Dissertation zur Erlangung des Doktorgrades

der Fakultät für Biologie

der Ludwig-Maximilians-Universität München

Analysis of sphingolipid-signaling at the plasma membrane of *Saccharomyces cerevisiae*

vorgelegt von

Florian Fröhlich

2010

Eherenwörtliche Versicherung

Ich versichere hiermit ehrenwörtlich, dass die vorgelegte Dissertation von mir selbstständig und ohne unerlaubte Hilfe angefertigt ist.

München, den ....

(Unterschrift)

Erklärung

Hiermit erkäre ich,

☐   Dass die Dissertation nicht ganz oder in wesentlichen Teilen einer anderen Prüfungskomission vorgelegt worden ist

☐   Dass ich mich anderweitig einer Doktorprüfung ohne Erfolg **nicht** unterzogen habe

München, den ....

(Unterschrift)

Diese Dissertation wurde von Prof. Dr. Stefan Jentsch betreut. Die Dissertation wurde eingereicht am 12.07.2010

      1. Gutachter: Prof. Dr. Stefan Jentsch
      2. Gutachter: Prof. Dr. Charles David

Tag der mündlichen Prüfung: 13.08.2010

1. Table of contents

Contents

2. List of Publications

Publication 1:

Walther TC*, Aguilar PS*, **Fröhlich F**, Chu F, Moreira K, Burlingame AL, Walter P. (2007) Pkh-kinases control eisosome assembly and organization. EMBO Journal 26(24), 4946-55.

Publication 2:

de Godoy LM*, Olsen J.V.*, Cox J*, Nielsen ML*, Hubner NC, **Fröhlich F**, Walther TC, Mann M. (2008) Comprehensive mass-spectrometry-based proteome quantification of haploid versus diploid yeast. Nature 455(7217):1251-4

Publication 3:

Fröhlich F*, Moreira K*, Aguilar PS, Hubner NC, Mann M, Walter P, Walther TC. (2009) A genome wide screen for genes affecting eisosomes reveals Nce102 function in sphingolipid signalling. Journal of Cell Biology, 185(7):1227-42

Publication 4:

Soufi B, Kelstrup CD, Stoehr G, **Fröhlich F**, Walther TC, Olsen JV. (2009) Global analysis of the yeast osmotic stress response by quantitative proteomics. Molecular BioSystems. 5(11):1337-46

Publication 5:

Fröhlich F and Walther TC. (2009) Comparing cellular proteomes by mass spectrometry. Genome Biology 10(10):240 Review

Publication 6:

Aguilar PS*, **Fröhlich F***, Rehman M*, Shales M*, Ulitsky I, Olivera-Couto A, Braberg H, Shamir R, Walter P, Mann M, Ejsing CS, Krogan NJ, Walther TC. (2010) A plasma membrane E-MAP reveals links between the eisosome, sphingolipid metabolism and endosomal tafficking. (2010) Nat Struct Mol Biol. [Epub ahead of print]

* These authors contributed equally to this work

3. Abbreviations

DHS	dihydrosphingosine
DHS-P	dihydrosphingosine phosphate
E-MAP	epistatic mini-array profile
ESR	electron spin resonance
FRAP	fluorescence recovery after photobleaching
GFP	green fluorescent protein
GPI	glycosylphophatidylinositol
GUV	giant unilamellar vesicle
IPC	inositol phosphoceramide
LCB	long chain base
L_o	liquid ordered
L_d	liquid disordered
MAPK	mitogen-activated protein kinase
MCC	membrane compartment occupied by Can1
MCP	membrane compartment occupied by Pma1
MCT	membrane compartment occupied by TORC2
MDCK	Madin-Darby canine kidney
MIPC	mannose-inositol-phosphoceramide
$M(IP)_2C$	mannose-$(inositol-P)_2$-ceramide
mTORC2	mammalian target of rapamycin complex 2
PA	phosphatidic acid
PC	phosphatidyl-choline
PDK1	phosphoinositide dependent kinase 1
PE	phosphatidyl-ethanolamine
PH domain	pleckstrin homology domain
PHS	phytosphingosine

PHS-P	phytosphingosine phosphate
PI	phosphatidyl-inositol
PIP	phosphoinositide
PI(4,5)P$_2$	phosphatidylinositol 4,5-bisphosphate
PS	phosphatidyl-serine
SDPE	1-stearoyl-2-docosahexaenoyl-*sn*-glycerophosphoethanol-amine
SGA	synthetic genetic array
SGK	serum glucocorticoid inducible kinase
SILAC	stable isotope labeling of amino acids in cell culture
SPT	serine palmitoyl transferase
SV40	simian virus 40
TORC2	target of rapamycin complex 2

4. Summary

The protein and lipid composition of eukaryotic plasma membranes is highly dynamic and regulated according to need. Despite its great plasticity, the plasma membrane retains some organizational features, such as its lateral organization into distinct domains. In the yeast, *Saccharomyces cerevisiae*, large immobile protein clusters, termed eisosomes, are important for plasma membrane organization. Eisosomes help to sort proteins into discrete domains, function in endocytosis and are implicated in cellular signaling. The major eisosome components Pil1 and Lsp1 were first identified as *in vitro* targets of the sphingolipid long chain base-regulated Pkh-kinases. However, it is not known if eisosomes are targets of Pkh-mediated sphingolipid signaling *in vivo*. In this thesis, I show that Pkh-kinases regulate eisosome formation in response to alterations of complex sphingolipid levels in the plasma membrane. I found that Pkh-kinase-dependent phosphorylation of Pil1 controls the assembly state of eisosomes. The combination of different unbiased, global analysis methods, such as proteomics and high content screening enabled me to identify Nce102 as a negative regulator of Pkh-kinases. Nce102 relocalizes between MCC domains, overlaying eisosomes, and the remainder of the plasma membrane in response to alterations in sphingolipid levels. Together with its regulatory function on Pkh-kinases that localize at eisosomes, this relocalization suggests that it is part of a sphingolipid sensor. Furthermore, I identified Rom2, a Rho1 GTPase exchange factor, as a novel regulator of sphingolipid metabolism. My data reveal several new insights into regulation of sphingolipid metabolism and plasma membrane organization. I provide a model how a homeostatic feedback loop may control sphingolipid levels. This likely will help in understanding how cells adjust processes, such as eisosome driven domain organization, endocytosis and actin organization to altered conditions. Furthermore, I anticipate that the datasets created in this thesis will serve as a resource for future studies on plasma membrane function.

5. Introduction

5.1 Architecture of the plasma membrane

5.1.1 Structure and components of the plasma membrane

The plasma membrane defines the boundary of eukaryotic cells by separating the cellular interior from the extracellular space. It surrounds all cells and is selectively permeable, thus controlling the movement of small water-soluble molecules in and out of the cell. The plasma membrane is primarily composed of proteins and lipids, each of which may be glycosylated. Molecules of both classes are approximately present in equal molar amounts. The basic structure of the plasma membrane is a lipid bilayer of approximately 30 Å (Lee, 2003).

All lipid molecules in the plasma membrane are amphiphatic. The chemistry of membrane lipids is modular and combinations of different headgroups and side-chains result in several thousand different lipid species. Based on their headgroup chemistry, lipids are classified into three major groups, phospholipids, sphingolipids, and sterols. (for examples see figure 1)

Phospholipids consist of a glycerol backbone to which different chemical groups can be attached. Two fatty-acyl chains are attached to carbon-1 and carbon-2 of the glycerol. Variations in chain length and saturation of these acyl chains further add to lipid heterogeneity. A phosphate group is bonded to the third glycerol carbon. The simplest phospholipid is thus phosphatidic acid (PA) where a phosphate is the polar headgroup. Various modifications of the phosphate with alcohols or sugars lead to other abundant phospholipids, specifically phsophatidyl-choline (PC), phosphatidyl-ethanolamine (PE), phosphatidyl-serine (PS) and phosphatidyl-inositol (PI).

The various modifications of the headgroups lead to different molecular shapes of phospholipids. PC has a cylindrical shape. PC moleulces can thus be arranged in a plane to form planar bilayers in aqueous phase. In such bilayers, the hydrophobic tails point to each other and the hydrophilic headgroups face the water. Other phospholipids, such as PE, have a more conical shape (Cullis and de Kruijff, 1979).

Conical shaped lipids are necessary in vivo to induce curvature in membranes, which is important to generate the rounded shape of vesicles, tubules and many organelles.

Besides their function in forming lipid bilayers, signaling functions and interactions with the cytoskeleton of phospholipids also participate in the organization of membrane domains. For example, Phosphoinsositols (PIs) are phosphorylated at several positions of their inositol ring. The resulting phosphoinositides (PIPs) are of low abundance in comparison to PIs, but are important for several processes including the recruitment of proteins to membranes. For example, many actin binding proteins have a conserved pleckstrin homology (PH) domain that binds PI(4,5)P$_2$, a phosphoinositide exclusively found in the plasma membrane. This way, PIP2 provides an anchor for the actin cytoskeleton at the plasma membrane. Together with its interactions with membrane proteins, this helps to organize the plasma membrane and align it with the actin cytoskeleton (Sechi and Wehland, 2000).

Sterols are another abundant lipid class in the plasma membrane. They consist of a polar headgroup, a planar steroid ring structure and a non polar hydrocarbon tail. The amphipathic character of sterols is due to the hydroxyl substituent on the steroid ring. Because of the small size and partial charge of the headgroup, and the resulting weak polar character of the molecule, it is too weak to form bilayers by itself. However, sterols are found abundantly in most eukaryotic plasma membranes. Sterols are incorporated in between phospholipids with their hydroxyl groups close to the polar headgroups of phospholipids. In this position, the steroid ring structures of sterols can immobilize the fatty acid chains of phospholipids close to the polar headgroups. This results in a less deformable membrane. In addition, during the lowering of temperature, cholesterol molecules intercalate with their bulky structure into the increasingly ordered phospholipid bilayers and therefore prevent membranes from freezing (Rottem et al., 1973).

Despite their near ubiquitous presence in most organisms, sterols are not essential for plasma membrane function. Nematodes for example have no sterols in the plasma membrane. In *Caenorhabditis elegans,* for example, sterols are just necessary as precursors for steroid hormones which is another important function of these lipids (Merris et al., 2003).
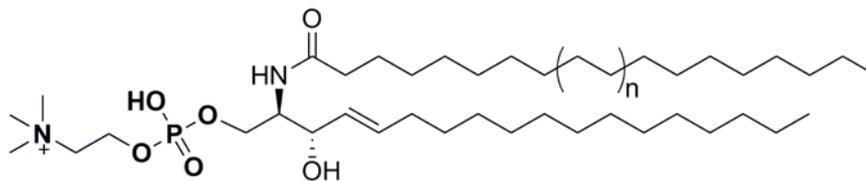
Phosphatidylcholine
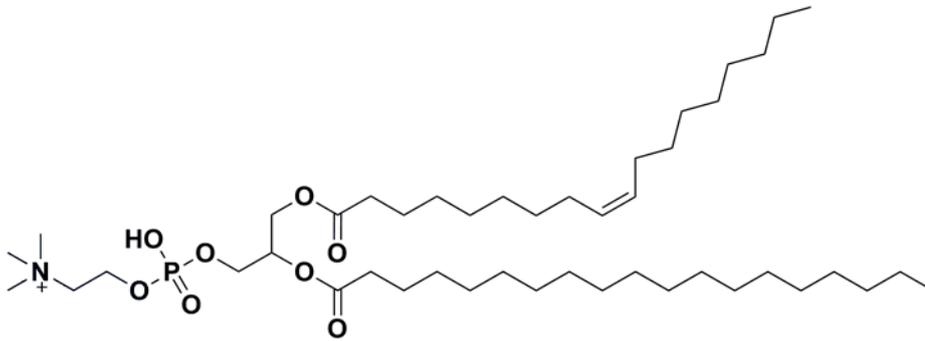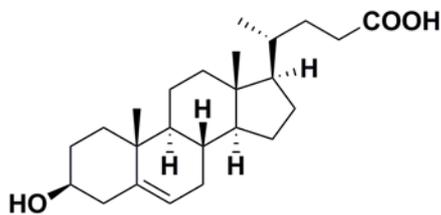
Cholesterol

Sphingomyelin

Figure 1: Structural formulas of phosphatidylcholine, cholesterol and sphingomyelin

Sphingolipids complete the description of lipid classes in the plasma membrane. They constitute 10-20 mol % of all plasma membrane lipids. Sphingolipids are characterized by an amide linkage of a fatty acid to a sphingoid long chain base. The latter are amino-alcohols with a hydrocarbon chain. The condensation reaction to form the amide takes place at the ER and yields ceramide. In mammalian cells, ceramides are transported by CERT proteins to the Golgi apparatus where they are flipped to the inner leaflet of the Golgi membrane (Hanada et al., 2003). There, different chemical groups, for example phosphocholine, can be further attached to

the C1 hydroxyl of ceramides. A phosphocholine headgroup attached to a ceramide yields sphingomyelin, the most abundant sphingolipid in eukaryotic cells.

Alternatively ceramides can be glycosylated by glucosylceramide synthases or galactosylceramide synthases. The glycan structure of the resulting glycosphingolipids can interact with lipids or proteins of neighbouring cells. Therefore glycosphingolipids play a role in cell recognition and signaling (Hakomori and Igarashi, 1995).

Additionally, sphingosines, ceramides and their phosphorylated derivates sphingosine-1-phosphate and ceramide-1-phosphate are second messengers and have been linked to a variety of cellular processes, such as apoptosis, proliferation and stress response (Chalfant et al., 1999; Pettus et al., 2005). Furthermore, sphingolipids are linked to several human diseases, such as diabetes (Summers, 2006), a range of cancers (Modrak et al., 2006; Ogretmen and Hannun, 2004), and Alzheimer´s disease (Han, 2005).

In comparison to the variability of sphingolipids in simple model organisms, they have a great diversity of sphingolipids in mammalian cell. The complexity in polar headgroups and fatty acids makes it difficult to study them. Therefore, the common baker´s yeast *Saccharomyces cerevisiae* has been used with great success to identify important enzymes in sphingolipid biology (Dickson and Lester, 2002). Since salient features of many biochemical pathways, including sphingolipid synthesis, are evolutionary conserved, these studies help to explain the complex processes in mammalian cells (Sims et al., 2004). Yeast sphingolipids are also in the focus of this work and their synthetic pathways will be described later in this thesis.

5.1.2 Membranes are two dimensional fluids

The first studies on the behavior of lipids in a bilayer were made with liposomes and planar bilayers, called "black membranes". Lipids with a polar headgroup that contained a spin label, such as a nitroxyl group, were incorporated into artificial membranes. The nitroxyl group contains an unpaired electron whose spin creates a paramagnetic signal. These signals can be recognized by electron spin resonance (ESR) spectroscopy. From the recorded spectra, the motion and behavior of a spin-labeled lipid can be deduced. These experiments showed that phospholipids do rarely flip between the two leaflets of a bilayer (on average less than once a month for each individual molecule). On the other side, lipids laterally exchange very rapidly with neighboring lipids (on average 10^7 times per second). Similar data were obtained from experiments with fluorescently labeled lipids. These and other results lead to a first commonly accepted model of plasma membrane structure, proposed by (Singer and Nicolson, 1972). It depicted a "fluid mosaic" of proteins and lipids, where proteins are freely floating around in a two dimensional, homogeneous fluid of lipids (Figure 2).
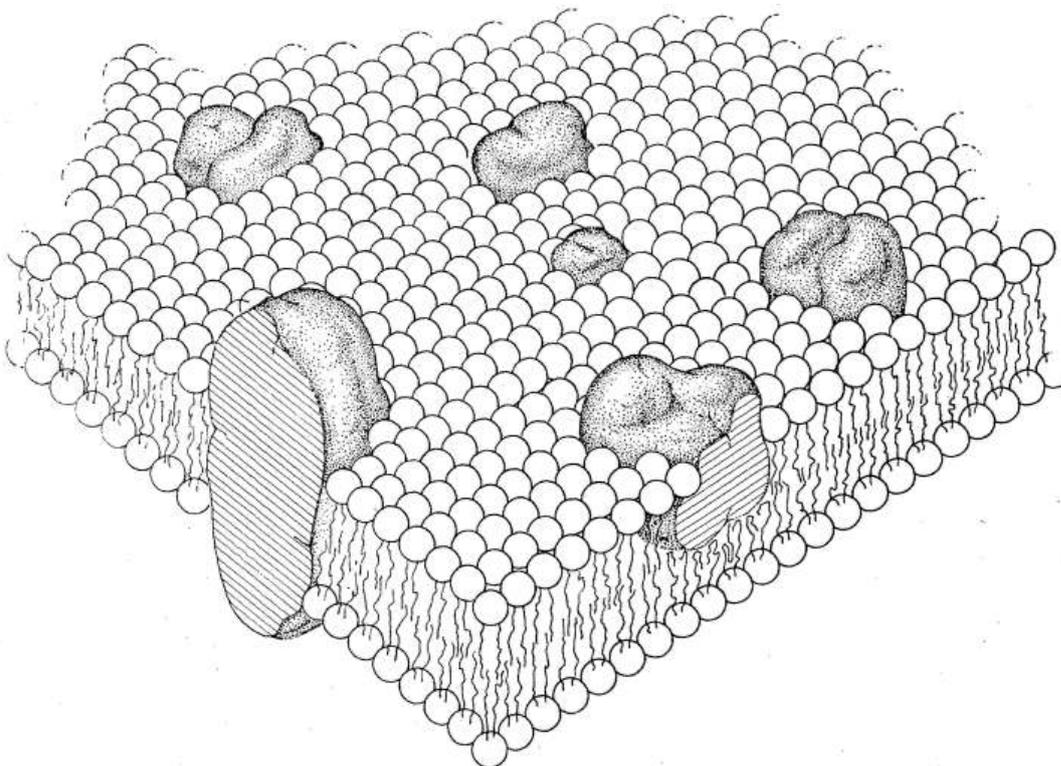
Figure 2: The fluid mosaic model of the plasma membrane (Singer and Nicolson 1972)

The fluidity of membranes is regulated to ensure that cellular processes, such as transport across the membrane, occur normaly. Consistent with this notion, such transport was inhibited when the bilayer fluidity was experimentally increased, (Friedlander et al., 1988). An artificial bilayer that contains only one type of phospholipid will change from a liquid state to a two dimensional crystalline state at a certain freezing point. This is a phase transition and its defining parameters - temperature and pressure - depend on attractive forces between lipids, length and saturation of the hydrocarbon chains. Especially, van der Waals attractions occur between the non-polar groups of the fatty acid chains and are responsible for the viscosity of a membrane.

5.1.3 Lipid rafts

In the last forty years, the model proposed by Singer and Nicolson was modified in several important ways: For example, it is now established that the lateral lipid distribution of the plasma membrane is not homogenous, but instead clusters and domains of distinct sizes and composition exist (Bagnat et al., 2000; Simons and Ikonen, 1997; van Meer and Simons, 1988)

The plasma membrane is the only organelle where high concentrations of sphingolipids are present (van Meer et al., 2008). The attractive forces between sphingolipids are just high enough to hold them together in small microdomains, called lipid rafts (Simons and Ikonen, 1997). The formation of microdomains represents a phase separation in the fluid lipid bilayer. The resulting domains are often described as liquid orderd (l_o) phase and liquid disordered (l_d) phase. When sphingomyelin, cholesterol and 1-stearoyl-2-docosahexaenoyl-*sn*-glycerophosphoethanol-amine (SDPE) were mixed in equal molar amounts, phase separation was shown in artificial membranes (Shaikh et al., 2001). By using fluorescently labeled lipid analogs, phase separation was also shown in giant unilamellar vesicles (GUVs), where it results in large domains visible by two photon microscopy (Kahya et al., 2003). The reasons why *in vivo* mostly very small raft microdomains are observed, whereas *in vitro* these phases coalesce to very large domains is not yet clear. One model to explain this is that *in vivo*, the plasma membrane is close to a critical point of phase transitions. The small clusers that are therefore disperse, but poised to cluster, which might be mediated by interaction with plasma membrane proteins or the cytoskeleton (Honerkamp-Smith et al., 2008; Honerkamp-Smith et al., 2009; Veatch et al., 2008)

Lipid rafts are formed by both, sphingolipids and sterols. The interaction between these two molecular classes may be stabilized by a hydrogen bond between the 3-hydoxyl group of the sterol and the amide group of the ceramide (Brown, 1998; Veiga et al., 2001). Because the much smaller sterols are positioned between sphingolipids with the long fatty acids and the large headgroups, this can be pictured as an umbrella of sphingolipids that shields the small sterols from too much exposure to the aqueous environment (Ikonen, 2008). The length of the fatty acyl chains and the concentration of sphingolipids also implies that lipid rafts, or l_o domains, are thicker

than the remainder of the membrane, as shown in planar lipid bilayer systems (Lawrence et al., 2003). This might provide a local environment in which proteins with unusually long transmembrane domains can preferentially incorporate and cluster together. For at least some cases, this was shown to affect the function of the proteins. For example, nanoclusters formed by glycosylphophatidylinositol (GPI) anchored proteins, in the outer leaflet of the cell surface are important for uptake of proteins by non-clathrin mediated endocytosis (Sharma et al., 2004b).

5.2   Mechanisms of plasma membrane organization

To accommodate communication and transport in and out of the cell under changing conditions, the plasma membrane is constantly remodeled and regulated according to need. However, despite its great plasticity, the plasma membrane retains some characteristic organizational features, including lateral organization in distinct domains. These phenomena can be distinguished into macro-phenomena that separate large parts of the membrane and micro-phenomena, such as lipid rafts that organize proteins and lipids into small areas of the membrane.

5.2.1   Macro-organization of the plasma membrane

An example of macro-organization is the separation of the apical and the basolateral membrane domains in epithelial cells. In polarized Madin-Darby canine kidney (MDCK) cells, the apical membrane is enriched in glycosphingolipids and sphingomyelin. In contrast, the basolateral membrane of these cells is rich in phosphatidylcholine. Both lipid classes are localized at the outer leaflet of the membrane and their mixing is prevented by tight junctions. The Golgi apparatus is the site of complex sphingolipid synthesis, where they are thought to form small clusters in the membrane. These clusters are believed to be sorting centers for proteins destined to the apical membrane (Simons and Ikonen, 1997). Consistent with this notion, (GPI) anchored proteins preferentially incorporate into these clusters and use their glycolipid anchors as apical sorting determinants (Brown and Rose, 1992).

The separation into apical and basolateral is important because the two domains face different environments and thus fulfill different functions.

5.2.2 Micro-organization of the plasma membrane

In contrast to macro-organization, micro organization of the plasma membrane ranges in dimensions from nanometers to a few microns. An example of protein-driven micro-organization in mammalian cells are small, flask-shaped invaginations of about 50-100nm in the plasma membrane, termed caveolae. The principal protein organizing these domains is caveolin. Each caveola contains 100-150 caveolin molecules that assemble into large, filamentous complexes (Fra et al., 1995). Caveloae are very static structures, as shown by fluorescence recovery after photobleaching (FRAP) experiments (Fernandez et al., 2002; Thomsen et al., 2002). It was also shown that cells with different fluorescently tagged caveolins do not exchange subunits after cell fusion. Instead, the fused cell maintained the originally labeled caveolae (Tagawa et al., 2005). Together these results indicate that caveolae, once they are formed, are very stable, immobile structures that do not exchange caveolins with a free cytoplasmic pool.
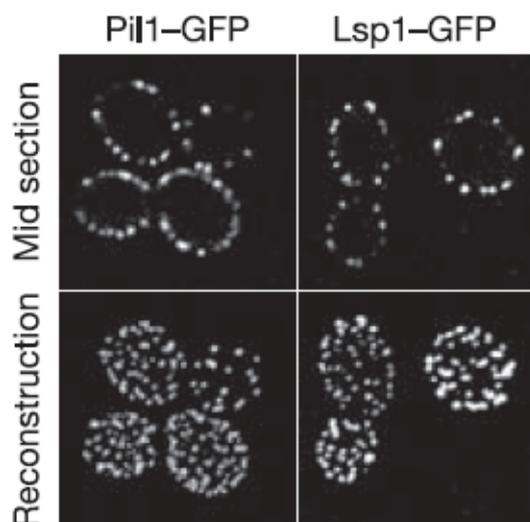
Interaction of caveolin with the plasma membrane is mediated by a scaffolding domain with many basic and aromatic amino acids that is thought to interact directly with cholesterol. This domain is followed by a 33 amino acid long intramembrane domain and a lipid anchor. The anchor mainly consists of palmitoylated cysteins. The intramembrane domain, thought to form a hairpin structure in the membrane, together with the anchor and the scaffolding domain mediate the interaction with the membrane. The self-assembly and the lipid binding properties of caveolin are the driving forces of membrane organization. Consistent with these properties, it was described that caveolae accumulate cholesterol and sphingolipids (Ortegren et al., 2004).

Besides their membrane organizing capabilities, caveloae have been associated with endocytosis. Some pathogens, such as the simian virus 40 (SV40), use caveloae as entry sites into the cells (Pelkmans et al., 2001). This might be achieved by fusion and fission of caveolae with internal compartments. It was also shown that caveolae internalization can be stimulated by cholera toxin, as well as by addition of exogenous cholesterol and glycosphingolipids (Sharma et al., 2004a).

5.2.3 Plasma membrane organization in *Saccharomyces cerevisiae*

Recently, a system for lateral plasma membrane organization has been discovered in the yeast *Saccharomyces cerevisiae*. In this model organism, large protein clusters, termed eisosomes, are localized in a peculiar, punctate pattern underneath the plasma membrane, which they organize into domains of distinct protein composition. An example for a protein in the eisosomal domain is the plasma membrane protein Sur7, which was shown to colocalize with eisosomes. Its localization completely collapsed upon deletion of the major eisosome component Pil1. Striking features of eisosomes are their uniform size, their stability over time and their composition of many copies of identical subunits. The main components of eisosomes are the two highly homologous proteins, Pil1 and Lsp1. Yeast cells possess around 25-45 eisosomes. Each eisosome consists of 2000-5000 Pil1 and Lsp1 proteins, as calculated from fluorescent intensity (Walther et al., 2006).

Eisosomes colocalize with a number of plasma membrane proteins that form a special compartment at this site, including the arginine permease Can1. The plasma membrane domain overlaying eisosomes is therefore named -membrane compartment occupied by Can1 (MCC). A normal yeast cell possesses around 25-45 MCCs that are mutually exclusive with a second domain called membrane compartment containing Pma1 (MCP) (Malinska et al., 2003). The MCP forms a continuous meshwork-like structure that covers most of the plasma membrane. Recently, a third domain was discovered that harbors the target of rapamycin complex 2 (TORC2) and is mutually exclusive with both other domains (Berchtold and Walther, 2009)

The MCC domain also harbors several other integral membrane

Figure 3: Eisosomes localize to the yeast cell cortex. Green fluorescent protein (GFP)-tagged Pil1 and Lsp1 are shown in midsections of yeast cells(upper panels) and in 3D reconstructions of the cells (lower panels). (Figure from (Walther et al., 2006))

proteins, such as the uracil/H+ symporter Fur4 or members of the Sur7 protein family. MCC domains are stable over time, as shown by FRAP experiments. MCCs also likely have a distinct lipid composition that is enriched in ergosterol, because they colocalize with membrane domains stained by fillipin, a fluorescent marker that binds to sterols (Grossmann et al., 2007). Since ergosterol preferentially localizes together with sphingolipids, it was hypothesized that MCCs represent raft like structures in *Saccharomyces cerevisae* (Malinska et al., 2003).

The concept of eisosomes being main organizers of the yeast plasma membrane was obtained from simple genetic experiments. When *PIL1* is deleted, localization of fluorescently tagged MCC markers completely collapses into a uniform plasma membrane signal with one or a few spots per cell. These are the sites where Lsp1, the second major eisosome component resides and they were therefore termed "eisosome remnants" (Walther et al., 2006). In addition, the regular distribution of ergosterol is also absent in *PIL1* deletion cells, resulting in a uniform staining of the plasma membrane with a few remnants (Figure 4). Together, these results suggest that lipids, most likely ergosterol together with sphingolipids, are not sufficient to form MCC domains in living yeast cells. On the other hand, it cannot be excluded that they are necessary to form domains. Most likely lipids and proteins, such as caveolin and Pil1 acting as a scaffold, are both necessary for membrane organization.
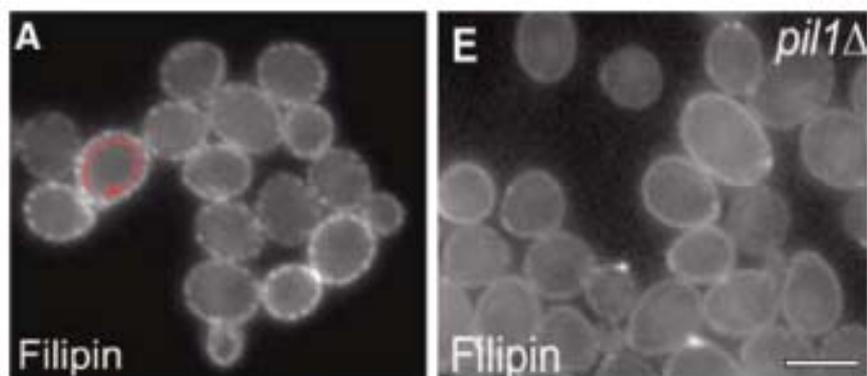
Figure 4: Eisosomes organize the plasma membrane. Fillipin stained WT (left) and *pil1Δ* (right) yeast cells. Pictures are taken from (Grossmann et al., 2007)

Eisosomes (from greek "eis" meaning into and latin "soma" meaning body) were initially described as static sites of endocytosis. When a lipophilc tracer, FM4-64 (Vida and Emr, 1995), is added to yeast cells, it forms endocytic intermediates that

colocalize with eisosomes. Interestingly, intermediates are formed only on some and not all eisosomes. It is unclear what distinguishes these "active" eisosomes from the other eisososmes. Endocytosis in yeast is actin dependent. However, the endocytic FM4-64 intermediates at eisosomes were still formed even if the actin cytoskeleton was depolymerized (Walther et al., 2006). There are two possible explanations for these results. One possibility is that eisosomes act in endocytosis upstream of actin in the formation of FM4-64 intermediates. The second possibility is that eisosomes mediate an actin independent endocytic pathway, similar to caveolae. Consistent with this, the uptake of the mating type receptor Ste3 is reduced in strains lacking normal eisosomes.

In addition to their function in endocytosis, eisosomes are implicated in cellular signaling. Pil1 and Lsp1 were first identified as inhibitors of the Pkh-kinases. Yeast has two Pkh-kinases that are highly similar and share at least one essential function. They are functional homologs of the mammalian phosphoinositide dependent kinase (PDK1). However, in contrast to PDK1 that binds phosphoinositides via its PH domain for plasma membrane recruitment and activation, Pkh-kinases do not contain such a domain and their activation *in vitro* does not depend on phosphoinositides (Casamayor et al., 1999). Pkh-kinases physically interact with eisosome components (Ho et al., 2002) and phosphorylate them *in vitro* (Zhang et al., 2004). In these in rwactions, phosphorylation of Pil1 and Lsp1 is oppositely regulated by long chain bases (LCBs). Pil1 phosphorylation is inhibited by LCBs, whereas Lsp1 phosphorylation is promoted by LCBs. These results make eisosomes an interesting target of sphingolipid signaling *in vivo*. One possibility is that eisosomes function as a signaling platform by clustering lipids and/or proteins together at the membrane, thereby facilitating their interaction.

5.3 Sphingolipids

5.3.1 Sphingolipid biosynthesis in *Saccharomyces cerevisiae*

The synthesis of sphingolipids starts with the condensation of serine with fatty acyl-CoA at the cytosolic leaflet of the ER to yield 3-ketodihydrosphingosine. This step is catalyzed by the serine palmitoyl transferase (SPT) and is rate limiting in the synthesis of sphingolipids. The SPT is a heterodimer composed of the proteins Lcb1 and Lcb2. A third protein, Tsc3, is necessary for optimal activity of the SPT and is essential for SPT activity at elevated temperatures (Gable et al., 2000), although the exact function of Tsc3 is still unknown. The second step of sphingolipid synthesis is catalyzed by Tsc10 that reduces 3-ketodihydrosphingosine to dihydrosphingosine (DHS) (Beeler et al., 1998). DHS is then attached via an amide linkage to a C26 fatty acid, catalyzed by either of two ceramide synthases Lag1 and Lac1 and yields N-acylsphiganine (dihydroceramide) (Guillas et al., 2001; Schorling et al., 2001). At this step also a third protein, Lip1, is involved. It was shown that Lip1 is necessary for the activity of the complex, but the mechanism how it functions is still unknown (Vallee and Riezman, 2005). Dihydroceramide is further hydroxylated at the C4 position by Sur2 to give phytoceramide. DHS can alternatively hydroxylated by Sur2 to yield phytosphingosine (PHS), which is then attached to a C26 fatty acid to yield phytoceramide (Haak et al., 1997). The chain length of DHS can be 16, 18 or 20 carbon atoms, and PHS contains either 18 or 20 carbon atoms.

The substrates required for ceramide synthesis, long chain bases and C26 fatty acids, are made in the ER. Synthesis of the latter requires several enzymes: Elo1, Fen1, Sur4, Tsc13, Phs1 and Acp1. C26 fatty acids are made from C14-C18 fatty acids and the elongation is achieved by a cycle of four reactions. The first step condenses malonyl-CoA with an acyl-CoA to yield 3-ketoacyl-CoA. The 3-ketoacyl-CoA is then reduced to 3-hydroxy acyl-CoA, which is reduced to an enol intermediate. The final step reduces the enol to yield an acyl-CoA that is two carbons longer than the starting compound (Beaudoin et al., 2002; Han et al., 2002; Oh et al., 1997; Toke and Martin, 1996).
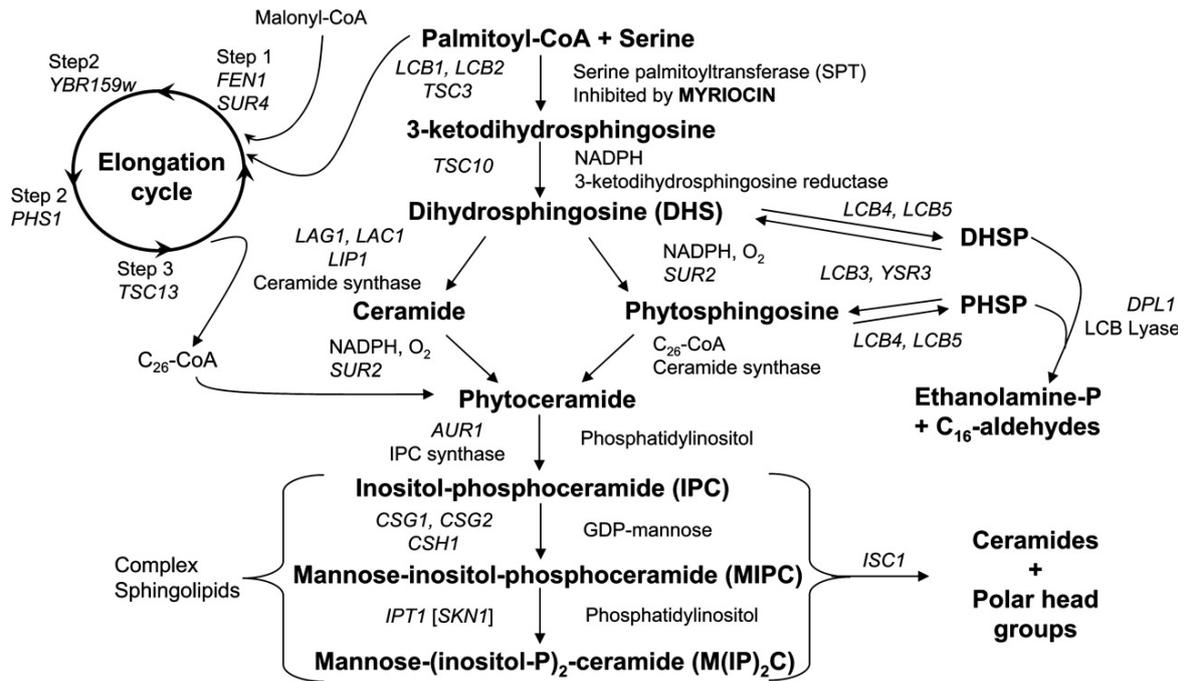
Figure 5: Sphingolipid metabolism in yeast (Dickson, 2008)

Once ceramides are made, they are transported from the ER to the Golgi apparatus. It is not clear if this is an active, transport in vesicles or a non-vesicluar transport that requires contact sites between ER and Golgi membranes. In mammalian cells, the CERT proteins are responsible for this transport, but yeast homologs have not been identified yet (Hanada et al., 2003). There is evidence that both pathways exist in yeast (Funato and Riezman, 2001). At the inner Golgi membrane, ceramides are modified by the inositol phopshoryl ceramide synthase (IPC synthase) Aur1 (Levine et al., 2000; Nagiec et al., 1997). An inositol phosphate is transferred from phosphatidyl inositol to the C_1 OH group of the ceramide to yield the first complex sphingolipid, inositol phosphoceramide (IPC).

For the next step in sphingolipid biosynthesis, the three enzymes Csg1, Csg2 and Csh1 are required (Uemura et al., 2003). They transfer a mannose from GDP-mannose to the inositol C_2-OH group. This results in a mannose-inositol-phosphoceramide (MIPC), which is the second complex sphingolipid in yeast.

In a final step of sphingolipis synthesis, a second inositol phosphate from phosphatidyl inositol is transferred to MIPC. This results in mannose-(inositol-P)$_2$-ceramide (M(IP)$_2$C). This reaction requires the *IPT1* gene. M(IP)$_2$C is the most

22

abundant of the complex sphingolipids in yeast, which – in analogy to the situation in mammalian cells- are all thought to reside in the outer leaflet of the plasma membrane. Only IPC might also be present in the vacuolar membrane, but its function there is unknown.

In comparison to the knowledge on sphingolipid synthesis, relatively little is known about the turnover of sphingolipids. There is some biological evidence that an enzyme with phospholipase C activity degrades sphingolipids. This activity is encoded by *ISC1* and hydrolyses the polar headgroup of all three complex sphingolipids, yielding ceramides (Sawai et al., 2000). Two genes have also been identified that encode ceramidases, *YDC1* and *YPC1* (Mao et al., 2000). These enzymes can hydrolyze the amide bond between the sphingosine and the fatty acid. However, single deletion of each of the genes has no effect on the viability of yeast, nor any other discernible phenotype. Thus, the biological relevance of the reactions catalyzed by the two genes remains unknown.

Sphingosines that are derived from breakdown of ceramides as well as *de novo* synthesized sphingosine can be phosphorylated. There are two LCB kinases in yeast, Lcb4 and Lcb5, which can produce PHS-1-phosphate (PHSP) and DHS-1-phosphate (DHSP). The function of these two molecules is not entirely clear. There is some evidence that they play a role in entry to the diaucix shift (Alvarez-Vasquez et al., 2007).

PHSP and DHSP can be either dephosphorylated by two LCB phosphatases, Lcb3 and Ysr3 or cleaved by an LCB lyase, Dpl1. Cleavage of LCB phosphates yields ethanolamine phosphate and a C_{16} aldhehyde. This pathway is the only exit from the sphingolipid biosynthesis pathway. Since double deletion of LCB3 and DPL1 is lethal for cells, it was suggested that high levels of LCB phosphates are toxic (Zhang et al., 2001). Sphingolipid metabolism in yeast is summarized in figure 5.

The basic metabolism of sphingolipids is conserved in mammalian cells, at least to the step of ceramides. In mammalian cells, inositol phosphates are not added to the ceramides. Instead, hydrophilic groups, such as phosphatidylcholine are added. The identification of yeast genes functioning in sphingolipid metabolism helped in many cases to identify their mammalian homologs. For example, the identification of the *LAG1/LAC1* genes helped to clarify the molecular function of the human LASS gene

23

family, which are now all shown to have ceramide synthase activity. Furthermore, some of the human *LASS* genes can complement the function of their yeast counterparts (Cerantola et al., 2007), thus demonstrating the evolutionary conservation of enzymatic function.

5.3.2 Regulation of sphingolipid levels

Even though many important enzymes for sphingolipid biosynthesis have been identified, very little is known about the regulation of sphingolipid levels. It is clear already that the relative amount of sphingolipids changes under different conditions and that this is important for plasma membrane function (Bagnat et al., 2000). Some studies focused on the transcriptional regulation of sphingolipid synthesis genes. So far, only *LAG1* and *LAC1* seem to be transcriptionally regulated. However, the changes in their expression levels are very low and do not influence the levels of sphingolipids (Kolaczkowski et al., 2004)

In contrast, it is known that sphingolipid intermediates fluctuate rapidly after a change in conditions. Cells that are shifted to a temperature of 37°C or 39°C show a 2-3 fold increase in C_{18}-PHS and C_{18}-DHS and a 100-fold increase in C_{20}-PHS and C_{20}-DHS. The increase in LCBs occurred within 5-10 min after heat shock and quickly returned to normal levels, even if the cells remained at an elevated temperature (Dickson et al., 1997; Jenkins et al., 1997). Sphingolipids cannot be stored in cells and the rapid increase of LCBs occurs through *de novo* synthesis. Since little transcriptional control is present and the responses are very fast, one would expect that most homeostatic controls occur via posttranslational modifications.

First evidence for this hypothesis comes from studies on the target of rapamycin complex 2 (TORC2), which is required for ceramide synthesis (Aronova et al., 2008). It signals through the downstream kinases Ypk1 and Ypk2, representatives of the AGC-kinase family, which includes human AKT. In agreement with a function in sphingolipid regulation, YPK1 was identified as a high copy suppressor in yeast cells that were grown in the presence of low concentrations of myriocin, an inhibitor of the SPT (Sun et al., 2000).

In analogy to mammalian systems, TORC2 is thought to phosphorylate an otherwise autoinhibitory sequence in the C-terminus of the Ypk-kinases (Kamada et al., 2005). Phosphorylation by TORC2 recruits Pkh-kinases, which can phosphorylate Ypk-kinases at their T-loop sequence. This is required for full activation of Ypk-kinases. Furthermore, Ypk-kinases are recruited to the plasma membrane after depletion of sphingolipids (Kobayashi et al., 2005), the place where TORC2 and Pkh-kinases localize.

In addition, TORC2 and Pkh-kinases share another essential downstream target. The proteins Slm1 and Slm2 were shown to physically interact with TORC2 (Tabuchi et al., 2006) and are also implicated in sphingolipid signalling (Daquinag et al., 2007). Some of their signals occur through the calcineurin phosphatase, but the exact output is unknown. One downstream effect of Slm-proteins is the inhibition of Isc1, the homolog of mammalian phospholipase C, cleaving sphingolipids (Tabuchi et al., 2006).

Together, these results indicate a complex signaling network that regulates the levels of sphingolipids. The main components of the network are conserved throughout evolution. However, our understanding of these processes is still rudimentary. New findings might help to understand complex processes in higher eukaryotes. This is of special interest, because misregulation of sphingolipid levels is linked to many common human diseases (see section 5.1.1).

5.3.3 Cellular processes regulated by sphingolipids

Sphingolipid intermediates participate in many important cellular processes, such as heat shock response, growth control, actin cytoskeleton organization, endocytosis and cell wall integrity. Isolation of a temperature sensitive mutant of the LCB1 gene, *lcb1-100,* helped in studying the functions of LCBs in these processes. Using this mutant, it was shown that these functions are regulated by signaling via Ypk- and Pkh-kinases. For example, *lcb1-100* yeast cells show an endocytic defect at the restrictive temperature (Friant et al., 2000). Overexpression of either Pkh1 or Pkh2 restored endocytosis in *lcb1-100* cells via activation of the protein kinase Pkc1, a downstream target of the Pkh-kinases (Inagaki et al., 1999). It was also shown that LCBs are required for actin organization. *lcb1-100* cells have depolymerized actin patches at the restrictive temperature. This defect was also rescued by the addition of exogenous PHS via the activation of Pkc1 through Pkh kinases (Friant et al., 2001)

Another link between sphingolipid signaling, endocytosis and Pkh-kinases is provided by eisososmes. Before my thesis, nothing was known about the regulation of Pkh-kinases *in vivo*, how and where they might phosphorylate eisosome components and what the cellular consequences of this might be. In addition, many apparent paradoxes persisted. For example, LCBs are synthesized in the ER, whereas Pkh-kinases localize to the plasma membrane. It is thus not clear how Pkh-kinases respond to the levels of LCBs. The overall aim of my thesis was therefore to determine how sphingolipid levels are perceived in the cell, how this information is relayed to eisosomes and what the cellular consequences of this signaling are.

5.4 Aims of the thesis

Eisosomes are static sites of endocytosis and help to organize the plasma membrane. Several lines of evidence suggest a connection between eisosomes and the Pkh kinases: 1) Pil1 and Lsp1, the main components of eisosomes, negatively regulate Pkh-kinase activity (Zhang et al., 2004). 2) The localization of overexpressed Pkh2 was very similar to the localization pattern of eisosomes (Roelants et al., 2002) 3) Both Pkh-kinases and eisosomes are linked to endocytosis (deHart et al., 2002; Friant et al., 2001; Walther et al., 2006).

Additionally, Pkh-kinases are regulated by LCBs, precursors of complex sphingolipids. LCBs are reported to function as signaling molecules that transduce stress signals (Friant et al., 2001). Therefore, I wanted to investigate if eisosomes are targets of sphingolipid signaling *in vivo,* possibly mediated by Pkh-kinases. I set out to identify proteins that have an effect on the localization of eisosomes either directly or through signaling via Pkh-kinases. To identify such proteins in an unbiased fashion, we incorporated a GFP tagged version of Pil1 in a comprehensive library of yeast gene deletion strains and visually screened for candidate genes encoding such proteins, using high throughput microscopy.

In a complementary approach, I employed high throughput genetics. Synthetic genetic array (SGA) screens are a common technique to compare the growth difference between a double mutant of two genes and the related single mutants (Tong et al., 2001). Classically, researchers focused on genes that show very strong phenotypes with each other or even lethality. A recently described modification of SGA screens is the so called epistatic mini-array profile (E-MAP) (Schuldiner et al., 2005). In this strategy, a large set of double mutants is created and the growth of each double mutant is measured. For each double mutant, a quantitative score is calculated that reflects the deviation of the growth rate of the individual mutant from the median of all mutants of the dataset. This quantative interaction score (or S-score) can display negative interactions (e.g. synthetic sick or lethal), as well as positive ones (e.g. suppression). The individual S-scores of each mutant can be compared with the S-scores of all other mutants and genes with similar interaction profiles can be clustered together. It has been shown that genes with very similar S-score profiles are likely to act in the same biological pathway (Schuldiner et al., 2005;

Ulitsky et al., 2008). We created a plasma membrane E-MAP that reveals insights into the connections between processes, such as eisosome assembly, endocytosis and sphingolipid biosynthesis.

In a third, complementary approach developed in this thesis, I investigated eisosome and sphingolipid biology in *Saccaromyces cerevisiae* by mass spectrometry based quantitative proteomics. In combination with SILAC (stable isotope labeling of amino acids in cell culture; (Ong et al., 2002), this methodology is a very usefull tool in cell biology (Blagoev et al., 2003; Foster et al., 2006; Vermeulen et al., 2007). In contrast to classical biochemical methods, such as a Western blot, many changes in the cell can be investigated quantitatively at the same time. Usually, lysine and arginine auxotrophic cells are grown in the presence of $[^{13}C_6/^{15}N_2]$L-lysine and $[^{13}C_6/^{15}N_4]$L-arginine, whereas control cells are grown with unlabeled amino acids. Proteins from both populations are mixed, and digested with proteases that cut only after lysines and arginines. The resulting peptides contain just one lysine or arginine and are analyzed in the mass spectrometer. Incorporation of the non-radioactive heavy amino acids results in a characteristic mass shift that can be distinguished in the mass spectra. Therefore, changes in the abundance of proteins can be analyzed quantitatively. I used these mass spectrometry based proteomics methods to identify new interaction partners of eisosomes, as well as posttranslational modifications of eisosome components.

6 Discussion

I used several systems biology approaches in my studies. In particular, I combined a number of unbiased, comprehensive methodologies, such as proteomics, high content screening and systematic genetics with hypothesis-driven biochemical and cell biological experiments.

High resolution mass spectrometry-based proteomics is a very powerful tool to study cell biology (Blagoev et al., 2003; Foster et al., 2006; Vermeulen et al., 2007). Quantitative proteomics enables comparison of changes of endogenous proteins under different conditions, and is therefore ideally suited to analyze the response of a system to changes in conditions or genetic alterations.

We used this technique to measure levels of all proteins in haploid yeast cells compared to their diploid counterparts. Most of the proteins showed a SILAC ratio in these experiments, allowing for a global view of proteome changes under each condition. Confirmation of abundance changes of many proteins by Western blots confirmed the MS-based quantification. Specifically, we could show that many proteins of the mating pathway are specific to haploid cells, as expected for this tightly regulated pathway (Dohlman and Slessareva, 2006). Interestingly, the overall correlation between SILAC ratios and changes in messenger RNA levels, derived from previous studies (Galitski et al., 1999), was poor. Only when the data was filtered for significant outliers the correlation coefficient increased. It is therefore likely that changes on the trascriptome level do not directly reflect changes of the proteome level. Similar findings were also obtained in a study analyzing the proteome and transcriptome of *Drosophila* cells (Bonaldi et al., 2008), suggesting that this is universal feature of biological systems (Publication 2).

Besides protein quantifications in cells under different conditions, mass spectrometry also allows for the quantification of changes in posttranslational modifications, such as phosphorylation. Therefore this method can be used to study complex networks of signal transduction. As a model for signal transduction, we investigated the osmotic stress response in yeast. We identified 3383 yeast proteins and 5534 unique phosphorylation sites, of which more than 15 % were changed significantly after 5 min of salt stress. Among the hits, we identified several proteins of the Hog1

mediated mitogen-activated protein kinase (MAPK) signal pathway, which is known to respond to osmotic stress and therefore confirms the quality of the dataset. In addition, several other pathways were regulated that were previously not recognized to be involved in osmotic stress resistance. Thus, our dataset will serve as a resource for future studies of the yeast response to salt stress (Publication 4).

Together, these studies illustrate the power of mass spectrometry based proteomics. Other people have, at the same time, combined MS-based proteomics with other techniques, such as cryo-electron tomography, to quantify the absolute abundances of proteins (Malmstrom et al., 2009). An overview of the currently used techniques, such as SILAC based proteomics and label free approaches, is given in (Frohlich and Walther, 2009) (Publication 5).

When work on this thesis commenced, very little was known about the function and composition of eisosomes. To identify new eisosome components, as well as posttranslational modifications of the core components, I started by affinity purifying Pil1 from yeast cells and analyzing its modifications and interactors by mass spectrometry.

This analysis of purified Pil1 led to the identification of at least 13 phosphorylation sites in the protein. At least four of these sites are important for the assembly state of eisosomes. A non-phosphorylatable mutant of Pil1-GFP that carries alanines at positions S45, S59, S230 and T233, showed a hyper-assembled phenotype. In contrast, a phospho-mimicking mutant of Pil1-GFP, where the same amino acids were mutated to aspartates, led to a reduced number of eisosomes with a corresponding increase in cytoplasmic signal. (Publication 1)

Another systems biology approach I used in this thesis was quantitative, systematic genetics, which I employed to generate a plasma membrane E-MAP. E-MAPs have previously been used to uncover complex biological processes, and to describe signaling networks and previously unrecognized protein-protein interactions (Fiedler et al., 2009; Schuldiner et al., 2005; Ulitsky et al., 2008). The plasma membrane E-MAP helped us to generate hypothesis on the regulation of sphingolipid metabolism, which will be discussed below. Besides that, I worked on two genes with the highest correlating genetic profiles compared with *PIL1, EMP70* and *YMR031C*. Analysis of the transmembrane protein Emp70 revealed a very complex localization. It is

possible that Emp70 plays a role in endocytosis, but this hypothesis needs further investigation. (Publication 6)

Another protein that consistently appeared in our screens linked to eisosomes was Ymr031c/Eis1. When I analyzed this protein, I found it to localize at eisosomes. In addition, SILAC based interaction proteomics confirmed that Ymr031C/Eis1, besides other proteins, physically interacts with eisosomes. This is consistent with another recent report, which also found the physical interaction of Ymr031c/Eis1 with eisosomes (Deng et al 2009 Mol Cell Prot). Based on its much lower abundance in comparison to eisosome core components, Ymr031C/Eis1 unlikely has a structural role at eisosomes, but instead may have regulatory function. This is also in line with data from our visual screen for genes affecting Pil1-GFP localization, the third high-throughput method I used, which shows that deletion of *YMR031C/EIS1* results in a phenotype similar to mutants in sphingolipid signaling. The question if and how Ymr031c/Eis1 participates in this signaling persists however.

In our systematic screen of gene deletions affecting Pil1-GFP localization, we identified 88 genes that are important for assembly of eisosomes. These are roughly three times more than identified in a similar screen that focused on localization of Can1 in MCC domains (Grossmann et al., 2008). It remains to be determined whether this difference is caused by different thresholding of phenotypes during the screen or biological differences between eisosomes and MCCs. Because Pil1 is necessary for the localization of MCCs, it is surprising that there is little overlap between the two screens. Only three genes were identified in both screens: *MNN1, SUR4* and *NCE102,* wich wil be discussed further below. (Publication 3)

Together the data presented in this thesis provide an example how different high throughput datasets can be combined to generate novel insights into biological questions. Many hypotheses that may be generated from these three different methods described here will need further investigation: For example, questions on the molecular function of Ymr031c/Eis1 or the connection between eisosomes and Emp70 remain to be adressed. Nonetheless, the data obtained from these approaches already served as a starting point for the main focus of this thesis, the analysis of sphingolipid signaling, and its relationship with eisosomes and plasma membrane organization.

Eisosomes organize the plasma membrane by clustering different proteins into a discrete domain (Grossmann et al., 2007; Walther et al., 2006). In my thesis, I showed that the major eisosome component Pil1 is a target of Pkh-kinases *in vivo*. I showed that Pkh-kinases localize to eisosomes and physically interact with them. This is consistent with previously published high throughput pull-down studies (Ho et al., 2002). Additionally, it was also shown previously that Pkh-kinases can phosphorylate the eisosome components Pil1 and Lsp1 *in vitro* (Zhang et al., 2004)*.* I found that either overexpression of Pkh-kinases or expression of a phospho-mimicking mutant of Pil1 results in disassembly of eisosomes. In contrast, more Pil1 assembles into eisosomes when Pkh-kinase activity is reduced in a temperature sensitive *pkh* mutant, or a non-phosphorylatable mutant of Pil1. Together with other data, this led me to conclude that Pil1 phosphorylation is critical for the assembly state of eisosomes. These results may be interpreted in two different ways: First, phosphorylation of Pil1 might be important for its assembly into eisosomes. Second, phosphorylation of Pil1 might lead to the disassembly of existing eisosomes. Of the two possibilities, I consider the latter more likely, because overexpression of Pkh-kinases from an inducible promoter leads to disassembly of existing eisosomes.

My data is different from findings by Luo et al (2008), who reported that a mutant form of Pil1 harboring five phosphosites mutated to alanines (S6A, S59A, T233A, S273A and S299A) could not assemble properly. Therefore they suggested that phosphorylation of Pil1 is important for the assembly of eisosomes, rather than disassembly. In my studies a mutant that lacks these five sites and even two additional sites (S6A, S45A, S59A, S230A, T233A, S273A and S299A) assembles properly into eisosomes. The reason for this difference is unclear at the moment, but might hint to the possibility that formation of eisosomes is regulated in a more complex fashion, and therefore dependent on conditions or different genetic background between the experiments.

Taken together, my results show that eisosome formation is dependent on phosphorylation of Pil1 by Pkh-kinases. Therefore, I used eisosome formation as a biological readout to identify regulators of Pkh-kinase activity. Pkh-kinases have been linked to LCB signaling in several studies (deHart et al., 2002; Friant et al., 2001). As expected from these studies, I could show that eisosome formation is dependent on sphingolipid signaling, mediated by Pkh-kinases. Eisosomes hyper-assemble after

addition of exogenous LCBs. In contrast, upon depletion of LCBs by inactivation of the serine palmitoyl transferase in *lcb1-100* cells or of its inhibition by myriocin, eisosomes disassemble. This phenotype was blocked by insertion of a non phosphorylatable *pil1(4A)* mutant. Apparently my results contradict published data that suggest an increase in Pkh activity by LCBs (Friant et al., 2001; Zanolari et al., 2000). However, this might be explained by the fact that these studies focused on different downstream targets of Pkh-kinases, such as the Pkc1 kinase. For Pil1 phosphorylation by Pkh-kinases though, also Zhang et al (Zhang et al., 2004) observed decreased activity *in vitro*, after addition of LCBs.

Taken together, these results suggest that the relative amounts of sphingolipids are sensed and transduced by Pkh-kinases to regulate eisosome formation and function, as well as other downstream targets. One of the targets phosphorylated by Pkh-kinases are Ypk-kinases, which are required for efficient ceramide synthesis. Moreover, Ypk-kinases are phosphorylated on a different site by TORC2, which is also required for normal ceramide synthesis (Kamada et al., 2005). From my studies presented here, I propose a model for a homeostatic feedback loop that regulates levels of sphingolipids. This model is shown in Figure 6.
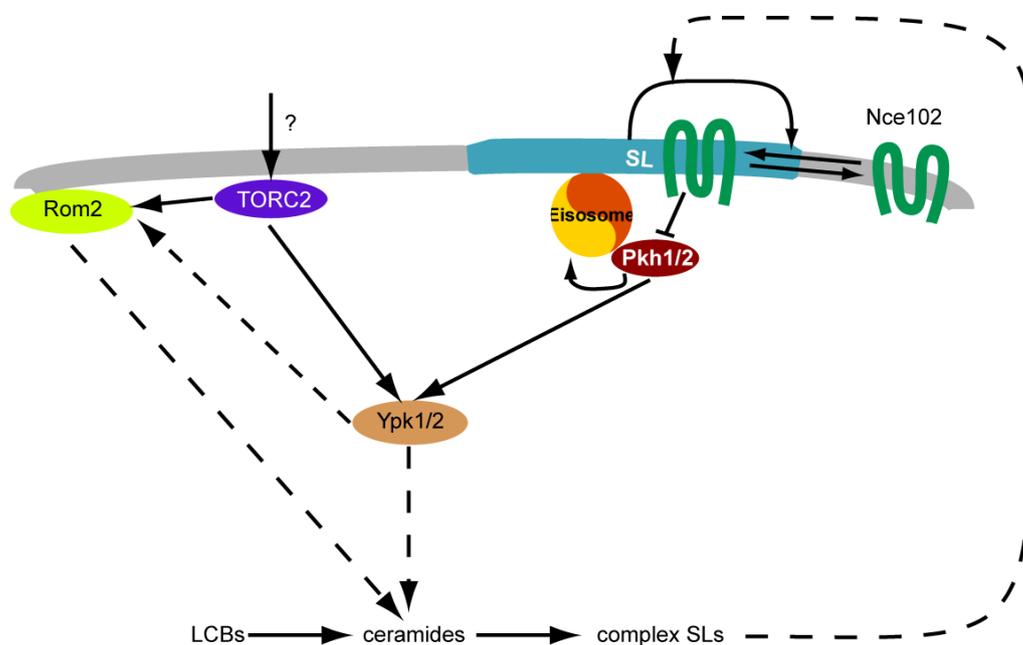
Figure 6: Model for a homeostatic feedback loop that controls sphingolipid levels. Nce102 (green) senses sphingolipid levels in the plasma membrane by distributing between the thick sphingolipid rich MCC (blue) and the rest of the plasma membrane (gray) depending on sphingolipid levels. It releases Pkh-kinases from inhibition by distributing away from MCCs under low sphingolipid levels. Pkh-kinases can activate Ypk-kinases, which also need TORC2 phosphorylation, functioning as a gain control, for full activation. Increased Ypk kinase activity stimulates ceramide synthesis, either directly or through signaling via Rom2.

In this model, Ypk-kinases are recruited to the plasma membrane when sphingolipids are depleted, as previously shown (Kobayashi et al 2005 JBC). This is also the place where Pkh-kinases and TORC2 are located, albeit in different membrane domains (Berchtold and Walther, 2009; Frohlich et al., 2009; Walther et al., 2007). For full activation, the Ypk-kinases have to be phosphorylated by both upstream branches. In analogy to mammalian systems, it is thought that TORC2 phosphorylates an otherwise auto-inhibitory sequence in the C-terminus of Ypk-kinases (Kamada et al., 2005), resulting in a recruitment of Pkh-kinases. Pkh-kinases phosphorylate Ypk-kinases at their T-loop sequence, which leads to a full activation of the Ypk-kinases (Inagaki et al., 1999). The upstream mechanisms of TORC2 regulation are still unclear. An interesting hypothesis is that TORC2 coordinates sphingolipid metabolism with levels of other lipids in the plasma membrane. Consistent with this notion, it was recently shown that TORC2 activity is modulated by both, the hydroxylation of sphingolipids and the levels of sterols (Guan et al., 2009). Phosphorylation of the autoinhibitory sequence of Ypk-kinases by TORC2 might in this scenario function as a gain control in the feedback loop, to adjust the magnitude of the Pkh-response dependent on the levels of other lipids in the plasma membrane.

The second branch, Ypk-activation is regulated by Pkh-kinases that respond to changes in sphingolipid levels. Using a combination of phosphoproteomics and a high throughput visual screen, I identified Nce102 as a negative regulator of Pkh-kinases. Upon deletion of *NCE102*, the phenotype of Pil1-GFP localization was very similar to that one of a phosphomimetic form of Pil1. This phenotype could be blocked by either the reduction of Pkh-kinase activity in *pkh1 pkh2* mutant cells or by the introduction of the non-phosphorylatable *pil1(4a)* mutant. Additionally, I could show that Pil1 is indeed more phosphorylated at some critical residues in *nce102Δ* cells, suggesting increased Pkh-kinase activity. I have also shown that Nce102 localization is highly sensitive to sphingolipid levels. At normal sphingolipid levels, Nce102 localizes to MCC domains where it is in close contact with the Pkh-kinases. Conversely, Nce102 leaves the MCC domains after depletion of sphingolipids and releases the Pkh-kinases from inhibition. These results suggest that Nce102 might be part of a sensor of complex sphingolipid levels in the plasma membrane that transduces this information to Pkh-kinases. In the simplest model, Nce102 regulates Pkh-kinase activity just by its juxtaposition to the kinases located at the MCC.

Nce102 localization to MCCs, which are thought to be enriched in ergosterol (Grossmann et al., 2007), could also implicate that Nce102 responds to ergosterol levels in the plasma membrane. However, deletion of nonessential *erg* mutants had no effect on Nce102 localization. Since sterols preferentially localize together with sphingolipids to form rafts, MCCs are thought to represent raft like domains in yeast (Malinska et al., 2003). Therefore Nce102 could either directly bind to sphingolipids or preferentially incorporate into a special membrane environment. Mechanistically, the latter may be an area of increased membrane thickness due to its elevated levels of sphingolipids. Alternatively, it was recently suggested that filipin stained domains are areas of free ergosterol, not complexed to sphingolipids (Jin et al., 2008). That would mean that Nce102 localizes to sphingolipid de-riched domains of the plasma membrane. In either of the two models, Nce102 leaves the MCC domains when sphingolipid levels are low, which corresponds to increased activity of Pkh-kinases towards Pil1 and potentially other targets, such as the Ypk-kinases.

In addition to the regulation by Nce102, activity of Pkh-kinases responds to levels of long chain base precursors that are synthesized in the ER. However, the addition of exogenous PHS did not rescue the observed phenotype of *NCE102* deletion towards Pil1 in my experiments. Additionally, inhibition of the IPC synthase by the drug aureobasidin, with a corresponding increase in LCBs and ceramides (Cerantola et al., 2009), has the same phenotype as the inhibition of the SPT. Therefore, the effect of LCB mediated Pkh-kinase activation is probably minor compared to the activation by Nce102 (Publication 3).

In addition, to this emerging picture of complex regulation of sphingolipid metabolism, I identified another protein that may be function in this regulation, using the plasma membrane E-MAP. In this E-MAP, phenotypic profiles of genes encoding sphingolipid metabolism highly correlate and therefore cluster together when all such profiles are compared. In this cluster, I found *ROM2*, a gene encoding a Rho1 GTPase exchange factor, arguing that it may have a regulatory function in sphingolipid metabolism. Particularly, *ROM2* has a very high correlation with profiles of genes that act early in the sphingolipid synthesis pathway. Furthermore, it clusters together with genes that encode two subunits of the ceramide synthase (*lag1Δ* and *lac1Δ*). Therefore, I hypothesize that it is an activator of the ceramide synthase. This is further supported by comparison of "shotgun lipidomic" analysis of mutants in sphingolipid synthesis

and *rom2Δ*. These experiments revealed that *rom2Δ* cells accumulate LCBs. One possibility to explain these data is that activation of Rom2 leads to increased long chain fatty acid synthesis. Long chain fatty acids are one of two substrates of ceramide synthase. Depletion of one of the two substrates leads to accumulation of the other substrate that is not being used, in this case LCBs (Publication 6).

The activation of the ceramide synthase by Rom2 might be achieved through regulation by TORC2. TORC2 was shown to regulate Rho1 and Rho2 by activation of Rom2 (Schmidt et al., 1997). This suggests an alternative pathway besides ceramide synthase activation via Ypk-kinases. An alternative model would be that TORC2 activates Rom2 via Ypk-kinases, a possibility not addressed in the studies of Schmidt et al.

Rom2 also localizes to the plasma membrane where it binds to $PI_{(4,5)}P_2$ via its PH domain (Audhya and Emr, 2002). Interestingly, it relocalizes from the cytoplasm to the plasma membrane after depletion of sphingolipid levels by myriocin (Kobayashi et al., 2005). A possible function of the TORC2/Rom2 module is therefore to coordinate the sphingolipid levels with $PI_{(4,5)}P_2$ levels in the plasma membrane.

Taken together, my data reveal several new insights into regulation of sphingolipid levels and plasma membrane organization. This might be important for the cell to maintain homeostasis of sphingolipids, as well as for the adjustment to altered conditions, for example during heat stress. Under heat stress conditions, cells control fluidity of the plasma membrane, which is regulated by sphingolipids (Guan et al., 2009). Ypk-kinases and Pkh-kinases are also linked to other cellular processes, such as endocytosis, actin cytoskeleton organization and the cell integrity pathway. It is possible that all these processes are coordinated to allow the cell to adapt to changing environments. For example, I could show that modulation of Pkh-kinase activity by deletion of *NCE102* led to altered plasma membrane organization, as observed for MCCs and MCPs. This might explain the effect of inactivation of Pkh-kinases on endocytosis (deHart et al., 2002). In line with this hypothesis, *nce102Δ* cells showed a reduction of endocytic foci at the plasma membrane, marked by the lipophilic dye FM4-64. Another group has furthermore reported that *nce102Δ* cells have altered endocytosis rates of some membrane transporters, for example accelerated uptake of Can1 (Grossmann et al., 2008).

It is already clear that the described pathways are just a small part of a much more complex signaling network. Recent studies have identified the proteins Orm1 and Orm2 as interactors and regulators of SPT (Breslow et al., 2010; Han et al., 2010). The authors showed that the phosphorylation of Orm-proteins is regulated by sphingolipid levels, but the responsible kinases/phosphatases are not yet identified. In addition, the phosphoinositide phosphatase Sac1 is part of the SPT/Orm complex. Sac1 had been described previously as a regulator of sphingolipid levels by generating substrates for complex sphingolipid synthesis (Brice et al., 2009). However, the identification of Sac1 as a member of the SPT/Orm-complex suggests a more direct role in this regulation. Another example was given by the identification of the proteins Slm1 and Slm2 as targets of TORC2 as well as Pkh-kinases. They have been linked through sphingolipid signaling via the phosphatase calcineurin. The exact output of this pathway is unknown, but it involves inhibition of Isc1, a homologue of the mammalian phospholipase C, which hydrolyses complex sphingolipids (Tabuchi et al., 2006).

The regulation of sphingolipid levels is not restricted to simple eukaryotes, such as yeast. The core components of my model, for example Pkh-kinases, Ypk-kinases, TORC2, as well as many enzymes of the sphingolipid synthesis pathway are evolutionary conserved. For some cases, it has been shown that mammalian homologs can complement the function of their yeast counterparts, for example the *LASS* genes, encoding ceramide synthases (Cerantola et al., 2007). However, mammals have at least six different ceramide synthases that are expressed in different tissues (Teufel et al., 2009). Therefore, it is unlikely that mammalian TORC2 (mTORC2) regulates all these enzymes directly, but it might regulate some of them through the Ypk homolog serum glucocorticoid inducible kinase (SGK). SGK belongs to the AGC kinase family which includes also Akt and PKB. Since all these kinases are known downstream targets of mTORC2, it is possible that they transduce mTORC2 signals to different ceramide synthases. In addition, SGK is also a known downstream target of the Pkh-kinase homolog PDK1 (Kobayashi and Cohen, 1999; Park et al., 1999). It will be exciting therefore to test whether a similar network is controlling sphingolipid metabolism in humans.

7 References

Alvarez-Vasquez, F., K.J. Sims, E.O. Voit, and Y.A. Hannun. 2007. Coordination of the dynamics of yeast sphingolipid metabolism during the diauxic shift. *Theor Biol Med Model*. 4:42.

Aronova, S., K. Wedaman, P.A. Aronov, K. Fontes, K. Ramos, B.D. Hammock, and T. Powers. 2008. Regulation of ceramide biosynthesis by TOR complex 2. *Cell Metab*. 7:148-158.

Audhya, A., and S.D. Emr. 2002. Stt4 PI 4-kinase localizes to the plasma membrane and functions in the Pkc1-mediated MAP kinase cascade. *Dev Cell*. 2:593-605.

Bagnat, M., S. Keranen, A. Shevchenko, and K. Simons. 2000. Lipid rafts function in biosynthetic delivery of proteins to the cell surface in yeast. *Proc Natl Acad Sci U S A*. 97:3254-3259.

Beaudoin, F., K. Gable, O. Sayanova, T. Dunn, and J.A. Napier. 2002. A Saccharomyces cerevisiae gene required for heterologous fatty acid elongase activity encodes a microsomal beta-keto-reductase. *J Biol Chem*. 277:11481-11488.

Beeler, T., D. Bacikova, K. Gable, L. Hopkins, C. Johnson, H. Slife, and T. Dunn. 1998. The Saccharomyces cerevisiae TSC10/YBR265w gene encoding 3-ketosphinganine reductase is identified in a screen for temperature-sensitive suppressors of the Ca2+-sensitive csg2Delta mutant. *J Biol Chem*. 273:30688-30694.

Berchtold, D., and T.C. Walther. 2009. TORC2 plasma membrane localization is essential for cell viability and restricted to a distinct domain. *Mol Biol Cell*. 20:1565-1575.

Blagoev, B., I. Kratchmarova, S.E. Ong, M. Nielsen, L.J. Foster, and M. Mann. 2003. A proteomics strategy to elucidate functional protein-protein interactions applied to EGF signaling. *Nat Biotechnol*. 21:315-318.

Bonaldi, T., T. Straub, J. Cox, C. Kumar, P.B. Becker, and M. Mann. 2008. Combined use of RNAi and quantitative proteomics to study gene function in Drosophila. *Mol Cell*. 31:762-772.

Breslow, D.K., S.R. Collins, B. Bodenmiller, R. Aebersold, K. Simons, A. Shevchenko, C.S. Ejsing, and J.S. Weissman. 2010. Orm family proteins mediate sphingolipid homeostasis. *Nature*. 463:1048-1053.

Brice, S.E., C.W. Alford, and L.A. Cowart. 2009. Modulation of sphingolipid metabolism by the phosphatidylinositol-4-phosphate phosphatase Sac1p through regulation of phosphatidylinositol in Saccharomyces cerevisiae. *J Biol Chem*. 284:7588-7596.

Brown, D.A., and J.K. Rose. 1992. Sorting of GPI-anchored proteins to glycolipid-enriched membrane subdomains during transport to the apical cell surface. *Cell*. 68:533-544.

Brown, R.E. 1998. Sphingolipid organization in biomembranes: what physical studies of model membranes reveal. *J Cell Sci*. 111 (Pt 1):1-9.

Casamayor, A., P.D. Torrance, T. Kobayashi, J. Thorner, and D.R. Alessi. 1999. Functional counterparts of mammalian protein kinases PDK1 and SGK in budding yeast. *Curr Biol*. 9:186-197.

Cerantola, V., I. Guillas, C. Roubaty, C. Vionnet, D. Uldry, J. Knudsen, and A. Conzelmann. 2009. Aureobasidin A arrests growth of yeast cells through both

ceramide intoxication and deprivation of essential inositolphosphorylceramides. *Mol Microbiol*. 71:1523-1537.

Cerantola, V., C. Vionnet, O.F. Aebischer, T. Jenny, J. Knudsen, and A. Conzelmann. 2007. Yeast sphingolipids do not need to contain very long chain fatty acids. *Biochem J*. 401:205-216.

Chalfant, C.E., K. Kishikawa, M.C. Mumby, C. Kamibayashi, A. Bielawska, and Y.A. Hannun. 1999. Long chain ceramides activate protein phosphatase-1 and protein phosphatase-2A. Activation is stereospecific and regulated by phosphatidic acid. *J Biol Chem*. 274:20313-20317.

Cullis, P.R., and B. de Kruijff. 1979. Lipid polymorphism and the functional roles of lipids in biological membranes. *Biochim Biophys Acta*. 559:399-420.

Daquinag, A., M. Fadri, S.Y. Jung, J. Qin, and J. Kunz. 2007. The yeast PH domain proteins Slm1 and Slm2 are targets of sphingolipid signaling during the response to heat stress. *Mol Cell Biol*. 27:633-650.

deHart, A.K., J.D. Schnell, D.A. Allen, and L. Hicke. 2002. The conserved Pkh-Ypk kinase cascade is required for endocytosis in yeast. *J Cell Biol*. 156:241-248.

Dickson, R.C. 2008. Thematic review series: sphingolipids. New insights into sphingolipid metabolism and function in budding yeast. *J Lipid Res*. 49:909-921.

Dickson, R.C., and R.L. Lester. 2002. Sphingolipid functions in Saccharomyces cerevisiae. *Biochim Biophys Acta*. 1583:13-25.

Dickson, R.C., E.E. Nagiec, M. Skrzypek, P. Tillman, G.B. Wells, and R.L. Lester. 1997. Sphingolipids are potential heat stress signals in Saccharomyces. *J Biol Chem*. 272:30196-30200.

Dohlman, H.G., and J.E. Slessareva. 2006. Pheromone signaling pathways in yeast. *Sci STKE*. 2006:cm6.

Fernandez, I., Y. Ying, J. Albanesi, and R.G. Anderson. 2002. Mechanism of caveolin filament assembly. *Proc Natl Acad Sci U S A*. 99:11193-11198.

Fiedler, D., H. Braberg, M. Mehta, G. Chechik, G. Cagney, P. Mukherjee, A.C. Silva, M. Shales, S.R. Collins, S. van Wageningen, P. Kemmeren, F.C. Holstege, J.S. Weissman, M.C. Keogh, D. Koller, K.M. Shokat, and N.J. Krogan. 2009. Functional organization of the S. cerevisiae phosphorylation network. *Cell*. 136:952-963.

Foster, L.J., A. Rudich, I. Talior, N. Patel, X. Huang, L.M. Furtado, P.J. Bilan, M. Mann, and A. Klip. 2006. Insulin-dependent interactions of proteins with GLUT4 revealed through stable isotope labeling by amino acids in cell culture (SILAC). *J Proteome Res*. 5:64-75.

Fra, A.M., E. Williamson, K. Simons, and R.G. Parton. 1995. De novo formation of caveolae in lymphocytes by expression of VIP21-caveolin. *Proc Natl Acad Sci U S A*. 92:8655-8659.

Friant, S., R. Lombardi, T. Schmelzle, M.N. Hall, and H. Riezman. 2001. Sphingoid base signaling via Pkh kinases is required for endocytosis in yeast. *EMBO J*. 20:6783-6792.

Friant, S., B. Zanolari, and H. Riezman. 2000. Increased protein kinase or decreased PP2A activity bypasses sphingoid base requirement in endocytosis. *EMBO J*. 19:2834-2844.

Friedlander, G., M. Shahedi, C. Legrimellec, and C. Amiel. 1988. Increase in Membrane Fluidity and Opening of Tight Junctions Have Similar Effects on Sodium-Coupled Uptakes in Renal Epithelial-Cells. *Journal of Biological Chemistry*. 263:11183-11188.

Frohlich, F., and T.C. Walther. 2009. Comparing cellular proteomes by mass spectrometry. *Genome Biol.* 10:240.

Funato, K., and H. Riezman. 2001. Vesicular and nonvesicular transport of ceramide from ER to the Golgi apparatus in yeast. *J Cell Biol.* 155:949-959.

Gable, K., H. Slife, D. Bacikova, E. Monaghan, and T.M. Dunn. 2000. Tsc3p is an 80-amino acid protein associated with serine palmitoyltransferase and required for optimal enzyme activity. *J Biol Chem.* 275:7597-7603.

Galitski, T., A.J. Saldanha, C.A. Styles, E.S. Lander, and G.R. Fink. 1999. Ploidy regulation of gene expression. *Science.* 285:251-254.

Grossmann, G., J. Malinsky, W. Stahlschmidt, M. Loibl, I. Weig-Meckl, W.B. Frommer, M. Opekarova, and W. Tanner. 2008. Plasma membrane microdomains regulate turnover of transport proteins in yeast. *J Cell Biol.* 183:1075-1088.

Grossmann, G., M. Opekarova, J. Malinsky, I. Weig-Meckl, and W. Tanner. 2007. Membrane potential governs lateral segregation of plasma membrane proteins and lipids in yeast. *EMBO J.* 26:1-8.

Guan, X.L., C.M. Souza, H. Pichler, G. Dewhurst, O. Schaad, K. Kajiwara, H. Wakabayashi, T. Ivanova, G.A. Castillon, M. Piccolis, F. Abe, R. Loewith, K. Funato, M.R. Wenk, and H. Riezman. 2009. Functional interactions between sphingolipids and sterols in biological membranes regulating cell physiology. *Mol Biol Cell.* 20:2083-2095.

Guillas, I., P.A. Kirchman, R. Chuard, M. Pfefferli, J.C. Jiang, S.M. Jazwinski, and A. Conzelmann. 2001. C26-CoA-dependent ceramide synthesis of Saccharomyces cerevisiae is operated by Lag1p and Lac1p. *EMBO J.* 20:2655-2665.

Haak, D., K. Gable, T. Beeler, and T. Dunn. 1997. Hydroxylation of Saccharomyces cerevisiae ceramides requires Sur2p and Scs7p. *J Biol Chem.* 272:29704-29710.

Hakomori, S., and Y. Igarashi. 1995. Functional role of glycosphingolipids in cell recognition and signaling. *J Biochem.* 118:1091-1103.

Han, G., K. Gable, S.D. Kohlwein, F. Beaudoin, J.A. Napier, and T.M. Dunn. 2002. The Saccharomyces cerevisiae YBR159w gene encodes the 3-ketoreductase of the microsomal fatty acid elongase. *J Biol Chem.* 277:35440-35449.

Han, S., M.A. Lone, R. Schneiter, and A. Chang. 2010. Orm1 and Orm2 are conserved endoplasmic reticulum membrane proteins regulating lipid homeostasis and protein quality control. *Proc Natl Acad Sci U S A.* 107:5851-5856.

Han, X. 2005. Lipid alterations in the earliest clinically recognizable stage of Alzheimer's disease: implication of the role of lipids in the pathogenesis of Alzheimer's disease. *Curr Alzheimer Res.* 2:65-77.

Hanada, K., K. Kumagai, S. Yasuda, Y. Miura, M. Kawano, M. Fukasawa, and M. Nishijima. 2003. Molecular machinery for non-vesicular trafficking of ceramide. *Nature.* 426:803-809.

Ho, Y., A. Gruhler, A. Heilbut, G.D. Bader, L. Moore, S.L. Adams, A. Millar, P. Taylor, K. Bennett, K. Boutilier, L. Yang, C. Wolting, I. Donaldson, S. Schandorff, J. Shewnarane, M. Vo, J. Taggart, M. Goudreault, B. Muskat, C. Alfarano, D. Dewar, Z. Lin, K. Michalickova, A.R. Willems, H. Sassi, P.A. Nielsen, K.J. Rasmussen, J.R. Andersen, L.E. Johansen, L.H. Hansen, H. Jespersen, A. Podtelejnikov, E. Nielsen, J. Crawford, V. Poulsen, B.D. Sorensen, J. Matthiesen, R.C. Hendrickson, F. Gleeson, T. Pawson, M.F. Moran, D. Durocher, M. Mann, C.W. Hogue, D. Figeys, and M. Tyers. 2002. Systematic

identification of protein complexes in Saccharomyces cerevisiae by mass spectrometry. *Nature*. 415:180-183.

Honerkamp-Smith, A.R., P. Cicuta, M.D. Collins, S.L. Veatch, M. den Nijs, M. Schick, and S.L. Keller. 2008. Line tensions, correlation lengths, and critical exponents in lipid membranes near critical points. *Biophys J*. 95:236-246.

Honerkamp-Smith, A.R., S.L. Veatch, and S.L. Keller. 2009. An introduction to critical points for biophysicists; observations of compositional heterogeneity in lipid membranes. *Biochim Biophys Acta*. 1788:53-63.

Ikonen, E. 2008. Cellular cholesterol trafficking and compartmentalization. *Nat Rev Mol Cell Biol*. 9:125-138.

Inagaki, M., T. Schmelzle, K. Yamaguchi, K. Irie, M.N. Hall, and K. Matsumoto. 1999. PDK1 homologs activate the Pkc1-mitogen-activated protein kinase pathway in yeast. *Mol Cell Biol*. 19:8344-8352.

Jenkins, G.M., A. Richards, T. Wahl, C. Mao, L. Obeid, and Y. Hannun. 1997. Involvement of yeast sphingolipids in the heat stress response of Saccharomyces cerevisiae. *J Biol Chem*. 272:32566-32572.

Jin, H., J.M. McCaffery, and E. Grote. 2008. Ergosterol promotes pheromone signaling and plasma membrane fusion in mating yeast. *J Cell Biol*. 180:813-826.

Kahya, N., D. Scherfeld, K. Bacia, B. Poolman, and P. Schwille. 2003. Probing lipid mobility of raft-exhibiting model membranes by fluorescence correlation spectroscopy. *J Biol Chem*. 278:28109-28115.

Kamada, Y., Y. Fujioka, N.N. Suzuki, F. Inagaki, S. Wullschleger, R. Loewith, M.N. Hall, and Y. Ohsumi. 2005. Tor2 directly phosphorylates the AGC kinase Ypk2 to regulate actin polarization. *Mol Cell Biol*. 25:7239-7248.

Kobayashi, T., and P. Cohen. 1999. Activation of serum- and glucocorticoid-regulated protein kinase by agonists that activate phosphatidylinositide 3-kinase is mediated by 3-phosphoinositide-dependent protein kinase-1 (PDK1) and PDK2. *Biochem J*. 339 (Pt 2):319-328.

Kobayashi, T., H. Takematsu, T. Yamaji, S. Hiramoto, and Y. Kozutsumi. 2005. Disturbance of sphingolipid biosynthesis abrogates the signaling of Mss4, phosphatidylinositol-4-phosphate 5-kinase, in yeast. *J Biol Chem*. 280:18087-18094.

Kolaczkowski, M., A. Kolaczkowska, B. Gaigg, R. Schneiter, and W.S. Moye-Rowley. 2004. Differential regulation of ceramide synthase components LAC1 and LAG1 in Saccharomyces cerevisiae. *Eukaryot Cell*. 3:880-892.

Lawrence, J.C., D.E. Saslowsky, J.M. Edwardson, and R.M. Henderson. 2003. Real-time analysis of the effects of cholesterol on lipid raft behavior using atomic force microscopy. *Biophys J*. 84:1827-1832.

Lee, A.G. 2003. Lipid-protein interactions in biological membranes: a structural perspective. *Biochim Biophys Acta*. 1612:1-40.

Levine, T.P., C.A. Wiggins, and S. Munro. 2000. Inositol phosphorylceramide synthase is located in the Golgi apparatus of Saccharomyces cerevisiae. *Mol Biol Cell*. 11:2267-2281.

Malinska, K., J. Malinsky, M. Opekarova, and W. Tanner. 2003. Visualization of protein compartmentation within the plasma membrane of living yeast cells. *Mol Biol Cell*. 14:4427-4436.

Malmstrom, J., M. Beck, A. Schmidt, V. Lange, E.W. Deutsch, and R. Aebersold. 2009. Proteome-wide cellular protein concentrations of the human pathogen Leptospira interrogans. *Nature*. 460:762-765.

Mao, C., R. Xu, A. Bielawska, Z.M. Szulc, and L.M. Obeid. 2000. Cloning and characterization of a Saccharomyces cerevisiae alkaline ceramidase with specificity for dihydroceramide. *J Biol Chem*. 275:31369-31378.

Merris, M., W.G. Wadsworth, U. Khamrai, R. Bittman, D.J. Chitwood, and J. Lenard. 2003. Sterol effects and sites of sterol accumulation in Caenorhabditis elegans: developmental requirement for 4 alpha-methyl sterols. *Journal of Lipid Research*. 44:172-181.

Modrak, D.E., D.V. Gold, and D.M. Goldenberg. 2006. Sphingolipid targets in cancer therapy. *Mol Cancer Ther*. 5:200-208.

Nagiec, M.M., E.E. Nagiec, J.A. Baltisberger, G.B. Wells, R.L. Lester, and R.C. Dickson. 1997. Sphingolipid synthesis as a target for antifungal drugs. Complementation of the inositol phosphorylceramide synthase defect in a mutant strain of Saccharomyces cerevisiae by the AUR1 gene. *J Biol Chem*. 272:9809-9817.

Ogretmen, B., and Y.A. Hannun. 2004. Biologically active sphingolipids in cancer pathogenesis and treatment. *Nat Rev Cancer*. 4:604-616.

Oh, C.S., D.A. Toke, S. Mandala, and C.E. Martin. 1997. ELO2 and ELO3, homologues of the Saccharomyces cerevisiae ELO1 gene, function in fatty acid elongation and are required for sphingolipid formation. *J Biol Chem*. 272:17376-17384.

Ong, S.E., B. Blagoev, I. Kratchmarova, D.B. Kristensen, H. Steen, A. Pandey, and M. Mann. 2002. Stable isotope labeling by amino acids in cell culture, SILAC, as a simple and accurate approach to expression proteomics. *Mol Cell Proteomics*. 1:376-386.

Ortegren, U., M. Karlsson, N. Blazic, M. Blomqvist, F.H. Nystrom, J. Gustavsson, P. Fredman, and P. Stralfors. 2004. Lipids and glycosphingolipids in caveolae and surrounding plasma membrane of primary rat adipocytes. *Eur J Biochem*. 271:2028-2036.

Park, J., M.L.L. Leong, P. Buse, A.C. Maiyar, G.L. Firestone, and B.A. Hemmings. 1999. Serum and glucocorticoid-inducible kinase (SGK) is a target of the PI 3-kinase-stimulated signaling pathway. *Embo Journal*. 18:3024-3033.

Pelkmans, L., J. Kartenbeck, and A. Helenius. 2001. Caveolar endocytosis of simian virus 40 reveals a new two-step vesicular-transport pathway to the ER. *Nat Cell Biol*. 3:473-483.

Pettus, B.J., K. Kitatani, C.E. Chalfant, T.A. Taha, T. Kawamori, J. Bielawski, L.M. Obeid, and Y.A. Hannun. 2005. The coordination of prostaglandin E2 production by sphingosine-1-phosphate and ceramide-1-phosphate. *Mol Pharmacol*. 68:330-335.

Roelants, F.M., P.D. Torrance, N. Bezman, and J. Thorner. 2002. Pkh1 and pkh2 differentially phosphorylate and activate ypk1 and ykr2 and define protein kinase modules required for maintenance of cell wall integrity. *Mol Biol Cell*. 13:3005-3028.

Rottem, S., J. Yashouv, Z. Ne'eman, and S. Razin. 1973. Cholesterol in mycoplasma membranes. Composition, ultrastructure and biological properties of membranes from Mycoplasma mycoides var. capri cells adapted to grow with low cholesterol concentrations. *Biochim Biophys Acta*. 323:495-508.

Sawai, H., Y. Okamoto, C. Luberto, C. Mao, A. Bielawska, N. Domae, and Y.A. Hannun. 2000. Identification of ISC1 (YER019w) as inositol phosphosphingolipid phospholipase C in Saccharomyces cerevisiae. *J Biol Chem*. 275:39793-39798.

Schmidt, A., M. Bickle, T. Beck, and M.N. Hall. 1997. The yeast phosphatidylinositol kinase homolog TOR2 activates RHO1 and RHO2 via the exchange factor ROM2. *Cell*. 88:531-542.

Schorling, S., B. Vallee, W.P. Barz, H. Riezman, and D. Oesterhelt. 2001. Lag1p and Lac1p are essential for the Acyl-CoA-dependent ceramide synthase reaction in Saccharomyces cerevisae. *Mol Biol Cell*. 12:3417-3427.

Schuldiner, M., S.R. Collins, N.J. Thompson, V. Denic, A. Bhamidipati, T. Punna, J. Ihmels, B. Andrews, C. Boone, J.F. Greenblatt, J.S. Weissman, and N.J. Krogan. 2005. Exploration of the function and organization of the yeast early secretory pathway through an epistatic miniarray profile. *Cell*. 123:507-519.

Sechi, A.S., and J. Wehland. 2000. The actin cytoskeleton and plasma membrane connection: PtdIns(4,5)P(2) influences cytoskeletal protein activity at the plasma membrane. *J Cell Sci*. 113 Pt 21:3685-3695.

Shaikh, S.R., A.C. Dumaual, L.J. Jenski, and W. Stillwell. 2001. Lipid phase separation in phospholipid bilayers and monolayers modeling the plasma membrane. *Biochim Biophys Acta*. 1512:317-328.

Sharma, D.K., J.C. Brown, A. Choudhury, T.E. Peterson, E. Holicky, D.L. Marks, R. Simari, R.G. Parton, and R.E. Pagano. 2004a. Selective stimulation of caveolar endocytosis by glycosphingolipids and cholesterol. *Mol Biol Cell*. 15:3114-3122.

Sharma, P., R. Varma, R.C. Sarasij, Ira, K. Gousset, G. Krishnamoorthy, M. Rao, and S. Mayor. 2004b. Nanoscale organization of multiple GPI-anchored proteins in living cell membranes. *Cell*. 116:577-589.

Simons, K., and E. Ikonen. 1997. Functional rafts in cell membranes. *Nature*. 387:569-572.

Sims, K.J., S.D. Spassieva, E.O. Voit, and L.M. Obeid. 2004. Yeast sphingolipid metabolism: clues and connections. *Biochem Cell Biol*. 82:45-61.

Singer, S.J., and G.L. Nicolson. 1972. The fluid mosaic model of the structure of cell membranes. *Science*. 175:720-731.

Summers, S.A. 2006. Ceramides in insulin resistance and lipotoxicity. *Prog Lipid Res*. 45:42-72.

Sun, Y., R. Taniguchi, D. Tanoue, T. Yamaji, H. Takematsu, K. Mori, T. Fujita, T. Kawasaki, and Y. Kozutsumi. 2000. Sli2 (Ypk1), a homologue of mammalian protein kinase SGK, is a downstream kinase in the sphingolipid-mediated signaling pathway of yeast. *Mol Cell Biol*. 20:4411-4419.

Tabuchi, M., A. Audhya, A.B. Parsons, C. Boone, and S.D. Emr. 2006. The phosphatidylinositol 4,5-biphosphate and TORC2 binding proteins Slm1 and Slm2 function in sphingolipid regulation. *Mol Cell Biol*. 26:5861-5875.

Tagawa, A., A. Mezzacasa, A. Hayer, A. Longatti, L. Pelkmans, and A. Helenius. 2005. Assembly and trafficking of caveolar domains in the cell: caveolae as stable, cargo-triggered, vesicular transporters. *J Cell Biol*. 170:769-779.

Teufel, A., T. Maass, P.R. Galle, and N. Malik. 2009. The longevity assurance homologue of yeast lag1 (Lass) gene family (review). *Int J Mol Med*. 23:135-140.

Thomsen, P., K. Roepstorff, M. Stahlhut, and B. van Deurs. 2002. Caveolae are highly immobile plasma membrane microdomains, which are not involved in constitutive endocytic trafficking. *Mol Biol Cell*. 13:238-250.

Toke, D.A., and C.E. Martin. 1996. Isolation and characterization of a gene affecting fatty acid elongation in Saccharomyces cerevisiae. *J Biol Chem*. 271:18413-18422.

Tong, A.H., M. Evangelista, A.B. Parsons, H. Xu, G.D. Bader, N. Page, M. Robinson, S. Raghibizadeh, C.W. Hogue, H. Bussey, B. Andrews, M. Tyers, and C. Boone. 2001. Systematic genetic analysis with ordered arrays of yeast deletion mutants. *Science*. 294:2364-2368.

Uemura, S., A. Kihara, J. Inokuchi, and Y. Igarashi. 2003. Csg1p and newly identified Csh1p function in mannosylinositol phosphorylceramide synthesis by interacting with Csg2p. *J Biol Chem*. 278:45049-45055.

Ulitsky, I., T. Shlomi, M. Kupiec, and R. Shamir. 2008. From E-MAPs to module maps: dissecting quantitative genetic interactions using physical interactions. *Mol Syst Biol*. 4:209.

Vallee, B., and H. Riezman. 2005. Lip1p: a novel subunit of acyl-CoA ceramide synthase. *EMBO J*. 24:730-741.

van Meer, G., and K. Simons. 1988. Lipid polarity and sorting in epithelial cells. *J Cell Biochem*. 36:51-58.

van Meer, G., D.R. Voelker, and G.W. Feigenson. 2008. Membrane lipids: where they are and how they behave. *Nat Rev Mol Cell Biol*. 9:112-124.

Veatch, S.L., P. Cicuta, P. Sengupta, A. Honerkamp-Smith, D. Holowka, and B. Baird. 2008. Critical fluctuations in plasma membrane vesicles. *ACS Chem Biol*. 3:287-293.

Veiga, M.P., J.L. Arrondo, F.M. Goni, A. Alonso, and D. Marsh. 2001. Interaction of cholesterol with sphingomyelin in mixed membranes containing phosphatidylcholine, studied by spin-label ESR and IR spectroscopies. A possible stabilization of gel-phase sphingolipid domains by cholesterol. *Biochemistry*. 40:2614-2622.

Vermeulen, M., K.W. Mulder, S. Denissov, W.W. Pijnappel, F.M. van Schaik, R.A. Varier, M.P. Baltissen, H.G. Stunnenberg, M. Mann, and H.T. Timmers. 2007. Selective anchoring of TFIID to nucleosomes by trimethylation of histone H3 lysine 4. *Cell*. 131:58-69.

Vida, T.A., and S.D. Emr. 1995. A new vital stain for visualizing vacuolar membrane dynamics and endocytosis in yeast. *J Cell Biol*. 128:779-792.

Walther, T.C., J.H. Brickner, P.S. Aguilar, S. Bernales, C. Pantoja, and P. Walter. 2006. Eisosomes mark static sites of endocytosis. *Nature*. 439:998-1003.

Zanolari, B., S. Friant, K. Funato, C. Sutterlin, B.J. Stevenson, and H. Riezman. 2000. Sphingoid base synthesis requirement for endocytosis in Saccharomyces cerevisiae. *EMBO J*. 19:2824-2833.

Zhang, X., R.L. Lester, and R.C. Dickson. 2004. Pil1p and Lsp1p negatively regulate the 3-phosphoinositide-dependent protein kinase-like kinase Pkh1p and downstream signaling pathways Pkc1p and Ypk1p. *J Biol Chem*. 279:22030-22038.

Zhang, X., M.S. Skrzypek, R.L. Lester, and R.C. Dickson. 2001. Elevation of endogenous sphingolipid long-chain base phosphates kills Saccharomyces cerevisiae cells. *Curr Genet*. 40:221-233.

8 Acknowledgments

9 Curriculum Vitae

Personal Data

Name:	Florian Fröhlich
Private adress:	Adlzreiter Str.19
	80337 München
	Germany
	froehlic@biochem.mpg.de
Phone:	private: 0179 6734931
	work: 089 8578 3442
Date of birth:	07/13/1981
Place of birth:	Kassel, Germany
Citizenship:	German

Education and Qualifications

10/2000 – 12/2005	Diploma, Biology, Georg-August Universität, Göttingen, Germany
09/1997 – 07/2000	A-levels (Abitur), Georg-Christoph Lichtenberg Gymnasium, Kassel, Germany

Research Experience

since 02/2007	**Max Planck Institute of Biochemistry, Organelle Architecture and Dynamics**, Munich, Germany, Dr. Tobias Walther, PhD
03/2006 – 12/2006	**Centre for Pharmacology and Toxicology, Department of Molecular Pharmacology**, Göttingen, Germany, Dr. Ralf Krätzner, Graduate student
03/2005 – 12/2005	**Centre for Pharmacology and Toxicology, Department of Molecular Pharmacology**, Göttingen, Germany, Prof. Dr. Wilhart Knepel, Diploma Thesis: *"In vitro* protein-protein interactions between domains of the transcription factors PAX6, PPARγ and RXRα"

Publications

Thakur SS, Geiger T, Chatterjee B, Bandilla P, **Fröhlich F**, Cox J, Mann M (2010) Deep proteome coverage in single-run liquid chromatography tandem mass spectrometry. Nature Biotechnology, [submitted]

Aguilar PS**, Fröhlich F**, Rehman M, Shales M, Ulitsky I, Olivera-Couto A, Braberg H, Shamir R, Walter P, Mann M, Ejsing CS, Krogan NJ, Walther TC. (2010) A plasma membrane E-MAP reveals links between the eisosome, sphingolipid metabolism and endosomal tafficking. (2010) Nature Structural and Molecular Biology, [Epub ahead of print]

Fröhlich F and Walther TC. (2009) Comparing cellular proteomes by mass spectrometry. Genome Biology 10(10):240 Review

Soufi B, Kelstrup CD, Stoehr G, **Fröhlich F**, Walther TC, Olsen JV. (2009) Global analysis of the yeast osmotic stress response by quantitative proteomics. Molecular BioSystems. 5(11):1337-46

Fröhlich F, Moreira K, Aguilar PS, Hubner NC, Mann M, Walter P, Walther TC. (2009) A genome wide screen for genes affecting eisosomes reveals Nce102 function in sphingolipid signalling. Journal of Cell Biology, 185(7):1227-42

de Godoy LM, Olsen J.V., Cox J, Nielsen ML, Hubner NC, **Fröhlich F**, Walther TC, Mann M. (2008) Comprehensive mass-spectrometry-based proteome quantification of haploid versus diploid yeast. Nature 455(7217):1251-4

Krätzner R, **Fröhlich F**, Lepler K, Schröder M, Röher K, Dickel C, Tzvetkov MV, Quentin T, Oetjen E, Knepel W. (2008) A peroxisome proliferator-activated receptor gamma-retinoid X receptor heterodimer physically interacts with the transcriptional activator PAX6 to inhibit glucagon gene transcription. Molecular Pharmacology 73(2), 509-517

Walther TC, Aguilar PS, **Fröhlich F**, Chu F, Moreira K, Burlingame AL, Walter P. (2007) Pkh-kinases control eisosome assembly and organization. EMBO Journal 26(24), 4946-55.

10 Declaration of Individual Contributions

Publication 1: Walther TC*, Aguilar PS*, **Fröhlich F**, Chu F, Moreira K, Burlingame AL, Walter P. (2007) Pkh-kinases control eisosome assembly and organization. EMBO Journal 26(24), 4946-55.

Florian Fröhlich performered the Western blots in figure 3. He created several plasmids that carry phosphomutants of Pil1 and analyzed them by live cell imaging. Furthermore, he affinity purified Pil1 to map phosphosites of the protein. He analyzed data from the mass spectrometrie experiments and extracted the spectra shown in the supplements.

Publication 2: de Godoy LM*, Olsen J.V.*, Cox J*, Nielsen ML*, Hubner NC, **Fröhlich F**, Walther TC, Mann M. (2008) Comprehensive mass-spectrometry-based proteome quantification of haploid versus diploid yeast. Nature 455(7217):1251-4

Florian Fröhlich established the protocols to label yeast cells with isotopically labeled lysine. He labelled the yeast cells, extracted proteins and digested the proteins for mass spectrometric analysis and participated in the analysis of the data.

Publication 3: **Fröhlich F***, Moreira K*, Aguilar PS, Hubner NC, Mann M, Walter P, Walther TC. (2009) A genome wide screen for genes affecting eisosomes reveals Nce102 function in sphingolipid signalling. Journal of Cell Biology, 185(7):1227-42

Florian Fröhlich designed and performed all experiments except the visual screen. He created all figures, except the ones corresponding to the visual screen. He co-wrote all parts of the paper.

Publication 4: Soufi B, Kelstrup CD, Stoehr G, **Fröhlich F**, Walther TC, Olsen JV. (2009) Global analysis of the yeast osmotic stress response by quantitative proteomics. Molecular BioSystems. 5(11):1337-46.

Florian Fröhlich established the protocols to label yeast cells with lysine. He provided the yeast strain used in this study and participated in SILAC labelling of the cells

Publication 5: **Fröhlich F** and Walther TC. (2009) Comparing cellular proteomes by mass spectrometry. Genome Biology 10(10):240 Review

Florian Fröhlich contributed the Figure and wrote the paper.

Publication 6: Aguilar PS*, **Fröhlich F***, Rehman M*, Shales M*, Ulitsky I, Olivera-Couto A, Braberg H, Shamir R, Walter P, Mann M, Ejsing CS, Krogan NJ, Walther TC. (2010) A plasma membrane E-MAP reveals links between the eisosome, sphingolipid metabolism and endosomal tafficking. (2010) Nat Struct Mol Biol. [Epub ahead of print]

Florian Fröhlich contributed Figure 3. He designed and performed the experiments shown in this figure. He contributed to the design of the experiments for the EMAP and all other figures in the paper. Furthermore, he generated many strains used in this study, used for example in the lipidomic experiments.

_____

Stefan Jentsch

11 Reprints of the Publications

Pkh-kinases control eisosome assembly and organization

Tobias C Walther[1,2,4,*], Pablo S Aguilar[1,4,5], Florian Fröhlich[2], Feixia Chu[1,3], Karen Moreira[1], Alma L Burlingame[1,3] and Peter Walter[1]

[1]Department of Biochemistry and Biophysics, Howard Hughes Medical Institute, University of California at San Francisco, San Francisco, CA, USA, [2]Organelle Architecture and Dynamics, Max Planck Institute of Biochemistry, Martinsried, Germany and [3]Mass Spectrometry Facility, Department of Pharmaceutical Chemistry, University of California at San Francisco, San Francisco, CA, USA

Eisosomes help sequester a subgroup of plasma membrane proteins into discrete membrane domains that colocalize with sites of endocytosis. Here we show that the major eisosome component Pil1 *in vivo* is a target of the long-chain base (LCB, the biosynthetic precursors to sphingolipids)-signaling pathway mediated by the Pkh-kinases. Eisosomes disassemble if Pil1 is hyperphosphorylated (i) upon overexpression of Pkh-kinases, (ii) upon reducing LCB concentrations by inhibiting serine-palmitoyl transferase in *lcb1*-mutant cells or by poisoning the enzyme with myriocin, and (iii) upon mimicking hyperphosphorylation in *pil1*-mutant cells. Conversely, more Pil1 assembles into eisosomes if Pil1 is hypophosphorylated (i) upon reducing Pkh-kinase activity in *pkh1 pkh2*-mutant cells, (ii) upon activating Pkh-kinases by addition of LCBs, and (iii) upon mimicking hypophosphorylation in *pil1*-mutant cells. The resulting enlarged eisosomes show altered organization. Other data suggest that Pkh signaling and sphingolipids are important for endocytosis. Taken together with our previous results that link eisosomes to endocytosis, these observations suggest that Pkh-kinase signaling relayed to Pil1 may help regulate endocytic events to modulate the organization of the plasma membrane.

*Corresponding author. Organelle Architecture and Dynamics, Max Planck Institute of Biochemistry, Am Klopferspitz 18, Martinsried, Bavaria 82152, Germany. Tel.: + 49 89 8578 3440; Fax: 49 89 8578 3430; E-mail: twalther@biochem.mpg.de
[4]These authors contributed equally to this work
[5]Present address: Institut Pasteur Montevideo, Uruguay

Introduction

To perform its many functions, the composition of the plasma membrane is highly dynamic and is continually remodeled according to need. In yeast cells, several plasma membrane transporters and signaling proteins are expressed on the surface in a conditional, tightly regulated manner. This regulation is achieved by the interplay between the delivery of proteins to the plasma membrane and their retrieval by endocytosis. The yeast plasma membrane contains patches of segregated plasma membrane proteins that are thought to be the functional equivalents of the lipid raft domains of mammalian cells (Malinska *et al*, 2003, 2004; Opekarova *et al*, 2005; Grossmann *et al*, 2006). The functional relevance of these domains is so far unclear, but one intriguing possibility is that they provide the framework for efficient regulation of different plasma membrane proteins by segregating them into different pools that can be recruited into a specialized lipid/protein environment and can be taken up separately by endocytosis.

Recently large, immobile complexes that mark sites of endocytosis were discovered and termed eisosomes (Walther *et al*, 2006). Eisosomes are positioned underneath the plasma membrane. Their striking features include their uniform pattern at the plasma membrane, their stability over time, their relatively uniform size, and their composition of many copies of identical subunits. How these features are achieved molecularly is largely unknown; even our knowledge of the composition of eisosomes is still incomplete. The two major subunits of eisosomes are the Pil1 and Lsp1 proteins. Pil1 most likely is the main organizer of eisosomes, since its deletion leads to collapse of the normal eisosome organization and relocation of all other known eisosome components to a few eisosome remnants in the cell periphery (Walther *et al*, 2006; Grossmann *et al*, 2007). This effect is specific to Pil1, since deletion of the homologous Lsp1 has no such consequences and also does not aggravate the effect observed in yeast cells lacking Pil1.

Their uniform size, firm anchoring underneath the plasma membrane, and seemingly stable assembly into complexes that do not readily exchange subunits with a free cytoplasmic pool suggests that eisosomes, once assembled, are static structures. As eisosomes are constructed of a few thousand copies each of their two major protein subunits Pil1 and Lsp1, their structure must form as a repeating arrangement of many identical units. Such assembly suggests a role as a scaffolding device that may recruit other components and perhaps modulate their activities by concentrating them locally in a specialized lipid/protein environment. As such, eisosomes have emerged as central players in the organization of the plasma membrane, since deletion the *PIL1* gene encoding one of their subunits leads to (i) large aberrant plasma membrane

invaginations associated with eisosome remnants and (ii) loss of the normal domain distribution of several plasma membrane proteins and sterol lipids (Walther *et al*, 2006; Grossmann *et al*, 2007). The distinct subcompartments in the plasma membrane that they organize comprise small, randomly distributed membrane patches that colocalize with eisosomes.

Tanner and co-workers recently termed the eisosome-organized membrane domains MCCs for 'Membrane Compartments occupied by Can1' (Grossmann *et al*, 2007), because they contain the arginine/proton symporter Can1, among other H^+-gradient driven symporters and Sur7, a plasma membrane protein that is genetically linked to the endocytic machinery. As MCCs are enriched in sterols, they provide a unique lipid environment for the membrane proteins that are embedded in it. The domains are thought to be the equivalent of lipid-ordered domains in higher eukaryotes (Malinska *et al*, 2003, 2004). Deletion of Pil1 leads to a collapse of MCCs (Grossmann *et al*, 2007), suggesting that eisosomes are essential to determine their size and organization in the plasma membrane. Disruption of the H^+ gradient across the plasma membrane also leads to release of Can1 and other transport proteins from MCCs, indicating that their localization of some membrane proteins can be dynamically controlled. Since functional studies suggest that their activity can strongly depend on the lipid environment (Lauwers and Andre, 2006), their recruitment into MCCs may provide an on/off switch. By contrast, other MCC constituents, such as Sur7, remain firmly anchored when the H^+ gradient is disrupted and hence may serve structural roles that help define the membrane domain. Pil1 emerges as the main organizer, because its deletion causes the remaining eisosome and the plasma membrane proteins recruited there to disperse or collapse.

Pil1 and Lsp1 were initially characterized as modifiers of Pkh signaling (Zhang *et al*, 2004). The central components of Pkh-signaling are two redundant kinases Pkh1 and Pkh2 that are functional homologues of the mammalian phosphoinositide-dependent kinase (PDK1) (Casamayor *et al*, 1999). The salient features of this signaling pathway are conserved (Inagaki *et al*, 1999; Sun *et al*, 2000; Roelants *et al*, 2002). Several laboratories have shown that Pkh-kinases are required for efficient endocytosis (Friant *et al*, 2001; deHart *et al*, 2002). Endocytosis in yeast is mediated by actin patches (Engqvist-Goldstein and Drubin, 2003) and the defect in endocytosis of cells deficient in Pkh signaling correlates well with a decrease in polarization of the actin cytoskeleton in these cells (Daquinag *et al*, 2007; TC Walther, PS Aguilar, and P Walter, unpublished observation). Again, salient features of this signaling seem conserved, since the mammalian Pkh homologue PDK1 also regulates the actin cytoskeleton, for example during insulin signaling (Dong *et al*, 2000).

Even though the molecular events leading to activation of Pkh-kinases are still only poorly understood, we know that they are regulated by the long-chain bases (LCBs), phytosphingosine (PHS), and dihydrosphingosine (DHS) (Friant *et al*, 2001). Consistent with this finding, it was shown that LCBs modulate yeast endocytosis via Pkh-kinase regulation (Zanolari *et al*, 2000; Friant *et al*, 2001; deHart *et al*, 2002). At least part of this regulation might occur through eisosomes, since the major eisosome components Pil1 and Lsp1 are phosphorylated by Pkh-kinases *in vitro* (Zhang *et al*, 2004).

Several lines of evidence point to a functional connection between eisosomes and Pkh signaling: (i) genetic evidence suggest that the major eisosome components Pil1 and Lsp1 negatively regulate Pkh-kinases (Zhang *et al*, 2004); (ii) we and others biochemically found Pkh1 and Pkh2 associated with eisosomes (F Fröhlich, Ivan Mattic, Matthias Mann, and TC Walther, unpublished observation; Ho *et al*, 2002; Krogan *et al*, 2006); (iii) cellular localization of Pkh1 is reminiscent of eisosomes (Roelants *et al*, 2002); (iv) both eisosomes and Pkh-kinases have purported roles in endocytosis (Friant *et al*,
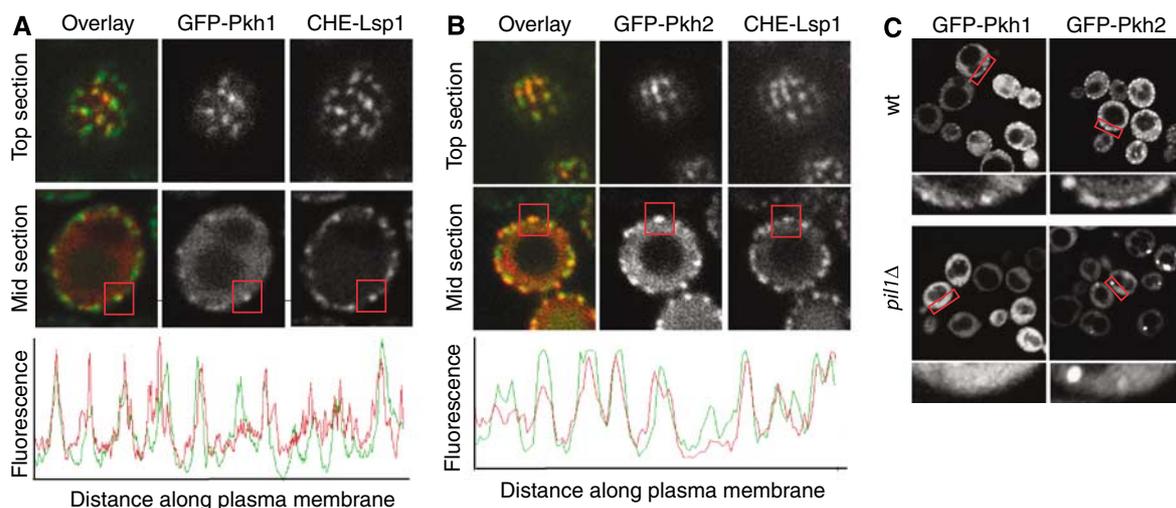
Figure 1 Pkh1 and Pkh2 are recruited to eisosomes. (**A**) 3GFP-Pkh1 expressed from the GAL promoter in a yeast strain expressing Lsp1-Cherry was imaged. Top- and mid-plane optical sections are shown for the single channel and an overlay in false colors (top panels). For midsections, the normalized intensity of the signal was plotted along a raced line underlying the cell surface (bottom panel). (**B**) Analogous analysis of Pkh2 localization. Boxes highlight colocalization of Pkh1 or Pkh2 with an individual eisosome. (**C**) Pil1 is required for localization of Pkh1 and Pkh2 to the plasma membrane. 3GFP-Pkh1 or 3GFP-Pkh2 was expressed from the GAL promoter either in wild-type cells (wt) or *pil1Δ* cells and imaged with a confocal microscope. Red boxes show area of the cell periphery that is shown in higher magnification below the corresponding image.

2001; deHart *et al*, 2002; Walther *et al*, 2006), and (v) Pkh-kinases phosphorylate Pil1 and Lsp1 *in vitro* (Zhang *et al*, 2004).

Here we investigated the effect of Pkh signaling on eisosomes and found that Pkh-kinases regulate aspects of eisosome assembly and organization. We suggest that this is part of a regulatory homeostasis mechanism that adjusts eisosome assembly in accordance to sphingolipid levels, perhaps providing negative feedback regulation to set eisosome abundance appropriately.

Results

Pkh-kinases localize to eisosomes

To further explore the connection of Pkh1 and Pkh2 with eisosomes, we first asked whether the Pkh-kinases associate with eisosomes *in vivo*. To this end, we expressed N-terminally GFP-tagged Pkh1 or Pkh2 in cells also expressing Cherry-tagged Lsp1 from its genomic locus. We found that the levels of GFP-Pkh1 and GFP-Pkh2 expressed from the PKH1 and PKH2 promoters were too low to detect the fusion proteins. We therefore overexpressed each fusion protein from the inducible GAL promoter, analyzing the earliest time points after induction that allowed reliable detection. As shown in Figure 1A, we observed robust induction of GFP fluorescence at a 1-h time point after shift from raffinose to galactose medium. Both GFP-Pkh1 and GFP-PKH2 localized to both a cytoplasmic pool and a distinct punctate pattern underlying the plasma membrane. For both kinases, the punctual staining colocalized with eisosomes marked by Lsp1-Cherry (Figure 1A and B). To get a quantitative impression of the degree of colocalization, we measured the relative fluorescence along the plasma membrane and overlayed the intensity profiles for either Pkh-kinase with the signal from Lsp1. For most eisosomes, we observed corresponding peaks of Pkh fluorescence (Figure 1A and B, lower panels).

To test whether eisosomes are required for the targeting of Pkh-kinases to the plasma membrane, we expressed GFP-Pkh1 and GFP-Pkh2 in wild-type and *pil1Δ* cells, in which eisosomes are disrupted. Instead of being distributed evenly around the cell periphery, eisosome remnants cluster in *pil1Δ* cells to one or a few spots along the cell periphery. Indeed, *pil1Δ* cells also mislocalized Cherry-Pkh1 and Cherry-Pkh2 to the cytosol (Figure 1C, top panels) and to a few spots along the cell periphery, presumably corresponding to eisosome remnants. These results suggest that both Pkh1 and Pkh2 are at least partially localized to eisosomes, and that Pkh1 but not Pkh2 requires Pil1 for this association.

Sphingolipid signaling controls eisosome assembly

Pkh-kinases are regulated by LCBs, which are metabolic precursors of sphingolipids. LCBs may have roles as signaling molecules, transmitting information about cell stress and/or information about the lipid composition of the plasma membrane (Dickson *et al*, 1997). *In vitro* experiments have shown that Pil1 and Lsp1 can be phosphorylated by Pkh-kinases (Zhang *et al*, 2004), suggesting that eisosomes might be a target of the LCB-signaling pathway.

To test this hypothesis, we monitored the effects of altering sphingolipid synthesis on eisosome assembly and organization. To this end, we used a temperature-sensitive allele of *LCB1* (*lcb1-100*), encoding serine-palmitoyl transferase,

which is the rate-limiting enzyme in LCB synthesis. In *lcb1-100* cells expressing Pil1-GFP, we observed a strong defect of eisosome assembly already at the permissive temperature (Figure 2A): cytoplasmic Pil1-GFP fluorescence was markedly increased compared with wild-type control cells. The effect is most clearly seen on a fluorescence profile of a line drawn through the diameter of the cell such that it bisects eisosomes, if visible, on either end (Figure 2A, lower panel). Accumulation of cytoplasmic Pil1-GFP was further aggravated after cells were shifted to the non-permissive temperature (Figure 2B). Under both permissive and non-permissive conditions, the total cellular Pil1-GFP levels were increased by roughly threefold (as assessed by western blotting, data not shown), perhaps due to a compensatory mechanism induced by failure to assemble eisosomes. To inhibit the synthesis of LCBs more acutely than possible with mutant cells that must be grown for many generations before analysis, we assessed the effects of myriocin, an inhibitor of Lcb1 (Fujita *et al*, 1994), on wild-type cells expressing Pil1-GFP. We imaged the cells 1 h after addition of myriocin (Figure 2C). Under these conditions the cellular Pil1 protein levels were unchanged (data not shown). The images show that cytoplasmic Pil1-GFP fluorescence increased and eisosome number at the cell periphery decreased. This experiment shows that LCB synthesis is required for maintenance of assembled eisosomes; due to the short time of myriocin treatment and the uniform phenotype observed, we can exclude that only newly formed eisosomes are affected by the drug.

Since inhibiting LCB synthesis affects eisosomes, we reasoned that, conversely, an increase in LCBs may also affect their assembly and organization. To test this possibility, we added exogenous LCBs to the medium. Indeed, addition of 25 μM PHS for 1.5 h yielded eisosomes that are about twofold brighter in the fluorescence images (Figure 2D). In addition to the increased fluorescence per eisosome, eisosomes appear elongated in the fluorescent images, perhaps indicative of two eisosomes becoming stacked next to one another.

Similar to the effects of myriocin, addition of aureobasidin, which blocks the synthesis of ceramide downstream of LCBs, led to comparable defects in eisosome assembly and organization. Thus taken together, these data show that both LCBs and ceramides regulate the assembly of eisosomes: increased LCB levels lead to more Pil1 assembled into eisosomes, whereas decreased LCB or ceramide levels lead to less Pil1 assembled.

Pil1 phosphorylation depends on Pkh-kinases

Since Pkh-kinases can localize to eisosomes and Pil1 has been shown to be a Pkh substrate *in vitro*, we asked whether Pil1 is also phosphorylated *in vivo* by Pkh-kinases. Western blot analysis with an antibody specific to Pil1 showed that Pil1 migrates as a doublet on denaturing gels (Figure 3A; Supplementary Figure S1). The slower-migrating form represents a phosphorylated Pil1, since it was sensitive to λ-phosphatase treatment. Dephosphorylation of Pil1 was inhibited by a preincubation with phosphatase inhibitors (Figure 3A).

We next asked whether Pil1 phosphorylation is dependent on Pkh-kinases. To this end, we examined the phosphorylation state of Pil1 in yeast cells bearing a temperature-sensitive allele of *PKH1* and a deletion of *PKH2* (Friant *et al*, 2001).
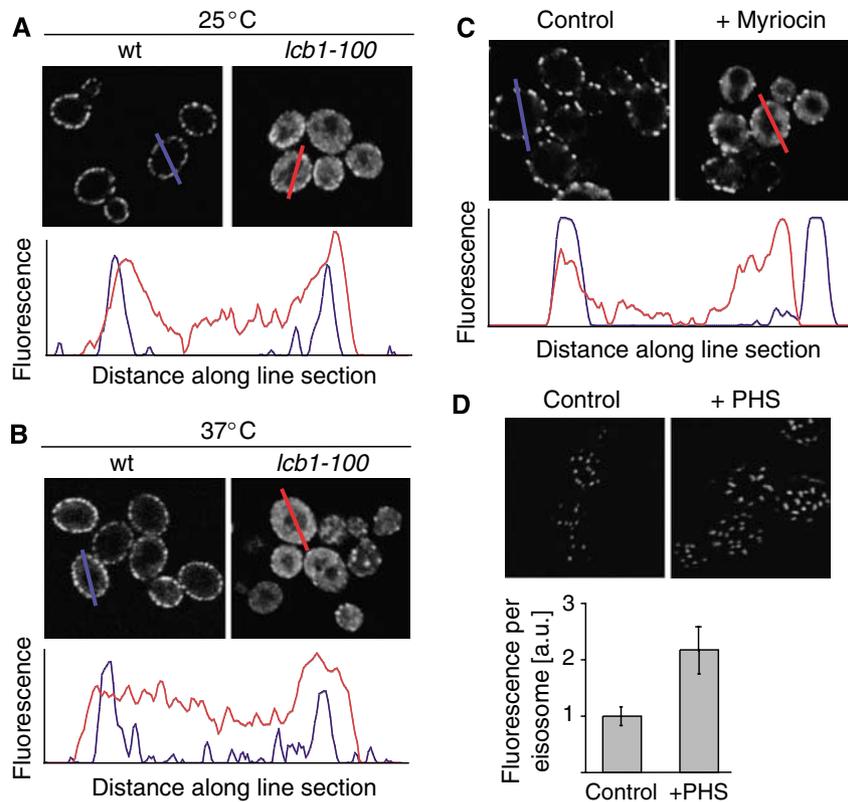
Figure 2 Sphingolipid signaling affects eisosome organization. (**A**) *LCB1* is required for normal eisosome assembly and organization. Pil1-GFP was expressed in either wt cells (left panel) or cells harboring a mutation in *LCB1* (*lcb1-100*). Cells were grown at 25°C and imaged with a confocal microscope. Representative middle sections are shown. Blue and red lines indicate the axis used for deriving the intensity profile plot shown below the images. (**B**) Elevated temperature aggravates the *lcb1-100* phenotype. Cells were grown for 1.5 h at 37°C and analyzed as in panel A. (**C**) Myriocin addition affects eisosome assembly and organization. Myriocin (5 μM) (right panel) or buffer was added to wt cells expressing Pil1-GFP and imaged by confocal microscopy after 1.5 h incubation at 30°C. (**D**) PHS addition leads to increased eisosome assembly. C16 PHS (5 μM) or buffer was added to wt cells expressing Pil1-GFP, incubated for 1 h and imaged as in panel C. The relative size of eisosomes was measured on confocal images and averages are shown. Standard deviates from the mean are shown as error bars.

Western blot analysis Pil1 of these strains showed that the phosphorylation of Pil1 is almost completely abolished under both permissive and restrictive conditions (Figure 3B). To further test the possibility that Pil1 is phosphorylated in a Pkh-kinase-dependent manner, we overexpressed Pkh1 and Pkh2 by placing each gene under control of the GAL promoter. At a 1.5-h time point after induction of either kinase, Pil1 phosphorylation was markedly increased (Figure 3C). Taken together our data establish Pil1 as a phosphoprotein that is a target of Pkh-kinase signaling *in vivo*.

To determine the sites of phosphorylation in Pil1, we partially purified Pil1 tagged with a tandem affinity purification tag or a myc-epitope and analyzed its phosphorylation by tandem mass spectrometry. This analysis revealed that Pil1 is phosphorylated at multiple sites. The MS/MS spectra of Pil1 showed phosphorylation of residues serines 16, 26, 45, 98, 163, 230, and 273, as well as of threonine 233 (a representative spectrum for this latter site is shown in Figure 3D; for the serine modifications see Supplementary Figures S2–S9). In addition, we found phosphorylation on serine 6 and serine 299, but these phosphorylated peptides were not detected in every preparation analyzed (F Chu and AL Burlingame, unpublished observation; Changhui Deng and Andrew Krutchinsky, personal communication). A large-scale analysis of the yeast phospho-proteome detected yet another phosphorylation site on serine 59 (Lyris de Godoy

and Matthias Mann, personal communication). As shown in Figure 2E, the many phosphorylation sites on Pil1 are distributed across the protein, leaving a central predicted coiled-coil domain (K165-A198) unphosphorylated.

To determine which site(s) are responsible for the shift in mobility observed in SDS–PAGE gels (Figure 3A), we mutated all residues alone and in various combinations to alanine. Surprisingly mutation of up to six sites did alter Pil1's electrophoretic mobility. When we mutated S273 in addition, the full magnitude of the shift was abolished. Kinetic experiments dephosphorylating Pil1 *in vitro* by addition of phosphatases did not show intermediates in mobility (F Fröhlich and T Walther, unpublished observation), indicating that phosphorylation of serine 273 alone is responsible for the shift in mobility. As such, the gel shift assay does not report comprehensively on the phosphorylation status of Pil1.

### Pkh signaling regulates eisosome assembly and organization

To address whether Pkh-kinase phosphorylation of Pil1 mediates the effect seen on eisosome assembly and organization upon inhibition of LCB synthesis and exogenously added LCBs, we next monitored the consequences of either inactivating or hyperactivating Pkh-kinases. First, we expressed Pil1-GFP in *pkh1^{ts} pkh2Δ* cells (Friant *et al*, 2001). Figure 4

A

λ-Phosphatase	−	+	+
Phosphatase inhibitors	−	−	+

P-Pil1
Pil1

B

Raffinose   Galactose

pGAL-*PKH1*   pGAL-*PKH2*   pGAL-*PKH1*   pGAL-*PKH2*

P-Pil1
Pil1

Pgk1

C

25°C   37°C

Δ*pil1*   wt   *pkh1^ts* Δ*pkh2*   wt   *pkh1^ts* Δ*pkh2*

P-Pil1
Pil1

Pgk1

D

Pil1-GFP   ΔPil1   Pil1-GFP 6A/T14A   Pil1-GFP 6A/S16A   Pil1-GFP 6A/S26A   Pil1-GFP 6A/S26A   Pil1-GFP 6A/S265A   Pil1-GFP 6A/S273A

E

b ions $AL_2L_3E_4{}^{23}L_5{}^{22}L_6{}^{21}D_7{}^{20}D^{19}S^{18}PV^{16}pT^{15}PGE^{12}TR^{10}PAYD^6G^5YE^3A^2S^1K$ y ions

F

S26
S16 S59
S6 S45 S98 S163 coiled coil T233 S230 S273 S299
1 ————————————————————————————————— 339
K165   A198

Figure 3 Pil1 is phosphorylated in a Pkh1/2-dependent manner. (**A**) Pil1 is a phosphoprotein. Extracts of wt cells were either incubated with buffer (left lane), λ-phosphatase (middle lane), or λ-phosphatase after 5 min preincubation with a mixture of phosphatase inhibitors (right lane) for 30 min, and analyzed by western blot against Pil1. The lower panel shows the same blot reprobed with an antibody against 3-phosphoglycerate kinase 1 (Pgk1) used as loading control. (**B**) Phosphorylation of Pil1 depends on Pkh-kinases. Extracts from either Δ*pil1*, wt, or pkh-ts cells grown at 25°C or shifted for 1.5 h to 37°C were analyzed as in panel A. (**C**) Overexpression of Pkh-kinases increases the levels of phosphorylated Pil1. Cells harboring *PKH1* (pGAL-*PKH1*) or *PKH2* (pGAL-*PKH2*) under the control of the GAL promoter were grown in raffinose-containing medium and shifted to galactose-containing medium for 1.5 h. Samples were analyzed as in panel A. (**D**) Ser273 is responsible for the shift in the mobility of phosphorylated Pil1 on SDS–PAGE gels. Extracts from cells either expressing wt Pil1-GFP or Pil1-GFP bearing a combination of seven amino acids mutated to alanine (S6, S45, S59, S230 T233, and S299, plus the residue indicated) were analyzed by western blot analysis. (**E**) A representative tandem MS spectrum is shown, in which threonine 233 of Pil1 is phosphorylated. Continuous sequence ions in the CID spectrum reveal the identity of the peptide, ^{222}ALLELLDDSPV*p*TPGETRPAYDGYEASK^{248}, and ions containing phosphate moiety (colored in red) indicate conclusively that Thr233 is phosphorylated. MS data for the remaining phosphorylation sites on Pil1 are provided in Supplementary Figures S2–S9. (**F**) Map of the identified phosphorylation sites on Pil1. A predicted central coiled-coil region is indicated in red.

shows that even at the permissive temperature *pkh1^ts pkh2*Δ cells display increased fluorescence intensity at the cell membrane and an abnormal eisosome organization. As best seen in the optical top sections, Pil1-GFP is found in elongated filamentous structures that coalesce into a reticular pattern, rather than in discrete, uniform punctate
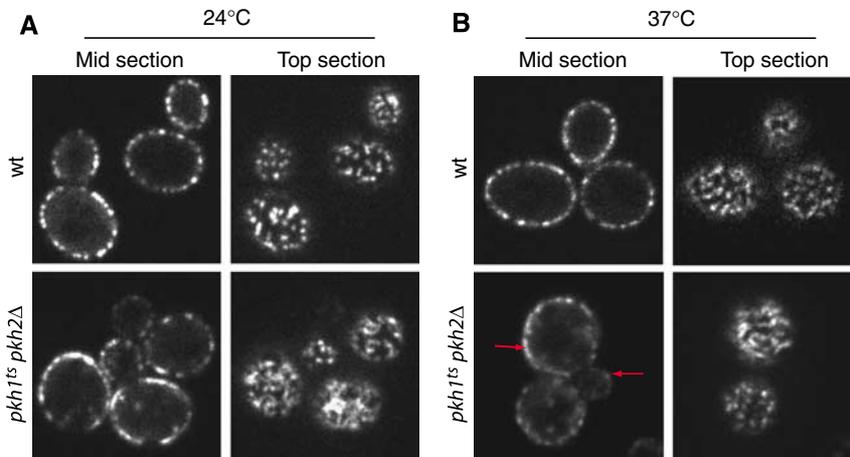
Figure 4 Inactivation of Pkh-kinases leads to increased Pil1 assembly. (**A**) Pil1-GFP was expressed either in control wt cells or cells with a deletion in *PKH2* and a temperature-sensitive allele of *pkh1* (*pkh1^ts pkh2Δ*). Cells were grown at 24°C and imaged by confocal microscopy. Representative optical midsections (left panels) or top sections (right panels) are shown. (**B**) Cells described in panel A were shifted to 37°C for 1.5 h and analyzed as described in panel A.

characteristic of eisosomes in wild-type cells. This effect was further enhanced by shifting the cells to the restrictive temperature for 1 h, and was more prominent in larger mother cells (Figure 4B, lower panels; compare signal at red arrows). By contrast, eisosomes remained well defined and of uniform size in wild-type cells shifted to the elevated temperature (compare Figure 4A and B, top panels).

Second, we overexpressed Pkh1 and Pkh2 from the GAL promoter and monitored the localization of Pil1-GFP. The Pil1-GFP signal at the cell periphery rapidly decreased upon expression of either kinase. At a 1.5-h time point after induction only a few bright spots remained (Figure 5A and B, middle panels). This effect was specific to the enzymatic activity of Pkh-kinases, since overexpression of a kinase-dead mutant form of Pkh1, Pkh1(K154R) had no effect on eisosome assembly or organization (Figure 5B). The decrease of fluorescence signal from eisosomes at the cell periphery is most evident by comparing line plots through the diameter of the cell (Figure 5A and C, graphs). Since this reaction occurred relatively rapid and happened in all cells expressing the kinase, we conclude that this decrease of Pil1-GFP signal in the cell periphery must result from disassembly of existing eisosomes. Some cells continued to show normal eisosome organization, presumably due to loss of the overexpression plasmid.

By contrast to eisosomes in wild-type cells, which are immobile, we frequently observed smaller Pil1-GFP foci that are detached from the plasma membrane in cells overexpressing either one of the Pkh-kinases. These structures were mobile within the cytoplasm, as apparent by time-lapse confocal microscopy (Figure 5D). We never observed mobile cytoplasmic Pil1-GFP foci in wild-type cells.

Pil1 phosphorylation can modulate its assembly into eisosomes

Taken together, the results presented so far show that (i) Pkh-kinases can localize to eisosomes, (ii) Pil1 phosphorylation is at least partially dependent on Pkh-kinases, and (iii) modulating Pkh-kinase activity leads to defects in eisosome assembly. To test whether the effect of Pkh-kinase activity on eisosome assembly and organization is directly due to

phosphorylation of Pil1 rather than to an indirect effect, we next mutated the mapped phosphorylation sites to either alanine, which cannot be phosphorylated, or to negatively charged aspartate, which mimics phosphorylated serine or threonine. We introduced the mutated variants in the context of the *PIL1-GFP* fusion gene into yeast strains as the sole copy of *PIL1*. When analyzed by confocal fluorescence microscopy, none of the single mutant Pil1 variants showed a significant effect on eisosome assembly or organization (data not shown), including serine 273, the single residue responsible for the mobility shift on SDS–PAGE gels. Likewise, deletion of the whole C-terminus up to residue 266 had no effect on eisosome assembly or organization (TC Walther, PS Aguilar, and P Walter, unpublished data). We therefore mutated combinations of residues. Figure 6 shows the results of two quadruple mutants in which serines 45, 59, and 230, and threonine 233 were changed to alanine (Figure 6A) or aspartate (Figure 6B). In *pil1(S45A,S59A,S230A,T233A)*—or *pil(4A)* for short—cells, we found a strong increase in the fluorescence of eisosomes compared with wild-type controls and a structural defect qualitatively similar to but not quite as strong as the phenotype of the temperature-sensitive Pkh-kinase mutant cells (Figure 6A, lower panel). Conversely, in *pil1(S45D,S59D,S230D,T233D)*—or *pil(4D)* for short—cells, we observed mainly cytoplasmic Pil1-GFP with only a few bright spots remaining (Figure 6B, lower panel). This phenotype is reminiscent of that observed in cells overexpressing either of the Pkh-kinases (compare to Figure 5) and indicates that phosphorylation of these four residues is sufficient to exert this effect. The effect of this mutation on eisosome organization and assembly is not further aggravated by mutation of the Pkh-kinases (Figure 6C). To test whether these residues are also required for the Pkh-kinase effect on eisosomes, we expressed *pil1(4A)* in cells overexpressing Pkh1 or Pkh2. We found that Pil1(4A) is much more resistant to the disassembly and clustering observed for wild-type Pil1 under these conditions (Figure 6D).

Together, these data suggest that phosphorylation of Pil1 by Pkh-kinases shifts the assembly equilibrium of Pil1 between a free, phosphorylated form and an eisosome-assembled, dephosphorylated form.
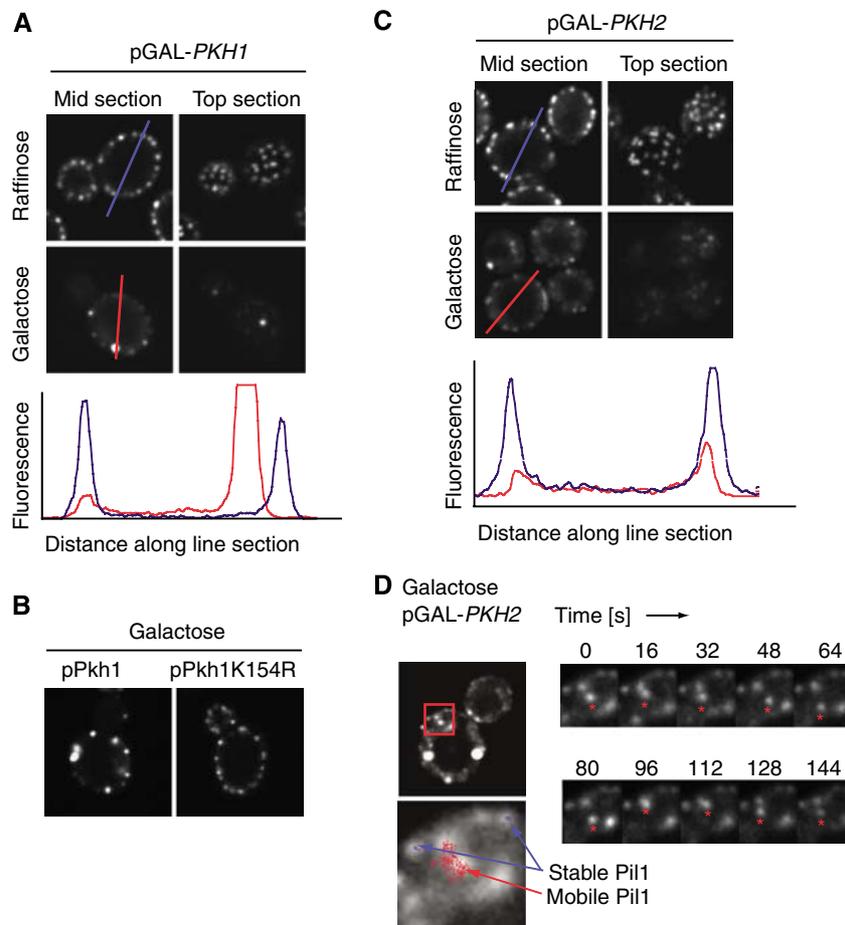
Figure 5 Overexpression of *PKH*-kinases leads to disassembly of eisosomes. (**A**) Pkh1 overexpression leads to eisosome disassembly. wt cells expressing Pil1-GFP and harboring *PKH1* under the control of the GAL promoter were grown in non-inducing raffinose-containing medium and shifted 1.5 h to galactose. Cells from both conditions were analyzed by confocal microscopy and representative midsections (left panels) or top sections (right panels) are shown. The red and blue lines indicate the axis that was used to derive the intensity profile shown in the lower panel for the wt and Pkh1-expressing cells, respectively. (**B**) The effect of Pkh1 overexpression on eisosomes is dependent on the catalytic activity of the protein. Pkh1 was mutated in the catalytic lysine 154 and overexpressed as in panel A. Representative confocal midsections are shown. (**C**) Pkh2 overexpression leads to eisosome disassembly. An analogous experiment was performed with cells expressing Pkh2. (**D**) Pkh overexpression leads to mobilization of eisosomes. The experiment was performed as described in panel B and short time-lapse movies were recorded. The left panel shows an overview of the imaged cell and on the right a subset of the recorded frames is shown. The asterisks indicate a mobile cluster of Pil1. To follow movement of the Pil1 clusters, we tracked individual clusters over time (left bottom panel). A track of a mobile Pil1 cluster representing a 40 s movie is shown in red, and eisosomes that remained stable are shown in two blue tracks.

Discussion

Eisosomes help sequester a subgroup of plasma membrane proteins into discrete membrane domains that colocalize with sites of endocytosis (Walther *et al*, 2006; Grossmann *et al*, 2007). Here we show that the major eisosome component Pil1 *in vivo* is a target of the LCB-signaling pathway mediated by the Pkh-kinases. We found that Pkh-kinases can localize with eisosomes, consistent with other observations that suggest physically association based on high-throughput interaction screens and pull-down studies (Ho *et al*, 2002; Krogan *et al*, 2006). Moreover, it was shown previously that Pkh-kinases can phosphorylate Pil1 *in vitro* (Zhang *et al*, 2004). We find that phosphorylation is a critical regulator of Pil1 assembly into eisosomes and affects their organization. Eisosomes disassemble if Pil1 is hyperphosphorylated (i) upon overexpression of Pkh-kinases, (ii) upon reducing LCB concentrations by inhibiting serine-palmitoyl transferase in *lcb1*-mutant cells or by poisoning the enzyme with myriocin, and (iii) upon mimicking hyperphosphorylation in *pil1(4D)*-mutant cells. Conversely, more Pil1 assembles into eisosomes if Pil1 is hypophosphorylated (i) upon reducing Pkh-kinase activity in *pkh1 pkh2*-mutant cells, (ii) upon modulation of Pkh-kinases activity by addition of LCBs, and (iii) upon mimicking hypophosphorylation in *pil1(4A)*-mutant cells.

The resulting enlarged eisosomes show altered organization. Other data suggest that Pkh signaling and sphingolipids are important for endocytosis (Zanolari *et al*, 2000). Taken together with our previous results that link eisosomes to endocytosis (Walther *et al*, 2006), these observations suggest that Pkh-kinase signaling relayed to Pil1 may help regulate endocytic events.

At a first glance, the view of eisosomes as stable, uniformly sized entities is at odds with the assembly-disassembly of Pil1 upon phosphorylation reported here, as we show that the assembly and organizational properties of eisosomes are subject to modulation by phosphorylation. There are multiple
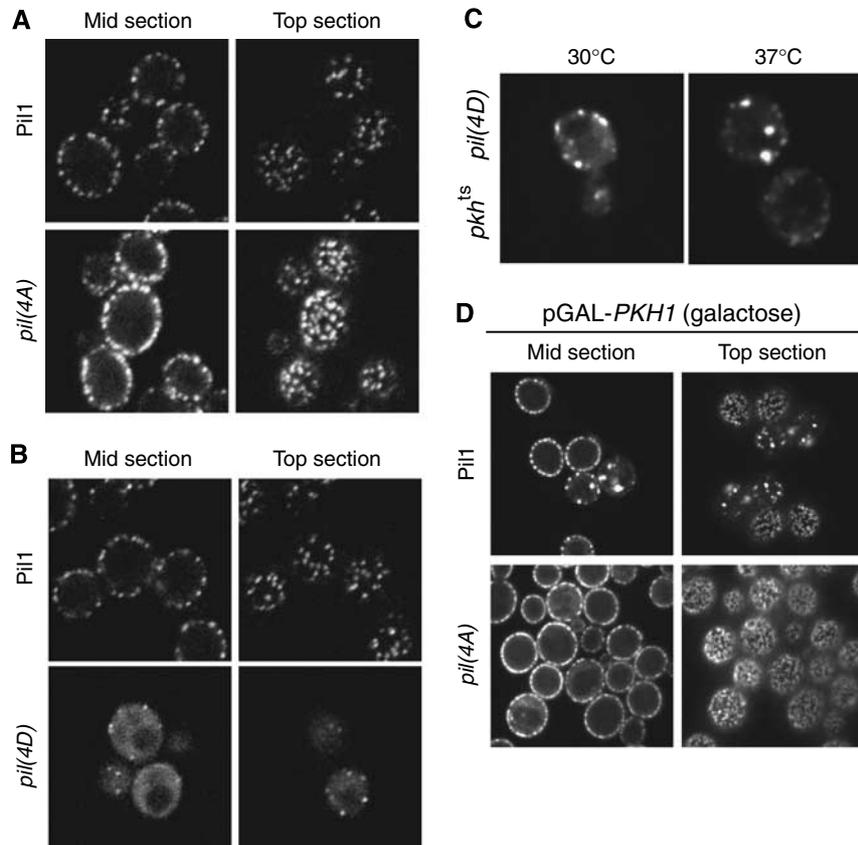
Figure 6 Phosphorylation of Pil1 regulates eisosome assembly. (**A**) Non-phosphorylatable Pil1 increases eisosome size. Pil1-GFP with serines 45, 59, 230, and threonine 233 mutated to alanine (*pil1(4A)*) was expressed as the only Pil1 and analyzed by confocal microscopy. Representative middle (left panels) and top sections (right panels) are shown. (**B**) Phospho-mimicking Pil1 mutants fail to assemble into eisosomes. Pil1 with the same residues indicated in panel A mutated to aspartate were analyzed as in panel A. (**C**) The *pil1(4D)* phenotype is dominant over the inactivation of Pkh-kinases. *pil1(4D)* was expressed in cells bearing a deletion in *PKH2* and a temperature-sensitive allele of *pkh1* (*pkh1^{ts}pkh2Δ*) grown at either 30°C (left panel) or 37°C (right panel). Representative confocal midsections are shown. (**D**) *pil1(4A)* is resistant to the effect of Pkh1 overexpression. wt Pil1-GFP (upper panels) and mutant Pil1(4A)-GFP (lower panels) were expressed in a cell with elevated Pkh1 levels expressed for 1.5 h form the *GAL* promoter in galactose-containing medium (see Figure 5A).

possible resolutions to this paradox. First, newly made Pil1 may be phosphorylated and its dephosphorylation may accompany its assembly into eisosomes as part of their biosynthesis pathway. Our result that turning on Pkh-kinases dissembles pre-existing eisosomes argues against the notion that this is the exclusive role of the modification, although it does not rule it out conclusively. Second, an assembly/ disassembly cycle of eisosomes may play role in their functional properties, yet be locally restricted so that under normal growth conditions only a few eisosomes in the cell are affected at any one time. This view would be consistent with our observation that endocytic events are restricted to a few active eisosomes at a time. Fluorescent photobleaching and recovery experiments may have missed the potentially dynamic behavior of only a few eisosomes. Third, the studies presented here may represent extreme end points of phosphorylation and dephosphorylation that do not truly reflect physiological conditions. The alternate actions of Pkh-kinases and cognate phosphatases under physiological conditions may only affect a subset of the total spectrum of potential phosphorylation sites on any particular Pil1 molecule, which could lead to local structural rearrangements within an eisosome without disrupting the complex as we observed upon extensive hyperphosphorylation. These

possibilities are not mutually exclusive, and the currently available information does not allow us to distinguish between them.

A second paradox results from comparison of our results with previous data that showed an induction of Pkh activity by LCBs (Zanolari *et al*, 2000; Friant *et al*, 2001; Liu *et al*, 2005). A possible resolution comes from the observation that LCBs induce the phosphorylation of certain targets (such as Lsp1), whereas the activity toward Pil1 is decreased (Zhang *et al*, 2004). These data are in good agreement with our results suggesting that inhibition of sphingolipid synthesis results in increased activity of Pkh-kinases toward Pil1 and hyperphosphorylation of the protein.

Third, it is currently unknown why we observe one or a few large clusters of Pil1 under conditions were most eisosomes disassemble. One possibility is that the normal distribution of eisosomes breaks down under these conditions, leading to a clustering of molecules that would normally be part of eisosomes, such as Lsp1. This would then provide an abnormally high concentration of binding sites for Pil1 at these sites, which would in turn recruit some of the solubilized Pil1.

Our data suggest that the relative concentrations of LCBs and/or sphingolipids and ceramides are sensed via

Pkh-kinases and transduced to Pil1 to regulate aspects of eisosome assembly and/or function. It is currently unknown how this sensing occurs at a molecular level. Since both inhibition of LCB and cermides synthesis have a similar effect on eisosomes, one possibility is that Pkh-kinases sense a property of the plasma membrane locally, perhaps in the membrane domain underlying eisosomes where those lipids are thought to be concentrated. Alternatively, and not mutually exclusive, LCBs or downstream metabolites may act as second messengers that bind the kinases and mediate the response of the Pkh-kinases. This is most likely part of a concerted cellular response to changing conditions that regulates endocytosis and adjusts the composition of the plasma membrane according to need.

Sphingolipids have been implicated in the regulation of many cellular processes such as cell growth, apoptosis, endocytosis, cell adhesion, and differentiation (Dickson, 1998; Futerman and Hannun, 2004; Dickson et al, 2006). In yeast, LCBs are massively increased during heat stress and the endocytic uptake of at least some highly abundant proteins, such as the uracil permease Fur4, is induced (Dickson et al, 1997; Jenkins et al, 1997; Bultynck et al, 2006). Moreover, Pkh-kinase-mediated regulation of endocytosis differentially affects the induced uptake of α-factor receptor Ste2 but not its constitutive recycling (Grosshans et al, 2006). Pkh-kinase regulation of endocytosis could thus potentially be used to selectively adjust the composition of the plasma membrane, suggesting that sphingolipid signaling might have a broad function in organizing the plasma membrane. Despite our astounding lack of knowledge regarding the regulation and physiological importance of this pathway, the potential of sphingolipid signaling as a drug target has already been demonstrated for myriocin, a compound that inhibits the generation of sphingolipids; myriocin was first characterized as an immune suppressive agent inducing apoptosis of cytotoxic T cells (Fujita et al, 1994). Such connections promise that expanding our most basic understanding of the mechanisms that organize the yeast plasma membrane may have profound implications for the physiology and pathology of mammalian cells.

Materials and methods

Yeast strains and plasmids
All yeast stains were generated in the W303 background. Lsp1-Cherry was introduced by homologous recombination using a PCR-based modification (Longtine et al, 1998) to generate the strain TWY566. The strain expressing Pil1-GFP was described in Walther et al (2006). PIL1-GFP was cloned into pRS306 and mutated using site-directed mutagenesis to generate plasmid pPIL4A (harboring substitutions S45A, S59A, S230A, T233A) or pPIL4D (harboring S45D, S59D, S230D, and T233D). Plasmids expressing seven mutations were generated in an analogous manner. Strains expressing either tagged or untagged versions of Pkh1 and Pkh2 were generated by transforming the following plasmids, which were generous gifts from Jeremy Thorner: for Pkh1 we transformed pAM73; for Pkh2, pAM79 (Casamayor et al, 1999) into a Pil1-GFP-expressing strain; for expression of 3GFP-Pkh1 or 3GFP-Pkh2, we transformed TWY566 with pFR37 or pER3, respectively (Roelants et al, 2002). pkh1^{ts}pkh2D strains were a generous gift from Howard Riezman (Friant et al, 2001).

Antibody generation
Antibodies against Pil1 were raised in rabbits against the full-length recombinant Pil1 protein expressed in Escherichia coli as a GST-fusion protein. The fusion protein was cleaved from the glutathione affinity column and further purified by ion-exchange chromatography on a MonoQ column. This protein was injected into rabbits in several boost cycles. Serum from rabbits was diluted 1:1000 for western blots.

Mapping of phosphorylation sites
For the analysis of Pil1 phosphorylation of Pil1, we froze cell from a 100 ml culture at OD = 0.7 in 500 μl buffer (150 mM KoAc, 20 mM HEPES, pH 7.8, 1 mM MgAc) in liquid nitrogen. We extracted total protein by bead milling and subsequently clarified the extract by two consecutive spins of 4 min, 1000 g. Extracts were incubated with λ-phosphatase according to the manufacturer's instructions (NEB) in the presence or absence of a cocktail of phosphatase inhibitors (Sigma). After 30 min the reaction was stopped by addition of sample buffer. A 20 μg weight of total protein was run on a 10% SDS–PAGE and analyzed by western blot.

Affinity purification of Pil1 from 1 l of yeast culture expressing Pil1-myc was accomplished as previously described (Walther et al, 2006). Pil1-myc and eluted from beads with sample buffer (0.24 M Tris, 8% SDS, 1 mM β-mercaptoethanol, 40% glycerol, and 0.4% bromophenol blue) and loaded onto 4–20% SDS–PAGE Criterion Ready Gels (Bio-Rad). In-gel digestions on Pil1 bands were carried out utilizing a procedure described at http://msf.ucsf.edu/in-gel.html. Typically, 100 ng of trypsin (porcine, side chain-protected; Promega, Madison, WI) was used for each gel band, and digestions were carried out at 37°C for 4 h. Peptides were extracted from gel pieces with 50 μl of 50% acetonitrile, 2% acetic acid three times, and the extraction solution was dried down to ~10 μl. An aliquot of the digestion mixture was injected into an Ultimate capillary LC system via an FAMOS Autosampler (LC Packings, Sunnyvale, CA), and separated by a 75 μm × 15 cm reverse-phase capillary column at a flow rate of ~330 nl/min. The HPLC eluent was fed directly into the micro-ion electrospray source of a QSTAR Pulsar QqTOF mass spectrometer (Applied Biosystem/MDS Sciex, Foster City, CA). Typical performance characteristics were >8000 resolution with 30 p.p.m. mass measurement accuracy in both MS and CID mode. LC-MS data were acquired in an information-dependent acquisition mode, cycling between 1-s MS acquisition followed by 3-s low-energy CID data acquisition. The centroided peak lists of the CID spectra were searched against the National Center for Biotechnology Information (NCBI) protein database using Batch-Tag, a program in the in-house version of the University of California San Francisco ProteinProspector package, considering phosphorylation on serine, threonine, and tyrosine as variable modifications. The CID spectra with putative phosphorylations were further inspected manually.

Microscopy
For fluorescence microscopy, yeast cells were grown to an OD = 0.6 in either YPD or, when selecting for Pkh expression plasmids, in synthetic medium lacking leucine. Cells were mounted onto coverslips previously coated with concanavalin A and directly imaged either with a Zeiss LSM 510 confocal microscope or an ANDOR/TiLL iMIC spinning-disk confocal microscope. Images were processed using ImageJ software (www.rsb.info.nih.gov/ij/).

Supplementary data
Supplementary data are available at The EMBO Journal Online (http://www.embojournal.org).

Acknowledgements

References

Bultynck G, Heath VL, Majeed AP, Galan JM, Haguenauer-Tsapis R, Cyert MS (2006) Slm1 and slm2 are novel substrates of the calcineurin phosphatase required for heat stress-induced endocytosis of the yeast uracil permease. *Mol Cell Biol* **26:** 4729–4745

Casamayor A, Torrance PD, Kobayashi T, Thorner J, Alessi DR (1999) Functional counterparts of mammalian protein kinases PDK1 and SGK in budding yeast. *Curr Biol* **9:** 186–197

Daquinag A, Fadri M, Jung SY, Qin J, Kunz J (2007) The yeast PH domain proteins Slm1 and Slm2 are targets of sphingolipid signaling during the response to heat stress. *Mol Cell Biol* **27:** 633–650

deHart AK, Schnell JD, Allen DA, Hicke L (2002) The conserved Pkh-Ypk kinase cascade is required for endocytosis in yeast. *J Cell Biol* **156:** 241–248

Dickson RC (1998) Sphingolipid functions in *Saccharomyces cerevisiae*: comparison to mammals. *Ann Rev Biochem* **67:** 27–48

Dickson RC, Nagiec EE, Skrzypek M, Tillman P, Wells GB, Lester RL (1997) Sphingolipids are potential heat stress signals in *Saccharomyces*. *J Biol Chem* **272:** 30196–30200

Dickson RC, Sumanasekera C, Lester RL (2006) Functions and metabolism of sphingolipids in *Saccharomyces cerevisiae*. *Prog Lipid Res* **45:** 447–465

Dong LQ, Landa LR, Wick MJ, Zhu L, Mukai H, Ono Y, Liu F (2000) Phosphorylation of protein kinase N by phosphoinositide-dependent protein kinase-1 mediates insulin signals to the actin cytoskeleton. *Proc Natl Acad Sci USA* **97:** 5089–5094

Engqvist-Goldstein AE, Drubin DG (2003) Actin assembly and endocytosis: from yeast to mammals. *Annu Rev Cell Dev Biol* **19:** 287–332

Friant S, Lombardi R, Schmelzle T, Hall MN, Riezman H (2001) Sphingoid base signaling via Pkh kinases is required for endocytosis in yeast. *EMBO J* **20:** 6783–6792

Fujita T, Inoue K, Yamamoto S, Ikumoto T, Sasaki S, Toyama R, Chiba K, Hoshino Y, Okumoto T (1994) Fungal metabolites Part 11. A potent immunosuppressive activity found in *Isaria sinclairii* metabolite. *J Antibiot* **47:** 208–215

Futerman AH, Hannun YA (2004) The complex life of simple sphingolipids. *EMBO Rep* **5:** 777–782

Grosshans BL, Grotsch H, Mukhopadhyay D, Fernandez IM, Pfannstiel J, Idrissi FZ, Lechner J, Riezman H, Geli MI (2006) TEDS site phosphorylation of the yeast myosins I is required for ligand-induced but not for constitutive endocytosis of the G protein-coupled receptor Ste2p. *J Biol Chem* **281:** 11104–11114

Grossmann G, Opekarova M, Malinsky J, Weig-Meckl I, Tanner W (2007) Membrane potential governs lateral segregation of plasma membrane proteins and lipids in yeast. *EMBO J* **26:** 1–8

Grossmann G, Opekarova M, Novakova L, Stolz J, Tanner W (2006) Lipid raft-based membrane compartmentation of a plant transport protein expressed in *Saccharomyces cerevisiae*. *Eukaryot Cell* **5:** 945–953

Ho Y, Gruhler A, Heilbut A, Bader GD, Moore L, Adams SL, Millar A, Taylor P, Bennett K, Boutilier K, Yang L, Wolting C, Donaldson I, Schandorff S, Shewnarane J, Vo M, Taggart J, Goudreault M, Muskat B, Alfarano C *et al* (2002) Systematic identification of protein complexes in *Saccharomyces cerevisiae* by mass spectrometry. *Nature* **415:** 180–183

Inagaki M, Schmelzle T, Yamaguchi K, Irie K, Hall MN, Matsumoto K (1999) PDK1 homologs activate the Pkc1–mitogen-activated protein kinase pathway in yeast. *Mol Cell Biol* **19:** 8344–8352

Jenkins GM, Richards A, Wahl T, Mao C, Obeid L, Hannun Y (1997) Involvement of yeast sphingolipids in the heat stress response of *Saccharomyces cerevisiae*. *J Biol Chem* **272:** 32566–32572

Krogan NJ, Cagney G, Yu H, Zhong G, Guo X, Ignatchenko A, Li J, Pu S, Datta N, Tikuisis AP, Punna T, Peregrin-Alvarez JM, Shales M, Zhang X, Davey M, Robinson MD, Paccanaro A, Bray JE, Sheung A, Beattie B *et al* (2006) Global landscape of protein complexes in the yeast *Saccharomyces cerevisiae*. *Nature* **440:** 637–643

Lauwers E, Andre B (2006) Association of yeast transporters with detergent-resistant membranes correlates with their cell-surface location. *Traffic (Copenhagen, Denmark)* **7:** 1045–1059

Liu K, Zhang X, Lester RL, Dickson RC (2005) The sphingoid long chain base phytosphingosine activates AGC-type protein kinases in *Saccharomyces cerevisiae* including Ypk1, Ypk2, and Sch9. *J Biol Chem* **280:** 22679–22687

Longtine MS, McKenzie III A, Demarini DJ, Shah NG, Wach A, Brachat A, Philippsen P, Pringle JR (1998) Additional modules for versatile and economical PCR-based gene deletion and modification in *Saccharomyces cerevisiae*. *Yeast (Chichester, England)* **14:** 953–961

Malinska K, Malinsky J, Opekarova M, Tanner W (2003) Visualization of protein compartmentation within the plasma membrane of living yeast cells. *Mol Biol Cell* **14:** 4427–4436

Malinska K, Malinsky J, Opekarova M, Tanner W (2004) Distribution of Can1p into stable domains reflects lateral protein segregation within the plasma membrane of living *S. cerevisiae* cells. *J Cell Sci* **117:** 6031–6041

Opekarova M, Malinska K, Novakova L, Tanner W (2005) Differential effect of phosphatidylethanolamine depletion on raft proteins: further evidence for diversity of rafts in *Saccharomyces cerevisiae*. *Biochim Biophys Acta* **1711:** 87–95

Roelants FM, Torrance PD, Bezman N, Thorner J (2002) Pkh1 and pkh2 differentially phosphorylate and activate ypk1 and ykr2 and define protein kinase modules required for maintenance of cell wall integrity. *Mol Biol Cell* **13:** 3005–3028

Sun Y, Taniguchi R, Tanoue D, Yamaji T, Takematsu H, Mori K, Fujita T, Kawasaki T, Kozutsumi Y (2000) Sli2 (Ypk1), a homologue of mammalian protein kinase SGK, is a downstream kinase in the sphingolipid-mediated signaling pathway of yeast. *Mol Cell Biol* **20:** 4411–4419

Walther TC, Brickner JH, Aguilar PS, Bernales S, Pantoja C, Walter P (2006) Eisosomes mark static sites of endocytosis. *Nature* **439:** 998–1003

Zanolari B, Friant S, Funato K, Sutterlin C, Stevenson BJ, Riezman H (2000) Sphingoid base synthesis requirement for endocytosis in *Saccharomyces cerevisiae*. *EMBO J* **19:** 2824–2833

Zhang X, Lester RL, Dickson RC (2004) Pil1p and Lsp1p negatively regulate the 3-phosphoinositide-dependent protein kinase-like kinase Pkh1p and downstream signaling pathways Pkc1p and Ypk1p. *J Biol Chem* **279:** 22030–22038

LETTERS

Comprehensive mass-spectrometry-based proteome quantification of haploid versus diploid yeast

Lyris M. F. de Godoy[1]*, Jesper V. Olsen[1]*, Jürgen Cox[1]*, Michael L. Nielsen[1]*, Nina C. Hubner[1], Florian Fröhlich[2], Tobias C. Walther[2] & Matthias Mann[1]

Mass spectrometry is a powerful technology for the analysis of large numbers of endogenous proteins[1,2]. However, the analytical challenges associated with comprehensive identification and relative quantification of cellular proteomes have so far appeared to be insurmountable[3]. Here, using advances in computational proteomics, instrument performance and sample preparation strategies, we compare protein levels of essentially all endogenous proteins in haploid yeast cells to their diploid counterparts. Our analysis spans more than four orders of magnitude in protein abundance with no discrimination against membrane or low level regulatory proteins. Stable-isotope labelling by amino acids in cell culture (SILAC) quantification[4,5] was very accurate across the proteome, as demonstrated by one-to-one ratios of most yeast proteins. Key members of the pheromone pathway were specific to haploid yeast but others were unaltered, suggesting an efficient control mechanism of the mating response. Several retrotransposon-associated proteins were specific to haploid yeast. Gene ontology analysis pinpointed a significant change for cell wall components in agreement with geometrical considerations: diploid cells have twice the volume but not twice the surface area of haploid cells. Transcriptome levels agreed poorly with proteome changes overall. However, after filtering out low confidence microarray measurements, messenger RNA changes and SILAC ratios correlated very well for pheromone pathway components. Systems-wide, precise quantification directly at the protein level opens up new perspectives in post-genomics and systems biology.

Yeast launched the genome era[6] and continues to be an informative model system for genomic and post-genomics technologies. It has also been a fruitful testing ground for mass spectrometry (MS)-based proteomics[7–10]. Repositories of yeast proteomics experiments contain about 4,000 proteins, albeit with varying confidence of identification[11]. Previously, we established that half of the yeast proteome could be detected with very high stringency by MS in a single experiment[12]. The phosphoproteome of pheromone signalling has already been investigated by a SILAC experiment[13]. Until now, no strategies have been described to comprehensively identify, much less to comprehensively quantify, two states of the yeast proteome against each other in a single experiment.

To develop methods for proteome-wide quantification, we metabolically labelled haploid and diploid yeast with arginine and lysine SILAC. We investigated three strategies to achieve deep coverage of the yeast proteome: extensive fractionation of proteins; fractionation of digested peptides; and accumulating and sequencing distinct mass ranges of peptides (Fig. 1, Methods). The second strategy, combining in-solution digest with peptide separation by isoelectric focusing, yielded the most proteins (3,987) and is by far the simplest.

Together, we identified 4,399 proteins with 99% certainty (Supplementary Table 4). Unambiguous identification only requires a few peptides per protein; however, on average we covered 32% of each protein sequence.

Previously, expressed yeast genes were detected by a fused tandem affinity tag (TAP)[14] or green fluorescent protein (GFP) tag[15] in genome-wide experiments (Fig. 2a and Table 1) and our data overlaps 89% with each of these tagging approaches. In addition, MS identified 510 proteins exclusively, including proteins in which the tag interferes with function, such as tail-anchored membrane proteins and proteins requiring carboxy-terminal modifications. As judged by MS, several hundred proteins previously reported at less than 50 copies per cell were part of different abundance classes over the whole dynamic range (Supplementary Fig. 5). Our data set is not biased against low-abundance proteins (Fig. 2b) or membrane proteins (30.9% of all proteins detected and 29.4% of the genome). Only 6% of yeast open reading frames (ORFs) were detected by both tagging methods but not by MS (Fig. 2a). This is less than the discrepancy between the tagging methods and includes 12 proteins that are inaccessible to MS due to a lack of appropriate tryptic or LysC cleavage sites, 33 proteins with overlapping genes (which we only counted as single identifications), 11 that have been removed from the database during the last three years, 8 dubious genes and 78 proteins for which no western blot quantification had been possible. Thus, of the accessible proteome, at most a few per cent of proteins are not detected. High-resolution data from the orbitrap instrument combined with efficient computational strategies led to very high peptide mass accuracy (average absolute mass deviation of 590 p.p.b.) and to very high identification rates for mass spectrometric peptide fragmentation (>53% on SILAC peptide pairs, Fig. 1d and Methods), contributing to the identification of essentially the entire yeast proteome expressed in log-phase cells.

Next, we determined the fold change of SILAC peptide pairs for relative proteome quantification between haploid and diploid yeast cells. In arginine and lysine double-labelled populations, we noticed that the proteomes were substantially different due to the presence of different sets of auxotrophic markers in the haploid and diploid strains (Supplementary Fig. 6). We therefore based our quantitative analysis on the lysine-labelled haploid S288C yeast strain and compared it to an isogenic diploid strain (Fig. 1b, c and Methods). A total of 1,788,451 SILAC peptide pairs were identified and quantified (median, 32 pairs per protein). Figure 3a and Supplementary Tables 6 and 7 show the ratios of all 4,033 quantified proteins and peptides from the lysine-labelling experiments. We achieved very high quantification accuracy, with 97.3% of the proteome changing less than 50% in abundance between haploid and diploid cells. Quantification after fractionation of digested peptides (Fig. 1b) showed excellent reproducibility ($R = 0.84$ on average; Supplementary Fig. 7). One-hundred-and-ninety-six proteins changed significantly ($P < 0.001$), and we confirmed the regulation of 29 of

---

[1]Proteomics and Signal Transduction, and [2]Organelle Architecture and Dynamics, Max-Planck-Institute for Biochemistry, Am Klopferspitz 18, D-82152 Martinsried, Germany.
*These authors contributed equally to this work.
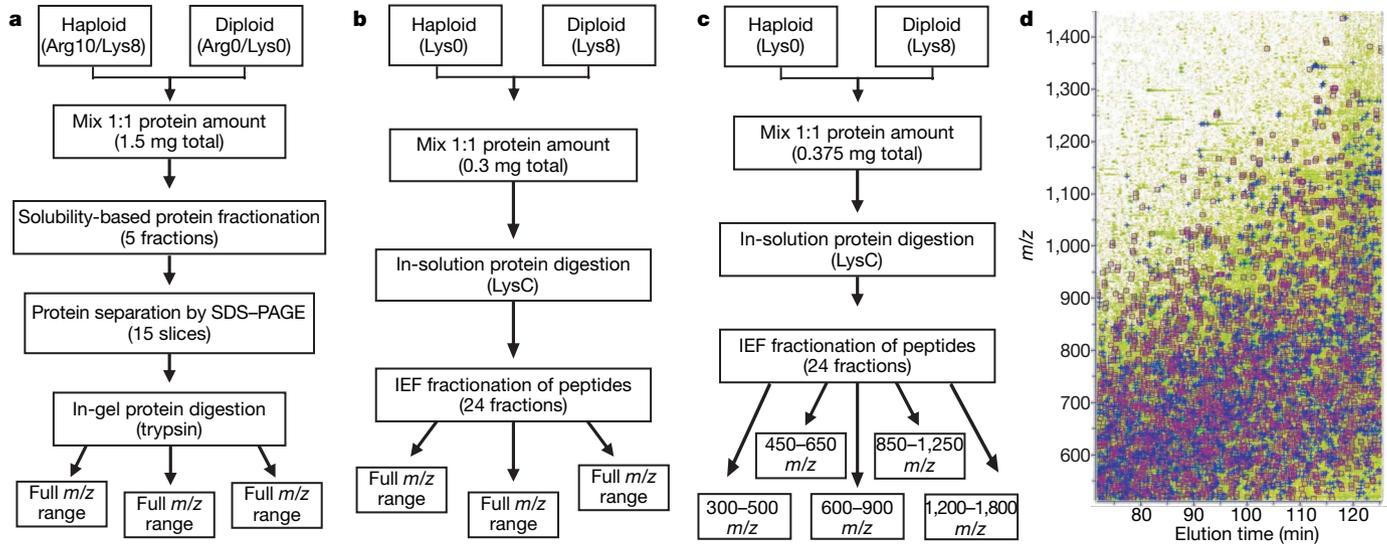
Figure 1 | Three strategies for in-depth quantification of the yeast proteome by SILAC labelling and high-resolution mass spectrometry.
a, Arginine and lysine SILAC labelling of haploid and diploid yeast. Arg10 is [$^{13}C_6$,$^{15}N_4$]L-arginine, Lys8 is [$^{13}C_6$/$^{15}N_2$]L-lysine, and Arg0 and Lys0 are the normal, non-substituted amino acids. Extensive fractionation followed by tryptic digestion and one-dimensional gel electrophoresis as well as online LC–MS/MS on a hybrid linear ion trap–orbitrap instrument yielded, through triplicate measurements, 3,639 identified proteins at high stringency using the MaxQuant algorithms (J.C. and M.M., submitted; Supplementary Table 1). **b**, Lysine SILAC labelling of haploid and diploid yeast. Triplicate measurements of in-solution digestion with endoprotease

LysC followed by isoelectric focusing into 24 fractions and online LC–MS/MS resulted in a proteome of 3,987 proteins (Supplementary Table 2). **c**, Same as **b** except that each isoelectric fraction is analysed five times with ion accumulation of a narrow *m/z* range for higher dynamic range. The signal-to-noise ratio and dynamic range improved by about a factor of five (Supplementary Fig. 1) and 3,779 proteins were identified (Supplementary Table 3). **d**, Typical contour plot of a single LC–MS/MS run. Peptide pairs eluting from the column (green) were automatically fragmented (blue crosses) and more than 60% of sequencing events on SILAC pairs resulted in successful identification (purple boxes).
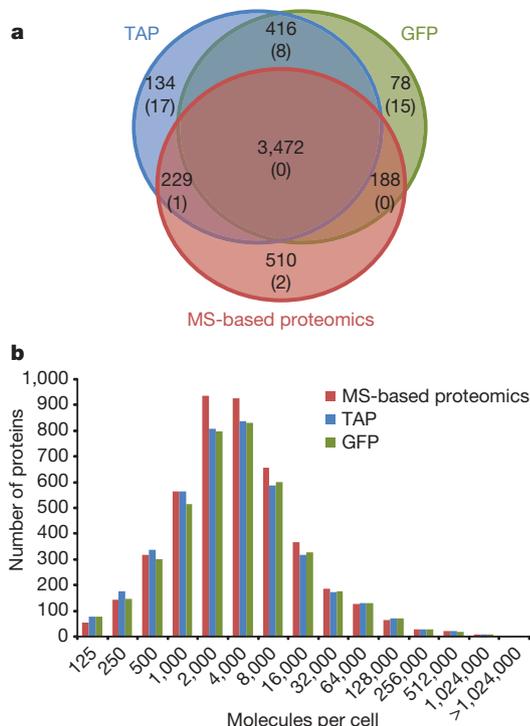
Figure 2 | Proteome coverage. a, Comparison of coverage of MS-based proteomics with GFP- and TAP-tagging methods[14,15]. Numbers are the identified proteins by each method and, in parentheses, the number of dubious open reading frames (ORFs). **b**, Identified proteins per copy number bin for MS-based proteomics and the two tagging approaches. Copy numbers were estimated by correlation between summed peptide intensity per protein and the quantitative western blotting data[14] (Methods).

the top-regulated ones by western blot against either the fused TAP or GFP tag from the systematic collection[14] (Supplementary Fig. 8). All ratios were in the same direction as that observed by MS-based proteomics. Kyoto Encyclopedia of Genes and Genomes (KEGG) pathway and Gene Ontology analysis (Supplementary Table 8) highlighted lysine biosynthesis as being upregulated in diploid cells ($P = 5 \times 10^{-6}$). This is due to heterozygosity for *LYS2*/*lys2* and illustrates the ability of proteome-wide quantification to pinpoint altered metabolic pathways (Supplementary Fig. 9a, c).

Pheromone signalling is required for mating of haploid cells and is absent from diploid cells[16]. The top ten haploid-specific proteins as determined by SILAC are components or transcriptional targets of pheromone signalling (Supplementary Table 9). Surprisingly, not all of its members are regulated equally (Fig. 3b). Key components of the signal transduction pathway and output factors were absent from diploid cells: the pheromone receptor (Ste2), the signal transducing G protein (consisting of Ste4, Ste18 and Gpa1), the mitogen-activated protein kinase (MAPK) scaffold protein Ste5, the MAPK Fus3 and the output transcription factor Ste12. In contrast, the

Table 1 | Yeast ORFs identified by SILAC-based quantitative proteomics

	Number of ORFs	TAP	GFP	nanoLC–MS
Total yeast ORFs	6,608	4,251	4,154	4,399
Characterized yeast ORFs	4,666	3,629	3,581	3,824
Uncharacterized yeast ORFs	1,128	581	539	572
Dubious yeast ORFs	814	26 (3%)	23 (3%)	3 (<1%)
Not present in ORF database		15	11	0

Comparative sequencing shows that 814 of the 6,608 yeast ORFs are never expressed (dubious ORFs, http://www.yeastgenome.org). Of these only six were identified in this experiment and three were validated by SILAC-assisted *de novo* sequencing of several peptides (Supplementary Table 5 and Supplementary Figs 2–4). Two of the three validated ones were reclassified as genuine yeast genes during writing of this manuscript (YGL041W-A and YPR170W-B). This leaves three potential false-positives (0.37% of 815) and suggests that our estimate of a false-positive identification rate of maximally 1% is conservative.

MAPKKKK Ste20, the MAPKKK Ste11 and the MAPKK Ste7 remained unchanged. For some of these kinases, such as Ste7 or Ste11, this is readily explained because they fulfil another function in the osmolarity-sensing and filamentous growth pathway[17]. For other proteins, such as the Far3/7/8/11 protein complex that mediates one pathway of cell cycle arrest during the pheromone response, this is unexpected and might indicate that they have another function in haploid cells. This suggests another repressive function of Far3 during the cell cycle. Consistently, its inactivation results in faster growth of haploid cells[18].

The proteins encoded by retrotransposons Ty1 and Ty2 are about ten times more abundant in haploid cells, consistent with regulation of specific Ty mRNAs by pheromone signalling in haploid cells and repression in diploid cells by the MAT**a**/α transcription factor[19,20]. We also found the Ty1 transcription activator Tec1 to be eight times more expressed in haploid cells. Little is known about the evolutionary advantage of restricting retrotransposition to haploid cells, but because most wild-type cells are diploid, the repression of transposition in these cells might be used to minimize the spread of detrimental effects through the population.

Cell wall components were statistically significantly reduced in diploid cells ($P = 2.7 \times 10^{-9}$; Supplementary Table 8). At first glance, this is surprising because diploid cells are on average twice as large as haploid cells and also have more cell wall. However, larger cells need less surface components in relation to 'bulk' proteins, and the observed downregulation (0.77) is very close to what would be expected from geometrical considerations: a sphere of double volume has $2^{2/3}$ the surface and thus should have $2^{2/3}/2 = 0.79$ the amount of surface proteins after normalization for the doubled volume. The list of differentially expressed factors also contains a number of uncharacterized genes, which can be mined for haploid-specific functions.

A longstanding question in functional genomics is to what extent changes in mRNA levels lead to changes of the active agents in the cell, the proteins[21]. Overall correlation of mRNA[22] and protein changes was poor ($R = 0.24$) and there were large populations of genes with mRNA but no protein change (Fig. 4a). However, after we filtered out low-level microarray signals (Supplementary Fig. 10), the correlation improved to 0.46 (Fig. 4b). Several of the remaining, discordant mRNA changes seem to be technical artefacts. For example, *INO1*, the protein level of which did not change, is the only representative of several co-regulated genes (for example, *CHO1* and

CHO2) that was found upregulated by microarray analysis. *CTS1*, which was downregulated according to microarray analysis, was upregulated when measured by SILAC and western blot. Several lysine biosynthesis pathway genes seem to be regulated at the protein but not the mRNA level (magenta in Fig. 4b). However, this is due to use of lysine auxotrophs in the MS but not the microarray experiments. Among genes only found upregulated by proteomics (blue in Fig. 4b), cell wall proteins were highly overrepresented ($P = 7.7 \times 10^{-8}$, see Methods). This could be due to the microarray experiment not detecting slight expression changes for this class of proteins. Strongly regulated genes in both data sets were mainly components of the pheromone response. Here, correlation between mRNA and protein changes was high ($R = 0.68$; Fig. 4c). However, actual fold changes determined by microarrays deviated considerably from the values provided by the SILAC quantification (Supplementary Table 10). This is probably due to technical differences (that is, microarray measurements are not strictly quantitative) combined with the fact that the level of mRNA change may not directly be translated into a change of protein level.

In summary, a combination of SILAC labelling, high-resolution MS and sophisticated computational proteomics allows accurate quantitative analysis of an entire proteome. Among several tested strategies, in-solution digest of unfractionated cell lysate followed by simple isoelectric focusing of the peptides proved most powerful.

Key advantages of MS-based proteomics are the ability to measure endogenous rather than tagged versions of proteins, which may have altered expression levels, and to quantify the entire proteome from one sample. Our comparison of the proteome with the transcriptome highlights several crucial points for systems-wide analysis. First, proteomics can directly measure small changes in the amounts of proteins, which might have important effects in the cell. Second, it shows that the relationship between mRNA and protein levels depends on the proteins investigated. This effect is likely to be even more notable in mammalian proteomes, which compared to yeast are more complex and subject to more post-transcriptional control. A mammalian cell is commonly thought to express 10,000 gene products, which would only be two to three times the number of genes expressed in yeast. Thus, we predict that essentially complete mammalian proteomes—with at least one representative protein per expressed gene—will be feasible with refined versions of our strategy[23]. The next challenge will then be proteome-wide identification of functionally important isoforms and modifications.
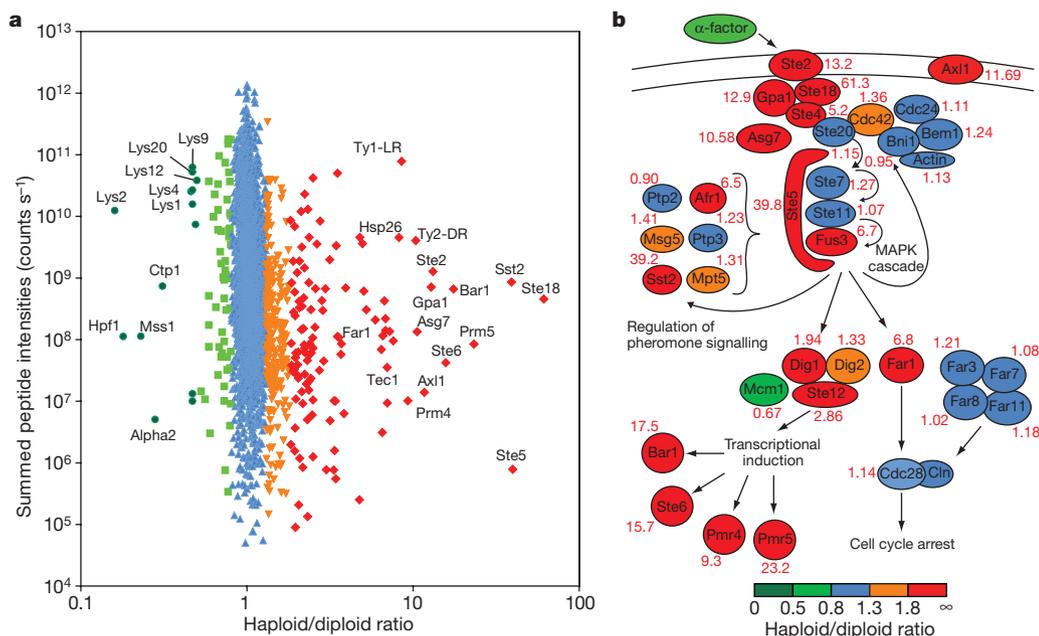
Figure 3 | Quantitative differences between the haploid and diploid yeast proteome. a, Overall fold change for the yeast proteome. **b,** Members of the yeast pheromone response are colour-coded according to fold change. The diploid to haploid ratio as determined by SILAC is indicated for each protein. Figure is adapted from ref. 13.
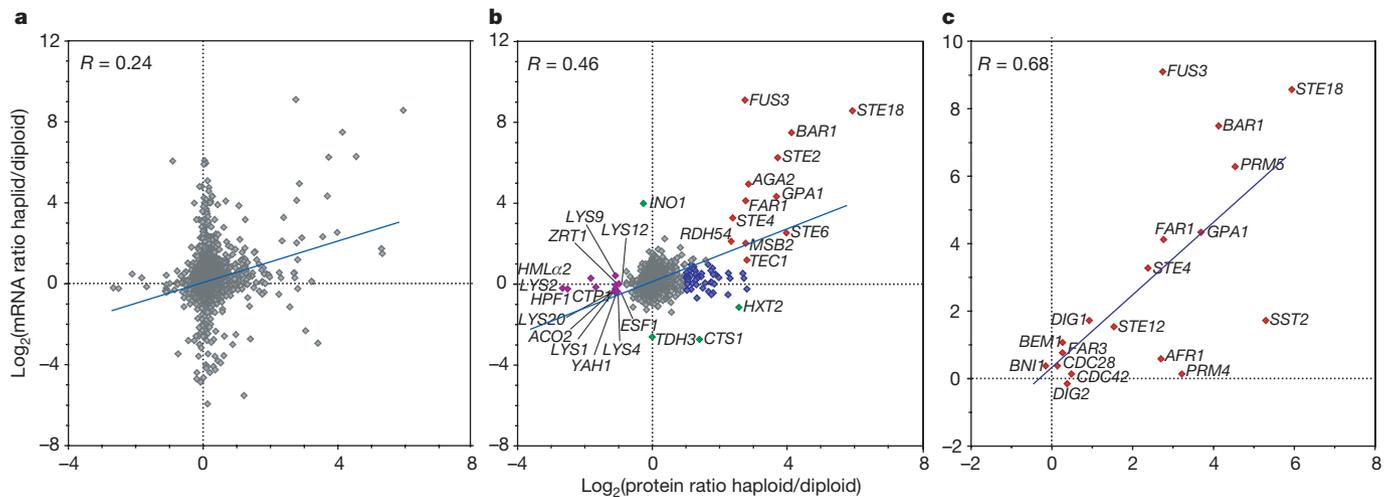
Figure 4 | Proteome and transcriptome changes of haploid versus diploid yeast. a, The overall correlation between protein and mRNA changes is poor ($R = 0.24$). **b**, After filtering out low mRNA signals, the data from **a** correlates better (Supplementary Fig. 10). Red, significantly upregulated as mRNA and protein; blue, significantly upregulated as protein; green, significantly changed as mRNA; and magenta, significantly downregulated as protein. **c**, Proteins involved in pheromone response (Fig. 3b) are co-regulated at mRNA and protein levels but actual protein ratios cannot be accurately predicted from changes of mRNA levels.

METHODS SUMMARY

Yeast diploid and haploid strains were SILAC-labelled as described[13] with $[^{13}C_6/^{15}N_2]$L-lysine-and/or $[^{13}C_6/^{15}N_4]$L-arginine. The diploid yeast strain TWY 809 was generated by crossing the wild-type BY4741 and BY4742. The haploid strain for lysine labelling was generated by sporulation of BY4743 and selection for the lysine auxotroph, MAT**a** cells. Yeast cells were lysed, mixed 1:1, fractionated by SDS–PAGE and in-gel digested with trypsin as described previously[12]. Alternatively, after mixing, proteins were digested in-solution by the endoproteinase LysC and the resulting peptide mixtures were fractionated by peptide isoelectric focusing. Each fraction was subsequently analysed by online liquid chromatography–tandem mass spectrometry (LC–MS/MS). All LC–MS/MS experiments were performed on an LTQ-Orbitrap (Thermo Fisher Scientific) mass spectrometer connected to an Agilent 1200 nanoflow HPLC system by means of a nanoelectrospray source (Proxeon Biosystems). MS full scans were acquired in the Orbitrap analyser using internal lock mass recalibration in real-time[24] whereas tandem mass spectra were simultaneously recorded in the linear ion trap. Peptides were identified from MS/MS spectra by searching them against the yeast ORF database (Stanford University) using the Mascot search algorithm[25] (http://www.matrixscience.com), and all SILAC pairs were quantified by MaxQuant (J.C. and M.M., submitted). For several of the top-regulated proteins, GFP- or TAP-tagged haploid and diploid strains were generated and the regulation was confirmed by western blot.

Full Methods and any associated references are available in the online version of the paper at www.nature.com/nature.

1. Aebersold, R. & Mann, M. Mass spectrometry-based proteomics. *Nature* **422**, 198–207 (2003).
2. Cravatt, B. F., Simon, G. M. & Yates, J. R. III. The biological impact of mass-spectrometry-based proteomics. *Nature* **450**, 991–1000 (2007).
3. Malmstrom, J., Lee, H. & Aebersold, R. Advances in proteomic workflows for systems biology. *Curr. Opin. Biotechnol.* **18**, 378–384 (2007).
4. Ong, S. E. *et al.* Stable isotope labeling by amino acids in cell culture, SILAC, as a simple and accurate approach to expression proteomics *Mol. Cell. Proteomics* **1**, 376–386 (2002).
5. Mann, M. Functional and quantitative proteomics using SILAC. *Nature Rev. Mol. Cell Biol.* **7**, 952–958 (2006).
6. Goffeau, A. *et al.* Life with 6000 genes. *Science* **274**, 563–567 (1996).
7. Shevchenko, A. *et al.* Linking genome and proteome by mass spectrometry: large-scale identification of yeast proteins from two dimensional gels. *Proc. Natl Acad. Sci. USA* **93**, 14440–14445 (1996).
8. Figeys, D. *et al.* Protein identification by solid phase microextraction-capillary zone electrophoresis-microelectrospray-tandem mass spectrometry. *Nature Biotechnol.* **14**, 1579–1583 (1996).
9. Washburn, M. P., Wolters, D. & Yates, J. R. III. Large-scale analysis of the yeast proteome by multidimensional protein identification technology. *Nature Biotechnol.* **19**, 242–247 (2001).
10. Peng, J. *et al.* Evaluation of multidimensional chromatography coupled with tandem mass spectrometry (LC/LC–MS/MS) for large-scale protein analysis: the yeast proteome. *J. Proteome Res.* **2**, 43–50 (2003).
11. King, N. L. *et al.* Analysis of the *Saccharomyces cerevisiae* proteome with PeptideAtlas. *Genome Biol.* **7**, R106 (2006).
12. de Godoy, L. M. *et al.* Status of complete proteome analysis by mass spectrometry: SILAC labeled yeast as a model system. *Genome Biol.* **7**, R50 (2006).
13. Gruhler, A. *et al.* Quantitative phosphoproteomics applied to the yeast pheromone signaling pathway. *Mol. Cell. Proteomics* **4**, 310–327 (2005).
14. Ghaemmaghami, S. *et al.* Global analysis of protein expression in yeast. *Nature* **425**, 737–741 (2003).
15. Huh, W. K. *et al.* Global analysis of protein localization in budding yeast. *Nature* **425**, 686–691 (2003).
16. Dohlman, H. G. & Slessareva, J. E. Pheromone signaling pathways in yeast. *Sci. STKE* **2006**, cm6 (2006).
17. Schwartz, M. A. & Madhani, H. D. Principles of MAP kinase signaling specificity in *Saccharomyces cerevisiae*. *Annu. Rev. Genet.* **38**, 725–748 (2004).
18. Blanc, V. M. & Adams, J. Evolution in *Saccharomyces cerevisiae*: identification of mutations increasing fitness in laboratory populations. *Genetics* **165**, 975–983 (2003).
19. Company, M., Errede, B. & Ty, A. 1 cell-type-specific regulatory sequence is a recognition element for a constitutive binding factor. *Mol. Cell. Biol.* **8**, 5299–5309 (1988).
20. Ke, N., Irwin, P. A. & Voytas, D. F. The pheromone response pathway activates transcription of Ty5 retrotransposons located within silent chromatin of *Saccharomyces cerevisiae*. *EMBO J.* **16**, 6272–6280 (1997).
21. Tyers, M. & Mann, M. From genomics to proteomics. *Nature* **422**, 193–197 (2003).
22. Galitski, T. *et al.* Ploidy regulation of gene expression. *Science* **285**, 251–254 (1999).
23. Cox, J. & Mann, M. Is proteomics the new genomics? *Cell* **130**, 395–398 (2007).
24. Olsen, J. V. *et al.* Parts per million mass accuracy on an orbitrap mass spectrometer via lock mass injection into a C-trap. *Mol. Cell. Proteomics* **4**, 2010–2021 (2005).
25. Perkins, D. N. *et al.* Probability-based protein identification by searching sequence databases using mass spectrometry data. *Electrophoresis* **20**, 3551–3567 (1999).

METHODS

Generation and SILAC-labelling of haploid and diploid yeast strains. The *Saccharomyces cerevisiae* diploid strain YLG1 was generated by crossing the haploid YAL6B MAT**a** strain[13] with one of its parental strains, Y15969 MATα (Euroscarf). The diploid yeast strain TWY 809 was generated by crossing the wild-type BY4741 and BY4742. The haploid strain for lysine labelling was generated by sporulation of BY4743 and selection for the lysine auxotroph, MAT**a** cells. The arginine and lysine double SILAC labelling was performed as described[13], with small modifications. In brief, cells from the haploid YAL6B strain, which has a *LYS1* and *ARG4* gene deletions and is therefore a double auxotroph for lysine and arginine, and the diploid YLG1 strain were grown in YNB liquid medium containing either 20 mg l^{-1} [^{13}C$_6$/^{15}N$_2$]L-lysine (Lys8) and 5 mg l^{-1} [^{13}C$_6$,^{15}N$_4$]L-arginine (Arg10; Isotec-Sigma) or 20 mg l^{-1} L-lysine and 5 mg l^{-1} L-arginine for ten generations, until they reached log-phase (D_{600} 0.7).

Lysis and protein fractionation strategy. Normal and heavy SILAC-labelled yeast cells were collected by centrifugation, resuspended in lysis buffer (150 mM potassium acetate, 2 mM magnesium acetate, 1× protease inhibitor cocktail (Roche), and 20 mM HEPES, pH 7.4) and frozen in liquid N$_2$. Haploid and diploid frozen cells were mixed 1:1 on the basis of protein amount (as determined by Bradford assay) and mechanically disrupted in a milling device (MM301 Ball Mill, Retsch), with 3 cycles of 3 min at 10 Hz, intercalated by immersion in liquid N$_2$. All further steps were performed at 4 °C. The extract was allowed to thaw and centrifuged for 4 min at 1,000*g*. The pellet was collected, washed twice with lysis buffer, resuspended in PBS containing 2% SDS, incubated for 5 min at 65 °C and spun down to remove debris (fraction 1). The sample was centrifuged for 10 min at 20,000*g* and the resultant pellet washed twice with lysis buffer and resuspended in PBS containing 2% SDS (fraction 2). The supernatant was brought to 60% (NH$_4$)$_2$SO$_4$, incubated for 10 min under rotation to allow protein precipitation, centrifuged for 10 min at 20,000*g* and the precipitated proteins resuspended in PBS containing 2% SDS (fraction 3). The concentration of (NH$_4$)$_2$SO$_4$ was raised to 80%, the sample processed as before, the precipitated proteins resuspended in PBS containing 2% SDS (fraction 4) and the remaining soluble proteins dialysed against PBS containing 2% SDS (fraction 5).

In-solution digestion. Proteins extracted from lysine-labelled haploid and diploid yeast were reduced for 20 min at room temperature (24 °C) in 1 mM dithiothreitol and then alkylated for 15 min by 5.5 mM iodoacetamide (IAA) at room temperature in the dark. Endoproteinase LysC (Wako) was added 1:50 (w/w) and the lysates were digested overnight at room temperature (12 h). Arginine- and lysine-labelled yeast proteins were digested with LysC in a similar manner, and the resulting peptide mixtures were diluted with Millipore water to achieve a final urea concentration below 2 M. Trypsin (modified sequencing grade, Promega) was added 1:50 (w/w) and digested overnight. Trypsin and LysC activity were quenched by acidification of the reaction mixtures with TFA to ~pH 2.

Peptide isoelectric focusing. In-solution digested peptides (75 μg) were separated according to their isoelectric point using the Agilent 3100 OFFGEL fractionator (Agilent, G3100AA). The system was set up according to the manual of the High Res Kit, pH 3–10 (Agilent, 5188-6424), but strips were exchanged by 24 cm Immobiline DryStrip, pH 3–10 (GE Healthcare, 17-6002-44), and ampholytes were substituted by IPG buffer, pH 3–10 (GE Helthcare, 17-6000-87), used 1:50. Peptides were focused for 50 kilovolt hours (kVh) at a maximum current of 50 μA, maximum voltage of 8,000 V and maximum power of 200 mW into 24 fractions. Each peptide fraction was acidified by adding 3% acetonitrile, 1% trifluoroacetic acid and 0.5% acetic acid, then desalted and concentrated on a reversed-phase C18 StageTip[26].

Gel electrophoresis and in-gel digestion. Each lysine- and arginine-labelled yeast protein fraction was boiled in 2× LDS buffer, separated by one-dimensional SDS–PAGE (4–12% Novex mini-gel, Invitrogen) and visualized by colloidal Coomassie staining. The entire protein gel lanes were excised and cut into 20 slices each. Every gel slice was subjected to in-gel digestion with trypsin[27]. The resulting tryptic peptides were extracted by 30% acetonitrile in 3% TFA, reduced in a Speed Vac, and desalted and concentrated on a reversed-phase C18 StageTip[26].

Mass spectrometric analysis. All MS experiments were performed on a nanoflow HPLC system (Agilent Technologies 1200) connected to a hybrid LTQ–orbitrap classic or XL (Thermo Fisher Scientific) equipped with a nanoelectrospray ion source (Proxeon Biosystems) as described[24] with a few modifications. In brief, the peptide mixtures were separated in a 15 cm analytical column (75 μm inner diameter) in-house packed with 3-μm C18 beads (Reprosil-AQ Pur, Dr. Maisch) with a 2 h gradient from 5% to 40% acetonitrile in 0.5% acetic acid. The effluent from the HPLC was directly electrosprayed into the mass spectrometer.

The MS instrument was operated in data-dependent mode to automatically switch between full-scan MS and MS/MS acquisition. Survey full-scan MS spectra (from *m/z* 300–2,000) were acquired in the orbitrap with resolution $R = 60,000$ at *m/z* 400 (after accumulation to a 'target value' of 1,000,000 in the linear ion trap).

The ten most intense peptide ions with charge states ≥2 were sequentially isolated to a target value of 5,000 and fragmented in the linear ion trap by collisionally induced dissociation. Fragment ion spectra were recorded with the LTQ detectors 'in parallel' with the orbitrap full-scan detection. For all measurements with the orbitrap detector, a lock-mass ion from ambient air (*m/z* 391.284286, 429.08875 or 445.120025) was used for internal calibration as described[24].

For mass range experiments (similar to 'gas-phase fractionation') all samples were analysed using survey scan MS spectra in one of the following mass regions: *m/z* 300–500, *m/z* 450–650, *m/z* 600–900, *m/z* 850–1,250 and *m/z* 1,200–1,800. Resolution, lock mass option, 'target value' and number of intense peptide peaks selected for isolation were identical to full-scan analysis (see below), except for the mass range analysis *m/z* 1,200–1,800 where charge states ≥1 were allowed for isolation. All survey scans where acquired using injection waveforms, which applies a filter on the injection ions and thereby ejects all ions outside of the selected mass range. This ensures optimal dynamic range because the ion trap will only be filled with a population of ions belonging to the mass range of interest.

Identification and quantification of peptides and proteins. The data analysis was performed with the MaxQuant software as described[13] supported by Mascot as the database search engine for peptide identifications. Peaks in MS scans were determined as three-dimensional hills in the mass-retention time plane. They were then assembled to isotope patterns and SILAC pairs by graph-theoretical methods. MS/MS peak lists were filtered to contain at most six peaks per 100 Da interval and searched by Mascot (Matrix Science) against a concatenated forward and reversed version of the yeast ORF database (*Saccharomyces* Genome Database SGDTM at Stanford University; http://www.yeastgenome.org). Protein sequences of common contaminants, for example, human keratins and proteases used, were added to the database. The initial mass tolerance in MS mode was set to 7 p.p.m. and MS/MS mass tolerance was 0.5 Da. Cysteine carbamidomethylation was searched as a fixed modification, whereas *N*-acetyl protein, *N*-pyroglutamine and oxidized methionine were searched as variable modifications. Labelled arginine and lysine were specified as fixed or variable modifications, depending on the previous knowledge about the parent ion. The resulting Mascot .dat files were loaded into the MaxQuant software[13] together with the raw data for further analysis. SILAC peptide and protein quantification was performed automatically with MaxQuant using default settings for parameters. Here, for each SILAC pair the ratio is determined by a robust regression model fitted to all isotopic peaks and all scans that the pair elutes in. SILAC protein ratios are determined as the median of all peptide ratios assigned to the protein. Absolute protein quantification was based on extracted ion chromatograms of contained peptides. To minimize false identifications, all top-scoring peptide assignments made by Mascot were filtered based on previous knowledge of individual peptide mass error, SILAC state and the correct number of lysine and arginine residues specified by the mass difference observed in the full scan between the SILAC partners. Furthermore, peptide assignments were statistically evaluated in a Bayesian model on the basis of sequence length and Mascot score. We accepted peptides and proteins with a false discovery rate of less than 1%, estimated on the basis of the number of accepted reverse hits.

Gene ontology and Pfam domain overrepresentation analysis. *P* values for the overrepresentation of gene ontology categories and protein domain content were based on a Wilcoxon–Mann–Whitney test for the presence–absence pattern of each category and the ratio significance as a continuous value. All *P* values below 0.01 are reported. To determine classes of proteins that show a high protein ratio but only low response on the transcript level, we defined a protein population with a protein ratio above two and a transcript ratio between one-half and two. We looked for enrichment of Gene Ontology terms in this class of proteins compared to the rest by calculating the *P* value according to the Fisher exact test.

SILAC-assisted peptide-sequence-tag searching for ambiguous ORFs. Fragment ion intensities in spectra from 'light' and 'heavy' forms of a SILAC peptide pair are highly correlated. The only difference between their spectra is that C-terminal fragment ions (*y*-ions) are offset by 8.014 Da or other multiples of the difference between normal and heavy labelled amino acids. Extraction of *y*-ions is therefore straightforward and examples are shown in Supplementary Figs 2–4 for each of the three ORFs initially assumed not to be expressed. Searching these SILAC confirmed fragment ions (*y*-ions) in the yeast database as peptide-sequence tags[28] unambiguously verified identification of the ORFs.

26. Rappsilber, J., Ishihama, Y. & Mann, M. Stop and go extraction tips for matrix-assisted laser desorption/ionization, nanoelectrospray, and LC/MS sample pretreatment in proteomics. *Anal. Chem.* **75**, 663–670 (2003).

27. Shevchenko, A. *et al.* Mass spectrometric sequencing of proteins silver-stained polyacrylamide gels. *Anal. Chem.* **68**, 850–858 (1996).

28. Mann, M. & Wilm, M. Error-tolerant identification of peptides in sequence databases by peptide sequence tags. *Anal. Chem.* **66**, 4390–4399 (1994).

A genome-wide screen for genes affecting eisosomes reveals Nce102 function in sphingolipid signaling

Florian Fröhlich,[1] Karen Moreira,[3] Pablo S. Aguilar,[4] Nina C. Hubner,[2] Matthias Mann,[2] Peter Walter,[3,5] and Tobias C. Walther[1]

[1]Organelle Architecture and Dynamics and [2]Proteomics and Signal Transduction, Max Planck Institute of Biochemistry, 82152 Martinsried, Germany
[3]Department of Biochemistry and Biophysics, University of California, San Francisco, San Francisco, CA 94158
[4]Institute Pasteur, CP 11400 Montevideo, Uruguay
[5]Howard Hughes Medical Institute, San Francisco, CA 94158

The protein and lipid composition of eukaryotic plasma membranes is highly dynamic and regulated according to need. The sphingolipid-responsive Pkh kinases are candidates for mediating parts of this regulation, as they affect a diverse set of plasma membrane functions, such as cortical actin patch organization, efficient endocytosis, and eisosome assembly. Eisosomes are large protein complexes underlying the plasma membrane and help to sort a group of membrane proteins into distinct domains. In this study, we identify Nce102 in a genome-wide screen for genes involved in eisosome organization and Pkh kinase signaling. Nce102 accumulates in membrane domains at eisosomes where Pkh kinases also localize. The relative abundance of Nce102 in these domains compared with the rest of the plasma membrane is dynamically regulated by sphingolipids. Furthermore, Nce102 inhibits Pkh kinase signaling and is required for plasma membrane organization. Therefore, Nce102 might act as a sensor of sphingolipids that regulates plasma membrane function.

Introduction

The plasma membrane is highly dynamic and crucial for communication of cells with their environment. It transduces numerous extracellular signals and transports molecules in and out of the cell. To accommodate these diverse tasks, it is highly organized, and plasma membrane processes are tightly coordinated, both spatially and temporally (Simons and Toomre, 2000; Anderson and Jacobson, 2002; Simons and Vaz, 2004). How the abundance of most lipids and proteins in the plasma membrane is regulated is largely unknown.

In the yeast *Saccharomyces cerevisiae*, the plasma membrane is laterally organized into spatial domains that have different protein and lipid composition. One type of domain harbors several integral membrane proteins, such as the arginine transporter Can1 and members of the Sur7 family of proteins and was accordingly termed membrane compartment

occupied by Can1 (MCC). MCCs were suggested to contain a distinct lipid composition enriched in ergosterol, as visualized by staining with filipin, a fluorescent marker binding this lipid (Malinska et al., 2003; Grossmann et al., 2007).
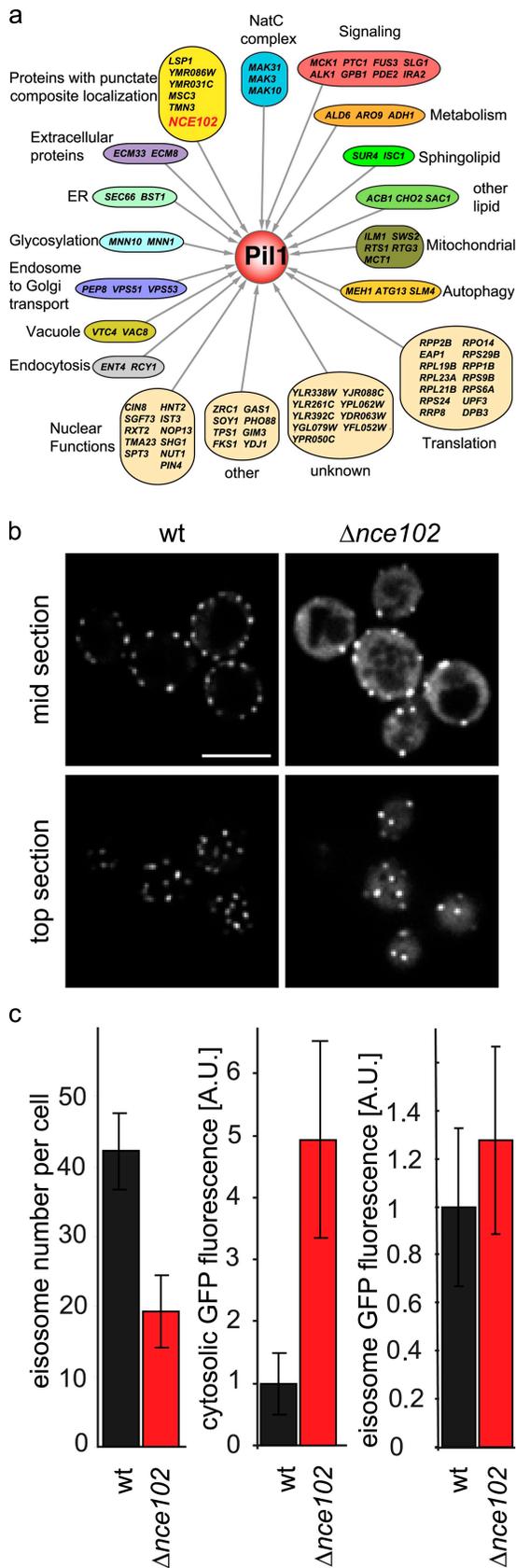
Yeast mother cells possess 25–45 MCCs that can be visualized as discrete foci in the plasma membrane. MCCs are mutually exclusive with a second domain, marked by the plasma membrane ATPase Pma1, termed membrane compartment occupied by Pma1 (MCP; Malinska et al., 2003, 2004). The organization of the plasma membrane in distinct spatial domains is at least in part mediated by large protein complexes termed eisosomes (Walther et al., 2006). Eisosomes lie underneath each MCC forming a punctate, distributed pattern in the cell cortex. When the gene encoding the major eisosome component Pil1 is deleted, MCCs and all remaining eisosome proteins investigated so far coalesce into one or a few punctae per cell (Walther et al., 2006; Grossmann et al., 2007). In addition to concentrating at such eisosome remnants, a significant fraction

Figure 1. **A functional genomic screen reveals genes required for eisosome organization.** (a) Genes with a Pil1 organization phenotype shown in functional groups. (b) Nce102 is required for normal eisosome organization. Images of Pil1-GFP expressed in wild-type (wt; left) or Δnce102 cells (right) are shown. (c) Number of eisosomes per mother cell (left), cytoplasmic Pil1-GFP fluorescence (middle), and Pil1-GFP fluorescence per eisosome (right). Error bars indicate SD. Bar, 5 μm.

of MCC transmembrane proteins, such as Sur7, localizes uniformly in the plasma membrane. Similarly, the ergosterol marker filipin looses its normal punctate eisosome localization in Δpil1 cells, distributes more evenly over the plasma membrane surface, and enriches at eisosome remnants (Grossmann et al., 2007).

One possible function of MCCs and eisosomes is to regulate protein and lipid abundance by sorting them into distinct, spatially separated pools where they are stabilized or from which they can be endocytosed selectively. Consistent with this notion, disruption of MCCs leads to increased turnover of some proteins normally localized there (Grossmann et al., 2008). The precise molecular function of eisosomes is still unclear, but it was suggested that they regulate sites of endocytosis based on their colocalization with endocytic intermediates visualized by the lipophilic dye FM4-64 and a hexose transporter GFP fusion protein (Walther et al., 2006). A clue of how eisosomes might be regulated is provided by the discovery that Pkh kinases localize at eisosomes and that Pil1 and Lsp1 are Pkh kinase substrates (Zhang et al., 2004; Walther et al., 2007; Luo et al., 2008).

Pkh kinases regulate physiology and plasma membrane functions such as actin patch organization, endocytosis, and eisosome assembly (Inagaki et al., 1999; Sun et al., 2000; Friant et al., 2001; deHart et al., 2002; Liu et al., 2005; Grosshans et al., 2006; Daquinag et al., 2007; Walther et al., 2007; Luo et al., 2008). These responses are mediated by their targets, including Ypk1 and Ypk2 (homologues of the mammalian serum glucocorticoid kinase), Sch9 (homologue of human AKT kinase), Pkc1 (atypical protein kinase C), and myosin-I. In addition, Pkh kinase phosphorylation of Pil1 regulates the assembly state of eisosomes (Walther et al., 2007; Luo et al., 2008).

Pkh kinases are regulated by sphingoid long chain bases such as phytosphingosine (PHS) and dihydrosphingosine, which are precursors in sphingolipid synthesis (Zhang et al., 2004). However, it is not known how Pkh kinases sense and respond to long chain bases. Pkh kinases and several other kinases of the signaling module are regulated by levels of long chain bases in vitro, but whether this is relevant in vivo and whether it is the only way to control Pkh kinase activity is not clear (Zhang et al., 2004; Liu et al., 2005).

In this study, we visually screened for genes that affect eisosome organization either directly or through altering Pkh kinase activity. We identified the transmembrane protein Nce102 as part of the sphingolipid–Pkh signaling network. Our functional experiments suggest that Nce102 might act as a sphingolipid sensor that modulates Pkh kinase activity to regulate plasma membrane organization and function.

Results

Nce102 is required for normal eisosome organization

To identify genes required for eisosome assembly and organization, we screened by fluorescence microscopy a systematic gene deletion collection into which we introduced GFP-labeled
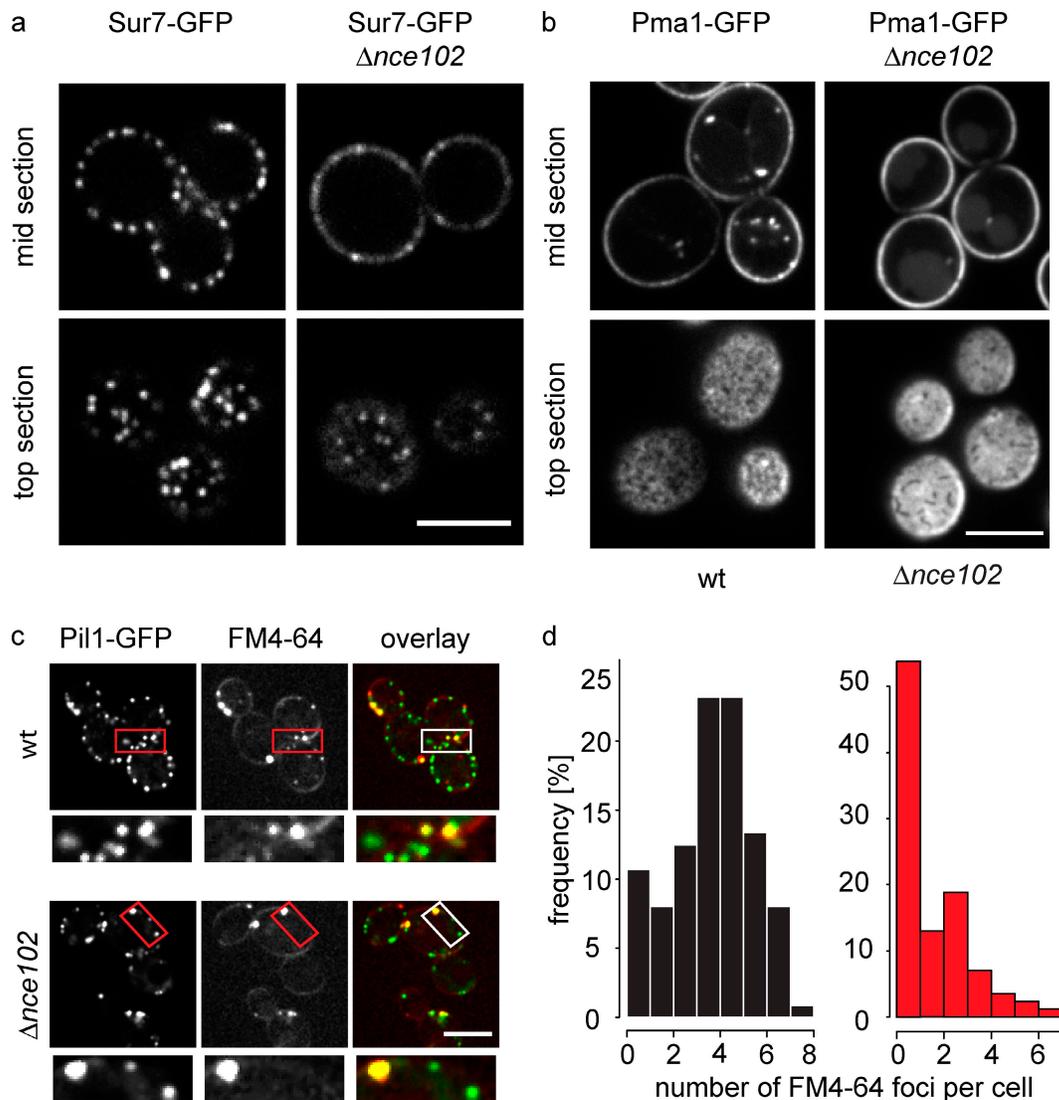
Figure 2. **NCE102 is required for normal plasma membrane organization.** (a and b) Sur7-GFP (a) and Pma1-GFP (b) were expressed in wild-type (wt) or Δnce102 cells, and representative confocal top (bottom) and mid sections (top) are shown. (c) Wild-type and Δnce102 cells expressing Pil1-GFP (green) were pulse labeled with FM4-64 (red) for 1 min, and representative images are shown. Boxes indicate the area magnified in the bottom panels. (d) Numbers of FM4-64 intermediates per cell (n > 50) from images as in c are shown as a histogram. Bars, 5 μm.

Pil1 fusion protein (Pil1-GFP; Fig. S1 a; Tong et al., 2001). To determine the effect of individual mutations on eisosomes, we grew the library in 96-well plates to mid-log phase and imaged cells with an automated microscope. Visual inspection of the images led to identification of 88 genes that affect eisosomes (Fig. 1 a).

To obtain quantitative data for the identified mutants, we collected confocal images and quantitated the number of eisosomes per cell, the cytosolic fluorescence signal representing unassembled Pil1-GFP, the integrated fluorescence on the cell surface, the size of individual eisosomes, and the percentage of cell surface covered with eisosomes (Fig. S1 a). The relative values for these parameters were used to cluster the genes according to the similarity of their phenotypes (Fig. S1 b).

For example, deletion of genes encoding subunits of the NatC complex involved in N-terminal protein acetylation

(*MAK3*, *MAK10*, and *MAK31*) showed a similar phenotype characterized by fewer eisosomes, increased cytoplasmic Pil1-GFP, and little change in the size of remaining eisosomes.

In addition, several hits (*YMR031C*, *YMR086W*, and *MSC3*) are good candidates for genes encoding previously not recognized eisosome components because they localize in a punctuate pattern at the cell periphery similar to eisosomes, and at least Ymr031c and Ymr086c were copurified with Pil1 (Huh et al., 2003; Grossmann et al., 2008; Deng et al., 2009).

In this study, we focused on Nce102 because it is the only hit in our screen previously found as a transmembrane plasma membrane protein (Cleves et al., 1996). To confirm the role of Nce102 in eisosome formation, we investigated the localization of Pil1-GFP in Δnce102 compared with wild-type cells. Consistent with the systematic genome-wide screen, confocal images showed a clear reduction of
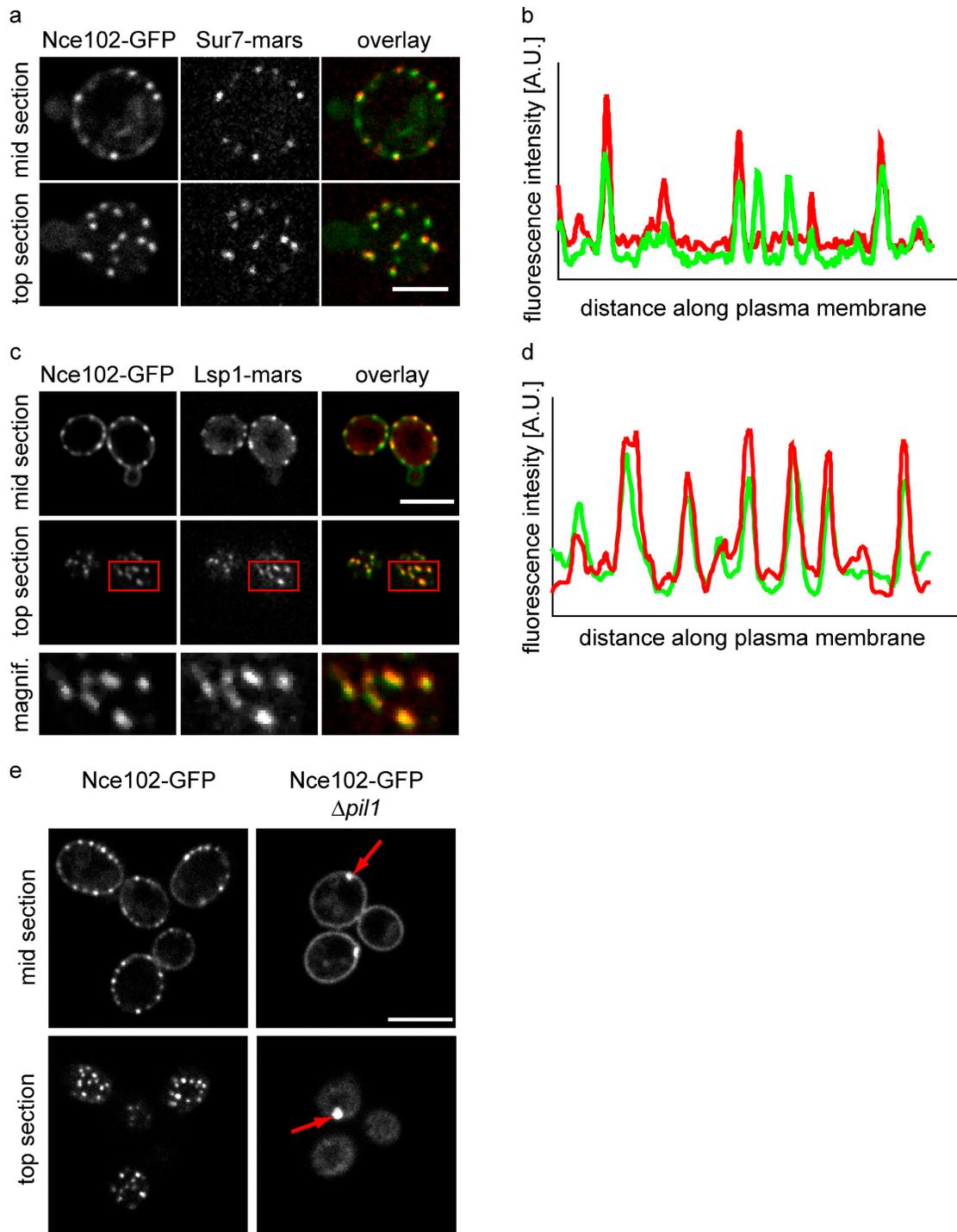
Figure 3. **Nce102 localizes to both MCC and non-MCC domains in the plasma membrane.** (a) Images from cells expressing Nce102-GFP (left; green in overlay) and Sur7-mars (middle; red in the overlay) are shown. (b) Intensity profiles of Nce102-GFP and Sur7-mars along the plasma membrane. (c) Images from cells expressing Nce102-GFP (left; green in overlay) and Lsp1-mars (middle; red in the overlay) are shown. Boxes indicate the area magnified in the bottom panels. (d) Intensity profiles of Nce102-GFP and Lsp1-mars along the plasma membrane. (e) Pil1 is required for normal Nce102 distribution. Wild-type (left) and *∆pil1* (right) cells expressing Nce102-GFP are shown. Arrows highlight eisosome remnants. Bars, 5 µm.

eisosome number and a wider spacing of remaining eiso-somes (Fig. 1 b). Quantitation revealed that deletion of *NCE102* results in a twofold decrease of eisosome number per mother cell and concomitant increase of cytosolic signal (Fig. 1 c).

Nce102 is required for membrane organization

Eisosomes organize MCCs, and mutation of *PIL1* results in mislocalization of all tested MCC components (Walther et al., 2006; Grossmann et al., 2007, 2008). Because *NCE102* deletion

has a strong effect on eisosomes, we asked whether *NCE102* is also required for plasma membrane organization. Indeed, compared with wild-type cells in which the MCC marker Sur7-GFP was organized in distinct domains, *Δnce102* cells showed only few clusters and more uniform localization of Sur7-GFP throughout the plasma membrane (Fig. 2 a). Furthermore, we observed a consistent but less pronounced phenotype on the MCP marker Pma1, which localized more uniformly in *Δnce102* cells compared with its normal localization in structured plasma membrane domains (Fig. 2 b).

Next, we asked whether Nce102 influences the formation of endocytic intermediates formed as foci at eisosomes by using the lipophilic tracer FM4-64 (Vida and Emr, 1995; Walther et al., 2006). FM4-64 foci formed after short chase periods of ~1 min and colocalized with eisosomes in both wild-type and *Δnce102* cells (Fig. 2 c). However, when we quantitated the number of foci, we found their number greatly reduced in *Δnce102* cells (median = 1 foci/cell; Fig. 2 d, right) compared with wild-type cells (median = 4 foci/cell; Fig. 2 d, left). Together, this shows that normal plasma membrane organization requires Nce102.

Nce102 localizes to the plasma membrane at MCC

To answer how Nce102 functions, we first investigated its subcellular localization. In agreement with a recent study that identified Nce102 as an MCC component, we found Nce102-GFP localizing in the plasma membrane and accumulating in foci reminiscent of MCCs (Fig. 3 a; Grossmann et al., 2008). This notion was further confirmed by colocalization of Nce102 with plasma membrane markers but not, for example, with cortical ER markers (unpublished data).

To test whether Nce102 foci are MCCs, we investigated their localization in respect to Sur7 tagged with the red fluorophore RFP-mars (Fischer et al., 2004), an MCC marker. Nce102 foci completely overlapped with Sur7-marked MCCs (Fig. 3, a and b) with significant levels of Nce102-GFP also diffusely localized in the remainder of the plasma membrane. As MCCs are membrane domains located over eisosomes, we additionally investigated Nce102-GFP localization in respect to eisosomes marked by Lsp1-mars and found that Nce102-GFP foci and eisosomes colocalize perfectly (Fig. 3, c and d). Because Nce102 is a multipass transmembrane domain protein, it is most likely located in the MCC and partially in the remainder of the membrane.

One hallmark of proteins localizing to eisosomes or MCCs is that they collapse to one or a few eisosome remnants in *Δpil1* cells (Walther et al., 2006; Grossmann et al., 2007). Indeed, Nce102-GFP localization in *Δpil1* cells also closely resembles that of MCC proteins such as Sur7. Most of Nce102-GFP localizes to one or a few eisosome remnants in *Δpil1* cells, whereas the remaining portion shows a uniformly distributed signal throughout the plasma membrane (Fig. 3 e).

Nce102 acts negatively on Pil1 phosphorylation

Because eisosome organization is sensitive to Pil1 phosphorylation, we expected to find genes in our screen that directly affect
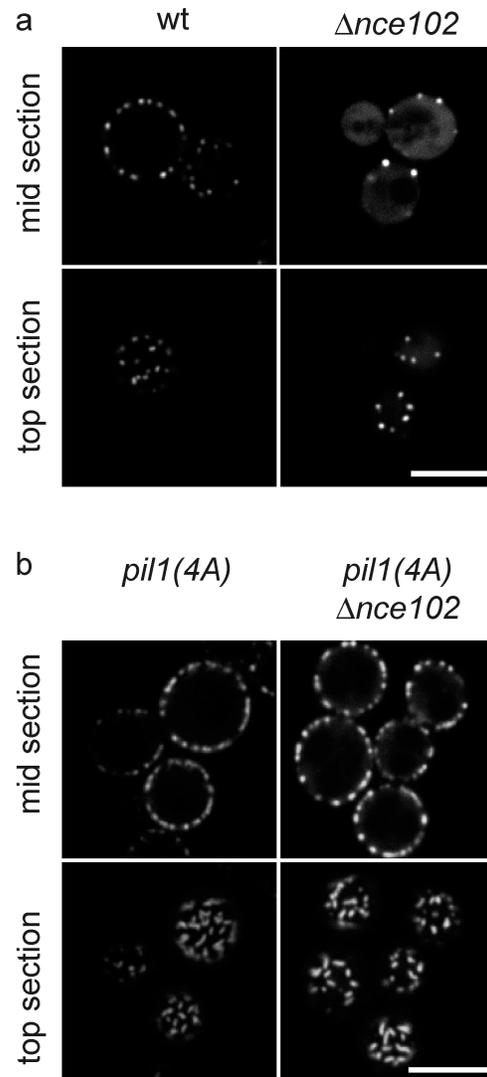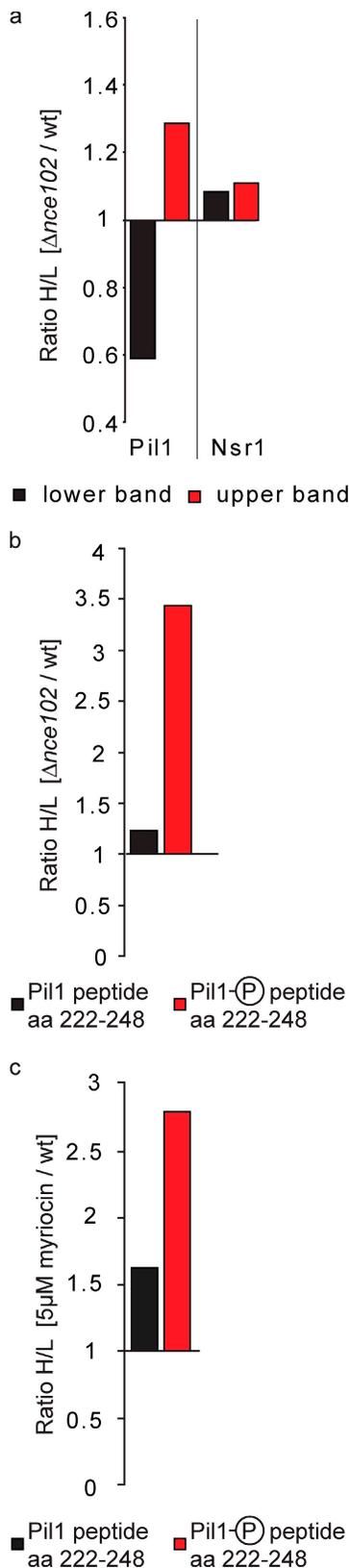

Figure 4. **Nonphosphorylatable Pil1 is resistant to *Δnce102*.** (a and b) Representative top and mid sections of wild-type (wt; left) or *Δnce102* cells (right) expressing Pil1-GFP (a) or nonphosphorylatable pil1(4A) fused to GFP (b) are shown. Bars, 5 μm.

the architecture, assembly, or stability of eisosomes and genes involved in signaling that modifies Pil1 phosphorylation. In fact, the *Δnce102* phenotype on Pil1-GFP localization closely resembles the phenotype of *pil1(4D)* mutant cells, bearing a phosphomimicking mutant of Pil1-GFP in which four residues that are phosphorylated in the wild-type protein are mutated to aspartate (S45D, S59D, S230D, and T233D; Fig. 1 b and Fig. S4 c; Walther et al., 2007).

Therefore, we tested genetically whether Nce102 acts on eisosomes by altering Pil1 phosphorylation that could then indirectly modulate eisosome assembly. If *Δnce102* effect is mediated by phosphorylation, we expect that a pil1(4A)-GFP mutant in which four residues that are required for the effect of Pkh kinases on eisosome assembly are changed to alanine (S45A, S59A, S230A, and T233A; Walther et al., 2007) blocks the effect of *NCE102* deletion. However, if Nce102's effect on eisosomes is independent of Pil1 phosphorylation state, we expect to see similar effects of *Δnce102* on wild-type Pil1 and pil1(4A).

Indeed, pil1(4A)-GFP localization was indistinguishable between Δnce102 and wild-type cells, showing slightly more eisosome pil1(4A) assembly at the plasma membrane compared with wild-type Pil1 (Fig. 4 b). Therefore, pil1(4A) is epistatic to Δnce102. Because Pil1 needs to get phosphorylated on residues mutated in pil1(4A) to develop the Δnce102 eisosome phenotype, we conclude that Nce102 acts upstream of Pil1 phosphorylation.

When combined with pil1(4D)-GFP, Δnce102 cells showed a similar, albeit slightly more severe phenotype than NCE102 pil1(4D)-GFP cells (Fig. S4 c), indicating that phosphorylation at additional sites can enhance eisosome disassembly. Previous work identified at least seven additional phosphorylation sites in Pil1, which may mediate this effect (Zhang et al., 2004; Walther et al., 2007; Luo et al., 2008). Together, pil1(4A) epistasis on Δnce102 and enhancement of the pil1(4D) phenotype by Δnce102 suggest that Nce102 negatively regulates Pil1 phosphorylation.

Nce102 inhibits Pil1 phosphorylation

To substantiate these findings, we determined whether the phosphorylation state of Pil1 is altered in Δnce102 cells. To this end, we purified Pil1 fused to a tandem affinity purification (TAP) tag from wild-type and metabolically heavy lysine-labeled Δnce102 cells (stable isotope labeling by amino acids in cell culture [SILAC]; Fig. S2 a; Ong et al., 2002) and analyzed it by two strategies. First, we mixed proteins of Pil1-TAP eluates 1:1 and separated them by SDS-PAGE, resulting in a clearly visible doublet of Pil1, where the upper band represents phosphorylated Pil1 (Walther et al., 2007). Separate analysis of the two bands by liquid chromatography (LC) mass spectrometry (MS)/MS revealed that contaminant proteins present in both bands have a 1:1 ratio of protein from wild-type and Δnce102 sample, as determined by comparing mean peptide peak intensities. In contrast, Pil1 from Δnce102 was 30% enriched in the upper phospho-Pil1 band (1.28 ratio, Pil1 heavy vs. light) and correspondingly decreased in the lower band (0.59 ratio, Pil1 heavy vs. light; Fig. 5 a; and Fig. S2, c and d).

In a second approach, we directly mixed, digested, and analyzed Pil1 pull-down eluates by LC-MS/MS (Fig. S2 a). From this approach, we identified many unphosphorylated peptides and, for example, the phosphorylated peptide harboring T233 of Pil1 from both wild-type and Δnce102 cells. Importantly, the phosphopeptide was more than threefold more abundant coming from the heavy lysine-labeled Δnce102 samples compared with the wild-type control (Fig. 5 b; and Fig. S2, e and f). The total amount of Pil1 was equal in both experiments because unphosphorylated peptides were present in a 1:1 ratio (Fig. S2 f). Together, these data demonstrate that Pil1 was present in a roughly equimolar ratio in both pull-down eluates but that phosphorylation at T233 was more than threefold increased in

Figure 5. **Pil1 phosphorylation is increased in Δnce102 cells.** (a) Pil1-TAP was purified from SILAC-labeled wild-type and Δnce102 cells, mixed in equal amounts, resolved by SDS-PAGE, and two resulting Pil1 bands were separately analyzed by MS. The contaminant Nsr1 was present in a 1:1 ratio from both strains in each band. Pil1 was 1.3-fold enriched in the upper band (red) and decreased to a ratio 0.6 in the lower band (black). (b) Pil1-TAP purified from SILAC-labeled wild-type and Δnce102 cells was analyzed by MS. Unphosphorylated Pil1 peptide amino acids 222–248 is shown in black, and the T233 phosphopeptide is shown in red. (c) Pil1-TAP purified from SILAC-labeled untreated cells or treated with myriocin for 1 h was analyzed as in b. Representative data of three experiments are shown. Ratio H/L denotes the mean ratio of the abundance of heavy- versus light-labeled peptides.
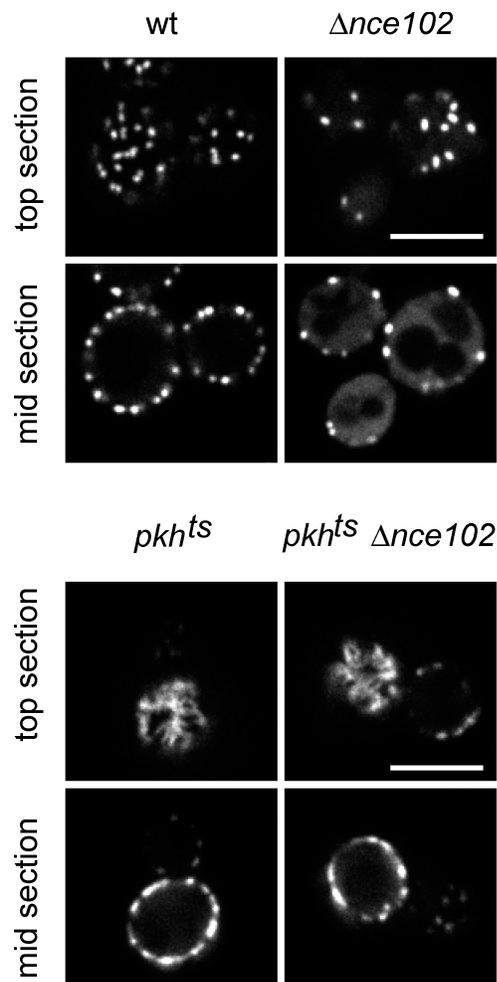
wt   Δnce102

pkh^ts   pkh^ts Δnce102

Figure 6. **Mutation of Pkh kinases is epistatic to Δnce102.** Optical top and mid sections of wild-type (wt; top left), Δnce102 (top right), pkh^ts (bottom left), or pkh1^ts Δnce102 (bottom right) cells expressing Pil1-GFP are shown. Bars, 5 μm.

Δnce102 cells. Therefore, the results of the two biochemical approaches converge, demonstrating that Pil1 phosphorylation is increased in Δnce102 cells.

Because Pil1 phosphorylation is inhibited by sphingoid bases (Zhang et al., 2004; Walther et al., 2007), we tested whether NCE102 deletion results in a similar effect on Pil1 phosphorylation as sphingolipid depletion. To this end, we measured the relative abundance of the Pil1 T233 phosphopeptide in cells where synthesis of sphingolipids was blocked for 1 h by myriocin, a drug targeting the serine palmitoyl transferase that catalyzes the rate-limiting step of sphingolipid synthesis, compared with wild-type cells. In this experiment, we detected a twofold increase of Pil1 phosphorylation at T233 after myriocin treatment compared with wild-type cells (Fig. 5 c and Fig. S2 g). This shows that the block of sphingolipid synthesis by myriocin and NCE102 deletion has a similar effect on Pil1 phosphorylation.

Nce102 acts on Pil1 via Pkh kinases

Several studies show that Pil1 phosphorylation is mediated by Pkh kinases (Zhang et al., 2004; Walther et al., 2007; Luo et al., 2008). Therefore, we asked whether the effect of Nce102

on Pil1 phosphorylation occurs through the Pkh kinase pathway. First, we determined the epistatic relationship between Pkh kinase mutants and Δnce102 using a yeast strain that harbors a deletion of PKH2 and a temperature-sensitive allele of PKH1 (pkh^ts; Friant et al., 2001). Already at the permissive temperature, these mutations lead to a strong over-assembly effect on eisosomes. Specifically, pkh^ts strains display large elongated threads of Pil1 at the plasma membrane with more of the membrane covered with Pil1 (Fig. 6; Walther et al., 2007). This phenotype is also very severe at the restrictive temperature, with most of the membrane covered with Pil1 (Fig. S4 e).

Combining pkh^ts and the Δnce102 mutations, we found that double-mutant cells show a Pil1-GFP phenotype indistinguishable from the pkh^ts phenotype at both 24 (Fig. 6) and 37°C (Fig. S4 e). This indicates that Pkh kinases are required to obtain the Δnce102 phenotype and shows that Nce102 acts upstream of Pkh kinases, inhibiting them in a linear pathway.

Nce102 acts downstream of long chain bases in sphingoid base signaling

Our data suggest that Nce102 acts on Pil1 phosphorylation by inhibiting Pkh kinases. Because Pkh kinases are regulated by sphingoid bases and both, a block of sphingolipid synthesis and Δnce102, lead to increased Pil1 phosphorylation, Nce102 itself may be controlled by sphingolipids, acting upstream of the Pkh kinases. Alternatively, Nce102 could be required for efficient synthesis of sphingolipids that are then sensed by the kinases by some other route. One more possibility is that Nce102 acts independently of sphingolipids to regulate Pkh kinases.

To distinguish between these possibilities, we tested whether Nce102 is required for the synthesis of sphingoid bases. If this was the case, addition of exogenous sphingoid base would rescue the Δnce102 phenotype. Exogenously added sphingoid bases can enter the cell and rescue a sphingoid base synthesis defect because addition of 5 μM PHS suppressed the Pil1-GFP phenotype of the lcb1-100 mutant (which impairs sphingolipid synthesis) both at the permissive and restrictive temperatures (Fig. 7 a). In contrast, the eisosome defect of Δnce102 cells was not rescued by addition of PHS under conditions that rescued the lcb1-100 mutant phenotype (Fig. 7 a) or by a 10-fold higher concentration of PHS (unpublished data). Quantitation of eisosome number and cytosolic Pil1 levels confirmed the visual evaluation (Fig. 7 b).

These data show that Nce102 is not required for sphingoid base synthesis but rather acts downstream of it. Because PHS has no additive effect on Δnce102 cells, sphingolipids and Nce102 act in the same pathway (Fig. 7 b).

To further test this hypothesis, we investigated the interaction between myriocin treatment and Δnce102. If both act independent from each other, we expect an additive effect between them. However, this is not the case. As shown in images and quantitation of eisosomes, myriocin has no further effect on eisosomes in Δnce102 cells, confirming that sphingolipid signaling and Nce102 act in the same pathway on eisosomes (Fig. 7, c and d).

We previously showed that Pil1 hyperphosphorylation caused by decreased sphingolipid synthesis causes eisosome disassembly (Walther et al., 2007). If our hypothesis is true and Nce102 is an inhibitor of Pil1 phosphorylation acting downstream
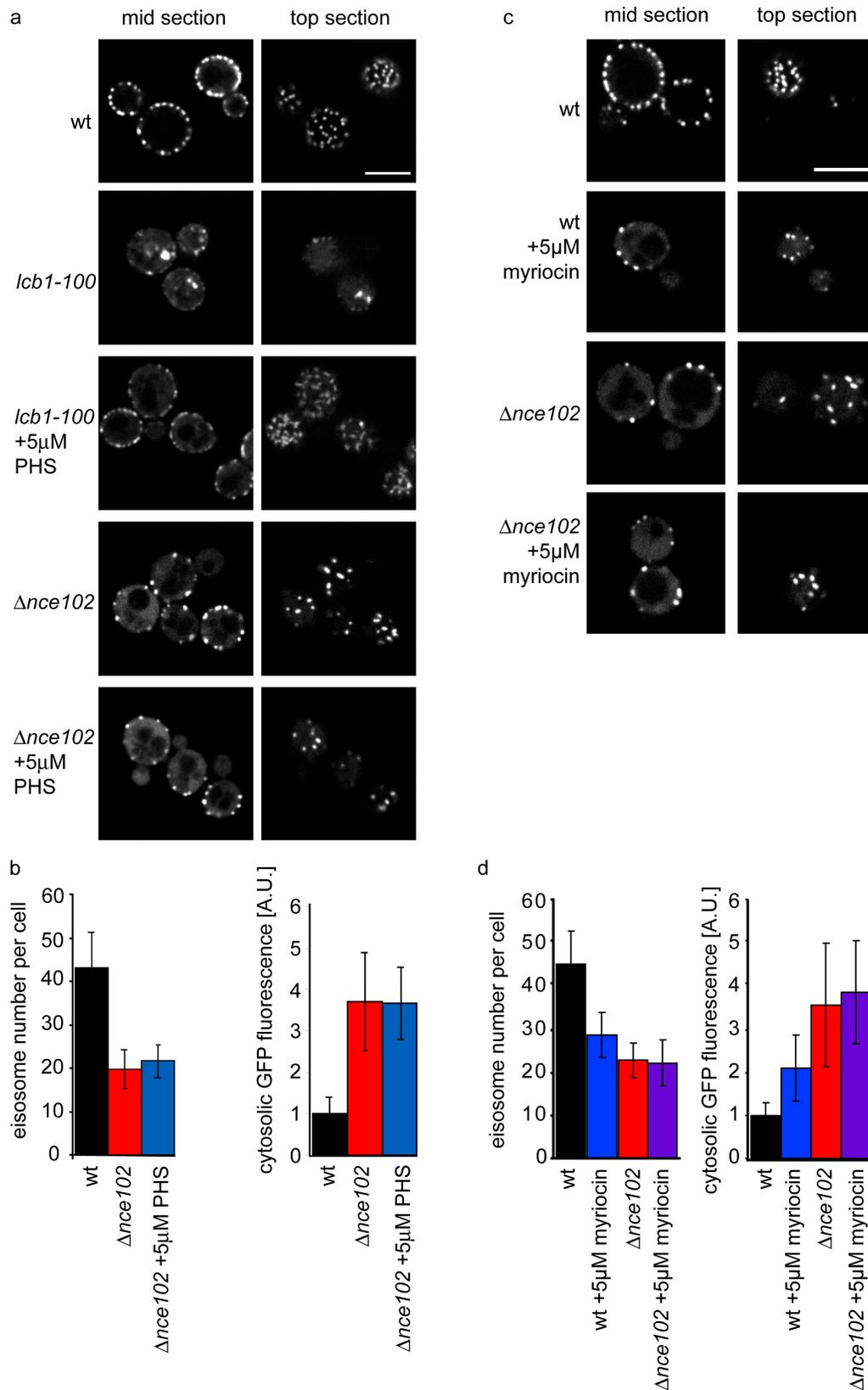
Figure 7. **Nce102 and sphingolipids act in the same pathway.** (a) *lcb1-100* but not Δ*nce102* is suppressed by sphingoid bases. Wild-type (wt), *lcb1-100,* or Δ*nce102* cells expressing Pil1-GFP were analyzed with or without addition of 5 µM PHS, and representative images are shown. (b) Eisosome number per mother cell (left) and cytosolic Pil1-GFP fluorescence (right) are shown. (c) Myriocin has no additive effect on Δ*nce102* cells. Wild-type and Δ*nce102* cells were treated for 1 h with 5 µM myriocin, and representative images are shown. (d) Quantitation of eisosome number per mother cell (left) and cytoplasmic Pil1-GFP fluorescence (right) of cells treated as in c. Error bars indicate SD. Bars, 5 µm.

of sphingolipids, we predict that overexpression of Nce102 will rescue eisosome disassembly when sphingolipid synthesis is decreased. To test this, we expressed Nce102-mars from the inducible Gal promoter in cells that have Pil1-GFP–marked eisosomes. When these cells are grown on raffinose, Nce102-mars is not expressed, and eisosomes appear normal, as these cells also express endogenous Nce102 (Fig. 8). When these cells grow on galactose, Nce102-mars is overexpressed (Fig. 8). Strikingly, when we blocked sphingolipid synthesis in these cells by treating them with myriocin, the normal effect of disassembling eisosomes apparent in control cells was completely blocked (Fig. 8). This shows that increasing Nce102 levels blocks the effect of inhibiting sphingolipid synthesis on eisosomes.

Together, our genetic experiments thus place Nce102 in a linear pathway inhibiting Pkh kinases and suggest a relationship: sphingoid bases → Nce102–| Pkh1/2 → Pil1 phosphorylation → eisosome disassembly. In this scenario, Nce102 would function as part of a sensor relay for sphingoid base or sphingolipid levels.

Nce102 localization responds to changes in sphingolipid levels

Because Nce102 negatively regulates Pkh kinases that localize to eisosomes, we next tested whether Nce102 distribution between MCCs at eisosomes and the rest of the plasma membrane is affected by sphingolipid levels. To this end, we determined Nce102-GFP localization after blocking sphingolipid synthesis. Strikingly, after a 1 h incubation of cells with myriocin, the punctate pattern of Nce102-GFP localization in MCCs disappeared, and the protein distributed diffusely across the plasma membrane (Fig. 9 a). Consistently, in intensity plots of surface images, myriocin-treated cells show a rather flat distribution of the Nce102-GFP signal, whereas control samples show many Nce102-GFP peaks corresponding to MCCs at eisosomes (Fig. 9 b). Relocalization of Nce102-GFP could be reversed by addition of exogenous PHS for a short time (15 min). In this case, the MCC pattern of Nce102-GFP localization reappeared, showing an even more pronounced pattern of Nce102-GFP foci than normal (Fig. 9 b).

Nce102 relocalization could be caused by redistribution of existing protein in the plasma membrane or new protein synthesis under conditions in which myriocin blocks the efficient incorporation of Nce102 in MCCs. To distinguish these possibilities, we added myriocin after a preincubation with the translation-blocking drug cycloheximide. During persistent translation block, Nce102 localized normally to MCCs and the remainder of the membrane (Fig. 9 c). Moreover, it still relocalized from MCCs after myriocin treatment, indicating that this phenomenon is not dependent on protein synthesis (Fig. 9 c). Similarly, when PHS was added to cells in which translation was blocked, Nce102 relocalization occurred normally (Fig. 9 c).

To test whether this effect is specific to the availability of sphingoid bases or a more general response to sphingolipid levels, we added aureobasidin to cells for 1 h. This drug inhibits complex sphingolipid synthesis from ceramide downstream of the formation of sphingoid bases (Nagiec et al., 1997). We observed the same Nce102-GFP redistribution in the plasma membrane after aureobasidin or myriocin addition (Fig. 9 a and

Pil1-GFP   pGalNce102-mars

raffinose

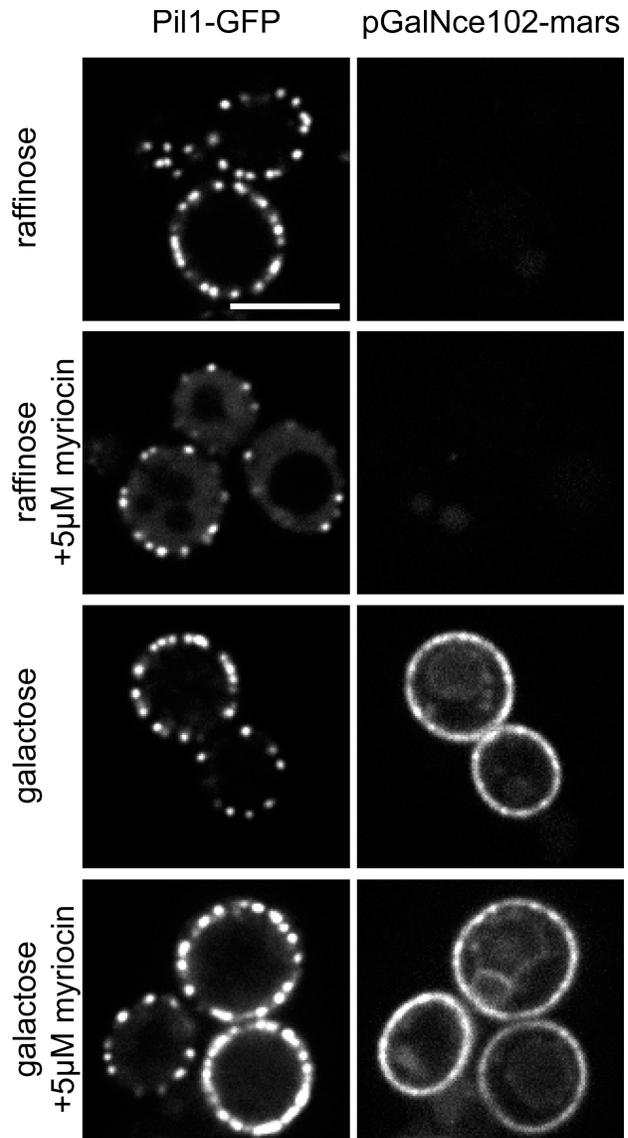raffinose +5µM myriocin

galactose

galactose +5µM myriocin

Figure 8. **Overexpression of Nce102 suppresses eisosomes disassembly after sphingolipid synthesis block.** Nce102-mars (right) controlled by the Gal promoter was either not expressed in raffinose-containing medium or induced in galactose-containing medium in Pil1-GFP (left) cells, which were incubated for 1 h with 5 µM myriocin as indicated. Bar, 5 µm.

Fig. S4). Consistent with the downstream block of sphingolipid synthesis by aureobasidin, addition of exogenous sphingoid bases did not result in reformation of the punctate Nce102 pattern (Fig. S4).

Together, these data suggest an equilibrium of two pools of Nce102-GFP localizing to MCCs at eisosomes or to spaces in between that is shifted by levels of sphingolipids. Consistent with this notion, addition of PHS to untreated cells shifted more Nce102-GFP into punctate structures, rendering them more pronounced (Fig. 9, a and b).

In the yeast plasma membrane, many proteins are sensitive to extraction by detergents to a different level, and Nce102 was previously described operationally as an abundant component of detergent-resistant membranes (Bagnat et al., 2000). To test whether Nce102 distribution between MCCs and the remainder

Figure 9. **Nce102-GFP localization depends on sphingolipid levels.** (a) Nce102-GFP was imaged under normal growth conditions (control), after addition of 5 µM myriocin for 1 h (myriocin), after sequential treatment with 5 µM myriocin for 1 h and 50 µM PHS for 15 min (myriocin→PHS), or after addition of 50 µM PHS for 15 min (PHS). Boxes indicate the area magnified in the bottom panels. (b) Fluorescence intensities of the area are shown plotted against xy image coordinates. (c) Nce102 redistribution is not dependent on new protein synthesis. Nce102-GFP cells were treated with myriocin or myriocin and PHS successively as in a after 10-min preincubation and continued presence of cycloheximide (CHX). (d) Nce102 partitions into detergent-resistant membranes dependent on sphingoid bases. Untreated Nce102-TAP–expressing cells and cells treated as in a were lysed in buffer containing 1% Triton X-100 and analyzed by gradient centrifugation and Western blotting against TAP (left). The same blots were probed with Pma1 antibodies (right). (e) pil1(4A)-GFP is resistant to disassembly after myriocin treatment. pil1(4A)-GFP–expressing cells were imaged after 1-h 5 µM myriocin incubation. (f) Redistribution of Nce102-GFP after myriocin treatment is independent of eisosome disassembly. Cells expressing pil1(4A) and Nce102-GFP were imaged before (left) and after 1 h treatment with 5 µM myriocin (right). (g and h) Sur7-mars does not behave like Nce102 after myriocin treatment. Wild-type Pil1 (g) or pil1(4A) (h) cells expressing Sur7-mars were treated with myriocin and imaged. wt, wild type. Bars, 5 µm.
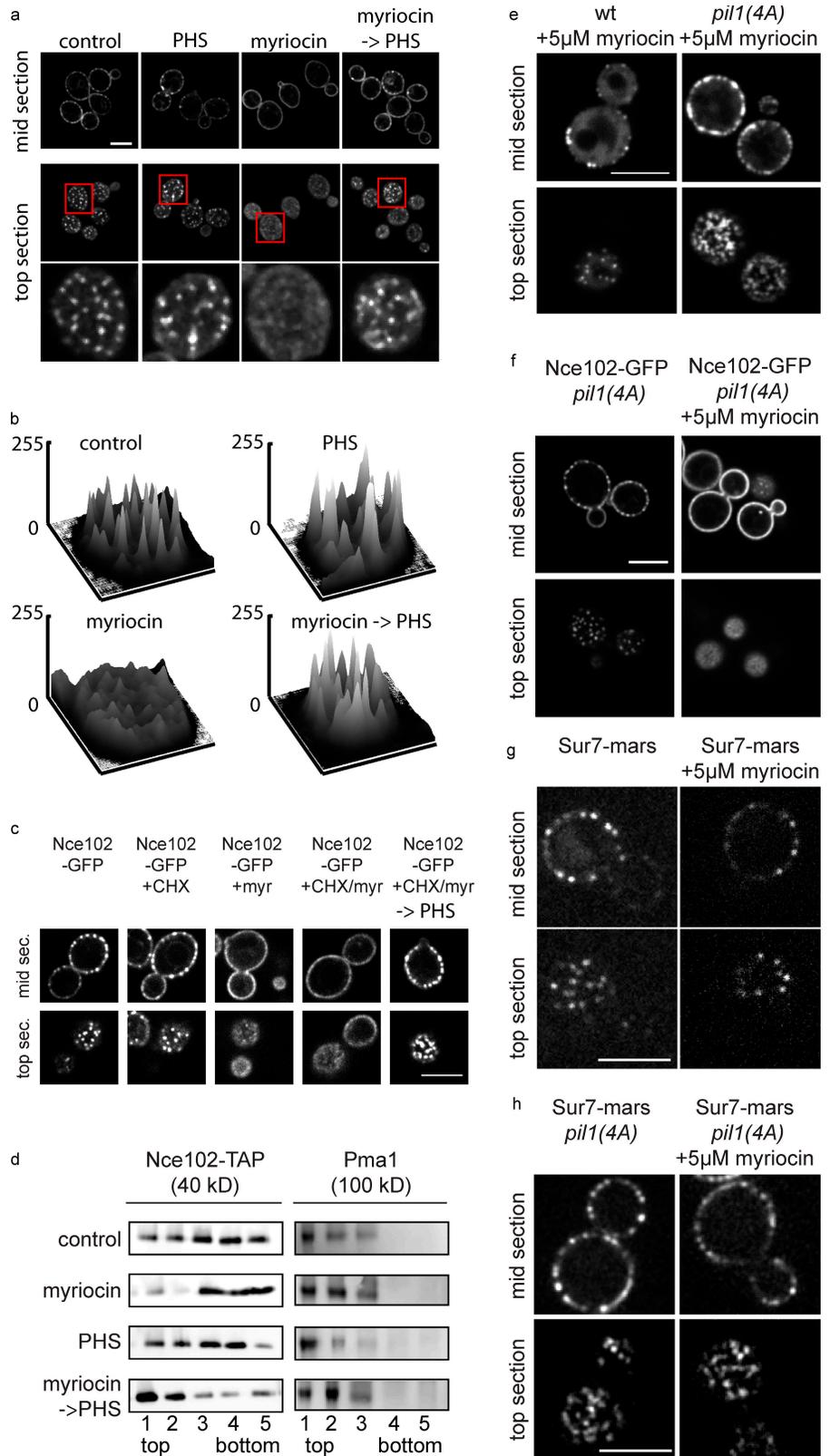
of the plasma membrane observed by microscopy is reflected in its partitioning between different membrane environments, we analyzed its solubility in a buffer containing 1% Triton X-100 at 4°C. Proteins partitioning into sphingolipid/ergosterol-rich domains show lower solubility in this buffer compared with

proteins embedded in mostly phospholipid bilayers. This difference can be tested in a velocity sedimentation gradient. Nce102 from untreated cells was present in most fractions of the gradient, indicating that it is localized both to detergent-resistant and other membranes (Fig. 9 d). When treated with myriocin, Nce102

partitioning changed toward the bottom of the gradient, indicating higher solubility. After short treatment of these cells with PHS, Nce102 redistributed to more detergent-insoluble membrane fractions at the top of the gradient. Pma1, a marker for MCP membranes, did not significantly alter its migration in the gradient after either myriocin or PHS treatment.

Together, these results show that relative levels of Nce102 in different plasma membrane domains are regulated by sphingolipids and that this redistribution is highly sensitive to changes in membrane composition because it can be observed after small perturbations that do not change Pma1 behavior. These data are consistent with the hypothesis that Nce102 sphingolipid-mediated redistribution is the mechanism by which Nce102 regulates Pil1 phosphorylation. In this model, Nce102 is recruited to MCCs at eisosomes under conditions of sufficient sphingolipids to repress Pkh kinase activity toward Pil1 and released from there when sphingolipid levels drop, for example, after inhibition of their synthesis by myriocin or aureobasidin. To test this, we determined the localization of Nce102-mars relative to Pkh kinases. Pkh2-GFP localizes in few very dim spots that colocalize with eisosomes and Nce102 foci (Fig. S5, a and b). Importantly, when we blocked sphingolipid synthesis with myriocin, Nce102-mars relocalized from these foci, leaving Pkh2-GFP behind (Fig. 5, c and d).

If Nce102 acts as a plasma membrane sphingolipid sensor, then its partitioning should be upstream and independent of the assembly state of eisosomes. Alternatively, Nce102 redistribution could be a consequence of eisosome disassembly after inhibition of sphingolipid synthesis. To test this directly, we used pil1(4A) mutant cells in which Pil1 cannot be sufficiently phosphorylated. Eisosomes are therefore resistant to activation of Pkh kinases (Walther et al., 2007). As expected, when cells that express pil1(4A)-GFP as their sole copy of Pil1 are incubated with myriocin, eisosomes remain stable because Pil1(4A) does not get sufficiently phosphorylated to disassemble (Fig. 9 e). To determine whether Nce102-GFP redistribution is caused by disassembly of eisosomes, we investigated the localization of Nce102-GFP in pil1(4A) cells. We found it to distribute normally in both MCCs and the remainder of the plasma membrane (Fig. 9 f). When we added myriocin to these cells, eisosomes remained assembled as a result of the pil1(4A) mutation, yet Nce102-GFP relocalized to become diffusely distributed throughout the plasma membrane (Fig. 9 f). To test whether this is a general property of MCC proteins, we performed similar experiments with cells expressing Sur7-mars. When we treated these cells with myriocin, the intensity of Sur7 signal in MCC decreased as Pil1 disassembled (Fig. 9 g; not depicted), but this could be completely blocked by expressing Pil1(4A) (Fig. 9 h). Thus, Nce102-GFP has a distinct behavior from other MCC components and redistributes in the plasma membrane dependent on sphingolipids but independently of the eisosome assembly state.

Discussion

We report a comprehensive screen for genes involved in Pil1-GFP localization. Recently, a similar screen using an MCC reporter identified 27 genes (Grossmann et al., 2008). Compared with that screen, we found roughly three times more genes affecting Pil1 localization ($n = 88$). It remains to be seen whether this difference is caused by different thresholding during the screen or biological differences between MCCs versus eisosomes. Because Pil1 and MCC components colocalize and PIL1 is required for normal MCC formation, it is surprising that there is little overlap between the two screens: only NCE102, SUR4, MNN10, and few biological processes were found in both. Examples include retrograde transport from the Golgi apparatus to the ER (VPS52 and VPS54 in the MCC screen; VPS51 and VPS53 in the Pil1 screen). Therefore, these genes and processes likely have a global effect on plasma membrane organization affecting MCCs and eisosomes. Genes that were identified only in one screen likely perform more specific functions; future experiments will, for example, show whether YMR086W, YMR031C, or genes encoding the NatC complex are important for eisosomes but not MCCs.

Besides genes globally affecting the plasma membrane, we expected to find genes impacting eisosome organization directly as well as genes that alter sphingolipid signaling, resulting in altered Pil1 phosphorylation and assembly. In the later class, we identified Nce102. Besides it, also SUR4, ISC1, and SAC1 are likely to act on eisosomes through sphingolipid signaling. Deletion of SUR4, required for fatty acid elongation during sphingolipid synthesis (Han et al., 2002; Paul et al., 2006), or deletion of ISC1, the homologue of mammalian neutral sphingomyelinase (Sawai et al., 2000), results in accumulation of complex sphingolipids. In our screen, both Δisc1 and Δsur4 cells showed hyperassembled Pil1-GFP, which is the opposite effect of depleting complex sphingolipids by inhibiting their synthesis (Table S2). In addition, it was recently reported that Δsac1 cells have elevated sphingoid bases and reduced levels of complex sphingolipids (Brice et al., 2009), and we found them to have fewer eisosomes and increased cytoplasmic Pil1-GFP signal (Table S2). We expect that other genes indentified will also turn out to play a role in sphingolipid biology.

In this study, we focused on the function of Nce102, a multispanning plasma membrane protein required for normal eisosomes, MCC formation, and plasma membrane organization. Initially, Nce102 was identified by Cleves et al. (1996) as required for nonclassical export of mammalian galectin from yeast. The mechanism of Nce102 function in this pathway was not investigated. Because the assay used requires solubilization of cell-associated galectin using high pH, it is possible that the basis of the effect could be altered protein extractability from Δnce102 cells because of their altered plasma membrane.

Our experiments revealed that Nce102 has fascinating properties, suggesting that it might act as part of a sphingolipid sensor. Most remarkable, its localization is dynamic and responsive to changes in sphingolipid levels: Nce102 partitions between two domains in the plasma membrane, MCCs overlying eisosomes and the rest of the plasma membrane. We show that the distribution between these two domains is controlled by sphingolipid availability. Nce102 localization to MCCs brings it into close contact with the underlying eisosomes and Pkh kinases (Fig. S5; Walther et al., 2007). Nce102 negatively regulates the activity of these kinases, and, in the presence of sphingolipids, blocks their downstream functions. Conversely, if sphingolipid

Figure 10. **Model for Nce102 function in sphingolipid sensing.** Nce102 (green) senses sphingolipid levels in the plasma membrane by distributing between the thick sphingolipid-rich MCC (blue) and the rest of the plasma membrane (gray) depending on sphingolipid levels. In the MCC, it inhibits Pkh kinases (red) that localize under this domain at eisosomes.
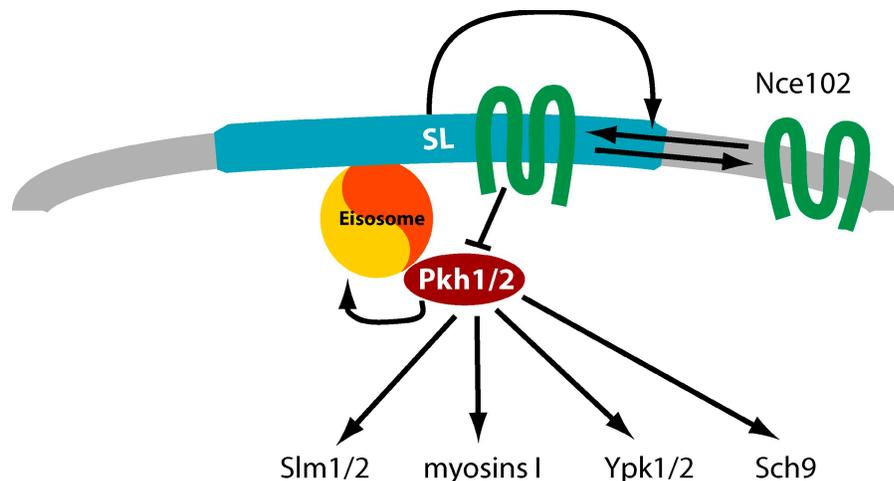
synthesis is blocked, Nce102 redistributes away from Pkh kinases (Fig. S5), alleviating their inhibition. Therefore, we propose a model that Nce102 acts as part of a sphingolipid-sensing mechanism and that its distribution in the plasma membrane regulates Pkh kinases (Fig. 10). In the simplest hypothesis, Nce102 could simply accomplish repression of the kinases by regulated juxtaposition to them, which is a common scheme in kinase signaling. Based on filipin staining, MCCs were suggested as sites of increased ergosterol concentration in the plasma membrane (Grossmann et al., 2007), and because sterols preferentially interact with sphingolipids, it is likely that sphingolipids are also concentrated there, forming detergent-resistant, liquid-ordered membrane domains or lipid rafts (Simons and Ikonen, 1997; Malinska et al., 2003) where Nce102 was found previously (Bagnat et al., 2000). Thus, it is possible that Nce102 also reacts to ergosterol levels in the plasma membrane. However, we did not observe an effect of nonessential *erg* mutants or block of sterol synthesis on eisosomes or Nce102 localization (unpublished data). Consistent with our model, Nce102 localizes to eisosome remnants that also show increased filipin staining, likely reflecting increased concentration of ergosterol and possibly sphingolipids (Grossmann et al., 2007). Alternatively, filipin might preferentially report on free sterols not in complex with sphingolipids, and staining of MCCs could actually indicate a lower concentration of sphingolipids in this compartment. This view is supported by a recent observation that filipin staining increases if sphingolipid synthesis is blocked (Jin et al., 2008). A further alternative is that Nce102 could directly bind sphingolipids, changing its affinities to other proteins that help localize it to MCCs and/or switching its activity as a Pkh kinase inhibitor on and off. In either model, Nce102 leaves the MCC when sphingolipid levels there are low, releasing its inhibition of Pkh kinases that now phosphorylate Pil1 and other targets. This is consistent with our observation that Nce102 detergent solubility changes after inhibition of sphingoid base synthesis, indicating that it partitions between different membrane environments. Most likely, this change corresponds to the relocalization of Nce102 from MCCs to the remainder of the membrane observed by microscopy. The interpretation of this result, however, remains vague, as most proteins in the yeast plasma membrane differ only in the degree

of their resistance to Triton X-100 detergent extraction. For example, the MCP marker Pma1 was also previously used as a marker for detergent-resistant lipid rafts (Bagnat et al., 2000; Lee et al., 2002; Malinska et al., 2003). The difference in Triton X-100 solubility between Nce102 and Pma1 after myriocin treatment might therefore indicate that these proteins differently partition into such lipid rafts or that the MCP is actually more complex and contains subdomains not easily resolved by light microscopy. Consistent with the later notion, TORC2 (Tor kinase complex 2) is localized at a distinct plasma membrane domain separate from MCC and MCP and is also partially detergent resistant (Aronova et al., 2007; Berchtold and Walther, 2009).

The sensing mechanism of sphingolipids in the plasma membrane by Nce102 suggested in this study is different from a previous model positing that soluble sphingoid bases in the cytoplasm directly control Pkh kinases (Zhang et al., 2004; Liu et al., 2005). It is possible that sphingolipids control the activity of Pkh kinases at many levels. Sphingoid bases could, for example, directly regulate Pkh kinases as in vitro experiments suggest (Zhang et al., 2004), and complex sphingolipids could affect signaling via Nce102. However, the in vivo effect of direct inhibition of Pkh kinase activity toward Pil1 by sphingoid bases is probably minor compared with the Nce102 pathway, as exogenously added PHS was not able to counteract the *Δnce102* hyperphosphorylation effect on eisosomes.

Our model of regulation of Pkh kinases by complex sphingolipids via the transmembrane protein Nce102 would also bridge the topological barrier between the cytoplasmic Pkh kinases and complex sphingolipids mainly concentrated in the outer leaflet of the plasma membrane (van Meer et al., 2008).

Downstream of sphingolipid sensing, the Nce102–Pkh pathway regulates phosphorylation of Pil1 that, when increased, always correlated with eisosome disassembly, e.g., in *Δnce102* cells. This effect could be blocked by mutating phosphorylated Pil1 residues to alanines that we previously found were required and sufficient for the effect of Pkh kinases on eisosomes (Walther et al., 2007). This is different from findings by Luo et al. (2008), who reported that a mutant form of Pil1 harboring five phosphosites mutated to alanine (S6A, S59A, T233A, S273A, and S299A) cannot assemble properly and argued that phosphorylation of Pil1

is important for assembly of eisosomes rather than disassembly. In this study, even a mutant that lacks these five sites and even two additional sites (S6A, S45A, S59A, S230A, T233A, S273A, and S299A) still assembles into eisosomes correctly (unpublished data). The reason for this difference is unclear but might indicate that additional pathways to the Nce102–Pkh kinase module regulate Pil1 phosphorylation in a complex fashion.

Besides phosphorylation of Pil1, Pkh kinases modify many plasma membrane functions. Therefore, as expected, $\Delta nce102$ cells show altered organization of the plasma membrane, as observed for MCCs, MCPs, and the endocytic foci marked by the lipophilic dye FM4-64. Recently, it was also shown that $\Delta nce102$ cells have accelerated endocytosis rates of some membrane transporters (Grossmann et al., 2008). Pkh kinases also participate in processes as diverse as cortical actin patch organization, cell integrity signaling, endocytosis, and eisosome organization (Inagaki et al., 1999; Sun et al., 2000; deHart et al., 2002; Roelants et al., 2002; Zhang et al., 2004; Liu et al., 2005; Grosshans et al., 2006; Walther et al., 2007; Luo et al., 2008). Regulation of these diverse processes may help control the composition of the plasma membrane according to need, perhaps constituting part of a negative feedback loop that targets genes involved in sphingolipid synthesis. Indeed, expression of such genes, e.g., *LCB2*, *FEN1*, and *SUR4*, is strongly negatively correlated to the expression of *NCE102* when the latter is regulated in response to various physiological conditions, e.g., during diauxic shift, nitrogen depletion, or heat shock (correlations for *NCE102/SUR4* are: diauxic shift, -0.94; nitrogen starvation, -0.66; and heat shock, -0.85; Fig. S3, b–d; DeRisi et al., 1997; Gasch et al., 2000). In addition, after prolonged incubation with PHS, we observed Nce102-GFP signal at the vacuole (unpublished data), perhaps reflecting an adaptation to recalibrate the set level of Pkh signaling after long times with high sphingolipids levels.

An important role of Nce102 in regulation of sphingolipids is also supported by the ability of its deletion to suppress the growth defect of a mutation in the serine palmitoyl transferase subunit *TSC3* (Schuldiner et al., 2005; unpublished data) or the growth inhibition caused by myriocin (Fig. S3 a), both of which reduce the first and rate-limiting step in sphingolipid synthesis.

Salient features of the sphingolipid–Nce102–Pkh kinase signaling network are likely conserved between yeast and other eukaryotes. Nce102 shares homology with the synaptogyrin/cellugyrin protein family (Belfort et al., 2005), but the molecular roles of these proteins are not understood. In contrast, mammalian PDK1 kinases (the homologues of yeast Pkh kinases) are well characterized, and the general architecture of downstream signaling is conserved (Casamayor et al., 1999). In either system, full activation of AGC kinases, such as AKT, Sch9, serum glucocorticoid kinase, or Ypk1/2, requires phosphorylation both by PDK1 (in mammalian cells) or Pkh kinases (in yeast) and in addition by the conserved kinase complex TORC2 (Powers, 2007). For yeast, TORC2 signaling has been implicated in the regulation of sphingolipid biosynthesis (Beeler et al., 1998; Tabuchi et al., 2006; Aronova et al., 2008). This effect of TORC2 is mediated by the Pkh kinase target Ypk2 (Aronova et al., 2008). Additionally, the Slm proteins were identified as targets of both the TORC2 and Pkh kinase signaling pathways

and to regulate a late step in the synthesis of complex sphingolipids (Tabuchi et al., 2006). It is therefore likely that the TORC2 and Pkh1/2 pathways collaborate to regulate sphingolipid metabolism in yeast. Given the similarity of the signaling pathway components and its architecture in higher eukaryotes, their output may also be evolutionarily conserved.

Materials and methods

Visual screen
To generate a library of deletion mutants each expressing Pil1-GFP, we performed a modification of the synthetic genetic array screen as described previously (Tong et al., 2001). In short, a *MAT*α strain containing a chromosomal copy of Pil1-GFP marked with a *NAT^R* marker, the *CAN1* gene disrupted by a construct that encodes the MATa promoter driving expression of the *HIS3* gene and the *LYP1* gene disrupted by a construct expressing *LEU2* from the MFα promoter (KEM108), was crossed to the *MAT*a deletion library BY4741 (each strain marked with *KAN^R*). Diploids were selected on G418 and nourseothricin and sporulated. From the sporulation, MATa haploids containing both Pil1-GFP and the deletion gene were selected with successive pinning on –HIS (selection for MATa cells), G418 (selection for the gene deletion from the library), canavanine (selection for haploid cells harboring *can1*Δ), S-(2-aminoethyl)-L-cysteine hydrochloride (selection for haploid cells harboring *lyp1*Δ), and nourseothricin (selection for Pil1-GFP)-containing media.

For imaging, cells were grown overnight to saturation in 384-well plates, transferred to 96-well plates, diluted, and grown for 9 h until they reached mid-log phase. Cells were transferred to glass-bottom 96-well plates coated with concanavalin A and imaged with a 40× high NA objective in an ImageXPress Micro (MDS Analytical Technologies). At least six different images were taken for each deletion strain.

The images were visually inspected using the software by the microscope manufacturer and classified using three categories: increased cytosolic Pil1-GFP fluorescence, altered number or eisosomes, and altered pattern of eisosomes. Strains that showed a phenotype in this first round of screening were regrown and imaged by using a confocal microscope (LSM510; Carl Zeiss, Inc.).

Two optical mid-section and two top-section images were taken for each strain, showing 15–40 cells per image. Images were visually analyzed, and several parameters of the Pil1-GFP signal on the surface of cells were quantitated using an image interpretation script developed in MATLAB that we named EISURAN (both the source code and an executable MATLAB file can be found at http://www.biochem.mpg.de/en/rg/walther/news/index.html). In short, EISURAN first subtracts background from the images and then finds the edge of a cell by image dilation. To facilitate the quantitation of signal from assembled Pil1, the script thresholds the image using Otsu's method (Otsu, 1979). From the resulting binary image, EISURAN calculates the number of positive pixels per cell, a measure for the area covered by eisosomes (percentage of cell surface covered by eisosomes). It then calculates the mean size of the connected clusters (mean pixel number per eisosome cluster on cell surface). To eliminate small background clusters, a minimum of 20 pixels are used for the lower cut off. In some conditions, very large values result caused by connection of eisosomes into very large clusters, which are sometimes string formed. To determine how much Pil1 is in individual eisosomes, EISURAN determines the mean intensity of each cluster by applying the binary image as a mask on the original image, integrating the intensity in each cluster, and averaging this intensity over all clusters in an image (mean integrated intensity per eisosome cluster on cell surface). Quantitation of eisosome number was based on the mean number of eisosomes counted by two independent observers in optical mid sections of mother cells (eisosome number; mean for the wild type = 11.5 ± 1.55).

The cytoplasmic signal was quantitated as the mean intensity of a 50 × 50–pixel area in the cytoplasm (cytoplasmic Pil1-GFP signal) visible in a confocal mid section of the cell using ImageJ (National Institutes of Health). The resulting values were averaged from at least 20 cells, analyzed by hierarchical clustering, and displayed using *R* software (http://www.r-project.org).

Yeast strains and plasmids
All yeast strains used as well as their genotypes are listed in Table S1. The starter strain used for the screen *Pil1-GFP::NAT^R* (KEM 108) was generated in the strain YMS196 (provided by N. Krogan, University of California,

San Francisco, San Francisco, CA) by tagging Pil1 with GFP using homologous recombination. *Nce102-GFP::HIS* and *Δnce102::NAT^R* were generated in the W303 wild-type strain by homologous recombination of PCR-generated fragments to yield strains TWY840 and TWY842, respectively (Janke et al., 2004). The *Δpil1:KAN^R NCE102-GFP::HIS* was similarly generated by homologous recombination, transforming the *NCE102-GFP* and marker into the *Δpil1* strain TWY226 to yield TWY836. Analogously, *Δnce102::NAT^R Pil1-GFP* was generated by transforming a *PIL1-GFP* fragment with an HIS marker into TWY842 to yield TWY837. The *Nce102-TAP:KAN^R* strain was generated by homologous recombination after transforming an Nce102-TAP fragment in the S288C wild-type strain to yield TWY897 (Janke et al., 2004). Strains harboring *pkh^ts* mutants and Pil1-GFP were described previously (Walther et al., 2007). *Δnce102::NAT^R* was generated by homologous recombination of a PCR fragment in a control strain with the same background as *pkh^ts* and used to derive a strain with *pkh1^ts Δpkh2::LEU Δnce102::NAT^R Pil1-GFP::URA* by crossing, sporulation, and selection of haploid cells to yield strain TWY932. All deletion strains were confirmed by PCR, and strains expressing tagged proteins were confirmed by PCR and Western blot analysis.

A *Δpil1::KAN^R Δnce102::NAT^R* strain was generated by crossing *Δpil1* strain TWY226 with the *Δnce102* strain TWY841. Sporulation and selection yield TWY898.

pRS306 plasmids containing the *PIL1* promoter, the wild type, or mutated ORF fused to GFP used for expression of phosphomimicking and nonphosphorylatable Pil1 were described previously (Walther et al., 2007) and were integrated into the URA locus of TWY898 to yield TWY931 and TWY934.

Pma1-GFP was created by PCR-mediated tagging in wild type or *Δnce102::NAT^R* to generate TWY958 and TWY1049, respectively. Similarly, *SUR7-GFP* strains were generated to yield TWY956 (wild type) and TWY1049 (*Δnce102*).

The pGalNce102-mars plasmid was created by cloning a fusion PCR product combining the Gal-promoter, the Nce102 ORF, and the mars sequence into the NotI and HindIII sites of pRS306. This plasmid was integrated into the *URA3* locus of TWY110 to yield TWY1222.

For SILAC labeling, the lysine auxotroph S288C strain TWY70 was transformed with a Pil1-TAP fragment to get the *Pil1-TAP:KAN^R* strain TWY1004 (Janke et al., 2004). To generate a *Pil1-TAP:KAN^R Δnce102:NAT^R* strain, TWY1004 was transformed with a *Δnce102* fragment yielding TWY1052 (Janke et al., 2004).

Yeast culture and drug treatment
Yeast cells were grown according to standard procedure. For microscopy, cells were grown in synthetic complete medium and bound to concanavalin A–treated coverslips. Myriocin (Sigma-Aldrich) and PHS (Sigma-Aldrich) were added in concentrations as indicated and incubated for 1 h or 15 min. Cycloheximide (Sigma-Aldrich) was added in a concentration of 100 µg/ml for 1 h and 15 min before treatment with other drugs.

For SILAC labeling, Pil1-TAP–expressing yeast cells in a wild-type or *Δnce102* background were grown in 1 l YNB liquid medium. *PIL1-TAP* cells were grown in the presence of 20 mg/l normal L-lysine, and *PIL1-TAP Δnce102* cells were grown in the presence of 20 mg/l L-lysine-U-$^{13}C_6$,$^{15}N_2$ overnight with at least 10 doublings to OD_{600} = 0.7.

Microscopy
For fluorescence microscopy, yeast cells were grown to OD = 0.6 in synthetic medium at 30°C unless indicated otherwise. Cells were mounted in synthetic media onto coverslips previously coated with concanavalin A and directly imaged with a spinning-disk confocal microscope (TiLL iMIC CSU22; Andoor) using a back-illuminated EM charge-coupled device camera (iXonEM 897; Andor) and a 100× 1.4 NA oil immersion objective (Olympus). From this setup, 16-bit images were collected using Image iQ (version 1.9; Andor) in the linear range of the camera. For presentation, images were filtered with a smoothening filter averaging 2 pixels, converted to 8-bit images, and cropped using ImageJ software (http://rsbweb.nih.gov/ij/).

FM4-64 assay
To measure the formation of early FM4-64 uptake intermediates, either wild-type or *Δnce102* cells were grown in mid-log phase to OD = 0.5. Approximately 5 ml cell culture was harvested by centrifugation and incubated on ice for 5 min. Cells were then labeled for 10 min with 40 µM FM4-64, washed three times in ice-cold medium, and resuspended in RT YPD for 5 min. Cells were killed by addition of 10 mM NaN$_3$ and NaF each and immediately analyzed by fluorescence microscopy.

Isolation of detergent-resistant membranes
Detergent-resistant membranes were isolated essentially as described previously (Bagnat et al., 2000). In brief, 20 ODs Nce102-TAP–expressing yeast cells were harvested by centrifugation. The pellets were washed once with water and lysed in TNE buffer (50 mM Tris-HCl, pH 7.4, 150 mM NaCl, and 5 mM EDTA) by vortexing with glass beads twice for 5 min each at 4°C. The lysate was cleared of unbroken cells by centrifugation at 500 g for 5 min and incubated with Triton X-100 (1% final) for 30 min on ice. 250 µl lysate was adjusted to 40% Optiprep by adding 500 µl of 60% Optiprep solution and overlaid with 1.2 ml of 30% Optiprep in TXNE (TNE and 0.1% Triton X-100) and 200 µl TXNE. The samples were centrifuged at 55,000 rpm for 2 h in a rotor (S55S; Sorvall), and five fractions of equal volume were collected from the top. Proteins of each fraction were precipitated with 10% trichloroacetic acid for 15 min on ice. Precipitates were resuspended in 50 µl 2× sample buffer (0.24 M Tris, pH 8.0, 8% SDS, 1 mM DTT, 40% glycerol, and 0.4% bromphenol blue) and heated at 65°C. 25-µl aliquots were loaded onto 12% SDS-PAGE gel and analyzed by Western blotting. Nce102-TAP was detected with a rabbit peroxidase antiperoxidase antibody (Sigma-Aldrich), Pma1 with a rabbit anti-Pma1 antibody (Santa Cruz Biotechnology, Inc.), and a horseradish peroxidase–coupled goat anti–rabbit IgG antibody (Santa Cruz Biotechnology, Inc.).

MS
700 ODs of light-labeled *PIL1-TAP* and heavy-labeled *PIL1-TAP Δnce102* cells were harvested by centrifugation resuspended in 5 ml of buffer (150 mM KOAc, 20 mM Hepes, pH 7.4, 10% glycerol, and complete protease inhibitor cocktail [Roche]) and phosphatase inhibitor cocktail (Sigma-Aldrich) and frozen in liquid nitrogen. Total protein was extracted by bead milling; the thawed lysates were incubated with Triton X-100 (1% final) for 30 min at 4°C and clarified by two consecutive spins of 4 min at 1,000 g. To immunopurify Pil1-TAP, equivalent amounts of the lysates of *PIL1-TAP* cells and *PIL1-TAP Δnce102* cells, according to the protein concentration, were incubated with IgG conjugated to agarose beads (GE Healthcare) for 2 h, washed, and eluted by TEV cleavage and centrifugation. The eluates were mixed, reduced for 20 min at RT in 1 mM DTT, and alkylated for 30 min by 5.5 mM iodoacetamide at RT in the dark. Nu-PAGE sample buffer (Invitrogen) was added, and the sample was loaded onto 4–12% Nu-PAGE Bis-Tris SDS-PAGE gels (Invitrogen). Two Pil1 bands were excised from the gel, and proteins were digested with endoproteinase LysC in gel overnight at RT. The resulting peptides were extracted with 30% acetonitrile and 3% trifluoroacetic acid, reduced in a speed vacuum centrifuge, and desalted and concentrated on a reversed-phase column (C18 StageTip; Rappsilber et al., 2003).

In a different approach, the mixed eluates were precipitated with chloroform/methanol and resuspended in 8 M urea. Proteins were alkylated, reduced, and directly digested in solution overnight at RT with LysC. Peptides were desalted and concentrated on StageTips. Peptides were eluted from the StageTips by passage of 2× 20 µl solvent B (80% acetonitrile and 0.5% acetic acid). The volume was reduced to 4 µl in a speed vacuum centrifuge, and 2 µl solvent A* (2% acetonitrile and 1% trifluoroacetic acid) was added to acidify the sample. Peptides were separated on line to the mass spectrometer by using an HPLC system (1200; Agilent Technologies). 5-µl samples were loaded with constant flow of 500 nl/min onto a 15-cm fused silica emitter with an inner diameter of 75 µm (Proxeon Biosystems) packed in house with reverse-phase 3-µm resin (ReproSil-Pur C18-AQ; provided by Dr. Maisch GmbH). Peptides were eluted with a segmented gradient of 10–60% solvent B over 110 min with a constant flow of 250 nl/min. The HPLC system was coupled to a mass spectrometer (linear trap quadrupole Orbitrap; Thermo Fisher Scientific) via a nanoscale LC interface (Proxeon Biosystems). The spray voltage was set to 2.2 kV, and the temperature of the heated capillary was set to 180°C.

The mass spectrometer was operated in positive-ion mode. Survey full-scan MS spectra (m/z = 300–1,600) were acquired with a resolution of 60,000 at m/z = 400 after accumulation of 1,000,000 ions. The most intense ions (up to five) from the preview survey scan delivered by the Orbitrap were sequenced by collision-induced dissociation (collision energy 35%) in the linear trap quadrupole after accumulation of 5,000 ions. Multistage activation was enabled in all MS/MS events to improve fragmentation of phosphopeptides. Maximal filling times were 1,000 ms for the full scans and 150 ms for the MS/MS. Precursor ion charge state screening was enabled, and all unassigned charge states as well as singly charged peptides were rejected. The dynamic exclusion list was restricted to a maximum of 500 entries with a maximum retention period of 90 s and a relative mass window of 10 ppm. Orbitrap measurements were performed enabling the lock mass option for survey scans to improve mass accuracy (Olsen et al., 2005). Data were acquired using the Xcalibur software (version 2.0.5).

Mass spectra were analyzed using the in house–developed software MaxQuant (version 1.0.1; Cox and Mann, 2008). The data were searched against the yeast database concatenated with reversed copies of all sequences (Moore et al., 2002; Peng et al., 2003) and supplemented with frequently observed contaminants (porcine trypsin, *Achromobacter lyticus* lysyl-endopeptidase, and human keratins) using Mascot (version 2.2.0; Matrix Science; Perkins et al., 1999).

Carbamidomethylated cysteines were set as fixed, oxidation of methionine, N-terminal acetylation and phosphorylation of serines, threonines, and tyrosines as variable modification. 0.5 D was set as maximum-allowed mass deviation for MS/MS peaks, and a maximum of three missed cleavages were allowed. Maximum false discovery rates were set to 0.01 both on peptide and protein levels. Minimum-required peptide length was six amino acids. Proteins with at least two peptides (thereof one uniquely assignable to the respective sequence) were considered identified.

Online supplemental material

Fig. S1 shows a flowchart of the screening process and the quantitation of Pil1-GFP mutant phenotypes. Fig. S2 shows mass spectrometric analysis of Pil1 phosphorylation in wild-type and *Δnce102* or myriocin-treated and -untreated control cells. Fig. S3 shows growth curves of *Δnce102* and wild-type cells untreated or treated with myriocin as well as microarray profiles of *NCE102* versus sphingolipid biosynthesis gene expression. Fig. S4 shows Nce102-GFP localization depending on sphingolipids, phosphomimicking Pil1 mutant being enhanced by deletion of *NCE102*, and epistasis between *Δnce102* and Pkh kinase mutants. Fig. S5 shows colocalization of Pkh2 and Nce102 depending on sphingolipid synthesis. Table S1 contains yeast strains used. Table S2 shows the phenotypes and classification of Pil1-GFP visual screen hits. Online supplemental material is available at http://www.jcb.org/cgi/content/full/jcb.200811081/DC1.

References

Anderson, R.G., and K. Jacobson. 2002. A role for lipid shells in targeting proteins to caveolae, rafts, and other lipid domains. *Science.* 296:1821–1825.

Aronova, S., K. Wedaman, S. Anderson, J. Yates III, and T. Powers. 2007. Probing the membrane environment of the TOR kinases reveals functional interactions between TORC1, actin, and membrane trafficking in *Saccharomyces cerevisiae. Mol. Biol. Cell.* 18:2779–2794.

Aronova, S., K. Wedaman, P.A. Aronov, K. Fontes, K. Ramos, B.D. Hammock, and T. Powers. 2008. Regulation of ceramide biosynthesis by TOR complex 2. *Cell Metab.* 7:148–158.

Bagnat, M., S. Keranen, A. Shevchenko, A. Shevchenko, and K. Simons. 2000. Lipid rafts function in biosynthetic delivery of proteins to the cell surface in yeast. *Proc. Natl. Acad. Sci. USA.* 97:3254–3259.

Beeler, T., D. Bacikova, K. Gable, L. Hopkins, C. Johnson, H. Slife, and T. Dunn. 1998. The *Saccharomyces cerevisiae* TSC10/YBR265w gene encoding 3-ketosphinganine reductase is identified in a screen for temperature-sensitive suppressors of the Ca2+-sensitive csg2Δ mutant. *J. Biol. Chem.* 273:30688–30694.

Belfort, G.M., K. Bakirtzi, and K.V. Kandror. 2005. Cellugyrin induces biogenesis of synaptic-like microvesicles in PC12 cells. *J. Biol. Chem.* 280:7262–7272.

Berchtold, D., and T.C. Walther. 2009. TORC2 plasma membrane localization is essential for cell viability and restricted to a distinct domain. *Mol. Biol. Cell.* 20:1565–1575.

Brice, S.E., C.W. Alford, and L.A. Cowart. 2009. Modulation of sphingolipid metabolism by the phosphatidylinositol-4-phosphate phosphatase Sac1p through regulation of phosphatidylinositol in *Saccharomyces cerevisiae. J. Biol. Chem.* 284:7588–7596.

Casamayor, A., P.D. Torrance, T. Kobayashi, J. Thorner, and D.R. Alessi. 1999. Functional counterparts of mammalian protein kinases PDK1 and SGK in budding yeast. *Curr. Biol.* 9:186–197.

Cleves, A.E., D.N. Cooper, S.H. Barondes, and R.B. Kelly. 1996. A new pathway for protein export in *Saccharomyces cerevisiae. J. Cell Biol.* 133:1017–1026.

Cox, J., and M. Mann. 2008. MaxQuant enables high peptide identification rates, individualized p.p.b.-range mass accuracies and proteome-wide protein quantification. *Nat. Biotechnol.* 26:1367–1372.

Daquinag, A., M. Fadri, S.Y. Jung, J. Qin, and J. Kunz. 2007. The yeast PH domain proteins Slm1 and Slm2 are targets of sphingolipid signaling during the response to heat stress. *Mol. Cell. Biol.* 27:633–650.

deHart, A.K., J.D. Schnell, D.A. Allen, and L. Hicke. 2002. The conserved Pkh–Ypk kinase cascade is required for endocytosis in yeast. *J. Cell Biol.* 156:241–248.

Deng, C., X. Xiong, and A.N. Krutchinsky. 2009. Unifying fluorescence microscopy and mass spectrometry for studying protein complexes in cells. *Mol. Cell. Proteomics.* 8:1413–1423.

DeRisi, J.L., V.R. Iyer, and P.O. Brown. 1997. Exploring the metabolic and genetic control of gene expression on a genomic scale. *Science.* 278:680–686.

Fischer, M., I. Haase, E. Simmeth, G. Gerisch, and A. Muller-Taubenberger. 2004. A brilliant monomeric red fluorescent protein to visualize cytoskeleton dynamics in *Dictyostelium. FEBS Lett.* 577:227–232.

Friant, S., R. Lombardi, T. Schmelzle, M.N. Hall, and H. Riezman. 2001. Sphingoid base signaling via Pkh kinases is required for endocytosis in yeast. *EMBO J.* 20:6783–6792.

Gasch, A.P., P.T. Spellman, C.M. Kao, O. Carmel-Harel, M.B. Eisen, G. Storz, D. Botstein, and P.O. Brown. 2000. Genomic expression programs in the response of yeast cells to environmental changes. *Mol. Biol. Cell.* 11:4241–4257.

Grosshans, B.L., H. Grotsch, D. Mukhopadhyay, I.M. Fernandez, J. Pfannstiel, F.Z. Idrissi, J. Lechner, H. Riezman, and M.I. Geli. 2006. TEDS site phosphorylation of the yeast myosins I is required for ligand-induced but not for constitutive endocytosis of the G protein-coupled receptor Ste2p. *J. Biol. Chem.* 281:11104–11114.

Grossmann, G., M. Opekarova, J. Malinsky, I. Weig-Meckl, and W. Tanner. 2007. Membrane potential governs lateral segregation of plasma membrane proteins and lipids in yeast. *EMBO J.* 26:1–8.

Grossmann, G., J. Malinsky, W. Stahlschmidt, M. Loibl, I. Weig-Meckl, W.B. Frommer, M. Opekarova, and W. Tanner. 2008. Plasma membrane microdomains regulate turnover of transport proteins in yeast. *J. Cell Biol.* 183:1075–1088.

Han, G., K. Gable, S.D. Kohlwein, F. Beaudoin, J.A. Napier, and T.M. Dunn. 2002. The *Saccharomyces cerevisiae* YBR159w gene encodes the 3-ketoreductase of the microsomal fatty acid elongase. *J. Biol. Chem.* 277:35440–35449.

Huh, W.K., J.V. Falvo, L.C. Gerke, A.S. Carroll, R.W. Howson, J.S. Weissman, and E.K. O'Shea. 2003. Global analysis of protein localization in budding yeast. *Nature.* 425:686–691.

Inagaki, M., T. Schmelzle, K. Yamaguchi, K. Irie, M.N. Hall, and K. Matsumoto. 1999. PDK1 homologs activate the Pkc1-mitogen-activated protein kinase pathway in yeast. *Mol. Cell. Biol.* 19:8344–8352.

Janke, C., M.M. Magiera, N. Rathfelder, C. Taxis, S. Reber, H. Maekawa, A. Moreno-Borchart, G. Doenges, E. Schwob, E. Schiebel, and M. Knop. 2004. A versatile toolbox for PCR-based tagging of yeast genes: new fluorescent proteins, more markers and promoter substitution cassettes. *Yeast.* 21:947–962.

Jin, H., J.M. McCaffery, and E. Grote. 2008. Ergosterol promotes pheromone signaling and plasma membrane fusion in mating yeast. *J. Cell Biol.* 180:813–826.

Lee, M.C., S. Hamamoto, and R. Schekman. 2002. Ceramide biosynthesis is required for the formation of the oligomeric H+-ATPase Pma1p in the yeast endoplasmic reticulum. *J. Biol. Chem.* 277:22395–22401.

Liu, K., X. Zhang, R.L. Lester, and R.C. Dickson. 2005. The sphingoid long chain base phytosphingosine activates AGC-type protein kinases in *Saccharomyces cerevisiae* including Ypk1, Ypk2, and Sch9. *J. Biol. Chem.* 280:22679–22687.

Luo, G., A. Gruhler, Y. Liu, O.N. Jensen, and R.C. Dickson. 2008. The sphingolipid long-chain base-Pkh1/2-Ypk1/2 signaling pathway regulates eisosome assembly and turnover. *J. Biol. Chem.* 283:10433–10444.

Malinska, K., J. Malinsky, M. Opekarova, and W. Tanner. 2003. Visualization of protein compartmentation within the plasma membrane of living yeast cells. *Mol. Biol. Cell.* 14:4427–4436.

Malinska, K., J. Malinsky, M. Opekarova, and W. Tanner. 2004. Distribution of Can1p into stable domains reflects lateral protein segregation within the plasma membrane of living *S. cerevisiae* cells. *J. Cell Sci.* 117:6031–6041.

Moore, R.E., M.K. Young, and T.D. Lee. 2002. Qscore: an algorithm for evaluating SEQUEST database search results. *J. Am. Soc. Mass Spectrom.* 13:378–386.

Nagiec, M.M., E.E. Nagiec, J.A. Baltisberger, G.B. Wells, R.L. Lester, and R.C. Dickson. 1997. Sphingolipid synthesis as a target for antifungal drugs. Complementation of the inositol phosphorylceramide synthase defect in a mutant strain of *Saccharomyces cerevisiae* by the *AUR1* gene. *J. Biol. Chem.* 272:9809–9817.

Olsen, J.V., L.M. de Godoy, G. Li, B. Macek, P. Mortensen, R. Pesch, A. Makarov, O. Lange, S. Horning, and M. Mann. 2005. Parts per million mass accuracy on an Orbitrap mass spectrometer via lock mass injection into a C-trap. *Mol. Cell. Proteomics.* 4:2010–2021.

Ong, S.E., B. Blagoev, I. Kratchmarova, D.B. Kristensen, H. Steen, A. Pandey, and M. Mann. 2002. Stable isotope labeling by amino acids in cell culture, SILAC, as a simple and accurate approach to expression proteomics. *Mol. Cell. Proteomics.* 1:376–386.

Otsu, N. 1979. A threshold selection method from gray-level histograms. *IEEE Trans. Sys.* 9:62–66.

Paul, S., K. Gable, F. Beaudoin, E. Cahoon, J. Jaworski, J.A. Napier, and T.M. Dunn. 2006. Members of the *Arabidopsis* FAE1-like 3-ketoacyl-CoA synthase gene family substitute for the Elop proteins of *Saccharomyces cerevisiae*. *J. Biol. Chem.* 281:9018–9029.

Peng, J., J.E. Elias, C.C. Thoreen, L.J. Licklider, and S.P. Gygi. 2003. Evaluation of multidimensional chromatography coupled with tandem mass spectrometry (LC/LC-MS/MS) for large-scale protein analysis: the yeast proteome. *J. Proteome Res.* 2:43–50.

Perkins, D.N., D.J. Pappin, D.M. Creasy, and J.S. Cottrell. 1999. Probability-based protein identification by searching sequence databases using mass spectrometry data. *Electrophoresis.* 20:3551–3567.

Powers, T. 2007. TOR signaling and S6 kinase 1: yeast catches up. *Cell Metab.* 6:1–2.

Rappsilber, J., Y. Ishihama, and M. Mann. 2003. Stop and go extraction tips for matrix-assisted laser desorption/ionization, nanoelectrospray, and LC/MS sample pretreatment in proteomics. *Anal. Chem.* 75:663–670.

Roelants, F.M., P.D. Torrance, N. Bezman, and J. Thorner. 2002. Pkh1 and pkh2 differentially phosphorylate and activate ypk1 and ykr2 and define protein kinase modules required for maintenance of cell wall integrity. *Mol. Biol. Cell.* 13:3005–3028.

Sawai, H., Y. Okamoto, C. Luberto, C. Mao, A. Bielawska, N. Domae, and Y.A. Hannun. 2000. Identification of ISC1 (YER019w) as inositol phosphosphingolipid phospholipase C in *Saccharomyces cerevisiae*. *J. Biol. Chem.* 275:39793–39798.

Schuldiner, M., S.R. Collins, N.J. Thompson, V. Denic, A. Bhamidipati, T. Punna, J. Ihmels, B. Andrews, C. Boone, J.F. Greenblatt, et al. 2005. Exploration of the function and organization of the yeast early secretory pathway through an epistatic miniarray profile. *Cell.* 123:507–519.

Simons, K., and E. Ikonen. 1997. Functional rafts in cell membranes. *Nature.* 387:569–572.

Simons, K., and D. Toomre. 2000. Lipid rafts and signal transduction. *Nat. Rev. Mol. Cell Biol.* 1:31–39.

Simons, K., and W.L. Vaz. 2004. Model systems, lipid rafts, and cell membranes. *Annu. Rev. Biophys. Biomol. Struct.* 33:269–295.

Sun, Y., R. Taniguchi, D. Tanoue, T. Yamaji, H. Takematsu, K. Mori, T. Fujita, T. Kawasaki, and Y. Kozutsumi. 2000. Sli2 (Ypk1), a homologue of mammalian protein kinase SGK, is a downstream kinase in the sphingolipid-mediated signaling pathway of yeast. *Mol. Cell. Biol.* 20:4411–4419.

Tabuchi, M., A. Audhya, A.B. Parsons, C. Boone, and S.D. Emr. 2006. The phosphatidylinositol 4,5-biphosphate and TORC2 binding proteins Slm1 and Slm2 function in sphingolipid regulation. *Mol. Cell. Biol.* 26:5861–5875.

Tong, A.H., M. Evangelista, A.B. Parsons, H. Xu, G.D. Bader, N. Pagé, M. Robinson, S. Raghibizadeh, C.W. Hogue, H. Bussey, et al. 2001. Systematic genetic analysis with ordered arrays of yeast deletion mutants. *Science.* 294:2364–2368.

van Meer, G., D.R. Voelker, and G.W. Feigenson. 2008. Membrane lipids: where they are and how they behave. *Nat. Rev. Mol. Cell Biol.* 9:112–124.

Vida, T.A., and S.D. Emr. 1995. A new vital stain for visualizing vacuolar membrane dynamics and endocytosis in yeast. *J. Cell Biol.* 128:779–792.

Walther, T.C., J.H. Brickner, P.S. Aguilar, S. Bernales, C. Pantoja, and P. Walter. 2006. Eisosomes mark static sites of endocytosis. *Nature.* 439:998–1003.

Walther, T.C., P.S. Aguilar, F. Frohlich, F. Chu, K. Moreira, A.L. Burlingame, and P. Walter. 2007. Pkh-kinases control eisosome assembly and organization. *EMBO J.* 26:4946–4955.

Zhang, X., R.L. Lester, and R.C. Dickson. 2004. Pil1p and Lsp1p negatively regulate the 3-phosphoinositide-dependent protein kinase-like kinase Pkh1p and downstream signaling pathways Pkc1p and Ypk1p. *J. Biol. Chem.* 279:22030–22038.
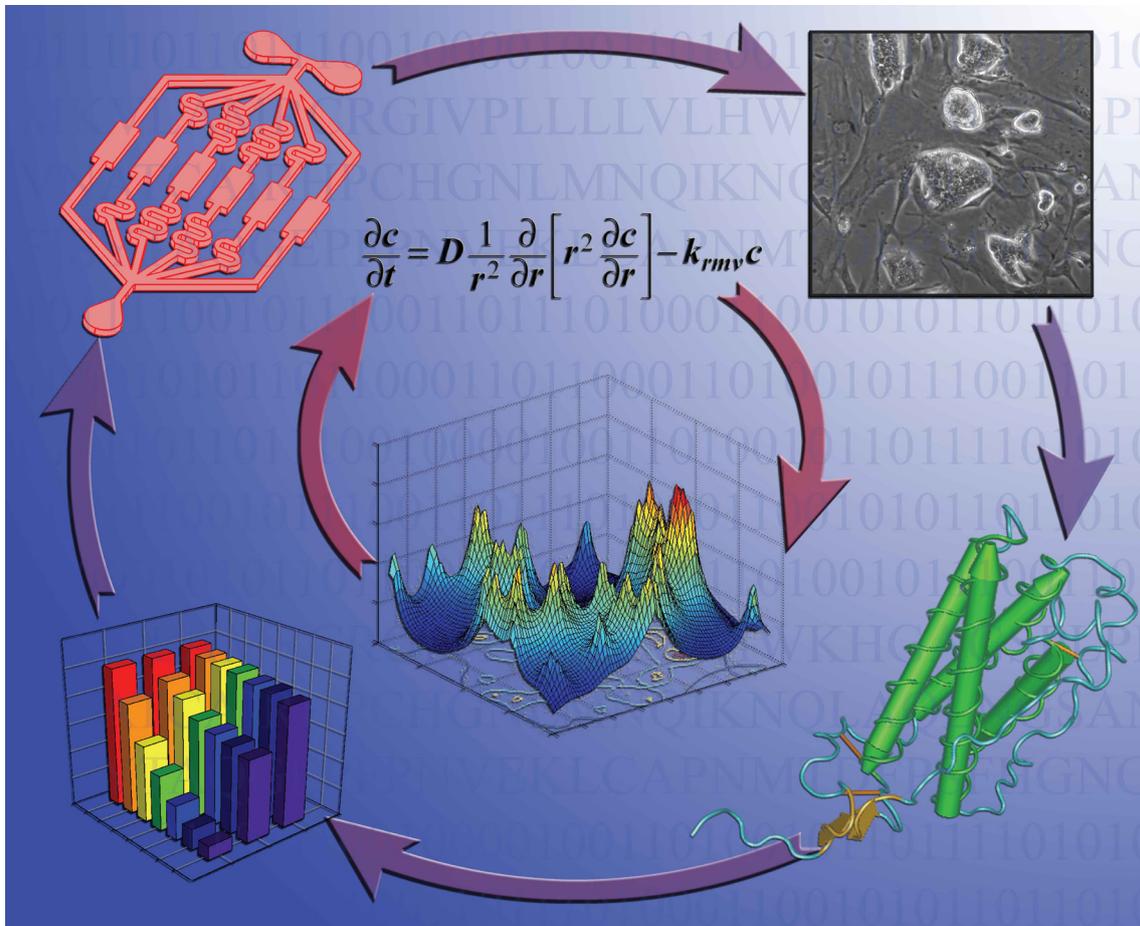
Molecular BioSystems

This article was published as part of the

2009 Emerging Investigators Issue

Highlighting the work of outstanding young scientists at the chemical- and systems-biology interfaces

Please take a look at the full table of contents to access the other papers in this issue.

$$\frac{\partial c}{\partial t} = D \frac{1}{r^2} \frac{\partial}{\partial r}\left[r^2 \frac{\partial c}{\partial r} \right] - k_{rmv}c$$

Global analysis of the yeast osmotic stress response by quantitative proteomics†‡

Boumediene Soufi,§[ab] Christian D. Kelstrup,§[ac] Gabriele Stoehr,[c] Florian Fröhlich,[d] Tobias C. Walther[d] and Jesper V. Olsen*[ac]

Information on extracellular signals and conditions is often transduced by biological systems using cascades of protein phosphorylation that affect the activity of enzymes, the localization of proteins and gene expression. A model to study signal transduction is the response of the yeast *Saccharomyces cerevisiae* to osmotic changes as it shares many central themes with information processing modules in higher eukaryotes. Despite considerable progress in our understanding of this pathway, the scale and dynamics of this system have not been addressed systematically yet. Here, we report a comprehensive, quantitative, and time-resolved analysis using high-resolution mass spectrometry of phospho-proteome and proteome changes in response to osmotic stress in yeast. We identified 5534 unique phosphopeptide variants and 3383 yeast proteins. More than 15% of the detected phosphorylation site status changed more than two-fold within 5 minutes of treatment. Many of the corresponding phosphoproteins are involved in the early response to environmental stress. Surprisingly, we find that 158 regulated phosphorylation sites are potential substrates of basophilic kinases as opposed to the classical proline-directed MAP kinase network implicated in stress response mechanisms such as p38 and HOG pathways. Proteome changes reveal an increase in abundance of more than one hundred proteins after 20 min of salt stress. Many of these are involved in the cellular response to increased osmolarity, which include proteins used for glycerol production that is up-regulated to counterbalance the increased osmolarity of the salt containing growth medium. Although the overall relationship between our proteome and published mRNA changes is poor we find an excellent correlation between the subset of osmotic shock up-regulated proteins and their corresponding mRNA changes.

Introduction

Changes of external conditions or signals from the environment often have far-ranging consequences in the cell. To mediate these responses, cells use networks of kinases that alter the phosphorylation status and concomitantly the activity of many factors. Due to their central importance to understanding cellular communication, such networks have been characterized in great detail over the past 30 years.[1] Until recently however, approaches to systematically characterize the global response

of cells to a specific signal have been missing. Advances in quantitative mass spectrometry close this gap and allow global profiling of the phosphorylation response.[2,3]

Here, we used this approach to globally determine changes of protein regulation in response to hyper-osmotic shock. Osmotic stress is used as a model to study signal transduction and is known to cause a multitude of cellular adaptations, which include changes in signal transduction, protein expression, and regulation of cell size and volume.[4,5] This response has been studied extensively using mRNA microarrays as well as hypothesis driven candidate-based approaches. Osmotic stress induced signaling can activate different signaling pathways. One of the well known transducers of the osmotic stress signal is the activation of the MAP kinase *high osmolarity glycerol* (HOG) pathway, which is the yeast counterpart of the human p38 MAPK pathway. Such mitogen-activated protein (MAP) kinase cascades are often involved in the immediate cellular response to various external stimuli such as growth factors, hormones, and environmental stresses.[6] Key genes involved in this pathway encode the Pbs2/Hog4 and Hog1 kinases.[7] Hog1 is known to bind and occupy regulatory elements of more than 30 different genes during periods of osmotic stress, which results in increased transcription.[8] However, little is still known about the effects of osmotic stress on protein level and the potential role of phosphorylation in the

cellular response to this stress. In addition, the full scope of signal transduction mediated by phosphorylation is so far unknown.

To globally address these questions, we employ stable isotope labeling of specific amino acids (SILAC)[9] in combination with high-resolution mass spectrometry and phosphopeptide enrichment,[10] in order to quantify changes in the phospho-proteome and proteome on a global level in response to osmotic stress.

Results and discussion

To generate an extensive, time-resolved dataset of proteome and phospho-proteome changes after hyper-osmotic stress we employed high-resolution mass spectrometry. To this end, we used three SILAC encoded populations of yeast cells auxotrophic for lysine[3,11] using either normal L-lysine, L-lysine-D4 or L-lysine-$^{13}C_6$, $^{15}N_2$ and compared the untreated control population with two hyper-osmotic stress conditions using 0.4 M NaCl for 5 and 20 min, respectively. Cells were subsequently lysed in 5% SDS containing buffer and proteins were digested in-solution by the endoproteinase LysC (see Fig. 1). In most proteomic experiments, trypsin that cleaves C-terminal to arginine and lysine is the preferred proteolytic enzyme to generate peptides suitable for mass spectrometric analysis. However, our previous experimental observations show that there is a high degree of arginine to proline conversion in yeast, convoluting the mass spectra obtained.[12] Therefore, we used labeling with only lysine followed by Lys-C digestion to generate peptides for mass spectrometric analysis. To obtain an in-depth proteome, we separated the complex peptide mixtures by iso-electric focusing into 12 fractions and analyzed each of these by online nanoflow HPLC-MS/MS on hybrid linear ion trap Fourier transform mass spectrometers (LTQ-FT Ultra and LTQ-Orbitrap XL). For phosphopeptide analyses, the LysC generated peptide mixtures were separated by strong-cation exchange (SCX) chromatography into 15 fractions, and phosphopeptides were enriched using TiO_2 in the presence of 2,5-DHB.[13] The phosphopeptide mixtures were analyzed by online LC-MS/MS, sequenced by multi-stage activated (MSA) collisionally induced dissociation (CID) and the resulting tandem mass spectra were searched against a yeast target-decoy database[14] using the Mascot algorithm. All raw MS and Mascot output files were analyzed together in the software suite MaxQuant,[15] where peptide identifications were filtered using stringent criteria of less than 1 percent final false-discovery rate on both peptide and protein level, and all identified peptides were quantified. This resulted in the identification of 26,620 unique peptide variants of which 5534 were unique phosphopeptides (Supplementary Table 3‡) and 3383 proteins (Supplementary Table 2‡). We included a replicate phosphoproteomics experiment in which we made use of the electron transfer dissociation (ETD) method[16] which is the latest generation phosphopeptide sequencing technology allowing for accurate localization of phosphosites in modified peptides. From the ETD experiment we can pinpoint 1588 phosphorylation sites (class A sites with high localization probability), of which 959 has previously been published and are publically available from Expasy.org. From the three CID experiments we localize 2924 class A sites (1621 already recorded at Expasy.org). Combining the ETD dataset with three CID experiments we all together identify peptides from 1728 yeast phosphoproteins and we localize 3084 unique phosphorylation sites. We calculated the phosphorylation site ratio as the relative difference between the phosphopeptide intensities observed from the untreated and the salt stressed states. We define increased phosphorylation of a protein as a result of an observed increased ratio of a phosphopeptide originating from the protein. Of all quantified class A phosphosites, 800 changed more than two-fold after 5 or 20 minutes of salt stress. This data show that osmotic stress regulates hundreds of proteins by altering their phosphorylation abundance on specific sites within a short time. Previous large-scale phosphoproteomics projects have shown that very few phosphorylation sites are only observed in one condition. This might reflect the overall "asynchronous" cell-cycle state of the cell populations and as a result of this most regulatory phosphorylation sites are present in low amounts in all cell populations.

This information rich dataset provides many novel and interesting insights into the osmotic stress response and forms a basis for future studies aiming at understanding the mechanisms of the osmotic stress response. Here, we discuss some examples of prominently regulated proteins and biological processes that were detected in our proteomics screen.

To confirm the activation of osmotic stress response in our system, we searched our phospho-proteome for an increase of proteins that are considered markers for this signaling pathway. We found for example serine-248 on Pbs2 had a 3 times higher induced level of phosphorylation. It is the MAP kinase kinase that plays a key role in cellular signaling after osmotic stress by directly phosphorylating and thereby activating the Hog1 MAP kinase pathway (Fig. S1‡). Likewise, we also observed increased abundance levels of phosphopeptides from other members of the HOG MAPK pathway such as Ste20 and Sln1. This data served as a positive control and confirmed the activation of stress signaling in the analyzed cells. In order to find the prominent protein kinases involved in osmotic stress signaling, we performed an unbiased motif analysis to search for enriched sequence motifs surrounding the phosphorylation sites in our dataset. To detect target sites with different extent of regulation, we applied a conservative cut-off for considering a phosphorylation site to be regulated and grouped the phosphorylation sites in three groups according to their SILAC ratio in response to osmotic stress such that phosphosites with a $\log_2$ ratio of one or more were considered up-regulated, sites with a $\log_2$ ratio less than -1 were down-regulated and the rest were considered as non-changing.

We developed an algorithm that tests for position-specific over-representation of amino acids compared to an average background frequency and used it to find enriched motifs between the up-regulated and non-changing phosphorylation class A sites. Specific amino acid groups were formed based on their chemical properties. Interestingly, as shown in the sequence logo plot (Fig. 2A) the most statistical significantly over-represented motif from the up-regulated class A phosphorylation sites conformed to basophilic sequence context
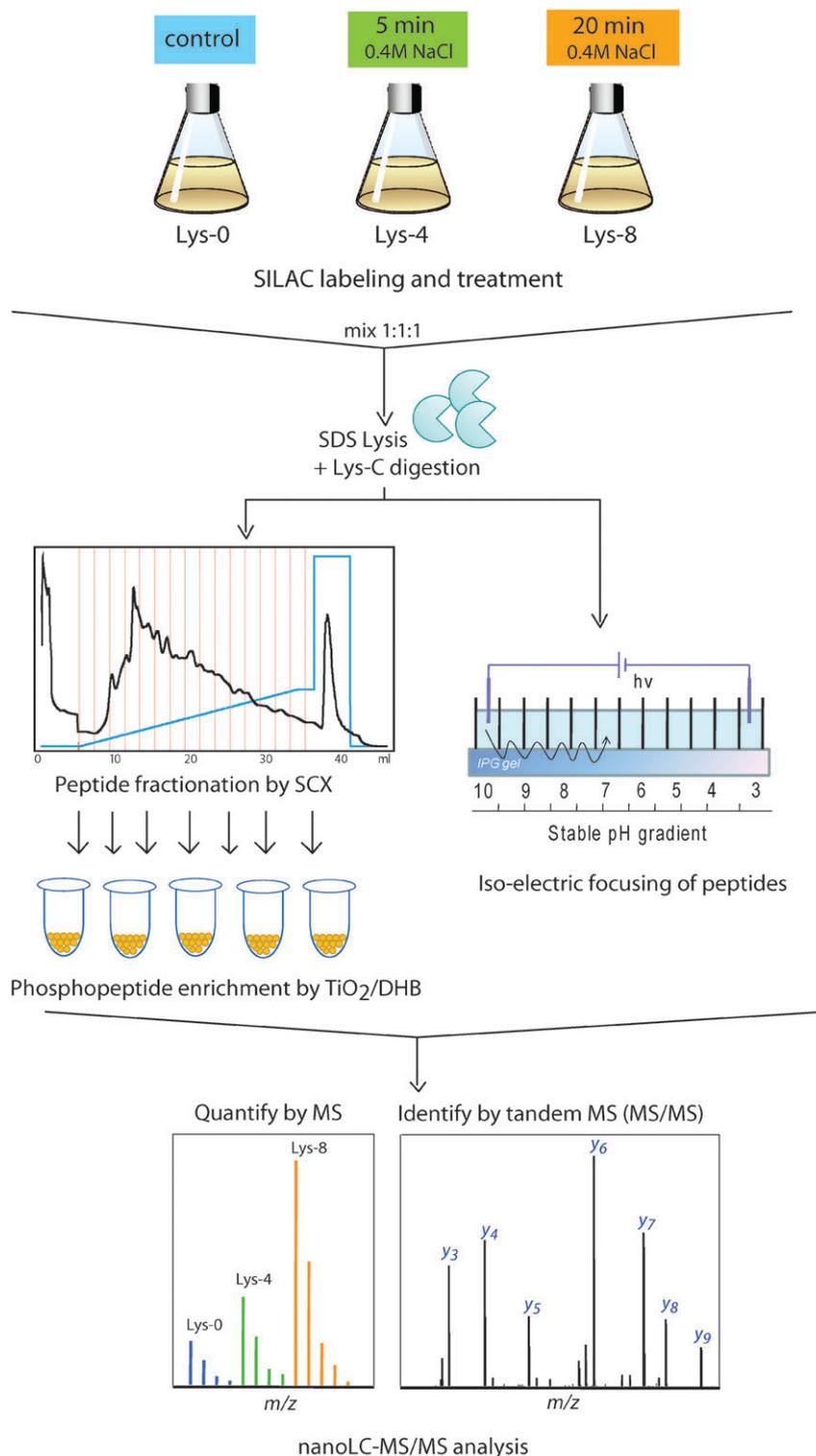
Fig. 1 Quantitative proteomics workflow. Control and treated yeast cells are labeled by different stable isotopic versions of lysine, lyzed in SDS, and mixed together. Protein extracts are digested by endoproteinase LysC, and phosphopeptides are enriched by a combination of strong cation exchange and TiO2 chromatographies. For proteome quantitation peptide digests were separated according to their pI-value by iso-electric focusing. Resulting peptide mixtures are separated on nanoflow HPLC and directly measured in a mass spectrometer. Relative peptide quantitation is based on the first stage of mass spectrometry (Full-scan MS), whereas peptide identification is achieved by fragmentation in the second stage of mass spectrometry (MS/MS).

[R/K]-X-X-[pS/T], which indicates activation of PKA- and CamKII-like kinases in response to osmotic stress. In contrast, the most overrepresented sequence motif among the non-changing phosphosites was highly enriched for acidic amino

acids surrounding the phosphorylated residue, suggesting that acidophilic kinases like the casein kinases are not activated by osmotic stress (Fig. 2B).

The second highest-enriched sequence motif of the remaining sequences conforms to the proline-directed MAP kinase [pS/T]-P motif for the upregulated phosphorylation
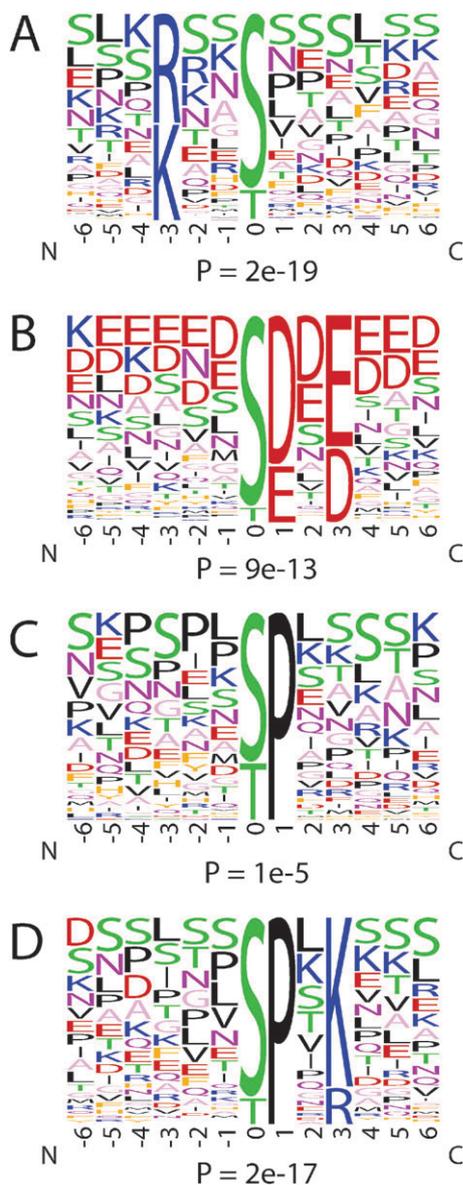

Fig. 2 Enriched phosphorylation site motifs. Logoplot of significant sequence motifs found in the dataset. The height of each amino acid represents its frequency at that position. (a) R/K-X-X-pS/pT/pY motif found in 32.0% of the up-regulated sequences compared to an average background frequency of 12.9% in the non-regulated sequences. (b) pS/pT/pY-D/E-X-D/E motif found in 13.1% of the non-regulated sequences compared to a background frequency of 1.1% in the up-regulated sequences. (c) pS/pT/pY-P motif found in 21.1% of the up-regulated sequences compared to an average background frequency of 6.3% in the non-regulated sequences. (d) pS/pT/pY-P-X-K/R motif found in 7.2% of the non-regulated sequences compared to an average background frequency of 1.2% in the up-regulated sequences.

sites, whereas for the non-changing sites there is a significant overrepresentation [pS/T]-P-X-[K/R] (Fig. 2C and 2D), which match exactly to the established CDK1/2 motif.[17] In concordance with this observation, Cdc28 which is the yeast single homolog of human CDKs and the master regulator of cell cycle progression, was found to have increased phosphorylation on tyrosine residue 19 after salt stress (Fig. S2‡). This residue is an inhibitory site of Cdc28 implying that upon exposure to osmotic stress, yeast cells immediately undergo cell cycle arrest, which would be a logical cellular response to this hazardous growth condition.

Moreover, many transcriptional regulators, which abundance on the protein level were unaffected by the osmotic shock treatment, showed increased phosphorylation site levels in our dataset (Fig. 3). At least five transcription factors (Msn2, Msn4, Hot1, Sko1 and Smp1) have been suggested to be directly controlled by the Hog1 MAP kinase in response to osmotic stress, although it is unclear how this control is exerted.[18,19] We find osmotic stress increases the relative levels of phosphorylation on specific sites on both Msn2 (serine-201, Fig. 3A) and Msn4 (threonine-142, Fig. 3B). The zinc finger proteins Msn2 and Msn4 are generic stress factors, which are controlled by PKA and Hog1 by an unknown mechanism. They are involved in the regulation of the Ctt1 and Hsp12 genes, both of which we find to be upregulated more than 7-fold on the protein level after 20 min of salt stress. Furthermore, we also find increased phosphorylation of serine-94 and -108 in the cyclic AMP response element (CRE)-binding basic-leucine zipper protein Sko1 induced, a critical regulator of osmotic stress-inducible genes (Fig. 3C). All of these proteins were previously implicated in the stress response; however, the regulatory mechanism remained unclear. Interestingly, we find that their phosphorylation is highly induced, indicating that this may represent a regulatory mechanism for these transcription factors.

We also find increased phosphorylation site levels on other transcriptional activators not previously implicated in the cellular stress response: for example, the AP1-like transcription factor Yap3 is phosphorylated on serine-128 and serine-133 (Fig. 3D). Since both of these phosphorylation sites are proline-directed, they might be direct targets of the Hog1 MAP kinase. Yap3 is thought to be a transcriptional activator that is involved in the environmental stress response and metabolism control pathways, but has not previously been implicated directly in osmotic stress. Interestingly, another member of this family of AP1-like proteins, Yap4, is induced 4-fold on the protein level within 5 minutes of salt stress (Supplementary Table 2‡).

Other transcriptional regulators like the glycolytic genes transcriptional activator Gcr2 are also phosphorylated in response to salt stress (Fig. 3E), whereas other transcription factors involved in other cellular responses such as the forkhead type Hcm1 appear to not be regulated (Fig. 3F) in terms of phosphorylation. We also confirm the activation of other known osmotic stress responders, for example, activation of serine/threonine-protein kinases Pkh1 and Hal5 as evidenced by the increased phosphorylation of specific sites on these proteins (Fig. S2‡). PKH1 phosphorylates and activates Ypk1 and Ypk2 and plays a role in the maintenance
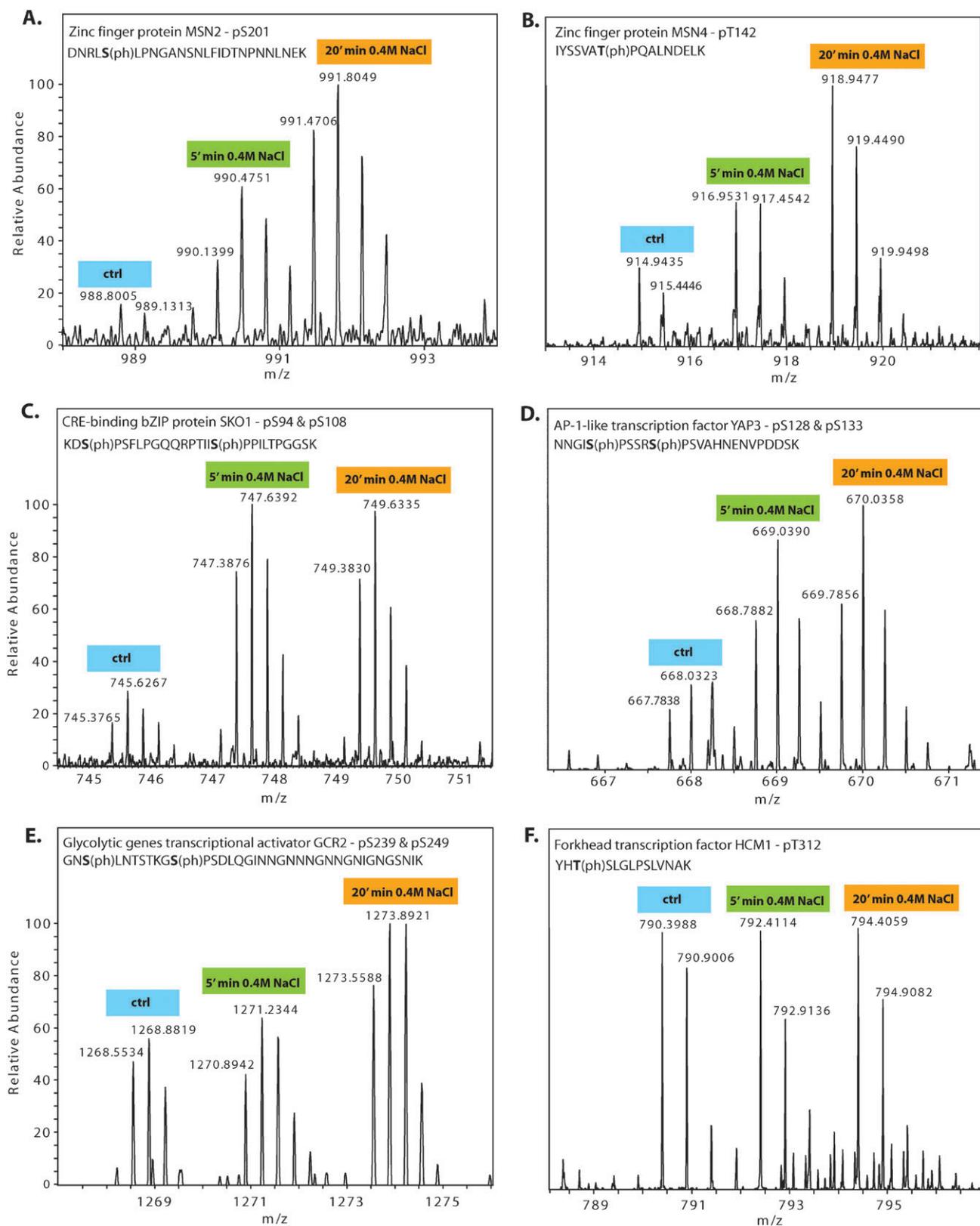
Fig. 3 Regulated phosphorylation sites on transcription factors. Transcriptional regulators showing increased levels of phosphorylation upon osmotic stress treatment after a time period of 20 min.

of the cell wall integrity during environmental stress.[20] Hal5 is known to help mediate adaptation to salt stress.[21]

We also measured the proteome changes after osmotic stress at two different time points and in three biological replicates.
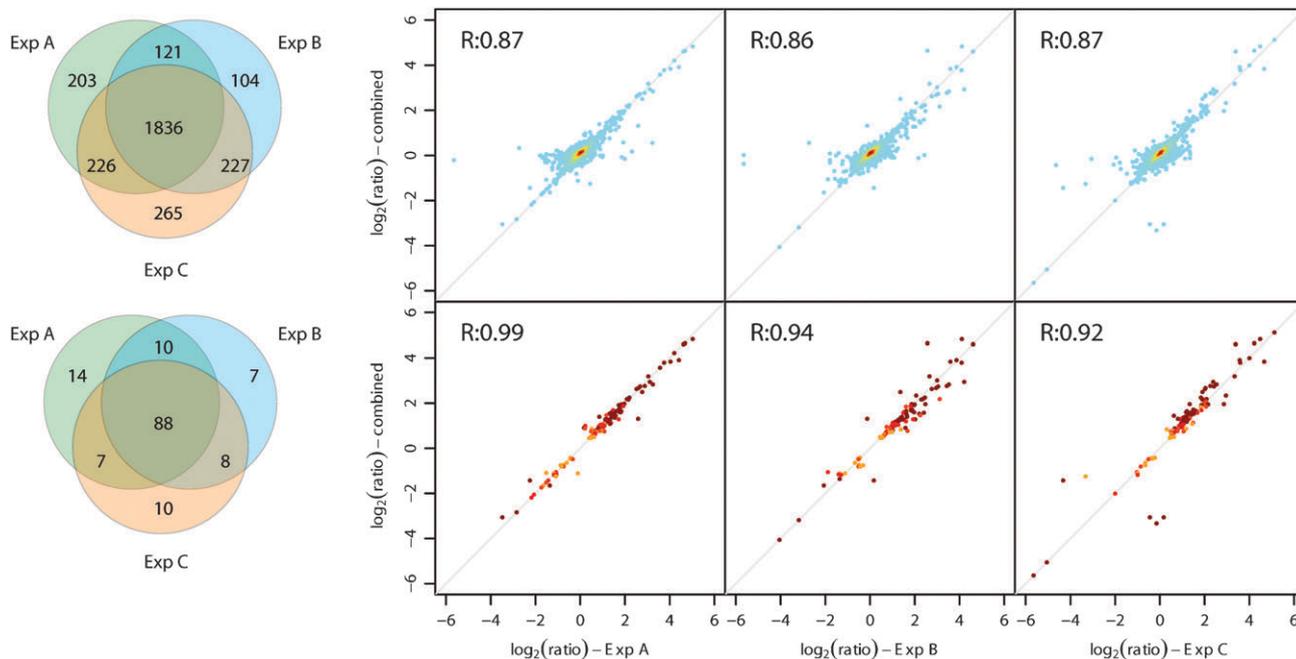
Fig. 4 Reproducibility of Proteome measurements between 0 and 20 min of salt stress. Venn diagrams show 61% overlap between all three biological replicates, and 80% overlap between two or more-both comparing all quantified proteins (top) or the subset that show a significant change (bottom). The ratio scatter plots show protein abundance change between 0 and 20 min of salt stress as measured in each experiment and plotted *versus* a combined ratio. The combined ratio is used as the quantization of each protein is measured with different precisions within each experiment depending on the number of underlying measured peptides (see ref. 15 for details). The Pearson correlation coefficient is shown in the top left corner of each plot. In the top 3 plots, coloring is done according to density, where 50% of the data points are colored red, 25% yellow, and the remaining 25% are light blue. The 3 lower plots only include proteins which are showing a significantly changed ratio and are colored from orange to red in increasing significance.

Reproducibility was observed with high correlation and overlap between the individual experiments (Fig. 4) with Pearson correlation coefficients of better than 0.86 for all comparisons. The figure legend to Fig. 4 provides more details and numbers. More than one hundred proteins are up-regulated ($p < 10^{-4}$) after 20 min, whereas less than fifty are down-regulated (Fig. 5).

To gain functional insights into the regulated proteins, we performed gene ontology (GO) enrichment analysis using the web-tool FatiGo (http://www.fatigo.org). This unbiased analysis revealed that proteins involved in the cellular stress response are highly over-represented in the group of up-regulated proteins ($p < 10^{-8}$), adding further to the confidence in our dataset. Likewise, proteins involved in the carbohydrate metabolism are significantly over-represented in this group ($p < 10^{-10}$).

To identify functional connections among the regulated proteins we mapped them to known metabolic and signal pathways using the metabolic pathway analysis tool at yeast genome.org. A significant number of the osmotic stress induced proteins are involved in carbon metabolism, *e.g.* glycolytic pathways (Fig. 6). Remarkably, all enzymes involved in the conversion of glycogen to glucose-6-phosphate are all regulated upon osmotic shock, which indicates an increased glycogen metabolism under stress conditions. Likewise, the enzymes directly involved in the glycerol biosynthesis branch of the pathway are specifically upregulated, for example, GPD1, an enzyme that converts dihydroxy-acetone-phosphate

from the glycolytic pathway to glycerol-3-phosphate, is up-regulated more than 3-fold. Also, HOR2 the rate-limiting enzyme that converts to glycerol-3-phosphate to glycerol is 4-fold induced within 20 min of osmotic stress. In contrast, all other members of the glycolytic pathway downstream of glyceraldehyde-3-phosphate are unchanged in abundance during osmotic stress. This could suggest that carbon metabolism redirected from pyruvate synthesis to increased production of glycerol, functions as an osmolyte that protects proteins in their native folded and functional states, and thereby aids in maintaining intra-cellular homeostasis during environmental stresses such as osmotic shock conditions. In addition to this role glycerol also increases the intracellular osmolarity in order to stop or slow down the efflux of water and influx of ions.

It is known that during osmotic stress, cells are more prone to oxidative stresses such as an increased level of hydrogen peroxide.[22] In line with this we find that the most up-regulated protein, catalase T (CTT1), is an enzyme that catalyzes the conversion of hydrogen peroxide to water and oxygen that thereby protects the cell from oxidative damage induced by hydrogen peroxide.

Under salt stress, Hog1 has been shown to bind directly to regulatory sequences of more than thirty genes and increases their mRNA expression within 15 min after hyper-osmotic shock.[8] To assess co-regulation of mRNA and protein changes upon osmotic stress, we compared our data with a previously published dataset on mRNA abundance.[23] The overall correlation between our proteome and the mRNA measurements
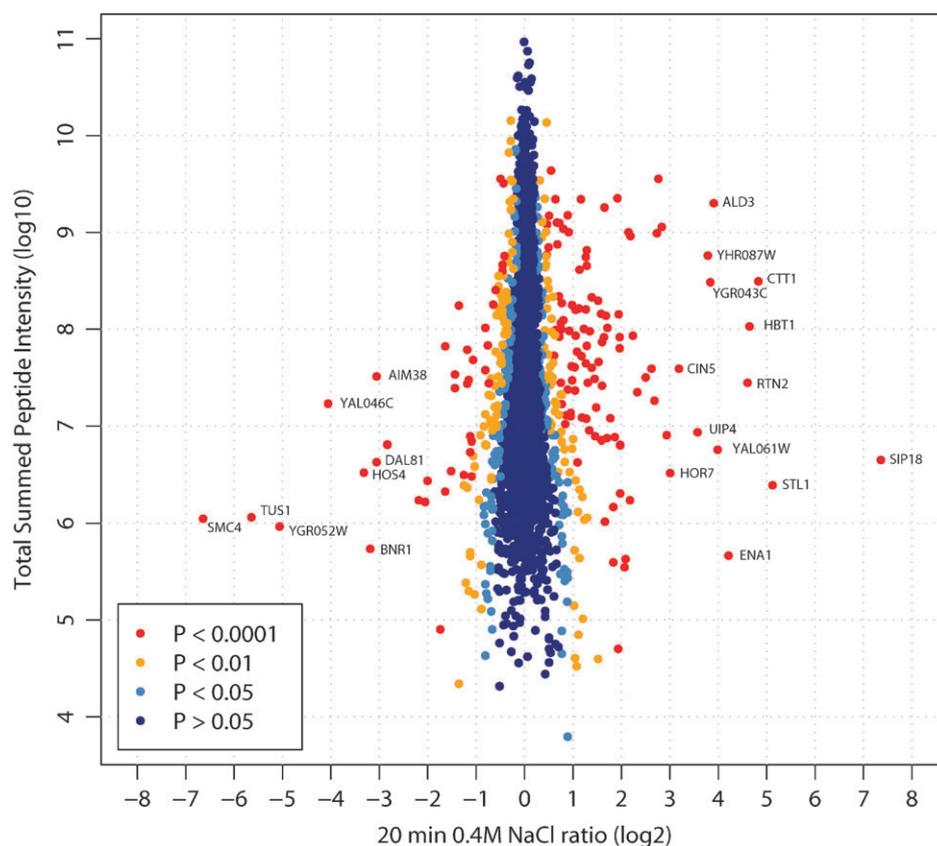
Fig. 5 Proteome changes after 20 min osmotic stress. Overall fold change for the yeast proteome as a function of protein intensity in the MS. Protein ratios are color-coded according to their ratio significance (significance B as described in ref. 15), which is calculated by estimating the variance of the distribution of all SILAC pair ratios, taking the summed peptide intensities into account, and reporting the *p*-value associated with the *z*-score for a given ratio. See Cox J *et al.*, *Nature Biotechnology*, **26**, 1367–1372 (2008). Data are normalized such that the median log-transformed ratio of all peptides identified were zero to correct for unequal sample mixing.

is poor (Fig. S3A‡), perhaps due to a combined effect of experimental differences, quantitation precision of the two different measuring techniques (MS *versus* microarray), and other differences inevitably present between labs. However, the induced change in protein abundance seems to correlate well with the corresponding mRNA changes observed by microarray studies (Supplementary Table 4 and Fig. S3B‡). Upregulated proteins include Hsp12, Ald3, Ctt1, which are known to be induced on both mRNA and protein levels under stress conditions. Down-regulated proteins include Rad9 and Hos4, both thought to be substrates of Cdc28. Down-regulation of protein can be exerted by two different mechanisms; a decrease in mRNA production or by active protein degradation, for example through the ubiquitin-proteasome pathway. The last type of regulation is only captured by quantitative proteomics screens, and might be the reason why some of the ratios of some of the significantly down-regulated proteins—for example Aim38, Mdr1, Nup157 and Rph1—are not reflected by changes in their mRNA.

Conclusion

We report global regulatory protein changes in yeast cells both at the proteome and phospho-proteome level upon osmotic stress. Our data confirm regulation of many proteins known to

be altered in abundance after salt stress and implicating a large number of novel proteins in the adaptation to high osmolarity conditions. For example, we find that although the stress-activated Hog1 MAPK pathway plays a pivotal role in the osmotic stress response in yeast, other kinase pathways also seem to play important roles. Furthermore, we find a significant correlation between protein changes and their mRNA and under these conditions, independently confirming the quality of our dataset. Interestingly, we observe that osmotic stress influences the expression of many more proteins than previously anticipated and the regulated proteins participate in many different aspects of cellular functions. Taken together, our data significantly expand the knowledge on osmotic stress mediators regulated on phosphorylation and protein level and will likely prove valuable for future studies in this field.

Methods

Cell culture, labeling and protein extraction

The yeast *Saccharomyces cerevisiae* strain S28CC was used in this study. It contains a lysine deficient gene which makes it compatible for the use with SILAC. Three different yeast cell cultures were grown in SILAC friendly YNB medium containing either 30 mg/L-Lysine, 30 mg/L-Lysine-D4, or
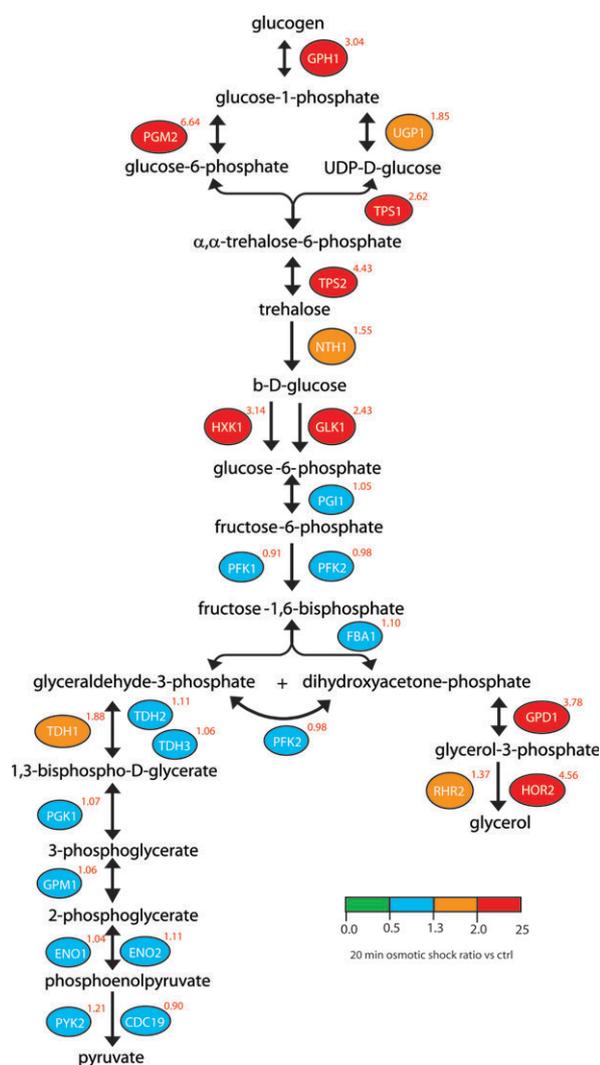
Fig. 6 The glycolytic metabolism and glycerol synthesis pathway. All enzymes of the yeast carbon metabolism pathway are colour-coded according to their osmotic fold-change. The 20 min osmotic shock to control ratio as determined by SILAC is indicated for each protein in red.

30 mg/L-Lysine-D8 for a total of ten generations to a final OD_{600} of 0.6. At this time, the yeast culture containing Lysine-D4 was shifted to 0.4 M NaCl for 5 min, and the yeast culture containing Lysine-D8 was subjected to 0.4 M NaCl for 20 minutes. Cells were harvested by centrifugation for 6 min at $4000 \times g$ at 4 °C, washed twice with ice-cold H_2O. Cell lysis and protein extraction was performed via a slightly modified version of the Filter Aided Sample Preparation (FASP) Method.[24] Briefly, yeast cells were re-suspended in a lysis solution containing 5% SDS, 100 mM Tris/HCL pH 7.6, 0.1 M DTT. Cells were incubated at 95 °C for 10 min. Precipitates were removed via centrifugation for 5 min. Proteins were mixed in a 1 : 1 : 1 ratio. Proteins were placed on a Millipore Centrifugal device (Microcon). SDS was removed through several washes with 8M Urea (pH 8.5 and pH 8.0) reduced cysteine thiols were alkylated by 0.55M iodoacetamide, and digested with LysC overnight. The resulting peptides were desalted using C18 Sep-Pak cartridges (Waters).

Peptide concentration was measured by UV spectrometer with a spectrum range of 240–340 nm. For proteome analysis, 100 mg of peptides were separated by iso-electric focusing (IEF) on an Agilent OFFGEL fractionator using the 13 cm IPG strip with pH = 3–10 followed by LC-MS analysis. All experiments were performed as three biological replicates.

Phosphopeptide fractionation and enrichment

To separate phosphopeptides from non-phosphorylated peptides we used strong cation exchange (SCX) chromatography. 8 mg of LysC digests were adjusted by tri-fluoroacetic acid (TFA) to pH 2.7. Precipitates were cleared by centrifuging at $17\,000 \times g$ for 10 min. The peptide mixture was loaded onto a 1 ml Resource S column (GE healthcare) connected to the Äkta Purifier chromatography system (Amersham biosciences). During loading, the flow-through from the column was collected. Peptides bound to the column were separated by a linear gradient of potassium dihydrogen phosphate in 30% acetonitrile and 0.1% TFA.[25] Fifteen fractions were collected via an automated fraction collector. Based on UV absorbance, some fractions containing low amount of peptides were pooled which resulted in 10 fractions. Each fraction was subjected to phosphopeptide enrichment with TiO_2 in the presence of 2,5-DHB. Due to the high peptide amount, the flow-through sample was sequentially incubated with TiO_2 beads for 3 times. Peptide samples originated from immunoprecipitation were adjusted by to a final concentration of 30% acetonitrile (MeCN) and pH 2.7.

Phosphopeptide enrichment by TiO_2 beads was essentially as described[26] with slight modifications. TiO_2 beads were pre-coated with 2,5-dihydroxybenzoic acid (2,5-DHB) and stored in a solution of 80% MeCN and 0.1% TFA. From this a 1 : 1 TiO_2 beads- slurry, 5 µl was added to each sample and rotated end-over-end for 30 min. After one time wash with 1 ml 30% MeCN/1% TFA and one time with 1 ml 50% MeCN/1% TFA, the phosphopeptides were eluted from TiO_2-C_8-StageTips into a 96-well plate with 2×20 µL of 20% acetonitrile (MeCN) in 15% ammonia-water solution (pH > 11) and dried to 2 µL in a speed-vac.

Mass spectrometric analysis

The dried phosphopeptide mixtures were acidified with 5% acetonitrile in 0.3% TFA to an end volume of 8 µL and analyzed by online nanoflow liquid chromatography tandem mass spectrometry (LC-MS/MS) as described previously[26] with a few modifications. Briefly, nanoLC-MS/MS-experiments were performed on an EASY-nLC™ system (Proxeon Biosystems, Odense, Denmark) connected to an LTQ-Orbitrap XL or 7-T LTQ-FT Ultra (Thermo Scientific, Bremen, Germany) through a nanoelectrospray ion source. The phosphopeptides were auto-sampled directly onto the 15 cm long 75 µm-inner diameter (i.d.) analytical column packed with reversed-phase C_{18} Reprosil AQUA-Pur 3 µm particles at a flow rate of 500 nl/min. The flow rate was reduced to 250 nl/min after loading, and the phosphopeptides were separated with a linear gradient of acetonitrile from 5–40% in 0.5% acetic acid for 100 minutes. The effluent from the column was directly electrosprayed into the mass spectrometer.

The LTQ Orbitrap XL and LTQ-FT Ultra instruments under Xcalibur 2.0 were operated in the data dependent mode to automatically switch between full scan MS and MS/MS acquisition. Survey full scan MS spectra (from m/z 300–2000) were acquired with resolution $R = 60\,000$ at m/z 400 (after accumulation to a 'target value' of 1 000 000 in the linear ion trap) in the orbitrap or at with resolution $R = 100\,000$ at m/z 400 ('target value' of 5 000 000) in the FTICR. The ten most intense multiply-charged ions ($z \geq 2$) were sequentially isolated and fragmented in the linear ion trap by collisionally induced dissociation (CID) at a target value of 5000 or a maximum ion time of 150 ms. All tandem mass spectra were acquired with the multi-stage activation (MSA) option enabled for neutral losses of m/z 32.66, 48.99 and 97.97. For all full scan measurements in the orbitrap detector a lock-mass ion from ambient air (m/z 445.120025) was used for internal calibration as described earlier.[27] For electron transfer dissociation (ETD) analysis, we employed an LTQ Orbitrap XL ETD instrument (Thermo Scientific) that was operated in a standard top10 ETD mode. Full-scans were analyzed in the orbitrap at $R = 60$ K with ETD spectra IT target values: 10 000, ETD ions: 300 000, and a maximum reaction time of 250 ms. The supplemental activation feature was enabled and recorded in parallel by the LTQ detector system. Anions and multiply-charged peptide ions were reacted for 100 ms to allow efficient ETD. Typical mass spectrometric conditions were: spray voltage, 2.2 kV; no sheath and auxiliary gas flow; heated capillary temperature, 200 °C; normalized CID collision energy 40% for MSA in LTQ. The ion selection threshold was set to 100 counts for MS/MS. An activation $q = 0.25$ and activation time of 30 ms for MSA acquisition were used.

Identification and quantification of peptides and proteins using MaxQuant

Raw FTICR and Orbitrap full-scan MS and ion trap MSA spectra were processed by MaxQuant as described[15] supported by Mascot (Matrix Science, London, UK) as the database search engine for peptide identifications. In brief, MaxQuant uses the entire elution profile of the full-scans, the isotope distribution, and possible SILAC pairs to determine the precursor mass with very high precision and an individualized mass accuracy which is a major part of the identification process.[28] MS/MS peak lists were filtered to contain at most six peaks per 100 Da interval and searched by Mascot against a concatenated forward and reversed version of the yeast ORF sequence database (Stanford University) supplemented with common contaminants such as human keratins and endoproteinase LysC. Tandem mass spectra were initially matched with a mass tolerance of 7 ppm on precursor masses and 0.5 Da for fragment ions, and strict LysC specificity and allowing for up to 3 missed tryptic cleavage sites. Cysteine carbamidomethylation (Cys + 57.021464 Da) was searched as a fixed modification. Labeled lysine was specified as fixed or variable modification, depending on prior knowledge about the parent ion. N-acetylation of protein (N-term + 42.010565 Da), N-pyro-glutamine (Gln −17.026549), oxidized methionine (+ 15.994915 Da) and phosphorylation of serine, threonine and tyrosine (Ser/Thr/Tyr + 79.966331 Da) were searched as

variable modifications. The resulting Mascot result files (*.dat) were loaded into the MaxQuant software together with the raw data for further processing. To minimize false identifications, all top-scoring peptide assignments made by Mascot were filtered based on previous knowledge of individual peptide mass error, SILAC state and the correct number of lysine residues specified by the mass difference observed in the full scan between the SILAC partners. Furthermore, peptide assignments were statistically evaluated in a Bayesian model on the basis of sequence length and required to have a Mascot score > 10. We accepted peptides and proteins with a false discovery rate of less than 1%, estimated on the basis of the number of accepted hits from the reverse database. Moreover, proteins can be identified by a single peptide that MaxQuant was not able to quantify (could not identify the SILAC triplet) and therefore these proteins will appear with an intensity of zero in the table.

Finally, to pinpoint the actual phosphorylated amino acid residue(s) within all identified phosphopeptide sequences in an unbiased manner, we calculated the localization probabilities of all putative serine, threonine and tyrosine phosphorylation sites using the PTM score algorithm as described.[26] As a further certainty localization measure, the likelihood of phosphate group transfer during fragmentation was considered,[29] where a high proton mobility of the peptide is equivalent to high phosphosite localization certainty. Certainty of localization was grouped into 3 groups, where class A sites indicate likely correct localization and is defined as peptides with localization probability above 0.75 and unlikely to be involved in gas phase phosphate group transfer defined as containing a mobile proton or with ETD evidence. Class B sites can be considered presumably correct requiring peptides to have a localization probability above 0.25 and match one or more of 22 known kinase motifs and not expected to be involved in phosphate group transfer defined as having a partially mobile or mobile proton or ETD evidence. Sites reported as class C are uncertain and needs further validation.

FatiGo. Statistical analysis of over- and under-represented genes in our osmotic stress regulated set of proteins was performed using the FatiGo software (www.fatigo.org)[30] using the non-regulated set of proteins identified as background. FatiGo performs functional enrichment analysis by comparing the two lists of proteins by means of a Fisher's exact test. Gene modules used in the test were defined to gene ontology (GO) and KEGG. We used a cut-off threshold of $p < 0.01$ for significance after adjusting for multiple testing.

Sequence logo plots

To identify enriched sequence motifs in our phosphorylation site dataset we developed a new algorithm that iteratively tests for position specific over-representation of any amino acid groups in a pre-aligned list of sequences compared to the average occurrence of the amino acid group in another list. In each round of iteration the most significant amino acid group is excluded in a position specific fashion from both lists. Statistical significant over-representation is calculated using R's (a programming language and software environment for statistical computing and graphics) implementation of the

Fisher's exact test. Grouping of amino acids were done by the basis of related chemical properties (acidic, basic, aromatic, aliphatic, hydrophilic, amide, polar and cyclic). The perl- package of WebLogo[31] was used internally in the algorithm to generate enriched sequence motifs as output.

For the motif analysis a sequence window of ± 6 amino acids in relation to a central phosphorylated residue was used. Phosphorylated peptide sequences upregulated more than two-fold were compared to a background of all non-regulated residues. This was followed by the inverse analysis. A cut-off of $p < 0.001$ was used on the Bonferroni adjusted p-values in this analysis.

Acknowledgements

References

1 T. Hunter and M. Karin, *Cell*, 1992, **70**, 375–387.
2 S. E. Ong and M. Mann, *Nat. Chem. Biol.*, 2005, **1**, 252–262.
3 L. M. de Godoy, J. V. Olsen, J. Cox, M. L. Nielsen, N. C. Hubner, F. Frohlich, T. C. Walther and M. Mann, *Nature*, 2008, **455**, 1251–1254.
4 S. Hohmann, *Microbiol. Mol. Biol. Rev.*, 2002, **66**, 300–372.
5 E. Klipp, B. Nordlander, R. Kruger, P. Gennemark and S. Hohmann, *Nat. Biotechnol.*, 2005, **23**, 975–982.
6 L. Chang and M. Karin, *Nature*, 2001, **410**, 37–40.
7 S. Hohmann, M. Krantz and B. Nordlander, *Methods Enzymol.*, 2007, **428**, 29–45.
8 D. K. Pokholok, J. Zeitlinger, N. M. Hannett, D. B. Reynolds and R. A. Young, *Science*, 2006, **313**, 533–536.
9 S. E. Ong, B. Blagoev, I. Kratchmarova, D. B. Kristensen, H. Steen, A. Pandey and M. Mann, *Mol. Cell. Proteomics*, 2002, **1**, 376–386.
10 B. Macek, M. Mann and J. V. Olsen, *Annu Rev Pharmacol Toxicol*, 2008, **49**, 199–221.
11 A. Gruhler, J. V. Olsen, S. Mohammed, P. Mortensen, N. J. Faergeman, M. Mann and O. N. Jensen, *Mol. Cell. Proteomics*, 2005, **4**, 310–327.
12 S. E. Ong, I. Kratchmarova and M. Mann, *J. Proteome Res.*, 2003, **2**, 173–181.
13 M. R. Larsen, T. E. Thingholm, O. N. Jensen, P. Roepstorff and T. J. Jorgensen, *Mol. Cell. Proteomics*, 2005, **4**, 873–886.
14 J. E. Elias and S. P. Gygi, *Nat. Methods*, 2007, **4**, 207–214.
15 J. Cox and M. Mann, *Nat. Biotechnol.*, 2008, **26**, 1367–1372.
16 J. E. Syka, J. J. Coon, M. J. Schroeder, J. Shabanowitz and D. F. Hunt, *Proc. Natl. Acad. Sci. U. S. A.*, 2004, **101**, 9528–9533.
17 J. A. Ubersax, E. L. Woodbury, P. N. Quang, M. Paraz, J. D. Blethrow, K. Shah, K. M. Shokat and D. O. Morgan, *Nature*, 2003, **425**, 859–864.
18 P. M. Alepuz, E. de Nadal, M. Zapater, G. Ammerer and F. Posas, *EMBO J.*, 2003, **22**, 2433–2442.
19 M. Proft, F. D. Gibbons, M. Copeland, F. P. Roth and K. Struhl, *Eukaryotic Cell*, 2005, **4**, 1343–1352.
20 K. Liu, X. Zhang, C. Sumanasekera, R. L. Lester and R. C. Dickson, *Biochem. Soc. Trans.*, 2005, **33**, 1170–1173.
21 J. Perez-Valle, H. Jenkins, S. Merchan, V. Montiel, J. Ramos, S. Sharma, R. Serrano and L. Yenush, *Mol. Cell. Biol.*, 2007, **27**, 5725–5736.
22 W. H. Mager, A. H. de Boer, M. H. Siderius and H. P. Voss, *Cell Stress Chaperones*, 2000, **5**, 73–75.
23 S. M. O'Rourke and I. Herskowitz, *Mol. Biol. Cell*, 2004, **15**, 532–542.
24 J. R. Wisniewski, A. Zougman, N. Nagaraj and M. Mann, *Nat Methods*, 2009, **6**, 359–362.
25 B. Macek, I. Mijakovic, J. V. Olsen, F. Gnad, C. Kumar, P. R. Jensen and M. Mann, *Mol. Cell. Proteomics*, 2007, **6**, 697–707.
26 J. V. Olsen, B. Blagoev, F. Gnad, B. Macek, C. Kumar, P. Mortensen and M. Mann, *Cell*, 2006, **127**, 635–648.
27 J. V. Olsen, L. M. de Godoy, G. Li, B. Macek, P. Mortensen, R. Pesch, A. Makarov, O. Lange, S. Horning and M. Mann, *Mol. Cell. Proteomics*, 2005, **4**, 2010–2021.
28 J. Cox and M. Mann, *J. Am. Soc. Mass Spectrom.*, 2009, **20**, 1477–1485.
29 A. M. Palumbo and G. E. Reid, *Anal. Chem.*, 2008, **80**, 9735–9747.
30 F. Al-Shahrour, P. Minguez, J. M. Vaquerizas, L. Conde and J. Dopazo, *Nucleic Acids Res.*, 2005, **33**, W460–464.
31 G. E. Crooks, G. Hon, J. M. Chandonia and S. E. Brenner, *Genome Res.*, 2004, **14**, 1188–1190.

Minireview

Comparing cellular proteomes by mass spectrometry

Florian Fröhlich and Tobias C Walther

Address: Organelle Architecture and Dynamics, Max Planck Institute of Biochemistry, Am Klopferspitz 18, 82152 Martinsried/Munich, Germany.

Correspondence: Tobias C Walther. Email: twalther@biochem.mpg.de

Abstract

Mass spectrometry and cryo-electron tomography together enable the determination of the absolute and relative abundances of proteins and their localization, laying the groundwork for comprehensive systems analyses of cells.

Biological systems are characterized by the dynamic interplay of their components, and to understand how individual parts act together it is crucial to know the composition of a system and how it changes over time. The protein components are of prime interest as they provide structure and carry out many functions in the cell. The transcriptome has been much used as a proxy to infer changes in protein expression, as techniques for measuring global RNA levels preceded those for measuring the proteome. However, when the levels of an mRNA and its corresponding protein are systematically compared, many differences in their abundance emerge, resulting in poor quantitative correlation overall between transcriptome and proteome [1-3]. Ways of measuring protein levels directly are therefore highly desirable, and breakthroughs in mass spectrometry (MS)-based proteomics are starting to enable this on a global scale.

In experiments recently published in *Nature*, Ruedi Aebersold and colleagues (Malmström *et al.* [4]) combined MS-based measurements of protein abundance in the bacterial pathogen *Leptospira interrogans*, the agent of Weil's disease, with imaging by cryo-electron tomography (CET) of distinct structures of known protein composition, such as the flagellar motor (in which the precise number and type of the protein subunits can be counted). The CET imaging provided a way of confirming the MS protein-quantitation data. The protein-abundance measurements then enabled the effect of the antibiotic ciprofloxacin on a large fraction of the *Leptospira* proteome to be determined. In this article we describe some of the recent developments in MS-based proteomics that enable such experiments, focusing on quantitative techniques that will eventually allow a complete inventory of cellular proteins. The goal for proteomics is the measurement of the absolute and relative abundances of proteins at high accuracy and with minimal effort. But currently this means a compromise between depth of analysis and measurement time.

Identifying proteins by mass spectrometry

Intact proteins are difficult to identify by MS because their sequence cannot be obtained by fragmentation and so MS-based proteomics relies on analysis of peptides obtained by proteinase digestion of the sample. By analogy with genome-sequencing methods, this approach has been called 'shotgun' proteomics. The resulting peptide mixtures are dauntingly complex and are fractionated before submitting them to MS. Several recent studies, including the determination of the yeast and *Leptospira* proteomes [2,4], used isoelectric focusing in so-called OFF-gels [5,6] as a first separation step. Following this initial fractionation, peptides are separated by liquid chromatography (LC) most commonly directly coupled to electrospray ionization of peptides (ESI) or less frequently to matrix-assisted laser desorption ionization (MALDI) to produce ions for MS.

In the next step, mass-to-charge (m/z) values of peptides and their ion intensities are determined by MS (MS[1] or 'parent ion' spectra). To reliably identify peptides, the (typically) 5 to 20 most abundant peptides are selected for further fragmentation, resulting in a sequence-characteristic spectrum (MS[2] or fragmentation spectrum) for each peptide that is used to search databases to identify the peptide (Figure 1a). In the determination of the *Leptospira* proteome, Malmström *et al.* [4] collected more than 415,000 MS[2] spectra that could be assigned to more than 18,000 unique peptides, leading to the identification of 2,221 proteins (61% of the predicted open reading frames). To analyze the complex peptide mixtures typical of proteomics very high mass resolution is required. Otherwise, MS spectra from different peptides overlap, making peptide identification and quantification potentially inaccurate and unreliable. Precision instruments, in particular orbital frequency resonance ion traps such as the Orbitrap [7], are therefore most widely used for proteomics.

Methods for comparative quantitative proteomics

A common goal in proteomics is the accurate quantification and comparison of the proteomes of cells in different physiological or developmental states. For *Leptospira*, the
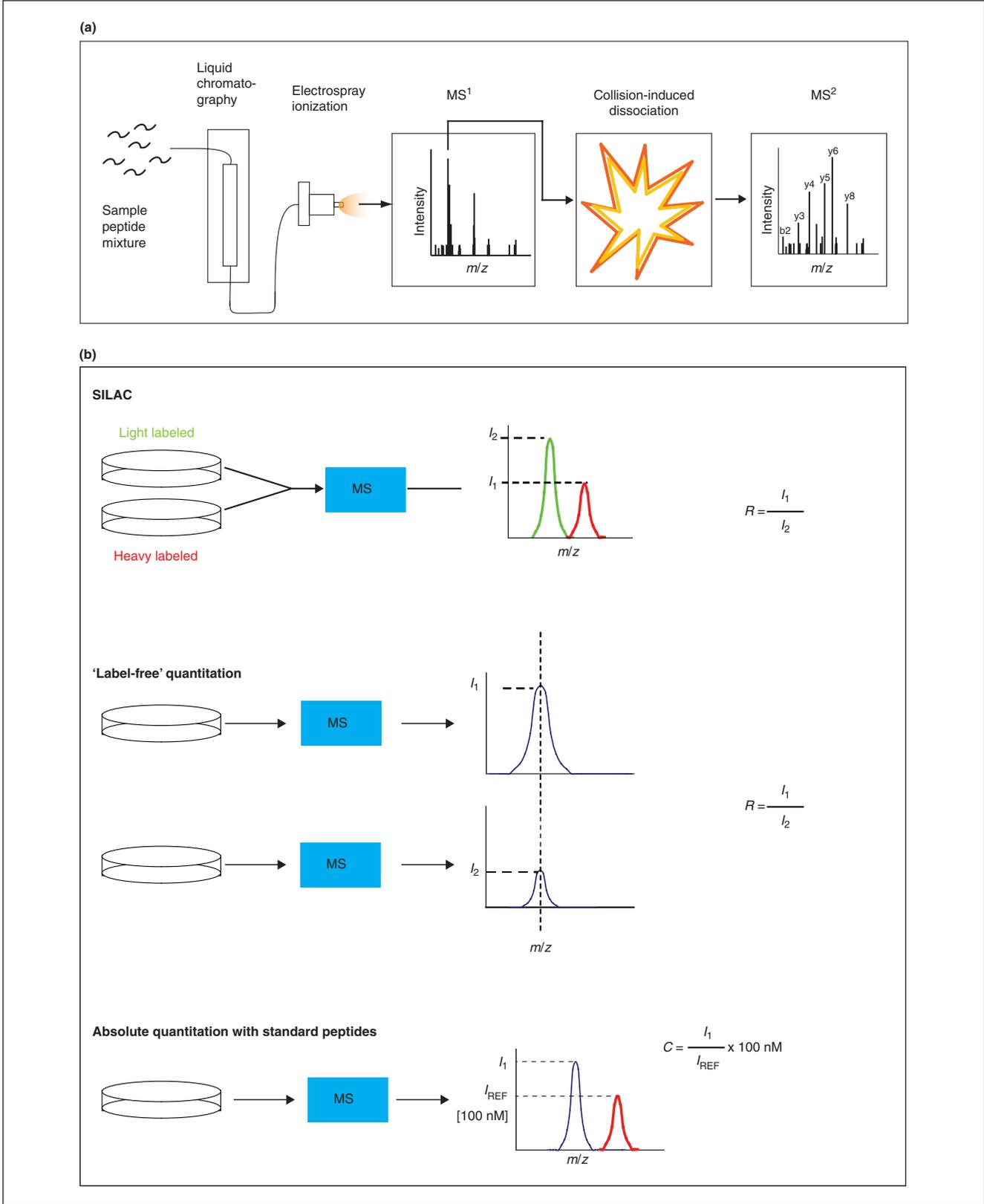
(a)

(b)

Figure 1

Quantitative MS-based proteomics. **(a)** Analysis of complex peptide mixtures by LC-MS[2]. Peptide mixtures are resolved by liquid chromatography, ionized through electrospray and resolved by MS[1]. Selected peptides are fragmented by collision with an inert gas and the resulting MS[2] spectra are recorded. **(b)** Quantitative proteomics strategies. In the SILAC technique, isotope-labeled peptide intensities (I) are compared in the MS[1] spectra. For 'label-free' quantitation, intensities of peptides are compared between different runs. Alternatively, standard peptides are spiked into the mixture to yield calibration for absolute peptide abundances. *R* refers to the ratio between either heavy and light peptides (SILAC panel) or ion intensities between different runs (label-free quantitation).

interesting question addressed by Malmström *et al.* [4] is how the proteome reacts to addition of an antibiotic. They took the approach of quantifying protein abundance directly using a label-free method, which we shall discuss later. Another approach would have been to derivatize the peptides from different conditions with isobaric labels that yield different, indicative, small molecules after fragmentation, a technique called isobaric tag for relative and absolute quantitation (iTRAQ) [8]. After fragmentation these derivatives yield distinctive small molecules indicative of the peptide. In such an experiment, the relative abundance of these indicators is used to quantify the relative abundance of the different peptides (and thus proteins) in the sample.

Metabolic labeling of proteins yields similar information, but avoids complications of *in vitro* coupling such as incomplete reactions. Samples are labeled *in vivo* with amino acids (lysine and arginine) labeled with heavy non-radioactive isotopes such as ^{13}C or ^{15}N, and compared with samples containing unlabeled amino acids, a technique called stable isotope labeling of cells in culture (SILAC) [9]. Peptides are then generated by digesting with proteinases (for example, trypsin) that cut specifically after labeled amino acids, thereby ensuring that each peptide contains at least one labeled amino acid. This results in a distinct shift in MS spectra between heavy and light peptides. The intensity ratio between peaks in a SILAC pair indicates the abundance ratio of proteins from which the peptides were derived (Figure 1b).

For more accurate measurements, multiple peptides from a protein are typically averaged and this analysis is now completely automated [10]. Because of the high resolving power of Orbitrap mass spectrometers, this methodology can be applied to very complex mixtures and closely spaced peaks can be well resolved. Together with only one previous fractionation step - isoelectric focusing - this experimental setup was used for the first quantitation of a eukaryotic proteome, that of *Saccharomyces cerevisiae*, in the haploid and diploid phases of the life cycle (4,399 proteins were identified and 4,033 quantitated from 1,788,451 SILAC pair peptides [2]). If the abundances of at least some proteins are known, as was the case in yeast, they can be used to calibrate the MS data and yield absolute protein measurements. Advantages of this approach include very accurate quantitation and the fact that no previous knowledge of proteins that change in abundance is

required. This is in contrast to the classical protein-detection methods, for example, immunoblotting, where reagents are often limiting and a clear hypothesis about which protein(s) to measure is required. SILAC, pioneered by the Mann laboratory, is now widely used for protein analyses in yeast, flies and even mice [1,2,11,12].

Label-free approaches

A limitation of SILAC experiments is that labeling is necessary but is not always possible - for example in human samples. One option is to compare SILAC-labeled reference extracts or recombinant proteins against samples of interest [13]. Alternatively, it may be desirable to find means of reliably quantifying protein abundance directly, an approach taken by Malmström *et al.* [4] for the characterization of *Leptospira* and its reaction to ciprofloxacin. Early methods of 'label-free' quantification used the frequency of peptide selection for fragmentation as a measure of their abundance - termed 'spectral counting' [14,15]. Because that technique uses an indirect measurement for peptide abundance and only works reliably for proteins with many available peptides, alternatives have been developed. Specifically, peptide-ion intensities in the parent MS[1] spectrum are used to quantify peptide abundances. For this method, reproducible identification of the same peptides in different LC-MS runs is crucial (Figure 1b). This is achieved by high mass-accuracy measurements, and also by aligning different runs based on the LC retention time of matched peptides between them [16]. Although still somewhat less accurate than quantification methods relying on isotope labels, this methodology makes a variety of clinical and environmental samples accessible, such as cancer or other biopsies.

In a series of papers including the *Leptospira* study, the peptide-ion intensity method has been further developed to calibrate MS measurements and yield absolute quantifications [4,6,17,18]. As standards for calibration, isotope-labeled reference peptides are spiked into samples. Comparison of the ion intensities of standards of known abundance and of the experimental peptides yields an absolute concentration for the latter (Figure 1b). In very complex mixtures, it can be difficult to detect such peptide pairs, but in principle, advances in instrumentation and development of analytic tools should eventually allow the measurement of most peptides in a mixture, including those spiked as a reference. In the meantime, targeted approaches such as selected reaction monitoring (SRM)

are promising. In these experiments, a series of mass analyzers (for example, a triple quadrupole MS) 'filters' only targeted peptides. In combination with isotope-labeled standards, the abundance of peptides is quantitated by comparison of parent ion pair intensities. As a result of effective filtering, SRM assays are performed very fast and can monitor a series of peptides. To obtain a calibration curve for the *Leptospira* proteome that can be extrapolated to determine the absolute abundances of all detected proteins, Malmström *et al.* [4] used 19 peptides to report on proteins ranging in abundance from 40 to 15,000 copies per cell. One appeal of this methodology is the rapid monitoring of a limited number of proteins, which would enable a comparison of abundance in many samples and the characterization of protein dynamics over time.

A potential problem with the peptide-ion intensity method is that parent ion scans are usually carried out using quadrupoles with high sensitivity and dynamic range but low mass accuracy, possibly leading to overlapping peaks and convolution of signals when analyzing complex mixtures. A remedy for this could be to acquire full high-resolution spectra by scanning MS and then select peptides for sequencing by an 'inclusion' list. Satisfyingly, in the case of *Leptospira* [4], the quantitation obtained using an SRM-derived calibration curve agreed very well with the counting by CET of the subunits in prominent cellular structures such as the flagella and the flagellar motor, or of methyl-accepting proteins in individual cells. This work shows how MS-based proteomics combined with high-resolution CET can yield information on protein abundance and localization.

Having obtained accurate measurements of the levels of individual proteins, it is then possible to compare proteomes under different physiological conditions. In the case of *Leptospira* [4], the comparison showed that the bacterium reacts to ciprofloxacin by strongly inducing the expression of a number of proteins (whose existence was previously only predicted from the genome sequence), but maintains overall protein concentration. The upregulated proteins might include interesting targets for combination therapy and the experiment shows in principle how this technology can be used for an unbiased systems characterization.

Over the past decade, developments in MS-based proteomics have greatly accelerated. In particular, new instrumentation and automation of MS-spectra interpretation enables the quantification of essentially whole-organism proteomes in single experiments. Tools to calibrate measurements are already leading to the determination of absolute protein abundances and specialized methods can be used to target subsets of proteins. All together, these developments predict that MS-based proteomics will become a staple technique in systems biology.

References
1. Bonaldi T, Straub T, Cox J, Kumar C, Becker PB, Mann M: **Combined use of RNAi and quantitative proteomics to study gene function in *Drosophila*.** *Mol Cell* 2008, **31:**762-772.
2. de Godoy LM, Olsen JV, Cox J, Nielsen ML, Hubner NC, Frohlich F, Walther TC, M Mann M: **Comprehensive mass-spectrometry-based proteome quantification of haploid versus diploid yeast.** *Nature* 2008, **455:**1251-1254.
3. Ideker T, Thorsson V, Ranish JA, Christmas R, Buhler J, Eng JK, Bumgarner R, Goodlett DR, Aebersold R, Hood L: **Integrated genomic and proteomic analyses of a systematically perturbed metabolic network.** *Science* 2001, **292:**929-934.
4. Malmström J, Beck M, Schmidt A, Lange V, Deutsch EW, Aebersold R: **Proteome-wide cellular protein concentrations of the human pathogen *Leptospira interrogans*.** *Nature* 2009, **460:**762-765.
5. Hubner NC, Ren S, Mann M: **Peptide separation with immobilized pI strips is an attractive alternative to in-gel protein digestion for proteome analysis.** *Proteomics* 2008, **8:**4862-4872.
6. Picotti P, Bodenmiller B, Mueller LN, Domon B, Aebersold R: **Full dynamic range proteome analysis of *S. cerevisiae* by targeted proteomics.** *Cell* 2009, **138:**795-806.
7. Hu Q, Noll RJ, Li H, Makarov A, Hardman M, Graham Cooks R: **The Orbitrap: a new mass spectrometer.** *J Mass Spectrom* 2005, **40:**430-443.
8. Ross PL, Huang YN, Marchese JN, Williamson B, Parker K, Hattan S, Khainovski N, Pillai S, Dey S, Daniels S, Purkayastha S, Juhasz P, Martin S, Bartlet-Jones M, He F, Jacobson A, Pappin DJ: **Multiplexed protein quantitation in *Saccharomyces cerevisiae* using amine-reactive isobaric tagging reagents.** *Mol Cell Proteomics* 2004, **3:**1154-1169.
9. Ong SE, Blagoev B, Kratchmarova I, Kristensen DB, Steen H, Pandey A, Mann M: **Stable isotope labeling by amino acids in cell culture, SILAC, as a simple and accurate approach to expression proteomics.** *Mol Cell Proteomics* 2002, **1:**376-386.
10. Cox J, Mann M: **MaxQuant enables high peptide identification rates, individualized p.p.b.-range mass accuracies and proteome-wide protein quantification.** *Nat Biotechnol* 2008, **26:**1367-1372.
11. Kruger M, Moser M, Ussar S, Thievessen I, Luber CA, Forner F, Schmidt S, Zanivan S, Fassler R, Mann M: **SILAC mouse for quantitative proteomics uncovers kindlin-3 as an essential factor for red blood cell function.** *Cell* 2008, **134:**353-364.
12. Liao L, Park SK, Xu T, Vanderklish P, Yates JR 3rd: **Quantitative proteomic analysis of primary neurons reveals diverse changes in synaptic protein content in fmr1 knockout mice.** *Proc Natl Acad Sci USA* 2008, **105:**15281-15286.
13. Hanke S, Besir H, Oesterhelt D, Mann M: **Absolute SILAC for accurate quantitation of proteins in complex mixtures down to the attomole level.** *J Proteome Res* 2008, **7:**1118-1130.
14. Liu H, Sadygov RG, Yates JR 3rd: **A model for random sampling and estimation of relative protein abundance in shotgun proteomics.** *Anal Chem* 2004, **76:**4193-4201.
15. MacCoss MJ, Wu CC, Liu H, Sadygov R, Yates JR 3rd: **A correlation algorithm for the automated quantitative analysis of shotgun proteomics data.** *Anal Chem* 2003, **75:**6912-6921.
16. Strittmatter EF, Ferguson PL, Tang K, Smith RD: **Proteome analyses using accurate mass and elution time peptide**

240.5

tags with capillary LC time-of-flight mass spectrometry. *J Am Soc Mass Spectrom* 2003, **14:**980-991.

17. Gerber SA, Rush J., Stemman O, Kirschner MW, Gygi SP: **Absolute quantification of proteins and phosphoproteins from cell lysates by tandem MS.** *Proc Natl Acad Sci USA* 2003, **100:**6940-6945.

18. Silva JC, Gorenstein MV, Li GZ, Vissers JP, Geromanos SJ: **Absolute quantification of proteins by LCMSE: a virtue of parallel MS acquisition.** *Mol Cell Proteomics* 2006, **5:**144-156.

---

nature structural & molecular biology

A plasma-membrane E-MAP reveals links of the eisosome with sphingolipid metabolism and endosomal trafficking

Pablo S Aguilar[1,9], Florian Fröhlich[2,9], Michael Rehman[2,9], Mike Shales[3,9], Igor Ulitsky[4,8], Agustina Olivera-Couto[1], Hannes Braberg[3], Ron Shamir[4], Peter Walter[5], Matthias Mann[6], Christer S Ejsing[7], Nevan J Krogan[3] & Tobias C Walther[2]

The plasma membrane delimits the cell and controls material and information exchange between itself and the environment. How different plasma-membrane processes are coordinated and how the relative abundance of plasma-membrane lipids and proteins is homeostatically maintained are not yet understood. Here, we used a quantitative genetic interaction map, or E-MAP, to functionally interrogate a set of ~400 genes involved in various aspects of plasma-membrane biology, including endocytosis, signaling, lipid metabolism and eisosome function. From this E-MAP, we derived a set of 57,799 individual interactions between genes functioning in these various processes. Using triplet genetic motif analysis, we identified a new component of the eisosome, Eis1, and linked the poorly characterized gene *EMP70* to endocytic and eisosome function. Finally, we implicated Rom2, a GDP/GTP exchange factor for Rho1 and Rho2, in the regulation of sphingolipid metabolism.

The plasma membrane is the defining feature of the cell, separating its interior from the exterior space. It controls exchange and communication processes between the cell and its environment. The delivery of cellular material to the plasma membrane or cell exterior is mediated by exocytosis. Conversely, endocytosis is used to take up plasma membrane and external components. In addition, many signaling processes occur at the plasma membrane simultaneously and are often regulated by the endocytosis of receptors or delivery of messenger molecules. To coordinate these processes and maintain cell integrity under changing conditions, both plasma-membrane protein and lipid composition are regulated and adjusted to external conditions. Despite impressive advances in our understanding of these individual processes, it is not well understood how they are coordinated.
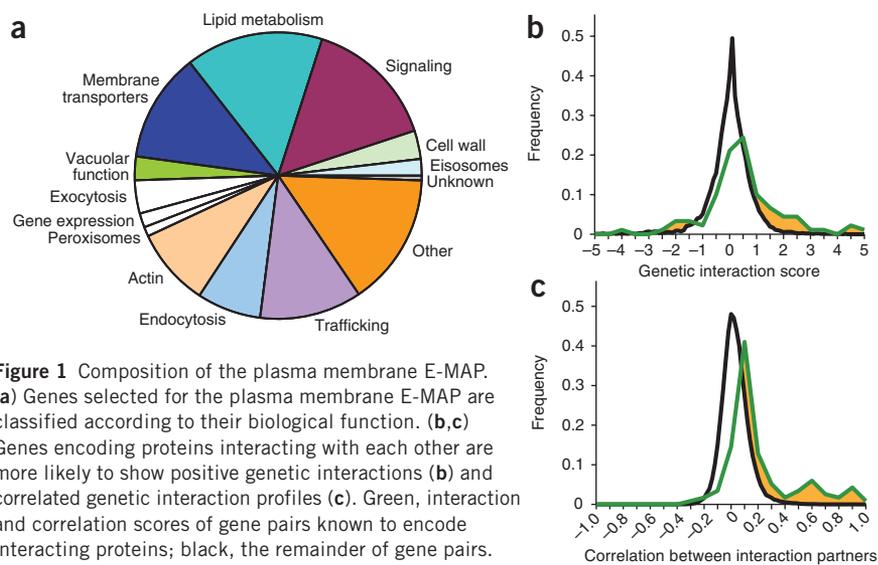
To accommodate its many functions, the plasma membrane is highly organized, both spatially and temporally. In *Saccharomyces cerevisiae*, several plasma-membrane domains of different composition are distinguishable by light microscopy. This organization is mediated, at least in part, by eisosomes, large protein complexes that underlie one of the domains, named MCC after the marker protein Can1 found there. When *PIL1*, encoding a major eisosome component, is deleted, cells have abnormal plasma-membrane structure with large invaginations and loss of MCC protein organization[1,2]. In addition, the endocytosis of several plasma-membrane proteins is either accelerated or delayed[2,3]. The molecular function of eisosomes is still unknown, but recent data show that they interact with sphingolipid-regulated Pkh-kinases, which phosphorylate their core components and are required for efficient endocytosis[4–6]. In addition to Pkh-kinases, Tor kinase complex 2 (TORC2) is implicated in sphingolipid metabolism regulation[7]. However, it is unclear how these different signaling pathways are controlled and coordinated as well as what their downstream effects are. Experimental evidence supports a model in which regulation of sphingolipid, sterol and glycerophospholipid levels in the plasma membrane are coordinated, but mechanistic insights as to how this is achieved are currently lacking[8,9]. To reveal functional links between the different processes, we generated a quantitative genetic-interaction map targeting a large set of genes implicated in plasma-membrane function.

Genetic interactions have long been used to dissect functional relationships between genes. Classically, researchers have looked for qualitative differences between observed phenotypes of double mutants and the phenotypes of the two related single mutants. More recently, we employed the epistatic miniarray profile (E-MAP) approach, a variation on synthetic genetic arrays[10]. This allows for the quantitative analysis of genetic interactions, including negative (for example, synthetic sick or lethal) as well as positive ones (for example, suppression)[11]. For this approach, a comprehensive set of double mutants is generated and their growth is measured. To determine individual genetic interactions, deviations of growth rates from the medians of all combinations with one particular gene are calculated for each combination as a quantitative interaction score

Figure 1 Composition of the plasma membrane E-MAP. (**a**) Genes selected for the plasma membrane E-MAP are classified according to their biological function. (**b**,**c**) Genes encoding proteins interacting with each other are more likely to show positive genetic interactions (**b**) and correlated genetic interaction profiles (**c**). Green, interaction and correlation scores of gene pairs known to encode interacting proteins; black, the remainder of gene pairs.

(or S-score)[12,13]. Each mutation has a genetic-interaction profile, or phenotypic signature, consisting of all its S-scores with all other genes in the E-MAP. A particularly useful parameter to judge the similarities of profiles is to compare correlations of two genes' interactions with all other genes in the set. In addition, bioinformatic extraction based on mathematical models can be applied to yield functional modules in an unbiased fashion from E-MAP datasets, and correlations and S-scores can be used to reveal their connections[14,15]. The E-MAP approach has been previously used to functionally interrogate several processes, and the dissection of genetic interactions from these E-MAPs has led to a deluge of biological insights in a variety of processes[11,16–18].

Here we report an E-MAP targeting plasma-membrane functions to generate previously unknown biological insight relating to plasma-membrane functions. Using this E-MAP, we have linked two new genes (*EMP70* and *EIS1*) to eisosome function and uncovered a link between GDP/GTP exchange protein Rom2 signaling and sphingolipid metabolism.

RESULTS

Overview of the plasma-membrane E-MAP

To address functional relationships between plasma-membrane processes, we systematically determined the genetic interactions among a set of 374 genes involved in plasma-membrane biology. We selected candidate genes encoding proteins functioning in membrane transport and organization, especially eisosomes, actin patches, endocytosis and exocytosis. In addition, we picked genes involved in ergosterol and sphingolipid metabolism, as these lipids are implicated in many plasma-membrane processes. Our selection criteria were based on available functional annotation (gene ontology terms) and a literature survey. We also included a diverse set of genes whose products localize to the plasma membrane and/or interact genetically or physically with previously characterized plasma-membrane genes/proteins. The selected genes were categorized into the functional groups presented in **Figure 1a** and **Supplementary Table 1**. We included a number of genes analyzed in previous systematic genetic studies to facilitate comparison between datasets[11,16,17]. From this set, we quantitated a total of 57,799 genetic interactions using the E-MAP approach (~83% of the possible interactions).

Previously, we found that gene pairs encoding physically interacting proteins are enriched for positive genetic interactions and show a higher propensity for having highly correlated genetic-interaction profiles[11,16,17]. To assess the richness and quality of the genetic-interaction data of the plasma-membrane E-MAP, we compared the

pairwise correlation of genetic-interaction profiles to a high-quality set of protein-protein interactions (PPIs)[19] and found that the power of the genetic map to predict PPIs is comparable to that of previously published E-MAPs (**Supplementary Fig. 1**). Furthermore, comparison of interaction scores or correlation coefficients of gene pairs encoding physically interacting proteins[19–21] (see **Supplementary Table 2**) among all plasma-membrane E-MAP gene pairs revealed that they have a higher likelihood to interact positively and to have correlated genetic-interaction profiles (**Fig. 1b,c**, yellow area under the green graph). Conversely, gene pairs with highly correlated interaction profiles and positive interactions are likely to physically interact.

To better visualize groups of interacting genes and their relationships, we used a previously developed algorithm that defines functional modules from quantitative genetic and PPI data[14] (**Supplementary Fig. 2**). This method identified 18 modules encompassing 53 genes (**Supplementary Fig. 2** and **Supplementary Table 3**). Genes in each module have similar genetic-interaction profiles and form a connected subnetwork in the PPI network. These modules corresponded to known protein complexes, such as the F-actin capping protein complex and the AP-3 adaptor, or to known pathways, such as sphingolipid metabolism, the HOG osmosensory pathway and ergosterol biosynthesis (**Supplementary Fig. 2**). To identify modules for which PPI data is not available, we performed the modular analysis without requiring PPI connectivity (**Supplementary Fig. 3**). This identified 29 modules encompassing 190 genes (**Supplementary Table 4** and http://acgt.cs.tau.ac.il/pmemap). This analysis yielded similar amounts of modules for the plasma membrane and the previously reported E-MAP on the early secretory pathway[11] (**Supplementary Table 5**). Additional information can be extracted by considering interactions of single genes with modules (data not shown).

Insights from hierarchical clustering of the genetic-interaction data

Each mutant engenders a genetic-interaction profile, or phenotypic signature, representing how it genetically interacts with all other mutants tested. Comparison of these profiles using hierarchical clustering (**Fig. 2**, **Supplementary Data** and http://interactome-cmp.ucsf.edu/plasma_membrane/) is a powerful and unbiased approach to identify genes of the same pathway. In the following, we provide a brief summary of several functional connections revealed by such gene clustering.

RVS161 and *RVS167* encode proteins that operate together in membrane remodeling during endocytosis[22]. As expected from their overlapping functions, *rvs161Δ* and *rvs167Δ* clustered together with high correlation (correlation = 0.54; **Fig. 2**, inserts 2). Consistent with previous reports, both share positive genetic interactions with a number of genes involved in fatty-acid elongation for sphingolipid synthesis, such as *FEN1* and *SUR4* (ref. 23) (**Fig. 2**, insert 2d). Notably, we observed positive interactions with genes encoding components of the Hog1 MAP-kinase cascade and the ergosterol biosynthesis pathway (*erg3Δ*, *erg5Δ*, *erg6Δ*, **Fig. 2**, inserts 2). In additions to changes in their sterols, these *erg* mutants have altered sphingolipid composition[8]. Thus, defects resulting from deletion of *RVS* genes could be compensated by *erg* mutants via changes in sphingolipids. Also in line with previous work, both *rvs161Δ* and *rvs167Δ* show negative interactions with actin
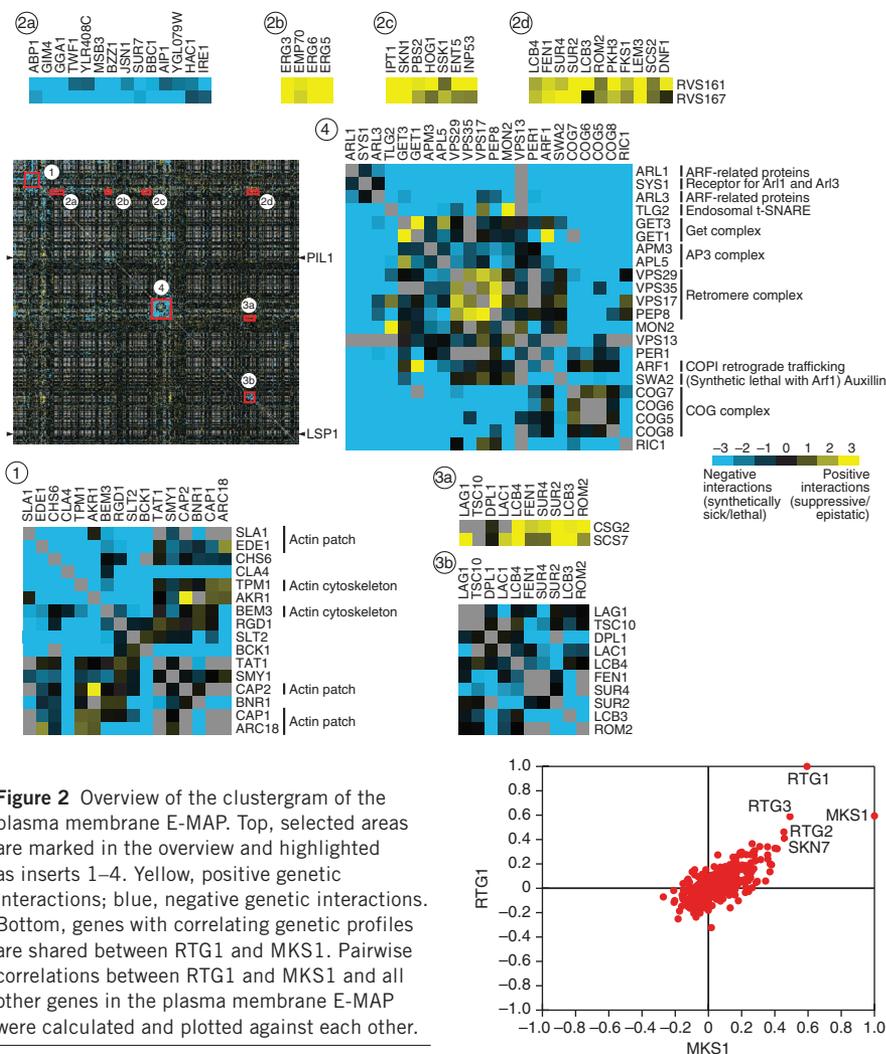
Figure 2 Overview of the clustergram of the plasma membrane E-MAP. Top, selected areas are marked in the overview and highlighted as inserts 1–4. Yellow, positive genetic interactions; blue, negative genetic interactions. Bottom, genes with correlating genetic profiles are shared between RTG1 and MKS1. Pairwise correlations between RTG1 and MKS1 and all other genes in the plasma membrane E-MAP were calculated and plotted against each other.

cytoskeleton genes, such as *BBC1*, *JSN1* and *BZZ1* (refs. 10,24–26) (**Fig. 2**, insert 2a). In addition, we found several previously unrecognized relationships, including negative interactions between the *RVS* genes and *ire1Δ* and *hac1Δ,* two mediators of the unfolded protein response (UPR) control system for endoplasmic reticulum function. Possibly, cells react to Rvs deficiency by altering lipid synthesis or transport, which in turn activates the UPR. Cells lacking the UPR in addition to the Rvs proteins could have decreased fitness. Consistent with this notion, a recent genome-wide study found the UPR activated in *rvsΔ* cells[27].

We also detected many genetic interactions and highly correlated profiles between genes encoding actin-patch components. For example, *sla1Δ* and *ede1Δ*, which function in endocytosis, are highly correlated (correlation = 0.64, **Fig. 2**, insert 1) and show a negative genetic interaction (interaction score = −7.7). Unexpectedly, given its function in exocytosis rather than endocytosis, we also found *chs6Δ* to be highly correlated with *sla1Δ* and *ede1Δ* (correlations *ede1Δ-chs6Δ* = 0.53 and *sla1Δ-chs6Δ* = 0.43; **Fig. 2**, insert 1). Furthermore, these three genes all result in negative genetic interactions when any two of them are combined. Collectively, this indicates that Chs6 might function in coordinating exo- and endocytosis, perhaps by delivering a subset of cargos to the plasma membrane[28]. In this scenario, *chs6Δ* would lead to the depletion of an endocytic factor from the plasma membrane and, as a consequence, a decrease in endocytosis efficiency. Combination with mutants defective in

this process would further decrease the fitness of the resulting strains.

We also observed many strong genetic interactions between trafficking complexes. Genes encoding the retromer complex (*VPS17*, *VPS29*, *VPS35*, *PEP8*), the COG complex (*COG5*, *COG6*, *COG7*, *COG8*) or the AP3 complex (*APM3*, *APL5*) all formed highly correlated clusters in the plasma-membrane E-MAP (**Fig. 2**, insert 4). In addition, potential new connections between these complexes and heretofore poorly characterized components of the endocytic machinery are apparent in these clusters. As an example, the retromer complex coclusters with deletion of *MON2* (correlation = 0.48), a gene encoding an evolutionarily conserved scaffolding protein functioning in endosome-to-Golgi trafficking[29]. Our data suggest that Mon2 acts together with the retromer in this process.

Many genes encoding members of signaling cascades showed strong genetic relationships. For example, two kinases of the cell integrity MAP kinase signaling module, Slt2 (the MAP kinase) and Bck1 (the MAP kinase kinase kinase)[30], showed one of the highest correlations (0.75). Similarly, genes encoding components of retrograde signaling (*RTG1*, *RTG2*, *RTG3* and *MKS1*) all cluster together (correlation = 0.44) indicating that all pairs have high correlation coefficients (for example, *MKS1/RTG1* correlation coefficient = 0.59; **Fig. 2**, bottom).

Functional links involving eisosomes

Although the eisosome has been linked to endocytosis regulation, details regarding its biological roles remain unresolved. To understand eisosome function *in vivo*, we genetically analyzed its core components, *PIL1* and *LSP1*. As the encoded proteins are >70% identical and are stoichiometric components of the eisosome, we expected very similar genetic profiles for them. Unexpectedly, *PIL1* and *LSP1* showed very different genetic interactions and, accordingly, cluster in different regions of the E-MAP (correlation = 0.038; **Fig. 2**, insert 4). This parallels the cell-biological observation that deletion of *PIL1* but not *LSP1* results in strong effects on plasma-membrane organization and protein turnover.

To gain further insight into eisosome function, we analyzed the triplet genetic motifs (TGMs) in which *pil1Δ* participates[17]. TGMs are the simplest motifs apart from binary interactions and can exist in four forms: type I (all three genes showing positive genetic interactions), type II (two positive and one negative), type III (two negative and one positive) and type IV (three negative interactions) (**Fig. 3a**). We have previously shown that genes with all positive genetic interactions (type I TGM) are enriched for functioning in the same pathway[17]. We therefore assembled a complete map of type I TGMs found in the plasma-membrane E-MAP (**Supplementary Fig. 4**). Because Pil1 has a more prominent role than Lsp1 in eisosome and plasma-membrane function, we extracted all type I TGMs involving *pil1Δ* (**Fig. 3b**). In this representation, we highlighted genes that are important for eisosome localization or are closely related to such genes (*YMR031c* and *EMP70*, respectively[31]; green nodes in **Fig. 3b**) and characterized them further.
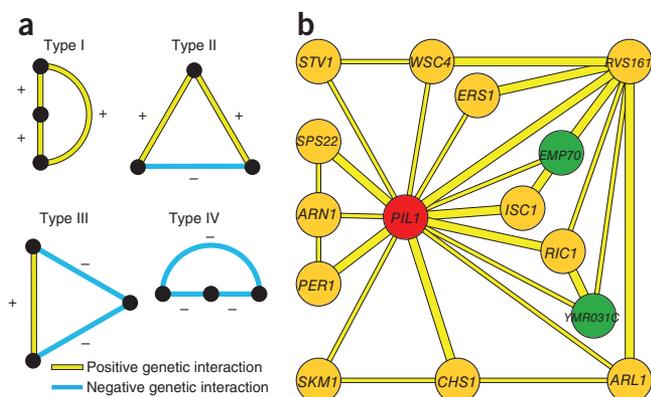
Figure 3 TGMs of the plasma membrane E-MAP. (**a**) All four potential TGMs are shown. Nodes in vertical order represent involvement in the same pathway; horizontal orientation indicates possible parallel pathways. (**b**) Type I TGMs that have *PIL1* as a node. Nodes in green represent a gene important for Pil1-GFP localization (*YMR031C*) or a homolog of such a gene (*EMP70*)[31].
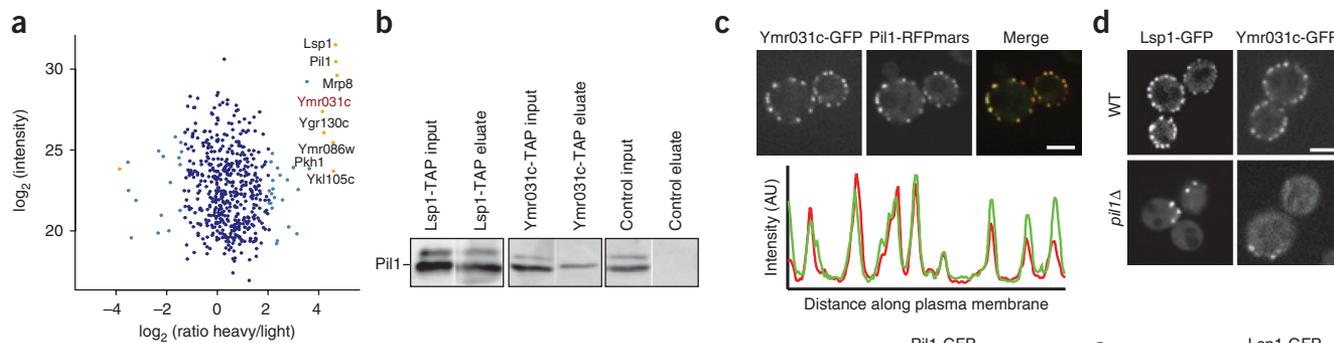
EIS1/YMR031c encodes a novel eisosome component

Because *ymr031cΔ* and *pil1Δ* have a positive genetic interaction and a correlated interaction profile (**Fig. 3b**), we tested whether the corresponding proteins physically associate. To this end, we fused the sequence encoding the green fluorescent protein (GFP) tag to *PIL1* at its endogenous location in the yeast genome and immune-purified the expressed Pil1-GFP from a yeast culture that was metabolically labeled with heavy, nonradioactive lysine (SILAC)[32]. In parallel, we performed a mock purification from control, light-labeled wild-type cells. We identified 533 proteins present over a 10,000-fold dynamic range in the mixed eluates from both purifications. As expected, we found Pil1 and Lsp1 as well as the recently identified eisosomes binding protein Mrp8 to be significant outliers, with a high ratio of labeled

to nonlabeled protein, indicating that they are specific interactors[2,33] ($P < 0.0001$; **Fig. 4a**). In addition, we found a number of other specific interactors, including Ymr031c, which is consistent with a recent report[34]. To independently confirm this observation, we performed immunoprecipitations of TAP-tagged Ymr031c and, as a control, Lsp1, and we found that both specifically precipitated Pil1 (**Fig. 4b**). To test whether Ymr031c colocalizes with Pil1, we fluorescently tagged both proteins. The signal from Pil1 and Ymr031c perfectly overlapped at eisosomes (**Fig. 4c**, upper panel; Pearson correlation = 0.81 ± 0.06). Consistent with these data, Ymr031c was recently detected at MCCs[3]. One prediction for a genuine eisosome component is that it relocalizes to eisosome remnants in a *PIL1* deletion strain[2]. We therefore investigated Ymr031c-GFP localization in *pil1Δ* cells and found that both Ymr031c and the eisosome component Lsp1 localized to one or a few eisosome remnants in the cell periphery (**Fig. 4d**). To investigate whether *YMR031c* has a role in eisosome architecture or assembly, we deleted it and analyzed the localization of eisosome core components in the resulting strain. For both Pil1 and Lsp1-GFP, we observed substantially increased cytosolic fluorescence in *ymr031cΔ* cells (**Fig. 4e,f**). Collectively, these data show that Ymr031c is physically associated with eisosomes and is required for their normal formation. We have therefore named this gene *EIS1*.

### *EMP70* is an early endosomal and vacuolar protein

In the genetic network of the plasma-membrane E-MAP, *EMP70* is the strongest candidate for a functional relationship with *PIL1* because (i) the two genes have highly correlated genetic profiles (correlation of *PIL1* and *EMP70* = 0.37 (*EMP70* has the most similar profile to *PIL1* of all the E-MAP genes); **Fig. 5a**); (ii) the two genes participate in two type I TGMs (**Fig. 3b**); and (iii) the Emp70 homolog Tmn2 is required for normal Pil1-GFP localization[31]. In addition, our modular analysis identified *EMP70* and *PIL1* as part of the same six-gene module (**Supplementary Fig. 3**; S-score between *PIL1* and *EMP70* = 1.78; **Supplementary Table 4**).

Figure 4 *YMR031C/EIS1* encodes an eisosome component. (**a**) Affinity purification and MS analysis of heavy labeled cells expressing GFP-tagged Pil1 and untagged control cells. Averaged peptide intensities are plotted against heavy/light SILAC ratios. Significant outliers ($P < 0.0001$) are colored in orange or light blue ($P < 0.05$); other identified proteins are shown in dark blue. (**b**) Pulldown purification from cells expressing tandem affinity-tagged Lsp1, Ymr031c or untagged control cells. Inputs and eluates from the pulldown were blotted and probed with antibodies against Pil1. (**c**) Colocalization of GFP-tagged Ymr031c with RFPmars-tagged Pil1. Representative confocal midsections are shown. The graph shows the intensity profiles for both channels along the perimeter of the cell. (**d**) *PIL1* is required for normal localization of Ymr031c. Ymr031c-GFP or Lsp1-GFP was expressed and imaged either in WT or *pil1Δ* cells. Representative confocal midsections are shown. (**e,f**) Ymr031c is required for normal eisosome formation. Pil1-GFP (**e**) or Lsp1-GFP (**f**) was expressed in *ymr031cΔ* or control cells. Representative midsections are shown. For each experiment, the number of eisosomes per cell, the GFP fluorescence per eisosome and the cytosolic GFP fluorescence were quantified from at least 100 cells and are shown below the images. Scale bars, 2.5 μm.
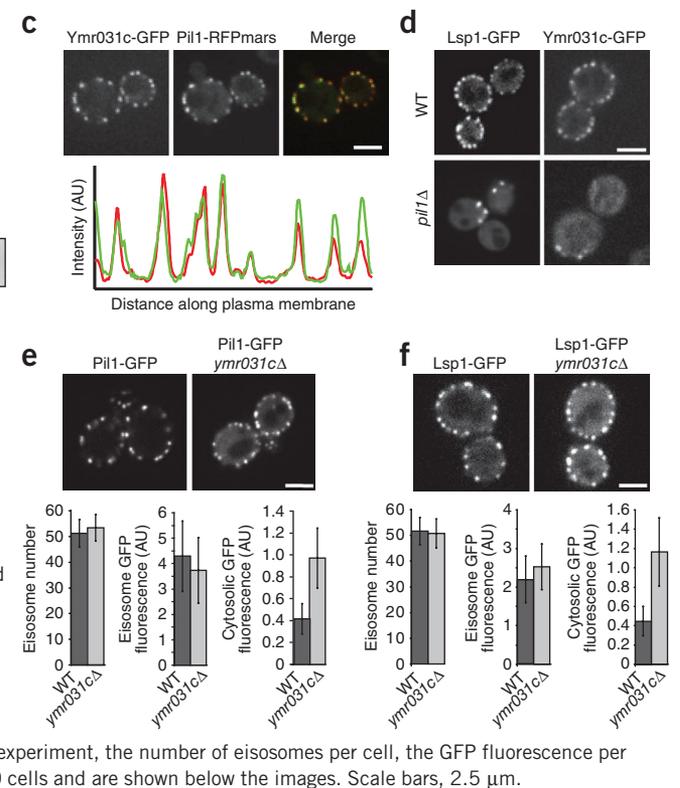
Figure 5 The eisosome-linked Emp70 is an early endosomal protein. (**a**) Genes with correlating genetic profiles are shared between *PIL1* and *EMP70* but not *PIL1* and *LSP1*. Correlation coefficients between the genetic profile of *PIL1* and each of the other 373 profiles in the E-MAP are plotted on the *x* axis against, on the *y* axis, either the similar set of values for the *LSP1* profile with all other profiles (blue) or those for *EMP70* with all other profiles (red). Labeled points indicate some genes with profiles that are positively correlated with both the profile of *PIL1* and that of *EMP70*. CC values in blue and red indicate the correlation coefficients for the full set of blue or red points plotted. (**b**) Emp70 colocalizes with Kex2. Emp70-GFP and Kex2-RFPmars were coexpressed and imaged. Representative confocal midsections are shown. (**c**) Emp70 localizes to an FM4-64 marked endocytic compartment. Cells expressing Emp70-GFP (green) were pulse labeled with FM4-64 (red) and imaged for 1 h. Images of midsections of cells at selected time are shown as indicated. (**d**) Emp70 localizes to the class E compartment in *SNF7* mutants. GFP-tagged Emp70 was expressed in cells harboring nonfunctional Snf7-RFPmars, resulting in the clustering of endosomal proteins in the class E compartment. Representative confocal midsections are shown. (**e**) Emp70-GFP foci localize to the cell periphery. Emp70-GFP (green) was expressed in cells harboring the fluorescent eisosomes marker Lsp1-MARS. Representative mid- (left) and top sections (right) are shown. Boxes highlight selected areas of colocalization. (**f**) *PIL1* is required for normal Emp70 localization to the cell periphery. Emp70-GFP was expressed in cells expressing the plasma membrane marker Ylr413w-RFPmars, and foci overlaying this marker were counted in more than 100 WT and *pil1Δ* cells. Results are shown as a histogram of number of spots opposed to the plasma membrane in each cell. (**g**) Quantitation of the organelle distribution of Emp70. Emp70-GFP was imaged in live cells and analyzed for colocalization with Kex2-RFPmars (*n* = 100), vacuolar FM4-64 (*n* = 91), Snf7-RFPmars (*n* = 93, diploid strain expressing one tagged Snf7 allele) and Lsp1-Cherry (*n* = 107). The relative area of overlap between signals was quantified as a percentage of total area occupied by Emp70 signal. Box plots representing maxima, 75th percentile, median, 25th percentile and minima are shown for the colocalization with each marker. Scale bars, 2.5 μm.
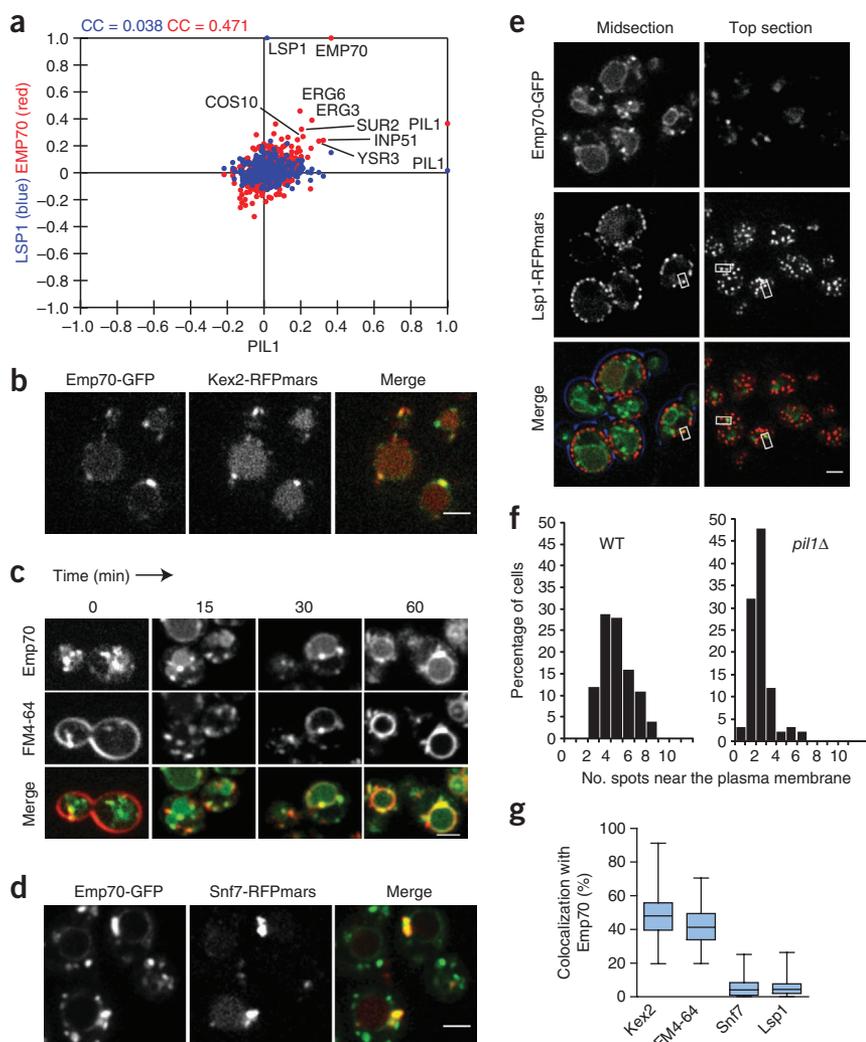
These genetic links prompted us to investigate *EMP70* in more detail (**Fig. 5**). We fluorescently tagged Emp70 with GFP and found that it localizes in a complex pattern consisting of a central ring reminiscent of vacuoles and several bright foci in the cytoplasm that often seem connected to the vacuole (**Fig. 5b** and **Supplementary Video 1**). Emp70 was previously found in an endosomal membrane fraction[35]. We therefore tested whether cytosolic Emp70 foci represent endosomes. We used a number of endosomal markers and found Emp70-GFP foci to colocalize with Kex2, marking the early endosome, which in yeast is functionally continuous with the trans-Golgi network. In contrast, Emp70 localization did not overlap with the late endosomal/prevacuolar marker Vps5 (**Fig. 5b** and **Supplementary Fig. 5a**).

To test whether the Emp70-labeled compartments are part of the endocytic route, we used the endocytosis tracer FM4-64. This lipid dye is incorporated in the plasma membrane, taken up by endocytosis and trafficked through the endosomal system to the vacuole[36]. We found in pulse-chase experiments that early FM4-64 intermediates colocalize with Emp70 foci (**Fig. 5c**, 0 min). As the dye migrated through the endocytic system, it also colocalized with a subset of Emp70-positive foci toward the end of the reaction but markedly less

at intermediate time points (**Fig. 5c**, 30 min). At the final time point, FM4-64 clearly labeled the vacuole delimiting membrane where it colocalized with the Emp70-GFP ring staining. Trafficking from early endosomes can be blocked by incubation of cells at 16 °C, which leads to the accumulation of FM4-64 (ref. 37). Emp70-GFP almost perfectly colocalized with FM4-64 when the latter was accumulated in such a '16 °C compartment', further arguing that Emp70 localizes to early endosomes (**Supplementary Fig. 5b**). Strains harboring a deleted or C-terminally tagged *SNF7* (an ESCRT-III gene) show a 'class E' vacuolar protein sorting defect. This is characterized by collapse of endosomes to one or a few large class E compartments[38,39]. Under these conditions, Emp70-GFP formed fewer, very large clusters that colocalized with Snf7-RFPmars marked class E compartments and showed reduced vacuolar membrane staining (**Fig. 5d**). From these data, we conclude that Emp70 localizes to early endosomes and the vacuole. To better characterize the localization of Emp70 in these two pools, we quantitated the relative amount of Emp70 colocalizing with markers for each organelle and found 48% of Emp70 to localize in the TGN/endosomal compartment and 41% at the vacuolar membrane (**Fig. 5g**).
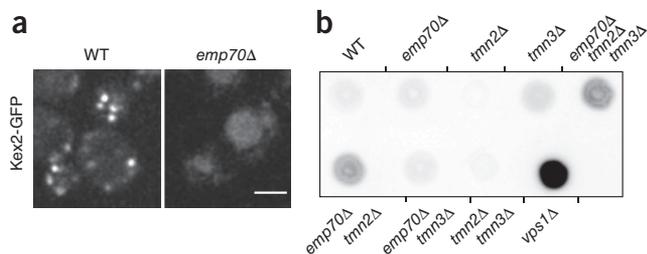
Figure 6 Emp70 is required for normal endosome function. (**a**) *EMP70* is required for normal localization of Kex2-GFP. Kex2-GFP was expressed in either WT or *emp70Δ* cells, and representative confocal midsections are shown. (**b**) Emp70 family members are required for late endosomal protein retrieval. Mutants of *EMP70, TMN2 or TMN3* were tested alone or in combination for CPY secretion. A representative colony blot is shown. Scale bar, 2.5 μm.

During our localization studies, we often observed early endosomal foci marked by FM4-64 dynamically associating with the plasma membrane. To test whether the genetic link of *EMP70* with *PIL1* was reflected in the recruitment of Emp70-GFP foci to eisosomes, we investigated the Emp70-GFP localization with respect to fluorescently tagged eisosomes. Strikingly, we found many spots of Emp70-GFP at eisosomes (**Fig. 5e**). In any given cell, 4% of the total Emp70-GFP signal colocalized with an eisosome marker (**Fig. 5g** and **Supplementary Video 2**). To test whether this association has functional relevance, we investigated the Emp70 localization in *pil1Δ* cells and found a marked reduction of foci close to the plasma membrane (**Fig. 5f**).

### EMP70 proteins are required for normal endosomal sorting

To test whether Emp70 is important for early endosome-to-vacuole trafficking, we analyzed Kex2-GFP localization in an *emp70Δ* strain and found a substantial Kex2 relocalization from early endosomes to the vacuole (**Fig. 6a**). Kex2 steady-state localization depends on signals that send it to early endosomes, which subsequently mature into late endosomes, from which Kex2 is actively retrieved[40,41]. It is possible that vacuolar mislocalization of Kex2 in *emp70Δ* cells results from a defect in retrieval from the late endosome or a complex-trafficking problem affecting early endosome function. Normally, if retrieval is compromised, vacuolar sorted carboxypeptidase Y (CPY) is secreted. We tested this and found that, in contrast to the control *vps1Δ*, *emp70Δ* alone does not lead to CPY secretion[42,43]. *EMP70* has two homologs in the genome, *TMN2* and *TMN3*. To address whether they could compensate for Emp70 function in its absence, we tested CPY secretion in strains with different combinations of the family members deleted. *TMN2* deletion alone had no effect, and *TMN3* deletion alone only a weak effect, on CPY sorting (**Fig. 6b**). In contrast, combining *emp70Δ* with either *tmn2Δ* or *tmn2Δ tmn3Δ* resulted in CPY secretion, showing that Emp70 is functionally redundant with Tmn2 in vacuolar protein sorting and that the Emp70 protein family is required for normal endosomal function.

Figure 7 Genetic interactions of sphingolipid metabolism. (**a**) Graphic representation of the sphingolipid synthesis pathway. Blue, negative genetic interactions; yellow, positive interactions. (**b**) Genes encoding enzymes acting in succession in sphingolipid synthesis show higher correlation than genes further apart in the metabolic network. For each gene pair in sphingolipid synthesis, the pathway distance of genes (that is, the number of metabolic intermediates between the catalyzed reactions) is plotted against the correlation coefficient of the gene pairs. The red line is a best-fit linear regression line fitted for all the data points on the graph.

Sphingolipid metabolism and its regulation

The plasma-membrane E-MAP interrogates relationships within metabolic networks that are important for plasma-membrane function, including sphingolipid metabolism (**Fig. 2**, inserts 3a and 3b, and **Fig. 7a**). Consistent with their common function, many of the sphingolipid pathway genes showed high correlation (>0.2). **Figure 7b** shows the distance of the action of enzymes in the pathway plotted against the correlation coefficient of the corresponding genes. The linear best fit on all data points revealed that genes encoding enzymes catalyzing subsequent steps are more highly correlated than genes further away in the metabolic network. Moreover, whereas most mutations in genes encoding enzymes catalyzing early steps of sphingolipid synthesis have negative genetic interactions with each other (**Fig. 2**, insert 3b, and **Fig. 7a**), they show positive genetic interactions when combined with mutations in genes acting late in complex sphingolipid formation (**Fig. 2**, insert 3a, and **Fig. 7a**). This might indicate that deficiency in late-acting enzymes leads to a buildup of toxic intermediates, which can be suppressed by deleting genes encoding upstream-acting enzymes. Precedence for this includes inhibition of Aur1, which converts ceramide to inositolphosphoceramide by aureobasidin A, leading to complex sphingolipids depletion and a concomitant accumulation of ceramide, which both contribute to toxicity[44].

The plasma-membrane E-MAP also revealed that *ROM2*, encoding a Rho1 GTPase exchange factor, has strong genetic connections to sphingolipid synthesis genes. For example, *ROM2* has correlated genetic profiles with *FEN1*, *SUR2*, *LCB3* and *SUR4*, all acting early,

a

CC = 0.611   CC = −0.201

b
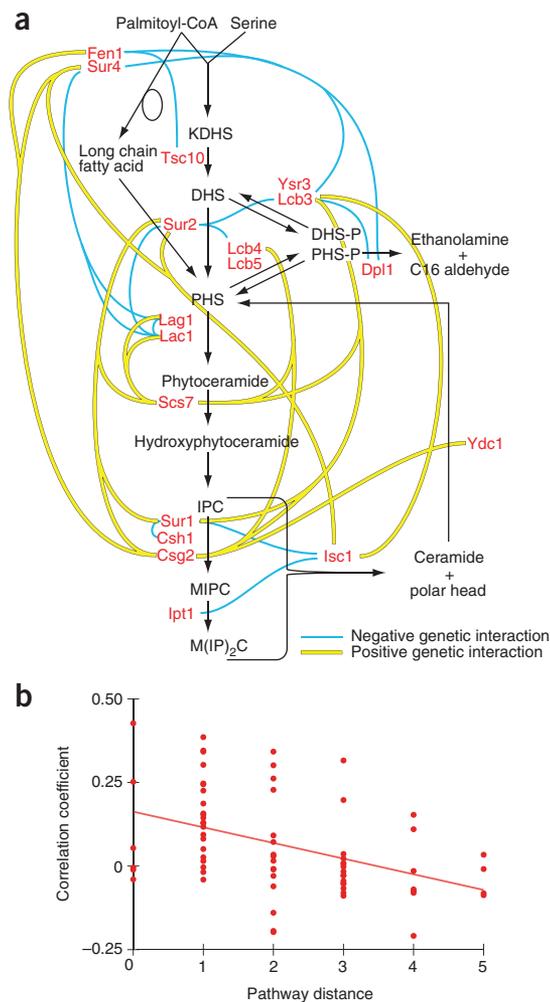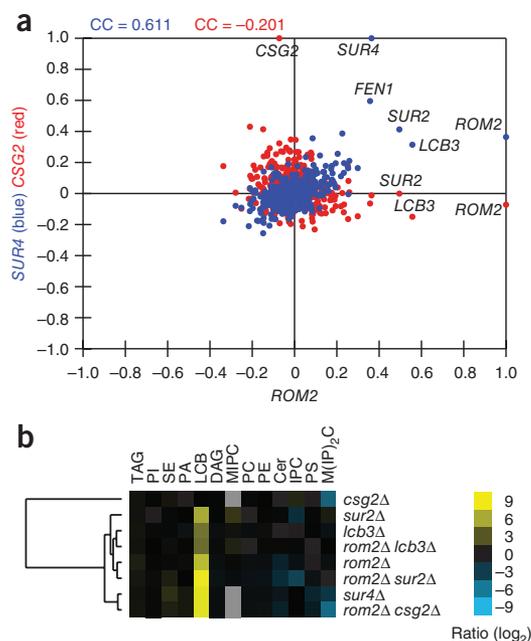
Figure 8 Rom2 interacts with sphingolipid metabolism. (**a**) Genes with correlating genetic profiles are shared between *SUR4* and *ROM2* but not between *CSG2* and *ROM2*. Correlation coefficients between the genetic profile of *ROM2* and each of the other 373 profiles in the E-MAP are plotted on the *x* axis against, on the *y* axis, either the similar set of values for the *SUR4* profile with all other profiles (blue) or those for *CSG2* with all other profiles (red). Labeled points indicate genes with profiles that are positively correlated with the profile of *ROM2*. CC values in blue and red indicate the correlation coefficients for the full set of blue or red points plotted. (**b**) Lipidome profiling of *rom2Δ* and selected sphingolipid metabolism mutants. Lipid class abundances were normalized to WT levels. Sterol esters (SE), phosphatidic acid (PA), triacylglycerol (TAG), long chain base (LCB) mannosylinositol phosphoceramide (MIPC), phosphatidylethanolamine (PE), diacylglycerol (DAG), phoshphatidylcholine (PC), phoshphatidylinositol (PI), ceramide (Cer), phosphatidylserine (PS) mannosylinositol-2-phosphoceramide (M(IP)$_2$C) and inositol phosphoceramide (IPC) levels are shown.

homeostasis. As an example of a physical interaction revealed from the E-MAP data, we investigated Eis1/Ymr031c and defined it as an eisosome component. Based on its much lower abundance compared to the eisosome core components, it might have a special architectural or regulatory role there. This is also a case where we combined data from the plasma-membrane E-MAP with our visual screen for genes affecting Pil1-GFP localization[31], which provides an example how the combination of different high-throughput datasets helps to uncover previously unrecognized relationships.

Mining of the plasma-membrane E-MAP also yielded information on more functional interactions not reflected in physical associations. The transmembrane protein Emp70 has a fascinatingly complex localization and genetically interacts with eisosome components. Particularly intriguing is the Emp70 pool localized in endosomal structures that often appear connected with the vacuolar membrane. This observation raises the possibility that endosomes reach out to the plasma membrane and pick up their cargo. It also suggests that at least parts of the endosomal membrane system might be a tubular network connected to the vacuole, but further detailed cell-biological studies will have to clarify this point.

We also used the plasma-membrane E-MAP to interrogate metabolic networks and their regulation. The strong correlation profiles of sphingolipid synthesis genes argues that novel functionally related genes could be found by using the genetic profiles from the plasma-membrane E-MAP. For example, genes that function in sphingolipid metabolism or are involved in its regulation would be expected to cluster with known sphingolipid synthesis genes. Using this logic, we identified Rom2 as a regulator of sphingolipid metabolism. Mechanistically, its activator function could occur either through ceramide synthesis activation by Rom2 or through negative regulation of ceramidase. Between these two hypotheses, we consider the first one more likely, as *rom2Δ* clusters with genes encoding ceramide synthase (*lag1Δ lac1Δ*) but not *ydc1Δ*, which encodes ceramidase (**Fig. 2**, insert 3b). This is consistent with previous findings that connect the Tor2 kinase pathway with Rho1-signaling via Rom2 as well as recent findings that TORC2 is required for ceramide biosynthesis[7,46]. This previous study[7] implicated an alternative branch of TORC2 signaling through the Ypk2 kinase in regulation of ceramide biosynthesis but did not rule out involvement of Rom2. The effect of *ROM2* deletion could either be directly on ceramide synthase or, alternatively, could block the synthesis of its substrate, long chain fatty acid–CoA. In the latter model, the depletion of long chain fatty acids would slow ceramide synthesis and would therefore lead to the accumulation of long chain bases, the second substrate of ceramide synthase. In either scenario, Rom2 has a stimulatory function in sphingolipid synthesis at the step converting long chain bases to ceramides. Consistent with this notion, the inhibition of sphingolipid synthesis by the antifungal drug myriocin leads to a relocalization of Rom2 from the plasma membrane[47]. Rom2 is recruited to the plasma membrane through the binding of phosphoinositol-(4,5)-bisphosphate (PI(4,5)P$_2$) by its pleckstrin homology domain, and reduction of PI(4,5)P$_2$ also relocalizes Rom2 (ref. 48). This raises the possibility that Rom2 serves to connect phosphoinositide and sphingolipid signaling pathways. The details of this regulation of sphingolipid metabolism remain to be worked out, but it shows how genetic interactions in the plasma-membrane E-MAP yield novel insights into metabolic networks and their regulation.

We anticipate that this dataset will fuel many more mechanistic studies. In particular, integration with other data from lipidomics, interaction proteomics or systematic visuals screens are likely to reveal novel insights into the regulation of plasma-membrane processes. In addition, many antifungal drugs target functions connected to the

but shows negative correlation with *CSG2* acting late in sphingolipid synthesis (**Fig. 8a**). In addition, a *ROM2* deletion mutation results in a strong synthetic sick phenotype with *lcb3Δ*, *sur2Δ dpl1Δ* and *ysr3Δ*, all genes encoding enzymes catalyzing different steps of sphingolipid metabolism (interaction score < −2; see **Fig. 2**, insert 3b, and data not shown). Together, this suggests that Rom2 is an activator of sphingolipid metabolism. To test this model, we profiled the lipidome of *rom2Δ* and several other mutants in the sphingolipid pathway by 'shotgun' lipidomics[45]. *ROM2* deletion resulted in a lipid phenotype similar to that of *sur2Δ* or *sur4Δ* cells (**Fig. 8b** and **Supplementary Table 6**). Particularly, *ROM2* deletion led primarily to accumulation of long chain bases and a small decrease of ceramides. This argues that Rom2 activates sphingolipid synthesis by regulating the conversion of long chain bases to ceramides.

DISCUSSION

The plasma-membrane E-MAP quantitatively describes interactions between genes involved in plasma-membrane processes. Together with previous studies, it shows that the E-MAP technology can be used to detect protein interactions and signaling pathways as well as to uncover complex biological connections. Here, we highlighted several examples of novel insights into plasma-membrane function derived from the E-MAP, focusing on its spatial organization and

plasma membrane, such as cell-wall and ergosterol synthesis. Probing the set of genes on the E-MAP presented here with a battery of drugs and comparing of the resulting drug profiles to the mutant profiles is an effective way to identify putative drug targets. This would facilitate the identification of compounds impinging on these various processes and could potentially have therapeutic value.

METHODS

Methods and any associated references are available in the online version of the paper at http://www.nature.com/nsmb/.

Note: Supplementary information is available on the Nature Structural & Molecular Biology website.

AUTHOR CONTRIBUTIONS

All authors contributed to every aspect of this work.

COMPETING FINANCIAL INTERESTS

The authors declare no competing financial interests.

1. Grossmann, G., Opekarova, M., Malinsky, J., Weig-Meckl, I. & Tanner, W. Membrane potential governs lateral segregation of plasma membrane proteins and lipids in yeast. *EMBO J.* **26**, 1–8 (2007).
2. Walther, T.C. *et al.* Eisosomes mark static sites of endocytosis. *Nature* **439**, 998–1003 (2006).
3. Grossmann, G. *et al.* Plasma membrane microdomains regulate turnover of transport proteins in yeast. *J. Cell Biol.* **183**, 1075–1088 (2008).
4. deHart, A.K., Schnell, J.D., Allen, D.A. & Hicke, L. The conserved Pkh-Ypk kinase cascade is required for endocytosis in yeast. *J. Cell Biol.* **156**, 241–248 (2002).
5. Friant, S., Lombardi, R., Schmelzle, T., Hall, M.N. & Riezman, H. Sphingoid base signaling via Pkh kinases is required for endocytosis in yeast. *EMBO J.* **20**, 6783–6792 (2001).
6. Walther, T.C. *et al.* Pkh-kinases control eisosome assembly and organization. *EMBO J.* **26**, 4946–4955 (2007).
7. Aronova, S. *et al.* Regulation of ceramide biosynthesis by TOR complex 2. *Cell Metab.* **7**, 148–158 (2008).
8. Guan, X.L. *et al.* Functional interactions between sphingolipids and sterols in biological membranes regulating cell physiology. *Mol. Biol. Cell* **20**, 2083–2095 (2009).
9. Tabuchi, M., Audhya, A., Parsons, A.B., Boone, C. & Emr, S.D. The phosphatidylinositol 4,5-biphosphate and TORC2 binding proteins Slm1 and Slm2 function in sphingolipid regulation. *Mol. Cell. Biol.* **26**, 5861–5875 (2006).
10. Tong, A.H. *et al.* Global mapping of the yeast genetic interaction network. *Science* **303**, 808–813 (2004).
11. Schuldiner, M. *et al.* Exploration of the function and organization of the yeast early secretory pathway through an epistatic miniarray profile. *Cell* **123**, 507–519 (2005).
12. Collins, S.R., Schuldiner, M., Krogan, N.J. & Weissman, J.S. A strategy for extracting and analyzing large-scale quantitative epistatic interaction data. *Genome Biol.* **7**, R63 (2006).
13. Schuldiner, M., Collins, S.R., Weissman, J.S. & Krogan, N.J. Quantitative genetic analysis in *Saccharomyces cerevisiae* using epistatic miniarray profiles (E-MAPs) and its application to chromatin functions. *Methods* **40**, 344–352 (2006).
14. Ulitsky, I., Shlomi, T., Kupiec, M. & Shamir, R. From E-MAPs to module maps: dissecting quantitative genetic interactions using physical interactions. *Mol. Syst. Biol.* **4**, 209 (2008).
15. Bandyopadhyay, S., Kelley, R., Krogan, N.J. & Ideker, T. Functional maps of protein complexes from quantitative genetic interaction data. *PLOS Comput. Biol.* **4**, e1000065 (2008).
16. Collins, S.R. *et al.* Functional dissection of protein complexes involved in yeast chromosome biology using a genetic interaction map. *Nature* **446**, 806–810 (2007).
17. Fiedler, D. *et al.* Functional organization of the *S. cerevisiae* phosphorylation network. *Cell* **136**, 952–963 (2009).
18. Wilmes, G.M. *et al.* A genetic interaction map of RNA-processing factors reveals links between Sem1/Dss1-containing complexes and mRNA export and splicing. *Mol. Cell* **32**, 735–746 (2008).
19. Collins, S.R. *et al.* Toward a comprehensive atlas of the physical interactome of *Saccharomyces cerevisiae. Mol. Cell. Proteomics* **6**, 439–450 (2007).
20. Gavin, A.C. *et al.* Proteome survey reveals modularity of the yeast cell machinery. *Nature* **440**, 631–636 (2006).
21. Krogan, N.J. *et al.* Global landscape of protein complexes in the yeast *Saccharomyces cerevisiae. Nature* **440**, 637–643 (2006).
22. Ren, G., Vajjhala, P., Lee, J.S., Winsor, B. & Munn, A.L. The BAR domain proteins: molding membranes in fission, fusion, and phagy. *Microbiol. Mol. Biol. Rev.* **70**, 37–120 (2006).
23. Revardel, E., Bonneau, M., Durrens, P. & Aigle, M. Characterization of a new gene family developing pleiotropic phenotypes upon mutation in *Saccharomyces cerevisiae. Biochim. Biophys. Acta* **1263**, 261–265 (1995).
24. Breton, A.M. & Aigle, M. Genetic and functional relationship between Rvsp, myosin and actin in *Saccharomyces cerevisiae. Curr. Genet.* **34**, 280–286 (1998).
25. Brizzio, V., Gammie, A.E. & Rose, M.D. Rvs161p interacts with Fus2p to promote cell fusion in *Saccharomyces cerevisiae. J. Cell Biol.* **141**, 567–584 (1998).
26. Friesen, H. *et al.* Characterization of the yeast amphiphysins Rvs161p and Rvs167p reveals roles for the Rvs heterodimer *in vivo. Mol. Biol. Cell* **17**, 1306–1321 (2006).
27. Jonikas, M.C. *et al.* Comprehensive characterization of genes required for protein folding in the endoplasmic reticulum. *Science* **323**, 1693–1697 (2009).
28. Valdivia, R.H., Baggott, J., Chuang, J.S. & Schekman, R.W. The yeast clathrin adaptor protein complex 1 is required for the efficient retention of a subset of late Golgi membrane proteins. *Dev. Cell* **2**, 283–294 (2002).
29. Efe, J.A. *et al.* Yeast Mon2p is a highly conserved protein that functions in the cytoplasm-to-vacuole transport pathway and is required for Golgi homeostasis. *J. Cell Sci.* **118**, 4751–4764 (2005).
30. Levin, D.E. Cell wall integrity signaling in *Saccharomyces cerevisiae. Microbiol. Mol. Biol. Rev.* **69**, 262–291 (2005).
31. Frohlich, F. *et al.* A genome-wide screen for genes affecting eisosomes reveals Nce102 function in sphingolipid signaling. *J. Cell Biol.* **185**, 1227–1242 (2009).
32. Ong, S.E. *et al.* Stable isotope labeling by amino acids in cell culture, SILAC, as a simple and accurate approach to expression proteomics. *Mol. Cell. Proteomics* **1**, 376–386 (2002).
33. Wang, H. *et al.* A complex-based reconstruction of the *Saccharomyces cerevisiae* interactome. *Mol. Cell. Proteomics* **8**, 1361–1381 (2009).
34. Deng, C., Xiong, X. & Krutchinsky, A.N. Unifying fluorescence microscopy and mass spectrometry for studying protein complexes in cells. *Mol. Cell. Proteomics* **8**, 1413–1423 (2009).
35. Schimmoller, F., Diaz, E., Muhlbauer, B. & Pfeffer, S.R. Characterization of a 76 kDa endosomal, multispanning membrane protein that is highly conserved throughout evolution. *Gene* **216**, 311–318 (1998).
36. Vida, T.A. & Emr, S.D. A new vital stain for visualizing vacuolar membrane dynamics and endocytosis in yeast. *J. Cell Biol.* **128**, 779–792 (1995).
37. Zheng, B., Wu, J.N., Schober, W., Lewis, D.E. & Vida, T. Isolation of yeast mutants defective for localization of vacuolar vital dyes. *Proc. Natl. Acad. Sci. USA* **95**, 11721–11726 (1998).
38. Babst, M., Wendland, B., Estepa, E.J. & Emr, S.D. The Vps4p AAA ATPase regulates membrane association of a Vps protein complex required for normal endosome function. *EMBO J.* **17**, 2982–2993 (1998).
39. Teis, D., Saksena, S. & Emr, S.D. Ordered assembly of the ESCRT-III complex on endosomes is required to sequester cargo during MVB formation. *Dev. Cell* **15**, 578–589 (2008).
40. Brickner, J.H. & Fuller, R.S. SOI1 encodes a novel, conserved protein that promotes TGN-endosomal cycling of Kex2p and other membrane proteins by modulating the function of two TGN localization signals. *J. Cell Biol.* **139**, 23–36 (1997).
41. Sipos, G. *et al.* Soi3p/Rav1p functions at the early endosome to regulate endocytic trafficking to the vacuole and localization of trans-Golgi network transmembrane proteins. *Mol. Biol. Cell* **15**, 3196–3209 (2004).
42. Robinson, J.S., Klionsky, D.J., Banta, L.M. & Emr, S.D. Protein sorting in *Saccharomyces cerevisiae*: isolation of mutants defective in the delivery and processing of multiple vacuolar hydrolases. *Mol. Cell. Biol.* **8**, 4936–4948 (1988).
43. Rothman, J.H., Howald, I. & Stevens, T.H. Characterization of genes required for protein sorting and vacuolar function in the yeast *Saccharomyces cerevisiae. EMBO J.* **8**, 2057–2065 (1989).
44. Cerantola, V. *et al.* Aureobasidin A arrests growth of yeast cells through both ceramide intoxication and deprivation of essential inositolphosphorylceramides. *Mol. Microbiol.* **71**, 1523–1537 (2009).
45. Ejsing, C.S. *et al.* Global analysis of the yeast lipidome by quantitative shotgun mass spectrometry. *Proc. Natl. Acad. Sci. USA* **106**, 2136–2141 (2009).
46. Schmidt, A., Bickle, M., Beck, T. & Hall, M.N. The yeast phosphatidylinositol kinase homolog TOR2 activates RHO1 and RHO2 via the exchange factor ROM2. *Cell* **88**, 531–542 (1997).
47. Kobayashi, T., Takematsu, H., Yamaji, T., Hiramoto, S. & Kozutsumi, Y. Disturbance of sphingolipid biosynthesis abrogates the signaling of Mss4, phosphatidylinositol-4-phosphate 5-kinase, in yeast. *J. Biol. Chem.* **280**, 18087–18094 (2005).
48. Audhya, A. & Emr, S.D. Stt4 PI 4-kinase localizes to the plasma membrane and functions in the Pkc1-mediated MAP kinase cascade. *Dev. Cell* **2**, 593–605 (2002).

ONLINE METHODS

E-MAP analysis. Generation and analysis of the quantitative genetic interaction data was carried out as previously described[11–13].

Detection of functional modules. Modules were identified using an algorithm described previously[14], which was applied to the S-scores in the plasma membrane E-MAP and a PPI network containing 49,010 interactions between 5,815 yeast genes, compiled from several databases[49–51]. The algorithm identifies a collection of modules and a set of module pairs by optimizing a probabilistic scoring function. This function takes into account both similarities of the S-score profiles and the raw S-scores by preferring modules of genes having high correlation coefficients (CC-scores) between members of the same complex and negative S-scores among members of a module pair. The significance of the CC-scores and S-scores was assessed by fitting Gaussian distributions using an expectation-maximization algorithm.

Yeast strains and culture. All yeast strains used are listed in **Supplementary Table 7**. C-terminal fusions and gene deletions were generated by homologous recombination of PCR-generated DNA fragments[52]. All single-, double- or triple-deletion strains were confirmed by PCR. Strains expressing tagged proteins were confirmed by PCR and fluorescence microscopy or western blot. Yeast cells were grown according to standard procedure. For SILAC labeling, Pil1-TEV-GFP–expressing and WT yeast cells were grown in the presence of 20 mg l^{-1} L-lysine-U-^{13}C$_6$,^{15}N$_2$ and normal L-Lysine, respectively, with at least ten doublings to an OD$_{600}$ = 0.7.

Microscopy. Cells were grown to an OD$_{600}$ = 0.6 in synthetic medium at 30 °C unless indicated. Cells were mounted in synthetic media onto concanavalin A coated cover slips and imaged with an ANDOR/TiLL iMIC CSU22 spinning disk confocal microscope, using an ANDOR iXonEM 897 EM CCD camera and an Olympus 100× 1.4 NA oil immersion objective. We collected 16-bit images using Andor Image iQ 1.9 in the linear range of the camera. For presentation, images were filtered with a smoothening filter averaging 2 pixels, converted to 8-bit images and cropped using ImageJ (http://rsb.info.nih.gov/ij/). For quantitation of colocalization, we collected stacks and extracted four-dimensional images for individual cells. The area of overlap was quantified dividing the total area of the Emp70 signal by the area of overlap determined using the RG2B colocalization ImageJ plugin.

FM4-64 uptake assay. Cells exponentially growing at an OD$_{600}$ = 0.7 (1 ml) were harvested, resuspended in 50 μl of medium and chilled on ice for 5 min. FM4-64 was added to a final concentration of 10 μM and incubated for another 10 min. Cells were washed with ice-cold medium, resuspended and incubated for different time points, after which cells were killed by 10 mM NaN$_3$ and 10 mM NaF and immediately analyzed by microscopy.

CPY secretion assay. The CPY secretion colony blot assay was performed as described using anti-CPY antibodies (Invitrogen-A6428)[53].

Proteomics. Protein extracts from 70 ODs of 'light' and 'heavy' labeled cells were obtained as described[31]. For immunopurification, equivalent amounts of proteins were incubated with anti-GFP AB-conjugated magnetic nanobeads (Miltenyi Biotech) for 5 min at 4 °C and loaded on μMacs columns (Miltenyi Biotech) in a magnetic μMacs Separator (Miltenyi Biotech), washed three times with 1 ml of lysis buffer with 1% (v/v) Triton-X100, three times with 1 ml of lysis buffer without Triton-X100 and eluted by TEV cleavage. Eluates were mixed, diluted 5× in 8 M urea, reduced for 20 min at room temperature (22 °C) in 1 mM DTT and then alkylated for 30 min by 5.5 mM iodoacetamide in the dark. Then, the eluates were digested, desalted and concentrated as described[31]. Peptides were separated on-line using an Easy nLC system (Proxeon Biosystems, Odense, Denmark). Samples (5 μl) were loaded as described[31]. Peptides were eluted with a segmented gradient of 2–60% solvent B over 102 min with a constant flow of 250 nl min^{-1}. The HPLC system was coupled to an LTQ-Orbitrap Velos mass spectrometer (Thermo Fisher Scientific) via a nanoscale LC interface (Proxeon Biosystems). The spray voltage was 2.2 kV, and the temperature of the heated capillary was 180 °C. Survey full scan spectra (m/z = 300–1600) were acquired in positive ion mode with a resolution of 60,000 at m/z = 400 after accumulation of 1,000,000 ions. Up to ten most-intense ions were sequenced by collision-induced dissociation in the LTQ. Precursor ion charge-state screening was enabled, and all unassigned charge states as well as singly charged peptides were rejected. The dynamic exclusion list was restricted to a maximum of 500 entries with a maximum retention period of 90 s and a relative mass window of 10 p.p.m. Orbitrap measurements were performed enabling the lock mass option for survey scans to improve mass accuracy[54]. Data were acquired using the Xcalibur software (version 2.1.0, Thermo Fisher Scientific) and MaxQuant, version 1.0.1 (ref. 55). The data was searched against the yeast database concatenated with reversed copies of all sequences[56,57] and supplemented with frequent contaminants using Mascot (version 2.2.0, Matrix Science[58]). Carbamidomethylated cysteines were set as fixed, whereas oxidation of methionine and N-terminal acetylation were set as variable modifications. Maximum allowed mass deviation for MS/MS peaks and missed cleavages were 0.5 and 3 Da, respectively. Maximum false-discovery rates (FDR) were 0.01 both on peptide and protein levels. Minimum required peptide length was 6 residues. Proteins with at least two peptides were considered identified.

Lipidomics. Cell were harvested from 20 ml logarithmically growing cultures in synthetic medium at 30 °C and washed in water at 4 °C. Cell pellets were frozen immediately in liquid nitrogen and were thawed later by adding 155 mM NH$_4$HCO$_3$ (pH 8), followed by cell disruption using zirconia beads (0.5 mm; BioSpec Products). Lipids were extracted from lysates as previously described[45] and analyzed using a LTQ Orbitrap XL mass spectrometer (Thermo Fisher Scientific) equipped with a robotic nanoflow ion source TriVersa NanoMate (Advion BioSciences Ltd.). MS survey scans were acquired in positive and negative ion mode using the Orbitrap analyzer with target mass resolution of 100,000 and automatic gain control set at 1e^5 as the target value[45].

49. Cherry, J.M. *et al.* SGD: *Saccharomyces* Genome Database. *Nucleic Acids Res.* **26**, 73–79 (1998).
50. Kanehisa, M. & Goto, S. KEGG: Kyoto encyclopedia of genes and genomes. *Nucleic Acids Res.* **28**, 27–30 (2000).
51. Reguly, T. *et al.* Comprehensive curation and analysis of global interaction networks in *Saccharomyces cerevisiae. J. Biol.* **5**, 11 (2006).
52. Janke, C. *et al.* A versatile toolbox for PCR-based tagging of yeast genes: new fluorescent proteins, more markers and promoter substitution cassettes. *Yeast* **21**, 947–962 (2004).
53. Mullins, C. & Bonifacino, J.S. Structural requirements for function of yeast GGAs in vacuolar protein sorting, α-factor maturation, and interactions with clathrin. *Mol. Cell. Biol.* **21**, 7981–7994 (2001).
54. Olsen, J.V. *et al.* Parts per million mass accuracy on an Orbitrap mass spectrometer via lock mass injection into a C-trap. *Mol. Cell. Proteomics* **4**, 2010–2021 (2005).
55. Cox, J. & Mann, M. MaxQuant enables high peptide identification rates, individualized p.p.b.-range mass accuracies and proteome-wide protein quantification. *Nat. Biotechnol.* **26**, 1367–1372 (2008).
56. Moore, R.E., Young, M.K. & Lee, T.D. Qscore: an algorithm for evaluating SEQUEST database search results. *J. Am. Soc. Mass Spectrom.* **13**, 378–386 (2002).
57. Peng, J., Elias, J.E., Thoreen, C.C., Licklider, L.J. & Gygi, S.P. Evaluation of multidimensional chromatography coupled with tandem mass spectrometry (LC/LC-MS/MS) for large-scale protein analysis: the yeast proteome. *J. Proteome Res.* **2**, 43–50 (2003).
58. Perkins, D.N., Pappin, D.J., Creasy, D.M. & Cottrell, J.S. Probability-based protein identification by searching sequence databases using mass spectrometry data. *Electrophoresis* **20**, 3551–3567 (1999).